NEW MEXICO DEPARTMENT OF TRANSPORTATION

RESEARCH BUREAU

Innovation in Transportation

Feasibility Analysis of Ultra High Performance Concrete for Prestressed Concrete Bridge Applications

Prepared by:
New Mexico State University
Department of Civil Engineering
Las Cruces, NM

June 2012

Prepared for:
New Mexico
Department of Transportation
Research.Bureau@state.nm.us
http://NMDOTResearch.com

In Cooperation with:
The US Department
of Transportation
Federal Highway Administration

Final Report
NM09MCS-01

JUNE 2012

USDOT FHWA SUMMARY PAGE

1. Report No. NM09MSC-01	2. Government Accession No.	3. Recipient's Catalog No.
4. Title and Subtitle: Feasibility Analysis of Ultra High Performance Concrete for Prestressed Concrete Bridge Applications – Phase I and II		5. Report Data 6. Performing Organization Code
7. Author(s): Brad D. Weldon, David V. Jáuregui, Craig M. Newtson, Christopher W. Taylor, Kristin F. Montoya, Srinivas Allena, Jesus Muro, Mohammed Talahat, Erin Lyell, and Eric T. Visage		8. Performing Organization Report No.
7. Performing Organization Name and Address Department of Civil Engineering New Mexico State University Box 30001, MSC 3CE Las Cruces, NM 88003		
12. Sponsoring Agency Name and Address NMDOT Research Bureau 7500B Pan American Freeway PO Box 94690 Albuquerque, NM 87199-4690		13. Type of Report and Period Covered Final Report: April 7, 2009 – June 30, 2012 14. Sponsoring Agency Code
15. Supplementary Notes		
16. Abstract UHPC is an emerging material technology in which concrete develops very high compressive strengths and exhibits improved tensile strength and toughness. In Phase I of this research project, a comprehensive literature and historical application review was completed to determine the characteristics and properties of UHPC currently being used in design applications. Trial designs and cost analyses on typical prestressed concrete bridges using UHPC were conducted and used to investigate the merits and feasibility of UHPC in prestressed concrete design in New Mexico. Based on the positive outcome of the feasibility study, UHPC mixture proportions using materials local to New Mexico were developed as Phase II of this research.		
17. Key Words ultra high performance concrete; UHPC; prestressed bridge design	18. Distribution Statement Available from NMDOT Research Bureau	

19.Security Classification Unclassified	20.Security Classification Unclassified	21. No. of pages 205	22. Price

Form DOT F 1700.7 (8-72)

THIS PAGE LEFT BLANK INTENTIONALLY

PROJECT NO. NM09MSC-01

FEASIBILITY ANALYSIS OF ULTRA HIGH PERFORMANCE CONCRETE FOR PRESTRESSED CONCRETE BRIDGE APPLICATIONS

Final Report
April 7, 2009 – June 30, 2012

A Report on Research Sponsored by:

Research Bureau
New Mexico Department of Transportation
7500B Pan American Freeway NE
PO Box 94690
Albuquerque, NM 887199-4690
(505) 841-9145
Research.bureau@state.nm.us
http://NMDOTResearch.com

Prepared by:

Brad D. Weldon, David V. Jáuregui, Craig M. Newtson
Christopher W. Taylor, Kristin F. Montoya, Srinivas Allena
Jesus Muro, Mohammed Talahat, Erin Lyell, and
Eric T. Visage

Department of Civil Engineering
New Mexico State University
PO Box 30001, MSC 3CE
(3035 S. Espina Street)
Las Cruces, NM 88003

PREFACE

The broad objective of the research program is to investigate the feasibility and limitations of Ultra High Performance Concrete (UHPC) for Prestressed Concrete Bridge Applications in New Mexico. UHPC is an emerging material technology in which concrete develops very high compressive strengths and exhibits improved tensile strength and toughness. In Phase I of this research project, a comprehensive literature and historical application review was completed to determine the characteristics and properties of UHPC currently being used in design applications. Trial designs and cost analyses on typical prestressed concrete bridges using UHPC were conducted and used to investigate the merits and feasibility of UHPC in prestressed concrete design in New Mexico. Based on the positive outcome of the feasibility study, UHPC mixture proportions using materials local to New Mexico were developed as Phase II of this research. Mixture proportions and the curing regimen were optimized for implementation of this material in bridge design in New Mexico. Finally, the resistance to freezing and thawing, alkali silica reaction, and delayed ettringite formation were established.

NOTICE

DISCLAIMER

ABSTRACT

This report presents the findings from two phases of research investigating the feasibility study on the advantages and limitations of implementing UHPC into prestress bridge design in New Mexico.

Ultra high performance concrete (UHPC) is an emerging material technology in which concrete develops very high compressive strengths and exhibits improved tensile strength and durability properties. Recent construction of three UHPC bridges in the United States has sparked interest in potentially using UHPC for prestressed bridge girders in New Mexico. UHPC offers many advantages including longer spans, improved durability, and smaller structural members, making it an appealing material to use in prestressed bridge construction.

In Phase I, two case studies on local bridges were conducted to investigate the feasibility of implementing UHPC in bridge design in New Mexico. The I-25/Doña Ana Interchange is a typical simple span bridge and the Sunland Park River Crossing is a typical continuous span bridge located in southern New Mexico. Using a modified procedure for flexure and shear design based on UHPC properties, bridge designs were developed considering the compressive strength, modulus of rupture, and modulus of elasticity of UHPC girder cross-section geometry, and prestressing strand diameter. Comparisons with the as-built bridge designs show that using UHPC with compressive strengths in the range between 15.0 ksi and 22.5 ksi (100 MPa and 150 MPa) leads to significant reductions in required girder lines while also reducing or eliminating mild steel shear reinforcement. Designs using both 0.6 in. (15 mm) and 0.7 in. (18 mm) strands were considered. Although 0.7 in. (18 mm) strands are not widely used, they could offer potential advantages in UHPC design; however, the larger strand size will have an initial implementation cost. Additionally, taking advantage of the tensile strength of UHPC, traditional mild steel stirrups can be significantly reduced or eliminated.

Compared to regular concrete, a cubic yard of commercially available UHPC (e.g., Ductal®) can cost as much as ten times more, making designers and precasters hesitant to adopt this material. An economic analysis on the bridge designs incorporating UHPC was conducted, assuming that local materials can be used to produce UHPC. Steel fibers are the most expensive constituent in UHPC, thus the possibility of reducing the percent of steel fibers from 2% to 1% was explored, where typical mild steel reinforcement was used along with the 1% volume of steel fibers. Results indicate that the initial high cost can be offset by careful selection of materials, reduced construction time and maintenance, and the increased service life of the structure. Costs were evaluated based on local material prices, design parameters of the bridge, modified production practices, and a projected maintenance schedule.

Based on the findings from Phase I of this research project, it was determined that more economical and readily available UHPC mixture proportions would be required for successful implementation of UHPC into bridge design in New Mexico. In Phase II of this research project, UHPC mixture proportions were developed and optimized along with the curing regimen required for use in local precast plants. The curing regimen was optimized for economy by using readily achievable temperatures for both the wet and dry curing periods. Finally a durability study was conducted and it was established that the UHPC developed using material local to New Mexico provides excellent resistance to freezing and thawing, alkali silica reaction, and delayed ettringite formation.

ACKNOWLEDGEMENTS

The authors would like to thank the project advocate, Bryce Simons, technical panel, Ray Trujillo, Ted Barber, Ben Najera, Jim Camp, Thiet Nguyen, and Robert Crossno and project managers, Keli Daniell, Virgil Valdez, and Michelle Langehennig (Research Bureau, NMDOT) for their guidance and support throughout the project. The research team at NMSU also acknowledges the assistance of several individuals: Ben Najera for CONSPAN® training and question answering; Dr. Benjamin Graybeal, FHWA Turner-Fairbank Research Center; Dr. Franz Josef Ulm, Massachusetts Institute of Technology; Dean Bierwagen, Iowa Department of Transportation; Brian Moore, Wapello County Engineer; Brain Keierleber, Buchannan County Engineer and Ned Johnson of Buchannan County; Dr. Sri Sritharan, Iowa State University, and Brian Silvis, Virginia Department of Transportation for their assistance gathering information and answering questions. Shannon Applegate and Steven Ruiz, Coreslab, Albuquerque; Phil Humphrey and Steve Darrah, BASF The Chemical Company; and Megan May, Fibercon International for assistance in determining cost of materials used in this study. The findings and conclusions in the paper are those of the authors and do not necessarily reflect the views of the organizations or the individuals acknowledged above.

THIS PAGE LEFT BLANK INTENTIONALLY

TABLE OF CONTENTS

Abstract ii
Acknowledgments iv
Figures x
Tables xiv
Notation xix

Phase I

Introduction 1
Literature Review 3
- Introduction and Background
- Composition of UHPC
  - Optimization of Granular Mixtures
  - Properties of UHPC
- Mechanical Properties
  - Compressive Strength
  - Flexural Strength
  - Modulus of Elasticity
  - Shrinkage-Swelling Behavior
  - Creep
- Durability Issues
  - Water Absorption
  - Chloride Penetration
  - Freeze-Thaw Durability
  - Alkali Silica Reaction
- Ductal®
- UHPC Structures
- Design
- Rapid Construction
- Ongoing Research

Case Studies 25
- Mars Hill Bridge, Wapello County, Iowa
  - Introduction
  - Bridge Description
  - Beam Description
  - Specifications
  - Project Timeline
  - Testing of Materials and Testing of Experimental Beams
  - Design and Analysis Methods Used in the Design of the UHPC Bridge Girders
  - Conclusion

Cat Point Creek Bridge, Richmond County, Virginia
Introduction
Bridge Description
UHPC Beam Description
Specifications
Analysis Methods
Conclusions
UHPC Parametric Study: Flexure....51
Parametric Flexure Study I-25/Doña Ana Interchange
CONSPAN® Flexure Analysis for I-25/Doña Ana Interchange
Effects of Modulus of Elasticity
Effects of Modulus of Rupture
Prestressing Strand Dimensions
Results of I-25/Doña Ana Interchange Utilizing 0.6 in. (15 mm) Diameter Strands
Results of I-25/Doña Ana Interchange Utilizing 0.7 in. (18 mm) Diameter Strands
Sunland Park Bridge – Two-Span Continuous and Three-Span Continuous Units
CONSPAN® Flexure Analysis for Sunland Park Two-Span Unit
Results of Sunland Park Bridge Two-Span Continuous Unit Utilizing 0.6 in. (15 mm) Diameter Strands
Results of Sunland Park Bridge Two-Span Continuous Unit Utilizing 0.7 in. (18 mm) Diameter Strands
CONSPAN® Flexure Analysis for Sunland Park Three-Span Unit
Results of Sunland Park Bridge Three-Span Continuous Unit Utilizing 0.7 in. (18 mm) Diameter Strands
UHPC Parametric Study: Shear....97
Design Shear Strength Procedure for Steel Fiber Reinforced UHPC
Shear Analysis of I-25/Doña Ana Interchange
Shear Analysis of Sunland Park Bridge
Parametric Study: Negative Moment Reinforcement in the Sunland Park Bridge....127
Results: Two-Span Unit
Results: Three-Span Unit
Summary of Parametric Study....133
Summary of I-25/Doña Ana Interchange Final Results
Summary of Sunland Park Bridge Two-Span Continuous Unit Results
Summary of Sunland Park Bridge Three-Span Continuous Unit Results
Hold Down Forces
Prestressing Steel Requirements
Confinement Steel....145
Economic Analysis....147
Introduction
Cost Comparison of UHPC Girders by Reducing Girder Size
Concrete Costs for I-25/Doña Ana Interchange
Concrete Costs for Sunland Park River Crossing Bridge

Prestressing Strand Comparison
I-25/Doña Ana Interchange Strand Comparison
Sunland Park River Crossing Strand Comparison
Steel Fiber Constituent Costs
Mild Steel Costs
I-25/Doña Ana Interchange Mild Steel Costs
Sunland Park Two-Span Unit Mild Steel Costs
Sunland Park Three-Span Unit Mild Steel Costs
Normal Strength Concrete Deck
I-24/Dona Ana Interchange Deck Cost
Sunland Park Two-Span Unit Deck Cost
Sunland Park Three-Span Unit Deck Cost
Total Present Cost Comparison
Total Cost for I-25/Doña Ana Interchange
Total Cost for Sunland Park Bridge Two-Span Unit
Total Cost for Sunland Park Bridge Three-Span Unit
Future Worth
I-25/Doña Ana Interchange Future Worth
Sunland Park Two-Span Unit Future Worth
Sunland Park Three-Span Unit Future Worth
Summary of Economic Analysis
Conclusions and Recommendations 173
Properties and Characteristics of UHPC
Conclusions from the Parametric Bridge Study
Conclusions of Economic Analysis

Phase II

Introduction – Phase II 179
Background… 181
Materials
Specimen Prepartation
Curing Regimen
Compressive Strength Results
Optimization of Mixture Proportions… 185
Fly Ash Optimization
Aggregate Top Size
Sand Optimization
Admixture Optimization
Compressive Strength Gain
Optimization of Curing Regimen… 195
Durability Testing… 197
Resistance to Freezing and Thawing
Results
Resistance to Alkali-Silica Reaction

Resistance to Delayed Ettringite Formation
Previous Research on DEF
Analysis for UHPC in New Mexico
Conclusions and Recommendations… 209
Mixture Proportions
Curing Regimen
Durability
Future Work
References.....213

FIGURES

FIGURE 2.1 Plot of Modulus of Elasticity Equations 2.6 and 2.7. 12
FIGURE 2.2 Example of PI Girder (Keierleber *et al.* 2007). 21
FIGURE 2.3 PI-Girder Bridge in Buchanan County Iowa. 21
FIGURE 3.1 Mars Hill Bridge: The First UHPC Bridge Constructed in the United States.. 26
FIGURE 3.2 Mars Hill Bridge Cross-Section. 26
FIGURE 3.3 Underside of Mars Hill Bridge. 27
FIGURE 3.4 Girder and Deck Overhang, Mars Hill Bridge. 27
FIGURE 3.5 IDOT BTCIIO 45 in. (1.14 m) Girder: (a) Typical (b) Modified. 29
FIGURE 3.6 Modified BTCIIO Girder Superimposed on a Typical BTCIIO. 29
FIGURE 3.7 Strands and Lifting Devices for BTCIIO. 31
FIGURE 3.8 Strand Layout and Mild Steel Reinforcement of the Modified BTCIIO Girder. 31
FIGURE 3.9 Test Prism from Flexural Testing of Mars Hill Bridge. 35
FIGURE 3.10 Close View of Crack Bridging Fibers in Test Prism. 35
FIGURE 3.11 Sample of 0.5 in. (12 mm) Steel Fibers Used in UHPC Mix for Mars Hill Bridge. 36
FIGURE 3.12 Second Bridge Built with UHPC in Richmond County, Virginia. 45
FIGURE 3.13 Cross-Section of Cat Point Creek Bridge. 46
FIGURE 3.14 Dimensions of the VDOT PCBT-45 (1.14 m). 47
FIGURE 3.15 VDOT PCBT Strand Layout and Mild Steel Reinforcement: (a) HPC (b) UHPC. 48
FIGURE 4.1 North Bound Structure of I-25/Doña Ana Interchange. 52
FIGURE 4.2 Cross-Section of I-25/Doña Ana Interchange, as Modeled in CONSPAN®... 52
FIGURE 4.3 Comparison of the Required Number of 0.6 in. (15 mm) Prestressing Strands based on Different Allowable Service Tensile Stress Limits for I-25/Doña Ana Interchange. 59
FIGURE 4.4 Comparison of the Required Number of 0.7 in. (18 mm) Prestressing Strands based on Different Tensile Stress Limits. 64
FIGURE 4.5 Two Span Unit of Sunland Park River Crossing. 66
FIGURE 4.6 Three-Span Unit of Sunland Park River Crossing. 66
FIGURE 4.7 Cross-Sectional Geometry of Sunland Park River Crossing Two-Span and Three-Span Units. 67

FIGURE 4.8 Comparison of the Required Number of 0.6 in. (15 mm) Prestressing Strands Based on Different Tensile Stress Limits for Sunland Park Bridge Two-Span Unit. 71

FIGURE 4.9 Comparison of the Required Number of 0.7 in. (18 mm) Prestressing Strands Based on Different Service Tensile Stress Limits for Sunland Park Bridge Two-Span Unit. 76

FIGURE 4.10 Comparison of the Required Number of 0.7 in. (18 mm) Prestressing Based on Different Service Tensile Stress Limits for Sunland Park Bridge Span 3 and 5. 81

FIGURE 4.11 Comparison of the Required Number of 0.6 in. (18 mm) Prestressing Strands for Span 4 Based on Different Service Tensile Stress Limits for Sunland Park Bridge Span 4. 85

FIGURE 4.12 Comparison of the Required Number of 0.7 in. (18 mm) Prestressing Strands Based on Different Service Tensile Stress. Limits for Sunland Park Bridge Spans 3 and 5. 90

FIGURE 4.13 Comparison of the Required Number of 0.7 in. (18 mm) Prestressing Strands Based on Different Service Tensile Stress Limits for Sunland Park Bridge Span. 95

FIGURE 5.1 Shear Envelopes for I-25/Doña Ana Interchange with Four BT-63 Girders Using 0.6 in. (15 mm) Strands. 101

FIGURE 5.2 Shear Envelopes for I-25/Doña Ana Interchange with Four Modified BT-54 Girders Using 0.7 in. (18 mm) Strands. 104

FIGURE 5.3 Shear Envelopes for I-25/Doña Ana Interchange with Four Modified BT-54 Girders Using 0.7 in. (18 mm) Strands and Traditional Mild Steel Stirrups. 106

FIGURE 5.4 Shear Envelopes for Sunland Park Bridge Two-Span Unit with Eight Modified BT-54 Girders Using 0.6 in. (15 mm) Strands. 109

FIGURE 5.5 Shear Envelopes for Sunland Park Bridge Two-Span Unit with Eight Modified BT-54 Girders Using 0.6 in. (18 mm) Strands and No. 5 (M16) Mild Steel Stirrups. 111

FIGURE 5.6 Shear Envelope for Sunland Park Bridge Two-Span Unit with Six BT-63 Girders Using 0.7 in. (18 mm) Strands. 113

FIGURE 5.7 Shear Envelope for Sunland Park Bridge Two-Span Unit for Six BT-63 Girders Using 0.7 in. (18 mm) Strands and No. 5 (M16) Stirrups. 115

FIGURE 5.8 Shear Envelopes for Sunland Park Bridge Three-Span Continuous Unit Using 0.6 in. (15 mm) Strands. 119

FIGURE 5.9 Shear Envelopes for Sunland Park Bridge Three-Span Unit for Eight BT-54 Girders Using 0.6 in. (15 mm) Strands and No. 3 (M8 Stirrups). 122

FIGURE 5.10 Shear Envelopes for Sunland Park Bridge Three-Span Unit for Six BT-63 Girder Using 0.7 in. (18 mm) Strands. 126

FIGURE 6.1 Negative Moment Reinforcement for Ten Modified BT-54 Girders. 129
FIGURE 6.2 Negative Moment Reinforcement for Eight Modified BT-54 Girders..... 130
FIGURE 6.3 Negative Moment Reinforcement for Six BT-63 Girders. 130
FIGURE 7.1 End View Cross-Section of Baseline Design (BT-63 Girders) with 28 - 0.6 in. (15 mm) Strands Employing HPC. 133
FIGURE 7.2 End View Cross-Section of Four BT-63 Girders with 42 - 0.6 in. (15 mm) Strands Employing UHPC. 134
FIGURE 7.3 End View Cross-Section of Four BT-54 Girders with 48 - 0.7 in. (18 mm) Strands Employing UHPC. 135
FIGURE 7.4 End View Cross-Section of Four BT-54 Girders with 48 - 0.7 in. (18 mm) Strands Employing UHPC. 135
FIGURE 7.5 End View Cross-Section of Ten BT-54 Girder with 40-15 mm (0.6 in.) Strands Employing HPC. 136
FIGURE 7.6 End View Cross-Section of Eight BT-54 Girders with 42-0.6 in. (15 mm) Strands Employing UHPC. 137
FIGURE 7.7 End View Cross-Section of Eight BT-54 Girders with 42-0.6 in. (15 mm) Strands Employing UHPC. 138
FIGURE 7.8 End View Cross-Section of Six BT-63 Girders with 38-0.6 in. (15 mm) Strands Employing UHPC. 139
FIGURE 7.9 End View Cross-Section of Ten BT-54 Girders with 32- 0.6 in. (15 mm) Strands Employing HPC. 140
FIGURE 7.10 End View Cross-Section of BT-54 Girder with 8 in. (203 mm) and 42 - 0.6 in. (15 mm) Strands Employing UHPC. 141
FIGURE 7.11 End View Cross-Section of BT-54 Girder with 7 in. (180 mm) 34 - 0.6 in. (15 mm) Strands Employing UHPC. 142
FIGURE 7.12 End View Cross-Section of BT-63 Girder with 34 - 0.7 in. (18 mm) Strands Employing UHPC. 143
FIGURE 9.1 NMDOT Mild Steel Reinforcement Requirements for a BT-63 Girder. 156
FIGURE 9.2 Cash Flow Diagram for Six HPC BT-63 Girders..... 168
FIGURE 9.3 Cash Flow Diagram for Four UHPC BT-63 Girders. 168
FIGURE 9.4 Cash Flow Diagram for Four UHPC BT-54 Girders. 168
FIGURE 9.5 Cash Flow Diagram for Ten HPC BT-54 Girders..... 169
FIGURE 9.6 Cash Flow Diagram for Eight UHPC BT-54 Girders. 169
FIGURE 9.7 Cash Flow Diagram for Six UHPC BT-63 Girders..... 169
FIGURE 9.8 Cash Flow Diagram for Ten HPC BT-54 Girders..... 170

FIGURE 9.9 Cash Flow Diagram for Eight UHPC BT-54 Girders. 170
FIGURE 9.10 Cash Flow Diagram for Six UHPC BT-63 Girders..... 170
FIGURE 13.1 Photograph of formation of slurry..... 185
FIGURE 13.2 Photograph of steel fibers being added to slurry..... 186
FIGURE 13.3 Photograph of test specimens. 187
FIGURE 13.4 Photograph of Tinius Olsen universal testing machine and specimen prior to loading. 188
FIGURE 15.1 Average relative dynamic modulus for mixtures 4-5..... 200
FIGURE 15.2 Average relative dynamic modulus for mixtures 7-9..... 201
FIGURE 15.3 Expansion versus time for UHPC mixtures without fibers. 204
FIGURE 15.4 Expansion versus time for UHPC mixtures with fibers. 204

TABLES

TABLE 2.1 Properties of UHPC Enhancing its Homogeneity and Strength (Dili and Santhanam 2004). 5
TABLE 2.2 Mixture Proportions (by fraction of cement) of UHPC from Literature. 7
TABLE 2.3 Durability of Ductal® (Lafarge 2009a). 18
TABLE 2.4 Physical Properties of Ductal® CS1000 (2009b). 18
TABLE 2.5 Typical Composition of Ductal® (Graybeal 2006b). 19
TABLE 2.6 Estimated Cost of NU UHPC Mixtures (Kleymann *et al.* 2006). 24
TABLE 3.1 Mars Hill Bridge Geometry. 28
TABLE 3.2 Comparison of the BTCIIO and Modified BTCIIO Girders. 29
TABLE 3.3 Materials Identity Card of Ductal® (Bierwagen and McDonald 2005). 33
TABLE 3.4 Results from UHPC Cubes (Degen 2005). 34
TABLE 3.5 Results from Prism Flexural Testing (Degen 2005). 34
TABLE 3.6 Moment of Test and Bridge Beams (Degen 2005). 37
TABLE 3.7 Shear Capacities of the Test Beam and the Bridge Beam (Degen 2005). 38
TABLE 3.8 Summary of Small Scale Test Beams. 39
TABLE 3.9 Design Parameters Used in the Design of the Mars Hill Bridge (Degen 2005). 39
TABLE 3.10 Cat Point Creek Bridge Geometry. 46
TABLE 4.1 Design Matrix for I-25/Doña Ana Interchange. 53
TABLE 4.2 Comparison of Prestressing Strand Properties. 55
TABLE 4.3 I-25/Doña Ana Interchange Using 0.6 in. (15 mm) Strands According to LFD Code. 57
TABLE 4.4 I-25/Doña Ana Interchange Using 0.6 in. (15 mm) Strands According to a Tensile Stress Limit of 1.16 ksi (8 MPa). 58
TABLE 4.5 Comparison of Tensile Stress Limits Results for I-25/Doña Ana Interchange Using 0.6 in. (15 mm) Strands To the Baseline Design. 60
TABLE 4.6 Results for I-25/Doña Ana Interchange Using 0.7 in. (18 mm) Strands According to LFD Code. 62
TABLE 4.7 Results for I-25/Doña Ana Interchange Using 0.7 in. (18 mm) Strands According to Tensile Stress Limit of 1.16 ksi (8.0 MPa). 63
TABLE 4.8 Comparison of Materials with Different Allowable Tensile Stress Limits for I-25/Doña Ana Interchange Using 0.7 in. (18 mm) Strands. 65

TABLE 4.9 Design Matrix for Sunland Park Bridge. 67

TABLE 4.10 Sunland Park Bridge Two-Span Unit Using 0.6 in. (15 mm) Strands According to LFD Code. 69

TABLE 4.11 Sunland Park Bridge Two-Span Unit Using 0.6 in. (15 mm) Strands According to a Limit Tensile Strength of 1.16 ksi (8 MPa). 70

TABLE 4.12 Comparison of Allowable Tensile Stress Limits for Sunland Park Bridge Two-Span Unit Using 0.6 in. (15 mm) Stands. 72

TABLE 4.13 Sunland Park Bridge Two-Span Unit Using 0.7 in. (18 mm) Strands According to LFD code. 74

TABLE 4.14 Sunland Park Bridge Two-Span Unit Using 0.7 in. (18 mm) Strands According to Tensile Limit of 1.16 ksi (8.0 MPa). 75

TABLE 4.15 Comparison of Allowable Tensile Stress Limits for Sunland Park Bridge Two-Span Unit Using 0.7 in. (18 mm) Strands. 77

TABLE 4.16 Sunland Park Bridge Spans 3 & 5 Using 0.6 in. (15 mm) Strands According to LFD Code. 79

TABLE 4.17 Sunland Park Bridge Span 3 & 5 Using 0.6 in. (15 mm) Strands According Tensile Limit Strength of 1.16 ksi (8 MPa). 80

TABLE 4.18 Comparison of Allowable Tensile Stress Limits for Sunland Park Bridge Spans 3 & 5 Using 0.6 in. (15 mm) Strands. 82

TABLE 4.19 Sunland Park Bridge Span 4 Using 0.6 in. (15 mm) Strands According to LFD Code. 83

TABLE 4.20 Sunland Park Bridge Span 4 Using 0.6 in. (15 mm) Strands According to Tensile Stress Limit of 1.16 ksi (8 MPa). 84

TABLE 4.21 Comparison of Allowable Tensile Stress Limits for Sunland Park Bridge Span 4 Using 0.6 in. (15 mm) Strands. 86

TABLE 4.22 Sunland Park Bridge Spans 3 and 5 Using 0.7 in. (18 mm) Strands According to LFD Code. 88

TABLE 4.23 Sunland Park Bridge Spans 3 and 5 Using 0.7 in Strands According to Allowable Tensile Stress of 1.16 ksi (8 MPa). 89

TABLE 4.24 Comparison of Allowable Tensile Stress Limits for Sunland Park Bridge Spans 3 & 5 Using 0.7 in. (18 mm) Strands. 91

TABLE 4.25 Sunland Park Bridge Span 4 Using 0.7 in. (18 mm) Strands According to LFD Code. 93

TABLE 4.26 Sunland Park Bridge Span 4 Using 0.7 in Strands According to Allowable Tensile Stress of 1.16 ksi (8 MPa). 94

TABLE 4.27 Comparison of Allowable Tensile Stress Limits for Sunland Park Bridge Span 4 Using 0.7 in. (18 mm) Strands. 96

TABLE 5.1 Shear Results for I-25/Doña Ana Interchange with Four BT-63 Girders Using 0.6 in. (15 mm) Prestressing Strands. 100

TABLE 5.2 Shear Results for I-25/Doña Ana Interchange Using 0.7 in. (18 mm) Prestressing Strands. 103

TABLE 5.3 Shear Results for I-25/Doña Ana Interchange Using 0.7 in. (18 mm) Prestressing Strands with No. 5 (M16) Mild Steel Stirrups. 105

TABLE 5.4 Shear Results for Sunland Park Bridge Two-Span Unit with Eight BT-54 Girders Using 0.6 in. (15 mm) Prestressing Strands. 108

TABLE 5.5 Shear Results for Sunland Park Bridge Two-Span Unit with Eight BT-54 Girders Using 0.6 in. (15 mm) Prestressing Strands with Stirrups. 110

TABLE 5.6 Shear Results for Sunland Park Bridge Two-Span Unit with Six BT-63 Girders Using 0.7 in. (18 mm) Prestressing Strands. 112

TABLE 5.7 Shear Results for Sunland Park Bridge Two-span Continuous Unit Using 0.7 in. (18 mm) Prestressing Strands and No. 5 (M16) Mild Steel Stirrups. 114

TABLE 5.8 Shear Results for Sunland Park Bridge Three-Span Unit with Eight Modified BT-54 Girders Using 0.6 in. (15 mm) Prestressing Strands Exterior Spans. 117

TABLE 5.9 Shear Results for Sunland Park Bridge Three-Span Unit With Eight BT-54 Girders Using 0.6 in. (18 mm) Prestressing Strands Interior Span. 118

TABLE 5.10 Shear Results for Sunland Park Bridge Three-Span Unit with BT-54 Girders Using 0.6in. (15 mm) Prestressing Strands Exterior Spans with Stirrups. ... 120

TABLE 5.11 Shear Results for Sunland Park Bridge Three-Span Unit with Eight BT-54 Girders Using 0.6in. (15 mm) Prestressing Strands Exterior Spans with Stirrups. 121

TABLE 5.12 Shear Results for Sunland Park Bridge Three-span Unit Using 0.7 in. (18 mm) Prestressing Strands Exterior Spans. 124

TABLE 5.13 Shear Results Sunland Park Bridge Three-Span Unit Using 0.7 in. (18 mm) Prestressing Strands Interior Span. 125

TABLE 6.1 Required Amount of Mild Steel Reinforcement in the Deck in the Maximum Negative Moment Region. 132

TABLE 9.1 I-25/Doña Ana Interchange Concrete Volumes and Costs. 148

TABLE 9.2 Sunland Park Two-Span Unit Concrete Volumes and Costs. 149

TABLE 9.3 Sunland Park Three-Span Unit Concrete Volumes and Costs. 150

TABLE 9.4 Dona Ana Strand Costs. 151

TABLE 9.5 Sunland Park Two-Span Unit Strand Costs. 152

TABLE 9.6 Sunland Park Three-Span Unit Strand Costs. 153

TABLE 9.7 Material Costs for a BT-63 Girder with Minimal Mild Steel Reinforcement and Steel Fibers at 2% Volume. 154
TABLE 9.8 Material Costs for a BT-63 Girder with Typical Mild Steel Reinforcement and Steel Fibers at 1% Volume. 154
TABLE 9.9 Material Costs for a BT-63 Girder with Typical Mild Steel Reinforcement Without Steel Fibers. 155
TABLE 9.10 Reinforcing Bar Requirements for As-Designed BT-63 Girders for the I-25/Doña Ana Bridge. 157
TABLE 9.11 Reinforcing Bar Requirements for Four BT-63 Girders for the I-25/Doña Ana Bridge..... 157
TABLE 9.12 Reinforcing Bar Requirements for Four BT-54 Girders for the I-25/Doña Ana Bridge..... 158
TABLE 9.13 Reinforcing Bar Requirements for As-Designed BT-54 Girders for Sunland Park Two-Span Unit. 159
TABLE 9.14 Reinforcing Bar Requirements for Eight BT-54 Girders for Sunland Park Two-Span Unit. 159
TABLE 9.15 Reinforcing Bar Requirements for Six BT-63 Girders for Sunland Park Two-Span Unit. 160
TABLE 9.16 Reinforcing Bar Requirements for As-Designed BT-54 Girders for Sunland Park Three-Span Unit. 161
TABLE 9.17 Reinforcing Bar Requirements for Eight BT-54 Girders for Sunland Park Three-Span Unit..... 161
TABLE 9.18 Reinforcing Bar Requirements for Six BT-63 Girders for Sunland Park Three-Span Unit. 162
TABLE 9.19 I-25/Doña Ana Interchange Deck Costs. 162
TABLE 9.20 Sunland Park Two-Span Unit Deck Costs. 163
TABLE 9.21 Sunland Park Three-Span Unit Deck Costs. 163
TABLE 9.22 I-25/Doña Ana Interchange Comparison Final Costs. 164
TABLE 9.23 Sunland Park Two-Span Unit Comparison Final Costs..... 165
TABLE 9.24 Sunland Park Three-Span Unit Comparison Final Costs..... 166
TABLE 9.25 I-25/Doña Ana Interchange Future Worth Results. 167
TABLE 9.26 Sunland Park Two-Span Unit Future Worth Results. 169
TABLE 9.27 Sunland Park Three-Span Unit Future Worth Results. 170
TABLE 12.1 Mixture proportions (by fraction of cement) of UHPC from literature. 181
TABLE 12.2 Grain size distribution of fine sand. 182

TABLE 12.3 Mixture proportions of UHPC. 183
TABLE 12.4 Compressive strength of UHPC mixtures. 184
TABLE 13.1 Compressive strength of UHPC mixtures. 188
TABLE 13.2 Compressive strength of UHPC mixtures with fly ash replacement (w/cm = 0.14). 189
TABLE 13.3 Effect of maximum size of aggregate on compressive strength. 190
TABLE 13.4 Effect of amount of sand on compressive strength. 190
TABLE 13.5 Effect of Rheomac on mixture proportions. 191
TABLE 13.6 Effect of Navitas 33 on mixture proportions. 192
TABLE 14.1 Compressive testing results for different curing regimens. 195
TABLE 15.1 Durability factors for UHPC mixtures with low sand (Series 1). 199
TABLE 15.2 Durability factors for UHPC mixtures with high sand (Series 1). 200
TABLE 15.3 Durability factors for UHPC mixtures with No. 4 maximum size aggregate (Series 3). 201
TABLE 15.4 UHPC batches tested 203
TABLE 15.5 Chemical and physical characteristics of cement, Silica fume and fly ash. 206
TABLE 16.1 Recommended Mixture Proportions. 209

Notation

a_{ij} - The parameter describing the loosening effects

A_w - Effective fiber area, in.^{2} (mm^2)

A_w^{eff} - Effective shear area, in.^{2} (m^2)

b_{ij} - Parameter describing the wall effects

C - Constant that accounts for Poisson's ratio and the geometry of the specimen

DC - dead load of structural components and non structural attachments, kip (kN)

DF - Durability factor of the test specimen

DW – Dead load of future wearing surface, psf (kN/m^2)

e - Voids index

E - Modulus of elasticity

E_D - Dynamic modulus of elasticity

E_n - Dynamic elastic modulus after n cycles

E_{rel} - Relative dynamic modulus after N cycles (%)

E_0 - Dynamic elastic modulus at zero cycles

f'_{ATT} - Compressive stress of UHPC after treatment

f'_c - Compressive strength of concrete, ksi (MPa)

h - Height of non-composite UHPC section, in. (mm)

IM - Design Lane Load, kip/ft (kN/m)

K_o - Initial Stiffness, ksi (MPa)

K_1 - Postcracking Stiffness, ksi (MPa)

L_f - Fiber Length, in. (mm)

LL - Loading of the design truck of the design tandem, kip (kN)

m - mass

M - Specified number of cycles at which the exposure is to be terminated

M_{SLS} - Design moment at the service limit state, kip-ft (kN-m)

M_{ULS} - Design moment at the service limit state, kip-ft (kN-m)

M_R^{SLS}- Moment capacity of the section at the service limit state, kip-ft (kN-m)

M_R^{ULS}- Moment capacity of the section at the ultimate limit state, kip-ft (kN-m)

n - Modular ratio

N - Number of cycles at which E_{rel} reaches the specified minimum value for discontinuing the test of the specified numbers of cycles at which the exposure is to be terminated (whichever is less)

RDM – relative dynamic modulus

V_c - Contribution of the UHPC to the sections shear strength, kip (kN)

V_f - Contribution of the crack-bridging 0.5 in. (13 mm) steel fibers, kip (kN)

V_p - Contribution of the inclined prestressing tendons to the sections shear strength, kip (kN)

V_R^{SLS} - Design strength of the section in shear at the service limit state, kip (kN)

V_R^{ULS} - Design strength of the section at the ultimate limit state, kip (kN)

V_v - Volume of Voids

V_s - Volume of the Solids

β_i - Virtual packing density (maximum packing density achievable with a given mixture of i class)

β_u - Angle of inclination of the compression strut with a lower bound of 30°

δ - Dynamic allowance for live load

ϕ - Strength reduction factor

Φ_c - Strength reduction factor for concrete

Φ_M - Strength reduction factor for Ductal® in flexure

Φ_V - Strength reduction factor for Ductal® in shear

γ_i - the virtual packing density of the mixture when class i is dominant

η - Load reduction factor

σ - Longitudinal stress near the support from the prestressing strands

σ_p - Residual UHPC tensile strength of UHPC, ksi (MPa)

Σ_1^- - Cracking Strength, ksi (MPa)

Σ_1^+ - Postcracking Strength

Σ_2 - Ductile Strength, ksi (MPa)

τ - Shear stress in the section, ksi (MPa)

τ_{lim} - Admissible shear stress in section, ksi (MPa)

ω_r - measured fundamental frequency

$[\omega]$ - crack dimension, in. (mm)

$[\omega]^{limit}$ - Crack width limit, in. (mm)

$[[\omega]]^{limit}_{reinforced}$ - Crack width limit in reinforced members, in. (mm)

$[[\omega]]^{limit}_{unreinforced}$ - Crack width limit in unreinforced members, in. (mm)

LAYOUT OF REPORT

This report covers two phases of research conducted for the New Mexico Department of Transportation, Transportation Research Bureau investigating the use of Ultra High Performance Concrete in prestressed concrete bridge design. This report is broken into two parts: (1) an investigation on the feasibility and limitations of Ultra High Performance Concrete for Prestressed Concrete Bridge Applications in New Mexico (Phase I); and (2) the development of mixture proportions for an Ultra High Performance Concrete using materials local to New Mexico (Phase II).

THIS PAGE LEFT BLANK INTENTIONALLY

PHASE I:

FEASIBILITY ANALYSIS OF ULTRA HIGH PEFORMANCE CONCRETE FOR PRESTRESSED CONCRETE BRIDGE APPLICATIONS

THIS PAGE LEFT BLANK INTENTIONALLY

1 INTRODUCTION – PHASE I

Ultra High Performance Concrete (UHPC) is an emerging material technology in which concrete develops very high compressive strengths and also exhibits improved tensile strength and toughness (Graybeal 2006). UHPC can achieve compressive strengths up to 29,000 pound force per square inch (psi) [200 Mega-Pascals (MPa)] and tensile strengths up to 7,000 psi (50 MPa). Several characteristics of UHPC offer advantages for structural applications, specifically prestressed concrete bridge design, including the following:

1. Increased strength and ductile behavior allowing the concrete to deform and support flexural and tensile forces, even after initial cracking.
2. The durability characteristics of the material are similar to those of an impermeable material reducing the effects of corrosion.
3. UHPC demonstrates a higher resistance to abrasion than that of normal strength concrete.
4. UHPC exhibits almost no shrinkage or creep, which makes the material very suitable for applications in prestressed concrete.
5. The material has the ability to replicate both the macro- and micro-texture of the formwork, resulting in high-quality textured or smooth surfaces.

Historically, conventional structural design has used concrete to support large compressive loads with supplemental reinforcement to resist tensile forces. With advances in technology such as UHPC the need for supplemental mild steel reinforcement may be reduced or eliminated. Advantages of using UHPC include: reduced material quantities; smaller geometry and weight of members; improved aesthetics; simpler detailing and construction; reduced maintenance; and increased lifespan. Recent events have shown the importance of durable long-lasting infrastructure. The use of UHPC is consistent with achieving goals of higher standards for U.S. infrastructure and meeting the increasing demands for reduced labor, materials, construction time, and environmental impact, while increasing safety, security, durability, and service life. With approximately 50% of bridges in New Mexico using prestressed concrete, incorporating UHPC in design has the potential to have a significant impact on the cost and performance of bridges in New Mexico.

THIS PAGE LEFT BLANK INTENTIONALLY

2 LITERATURE REVIEW

2.1 INTRODUCTION AND BACKGROUND

The introduction of high strength concrete began with the development of reactive powder concrete (RPC) by Bache (1981) in the early 1980's. Richard and Cheyrezy (1995) implemented several new principles to produce ultra high performance concrete (UHPC). UHPC is a new type of ultra high strength and high ductility concrete first developed in the 1990's by Richard and Cheyrezy at Bouygues′ laboratory in France (2000). UHPC is composed of particles of similar sizes and stiffness which reduces the differential tensile strain and increases the ultimate load-carrying capacity of the material. The particles consist of cement, sand, silica fume, silica flour, superplastizer, water, and optional high-strength steel fibers or non-metallic fibers (2006).

UHPC can simultaneously have compressive strengths exceeding 29.0 kilo-pound per square inch (ksi) (200 MPa), tensile strengths of 2.9 to 7.3 ksi (20 to 50 MPa), and durability properties that significantly exceed those of current high-performance concretes (Gao *et al.* 2005). At such high strengths, the coarse aggregate is the weakest link in concrete (Dili and Santhanam 2004). Development of shear and tensile stresses at the paste-aggregate interface when compressive force is applied causes cracks in the paste of traditional concrete. According to Richard and Cheyrezy (1995), the size of the equatorial crack is directly proportional to the diameter of the aggregate particle. Consequently, elimination of coarse aggregate greatly improves the mechanical strength of UHPC. Advantages to having high strength are that UHPC structures can be built with less structural weight, greater structural spans, and have better seismic resistance compared to conventional concrete structures.

Richard and Cheyrezy (1995) recommended the following principles to develop UHPC:

- Removal of coarse aggregate to enhance the homogeneity of concrete.
- Use of silica fume for pozzolanic reaction.
- Optimization of the granular mixture for enhancement of compacted density.
- Application of pre-setting pressure for better compaction.
- Post-setting heat treatment to enhance the mechanical properties of the microstructure.
- Addition of steel fibers to achieve ductility.

This material differs from conventional concrete not only from the strength aspect, but also in terms of durability. UHPC is more durable because the low water-to-cementitious materials ratio results in very low porosity (Roux *et al.* 1996). The possibility of achieving high strength, durability, and improved ductility with the use of ultra high strength concrete encourages researchers and engineers to use this modern material in many practical applications like nuclear waste containment structures, high rise structures, long span bridges, and walkways.

Benefits of using UHPC for an I-girder included rapid completion of formwork and little need for supplemental vibration because UHPC has been observed to be nearly self-placing (Rebebtrost and Cavill 2006). The ability of UHPC to be reinforced internally by fiber reinforcement allows for the reduction or elimination of most mild steel reinforcement, which greatly simplifies the I-girder formwork preparation. Without taking any special precautions to release the formwork during setting, no shrinkage cracks were observed in the girders during testing (Graybeal 2006a).

The only readily available UHPC in the United States is marketed by Lafarge Inc. under the name Ductal®. This product is shipped to precasters in three components; the dry materials are pre-blended in bulk bags, while the steel fibers and chemical admixtures are packaged separately. The cost of this product varies significantly based on the amount being used, but is approximately \$750/yd^3 (\$980/m^3) for the materials (Kleymann *et al.* 2006).

2.2 COMPOSITION OF UHPC

2.2.1 Optimization of Granular Mixtures

Optimization of granular mixtures can be achieved by calculating the packing density (ratio of volume of solids to the total unit volume) using packing models such as the solid suspension model (SSM) for granular mixtures proposed by Ferraris and Larrard 1998. The following equations are cited by Ferraris and Larrard:

$$\gamma = \min(\gamma_i) \text{ for } i = 1 \ldots n \qquad \text{Equation 2.1}$$

$$\gamma_i = \frac{\beta_i}{1 - \sum_{j=1}^{i-1}\left[1 - \beta_i + b_{ji}\left(1 - \frac{1}{\beta_j}\right)\right]\gamma_j - \sum_{j=i+1}^{n}\left[1 - \frac{a_{ij}\beta_i}{\beta_j}\right]\gamma_j} \qquad \text{Equation 2.2}$$

where, β_i is the virtual packing density (maximum packing density achievable with a given mixture of i class, granular size class defined by sieve size); γ_i is the virtual packing density of the mixture when class i is dominant; and a_{ij} and b_{ji} are the parameters describing the loosening and wall effects. The disturbance in the coarse grain arrangement when an isolated fine grain is introduced in an interstice of a coarse grain packing is the loosening effect. The wall effect is defined as the disturbance in the packing of a small grain in the vicinity of an isolated coarse grain (Elkim 2009).

Software programs such as the language independent size distribution analyzer (LISA) can also be used for modeling the granular mixtures (Shaheen and Shrive 2006). LISA is a program that evaluates particle packing and composite particle size distribution. Roux *et al.* (1996) reported that optimization of the granular mixture reduces the porosity of UHPC and the size of the micropores can be decreased by post-setting heat treatment. The authors also indicated that the application of pre-setting pressure removes air bubbles and expels excess water from the paste.

Shaheen and Shrive (2006) have reported that the air voids and water pockets disappear after applying a pre-setting pressure between 0.0 and 3.77 ksi (0.0 and 26.0 MPa). The authors observed that the application of higher pressure results in lower values of compressive strength. This could be due to microcracking upon release of the pre-setting pressure. A mixture that was proportioned using the linear packing density model for granular mixtures and cured at 194°F (90°C) for four days resulted in a compressive strength of 34.22 ksi (236.0 MPa) (Ferraris and Larrard 1998).

2.2.2 Properties of UHPC

Dili and Santhanam (2004) described the salient properties of UHPC and suggested how to achieve them. Table 2.1 presents the properties of their UHPC and describes the different constituents in UHPC and the parameters of their selection described by the authors.

TABLE 2.1 Properties of UHPC Enhancing its Homogeneity and Strength (Dili and Santhanam 2004).

Property of UHPC	Description	Recommended Values
Reduction in aggregate size	Coarse aggregates are replaced by fine sand, with a reduction in the size of coarsest aggregate by a factor of about 50	Maximum size of fine sand is 0.0236 in. (600 μm)
Enhanced mechanical properties	Improved mechanical properties of the paste by the addition of silica fume	Young's modulus values range between 7,250 to 10,900 ksi (50,000 to 75,000 MPa)
Reduction in aggregate-to-matrix ratio	Limitation of sand content	Volume of the paste is at least 20% greater than the voids index of non-compacted sand

Dili and Santhanam (2004) suggested that the coarse aggregate should be replaced by fine sand and the coarsest aggregate size should be reduced by a factor of 50 (Table 2.1). The recommended maximum size of the aggregate was reported as 0.0236 inches (in.) (600 μm). This reduced size of the aggregate particles may be used to improve the homogeneity of the mixture. However, particles sizes below 0.0059 in. (150 μm) should be avoided to prevent interference with the largest cement particles [0.00315 to 0.00394 in. (80 to 100 μm)] (Richard and Cheyrezy 1995).

Dili and Santhanam (2004) reported that the mechanical, chemical, and thermo-mechanical types of failures can be eliminated by using reduced particle sizes. This may be attributed to the increased homogeneity of the UHPC mixtures due to the elimination of coarse aggregate. Similarly, failure due to the disturbance of the mechanical stress field can be avoided by improving the mechanical properties such as modulus of elasticity by incorporating silica fume. It was also reported that the aggregate-to-matrix ratio should be reduced (by limiting the sand content). The reason for the reduction in sand content was explained by Richard and Cheyrezy (1995); aggregates form a rigid skeleton of contiguous granular elements that restrains a major portion of paste shrinkage resulting in increased porosity. The volume of the paste should be at least 20% greater than the voids index, e, (voids ratio) of the non-compacted sand (Dili and Santhanam 2004, Richard and Cheyrezy 1995). The voids index is expressed as:

$$e = V_v / V_s \qquad \text{Equation 2.3}$$

where, V_v is the volume of voids and V_s is the volume of solids.

Quartz powder is used for maximum reactivity during post-setting heat treatment. The reactivity of quartz powder is mainly due to the smaller particle size [196.9 - 984.3 μin. (5.0 - 25 μm)]. Steel fibers between 0.15 and 1 in. [13 and 25 millimeters (mm)] long with diameters from 0.006 to 0.0078 in. (0.15 to 0.2 mm) should be used to improve ductility. Use of a superplasticizer that does not cause initial set retardation is recommended for significant reduction in the water-to-cementitious materials ratio. Silica fume should be used to fill the voids between cement particles, to enhance paste rheology, and to produce secondary hydrates.

Relative density of the concrete (ratio of density of the concrete to the compacted density of the mixture) indicates the amount of packing of the concrete. It was reported that the optimum water content is analyzed using relative density (Dili and Santhanam 2004). To get the maximum density, water content should be kept optimum since the packing density of concrete was calculated without considering the fractions of water and air. Dili and Santhanam (2004) reported that the mixture proportions should be such that the packing density is maximized.

In the process of mixture optimization, different curing techniques and temperatures should be considered (Matte and Moranville 1999). Matt and Moranville used carbon fibers in place of steel fibers to avoid any possibility of corrosion with little compromise in strength. A post-setting heat treatment temperature of 212°F (100°C) and a pre-setting pressure of 3.8 ksi (26.0 MPa) were used. The constituents of the mixture and proportions (by fraction of cement mass) proposed by various investigators [Richard and Cheyrezy (1995), Shaheen and Shrive (2006), and Matte and Moranville (1999)] are presented in Table 2.2. From Table 2.2, it is evident that the optimum water-to-cement and water-to-cementitious materials ratios for fiber reinforced concrete ranges from 0.13 to 0.2 and 0.11 to 0.15, respectively. The range of superplasticizer content used is between 0.016 and 0.019 by fraction of cement mass.

TABLE 2.2 Mixture Proportions (by fraction of cement) of UHPC from Literature.

Constituent	Richard and Cheyrezy (1996)				Shaheen and Shrive (2006)		Matte and Moranville (1999)
	Plain		Steel fibers 0.5 in. (12.7 mm)		Plain	Carbon Fibers 0.12 in (3.0 mm) long	Steel fibers
Portland cement	1	1	1	1	1	1	1
Silica fume	0.25	0.23	0.25	0.23	0.23	0.23	0.325
Quartz sand	1.1	1.1	1.1	1.1	1.1	0.5	1.43
Quartz powder	-	0.39	-	0.39	-	-	0.3
Crushed quartz	-	-	-	-	0.39	0.39	-
Superplasticizer	0.016	0.019	0.016	0.019	0.019	0.019	0.018
Steel fibers	-	-	0.175	0.175	-	-	0.275
Carbon fibers	-	-	-	-	-	0.125	-
Water	0.15	0.17	0.17	0.19	0.13	0.13	0.2
w/c[1]	0.15	0.17	0.17	0.19	0.13	0.13	0.2
w/cm[2]	0.12	0.138	0.136	0.154	0.11	0.11	0.15
Pre-setting pressure, ksi (MPa)	-	-	-	-	26.0 (3.8)	26.0 (3.8)	-
Post-setting heat treatment temperature, °F (°C)	68 (20)	194 (90)	68 (20)	194 (90)	212 (100)	212 (100)	194 (90)

[1] w/c = water to cement ratio
[2] w/cm = water to cementitious ratio

2.3 MECHANICAL PROPERTIES

Compared with normal strength concrete (NSC), UHPC beams without reinforcement have a high load capacity. Even the initial cracking load of UHPC beams is higher than the ultimate load of same size conventional concrete beams. Usually, conventional concrete beams fail in a brittle manner where the ultimate load is close to the initial cracking load. However, the flexural capacity of UHPC beams after the main crack occurs is greatly improved. The failure of UHPC beams is plastic; most of steel fibers pull out of the cement matrix rather than snap resulting in improved post-cracking behavior. As crack width increases, the load decreases gradually and a great deal of energy is absorbed during the fibers' pullout process (Gao *et al.* 2005).

The standard curing procedure suggested by the manufacturer is steam curing at 195°F (90.6°C) for 48 hours. Studies have shown that the method of curing can have a large impact on the properties of UHPC. Ambient air curing compared to steam curing will produce significantly different results (Kleymann *et al.* 2006).

2.3.1 Compressive Strength

Compressive strength is significantly affected by the curing method applied to the UHPC. Based on results from Graybeal's (2006b) study, the average 28-day compressive strength of UHPC was determined for different curing regimens. Steam-treated UHPC was found to have a compressive strength of 28.0 ksi (193.0 MPa) with a 95% confidence interval of 27.7 to 28.3 ksi (191.0 to 195.0 MPa). Untreated UHPC had a compressive strength of 18.3 ksi (126.0 MPa) with a 95% confidence interval of 17.9 to 18.7 ksi (123.0 to 129.0 MPa). Tempered steam-treated UHPC had a compressive strength of 24.8 ksi (171.0 MPa) with a 95% confidence interval of 24.3 to 25.3 ksi (168.0 to 174.0 MPa). The tempered steam treatment is very similar to the steam treatment, except that the temperature inside the steam chamber was limited to 140°F (60°C). Finally, delayed steam-treated UHPC had a compressive strength of 24.8 ksi (171.0 MPa) with a 95 percent confidence interval of 24.3 to 25.3 ksi (168.0 to 174.0 MPa).

Although these results seem quite high for concrete, they are likely lower than would normally be observed with this UHPC. Two factors clearly influence the compressive strength, the environment that UHPC is kept in before any steam-based treatment, and the steaming environmental conditions. In Graybeal's (2006b) study, the UHPC was demolded as soon as it had sufficient strength to maintain its geometric integrity. At this age, the UHPC is still rather permeable and is susceptible to moisture loss that likely resulted in lower strength values. Second, the UHPC manufacturer recommends 48 hours of steam treatment. In Graybeal's (2006b) study, the UHPC received only 44 hours of steam treatment with two hours of ramping up and down from room temperature.

Collepardi *et al.* (2007) conducted experiments with three types of UHPC concrete mixtures; a traditional UHPC mixture with only ground quartz sand and two modified UHPC mixtures

where the quartz sand was replaced fully and partly (about 47%) with graded aggregate that had a top size of 0.315 in. (8.0 mm). The water-to-cement ratio was slightly decreased in the modified UHPC mixtures. Compressive strength tests were conducted on 1.6 in. (40 mm) cubes and the microstructure of the concrete was examined using scanning electron microscopy. Specimens cured at room temperature or steam cured at 194°F (90°C) exhibited compressive strengths ranging from 23.2 to 26.1 ksi (160.0 to 180.0 MPa), whereas the compressive strength of specimens cured in an autoclave at 320°F (160°C) was in the range of 27.6 to 30.5 ksi (190.0 to 210.0 MPa). Based on the strengths obtained, it was evident that the partial replacement of ground quartz sand with graded sand had little effect on compressive strength.

Dili and Santhanam (2004) investigated the mechanical properties of UHPC and high performance concrete (HPC). Cubes with dimensions of 2.0 in. (51 mm) were tested for compressive strength after being cured at 194°F (90°C). The greatest compressive strengths observed by Dili and Santhanam for UHPC and HPC were 29.0 (200.0 MPa) and 10.88 ksi (75.0 MPa), respectively. They reported that the compressive strength at early age is greater for UHPC than for HPC. A significant increase (30 to 50%) in compressive strength due to heat treatment and the use of steel fibers was reported for UHPC.

Shaheen and Shrive (2006) proportioned UHPC mixtures to produce a concrete with very high compressive strength, toughness, and superior durability with minimum heat treating temperature, pre-setting pressure, and carbon fiber content (see Table 2.2 for mixture proportions). A specially designed mold with 157.5 μin. (4 μm) wide horizontal grooves was used to cast cylindrical specimens. The grooves were included to allow excess water and air bubbles to escape after the pre-setting pressure was applied. Mixing was performed for 10 to 15 minutes at a rate of 30 revolutions per minute. The thick and viscous mixture was consolidated for 5 to 10 minutes using a vibrating table. A pre-setting pressure of 3.8 ksi (26.0 MPa) was applied to cylinder specimens for 24 hours. Then, the cylinders were cured at a temperature of 302°F (150°C). The other curing regimens investigated by Shaheen and Shrive (2006) were: fogging at 60% relative humidity, autoclave oven at different temperatures up to 752°F (400°C), and room temperature [73.4°F (23°C)].

Shaheen and Shrive (2006) used carbon fibers and greater heat treatment to obtain compressive strengths as high as 40.9 ksi (282.0 MPa). It was observed that the application of a pre-setting force between 3.77 and 7.54 ksi (26.0 and 52.0 MPa) improved the compressive strengths considerably. However, application of greater pressure hinders the compressive strengths. This may be due to microcracking in the concrete caused by the expansion of compressed aggregates upon release of pressure.

2.3.2 Flexural Strength

Collepardi *et al.* (2007) also investigated the flexural strength of UHPC specimens using one traditional UHPC and two modified UHPC mixtures where the quartz sand was replaced fully and partially with graded aggregate that had a top size of 0.315 in. (8.0 mm). Flexural strengths were determined at 3, 7, and 28 days using a third point load method on 6.0 in. x

6.0 in. x 24 in. (150 mm x 150 mm x 600 mm) beams and a central point loading method on 1.6 in. x 1.6 in. x 6.5 in. (40 mm x 40 mm x 160 mm) specimens. Specimens were cured at three different temperatures, 68°F (20°C), 194°F (90°C), and 320°F (160°C). Collepardi *et al.* (2007) reported that the flexural strength was reduced when all the fine sand was replaced by coarse aggregate. The authors explained the reason for the lower flexural strengths in terms of homogeneity and bond strength. The authors also mentioned that the flexural strength of 1.6 in. x 1.6 in. x 6.5 in. (40 mm x 40 mm x 160 mm) specimens was greater than the flexural strength of 6.0 in. x 6.0 in. x 24.0 in. (150 mm x 150 mm x 600 mm) beams which agrees the results published by Richard and Cheyrezy (1994).

Dili and Santhanam (2004) investigated the flexural behavior of 1.6 in. x 1.6 in. x 6.5 in. (40 mm x 40 mm x 160 mm) specimens that included both plain and fiber reinforced specimens. They reported that the flexural strength of fiber reinforced UHPC and HPC specimens was greater than the flexural strength of the plain specimens. However, the flexural strength of UHPC specimens was significantly greater than that of HPC specimens. It was also observed that the flexural strength of both fiber reinforced and plain UHPC and HPC specimens was greater for the specimens cured in hot water at a temperature of 194°F (90ºC) compared to specimens cured under normal conditions.

2.3.3 Modulus of Elasticity

The design compressive strength of UHPC is much greater than the compressive strength of NSC and HPC. As a result the traditional ACI 318-08 equation (Equation 2.4) used to predict the modulus of elasticity for NSC is no longer valid when dealing with UHPC because UHPC exceeds the applicable range of f_c' this equation.

$$E_c = w_c^{1.5} \times 33{,}000\sqrt{f_c'}\ (\text{psi}) \qquad \text{Equation 2.4}$$

Furthermore, the ACI Committee 363 relationship (Equation 2.5) for HPC which is valid for compressive strengths of 3.0 to 12.0 ksi (20.7 to 82.7 MPa) does not apply to UHPC; again UHPC exceeds the applicable range of f_c'.

$$E_c = 40{,}000\sqrt{f_c'} + 1.0 \times 10^6\ (\text{psi}) \qquad \text{Equation 2.5}$$

However, there is a proposed relationship in the Association Française de Génie Civil/Service d'études Techniques des Routes et Autoroutes (AFCG/SETRA) recommendations for predicting the modulus of elasticity of UHPC, as well as NSC and HPC.

$$E_c = 262{,}000 \times \sqrt[3]{f_{ATT}'}\ (\text{psi}) \qquad \text{Equation 2.6}$$

where, f_{ATT}', is the compressive stress of UHPC after thermal treatment. This equation is found to most accurately predict the values for the modulus of elasticity based on the method of least squares in a study by Michigan Tech (2008).

Collepardi *et al.* (2007) determined the modulus of elasticity of specimens of three types of UHPC concretes (original UHPC mixture with only ground quartz sand and two modified UHPC mixtures where the quartz sand was replaced fully and partially with graded aggregate). They reported the value of elastic modulus as approximately 5,800 ksi (40,000 MPa) which was lower than the value reported by Richard and Cheyrezy (1994) [7.25 to 8.70 ksi (50,000 to 60,000 MPa)].

Wen-yu *et al.* (2007) reported a static modulus value of 6,790 ksi (46,800 MPa) which was comparable to the values obtained by the other investigators.

In Graybeal's study (2006b), tests were also conducted to determine the modulus of elasticity of this UHPC. In general, between 20 and 30 cylinders were tested at one month of age for each curing regime. The overall modulus of elasticity results include a stiffness of 7,650 ksi (52,800 MPa) for steam-treated, 6,200 ksi (42,800 MPa) for untreated, 7,400 ksi (51,000 MPa) for tempered steam-treated, and 7,300 ksi (50,300 MPa) for delayed steam-treated UHPC. The following equation was developed by Graybeal to approximate the modulus of elasticity:

$$E_c = 46{,}200\sqrt{f'_c}\ (psi) \qquad \text{Equation 2.7}$$

Figure 2.1 illustrates equations 2.6 and 2.7 over the applicable range of compressive strengths of UHPC.

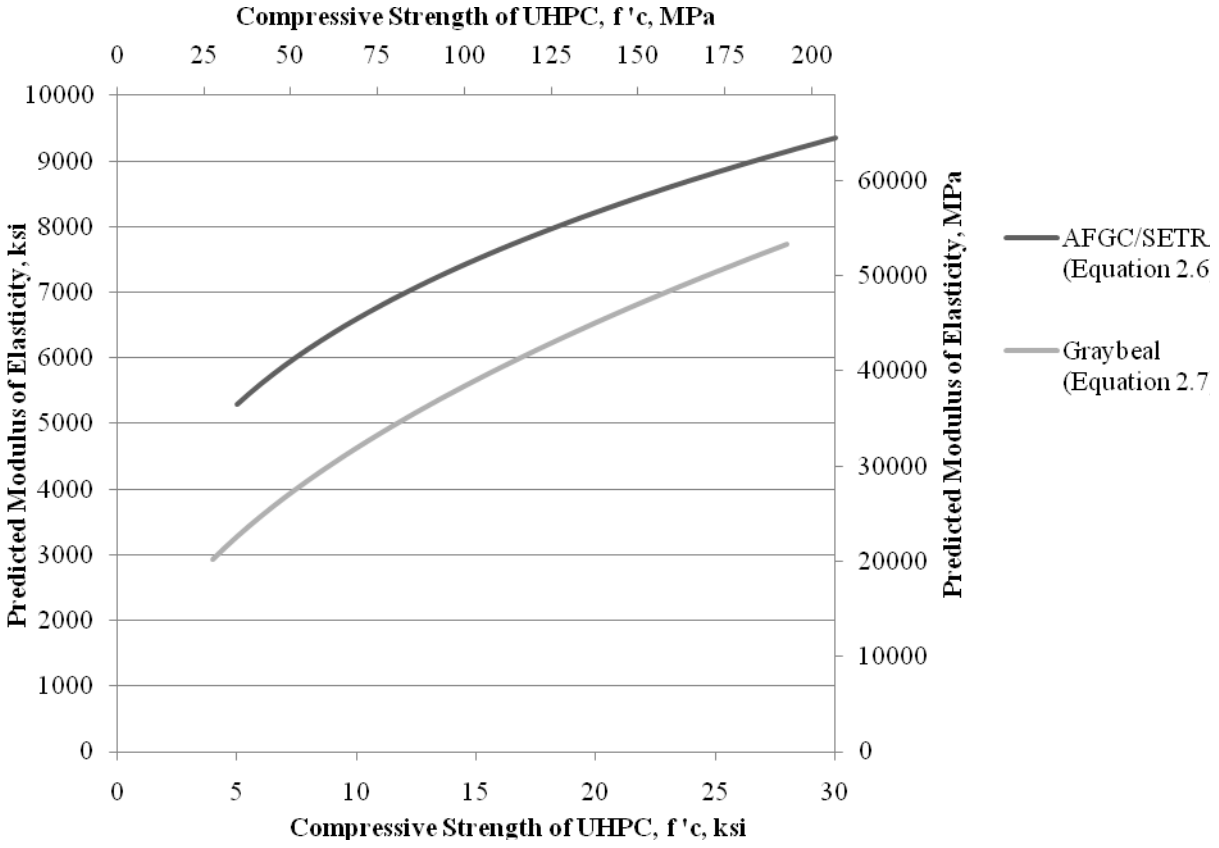

FIGURE 2.1 Plot of Modulus of Elasticity Equations 2.6 and 2.7.

2.3.4 Shrinkage-Swelling Behavior

Collepardi *et al.* (2007) studied the shrinkage and swelling behavior of three types of UHPC mixtures: the original UHPC mixture with only ground quartz sand and two modified UHPC mixtures where the quartz sand was replaced fully and partially (approximately 47%) with graded aggregate with a top size of 0.315 in. (8.0 mm). The specimens were exposed to air with a relative humidity of 65% for 30 days and then placed in water. It was reported that there was no significant change in the shrinkage-swelling behavior as a function of the aggregate-cement ratio of the UHPC specimens. This can be attributed to the very dense microstructure of the cement paste. However, it was reported that the shrinkage of the steam cured [194ºF (90ºC)] UHPC specimens was less than 50% of the shrinkage for specimens cured at room temperature.

Steel fibers are important for controlling the extension of cracks. It is the tension function of steel fibers that makes the depth of the tension zone in beams smaller and the overall rigidity of the beam greatly improved. The failure of UHPC beams is nearly plastic, and most of the steel fibers pull out of the cement matrix rather than snap. This allows the load to decrease gradually as the crack widths increase, and a great deal of energy is absorbed during the process of steel fibers pulling out of the cement matrix. Therefore, the ductility of UHPC beams is improved (Gao *et al.* 2005).

A large amount of shrinkage can occur in UHPC due to the high cement content and the lack of an aggregate skeleton. Early-age shrinkage can be especially large in UHPC, and the highest rate of shrinkage tends to occur during the period of early age strength gain. Because of this, traditional shrinkage measurement techniques can miss shrinkage that is occurring as the UHPC is beginning to set. Graybeal (2007) used embedded vibrating wire gages to measure this early age shrinkage. Results show that the shrinkage began to occur 20 hours after casting, and by 30 hours after casting over 300 microstrain of shrinkage had already occurred. Air cured UHPC exhibited approximately 35 microstrain shrinkage per day from the second through the sixth day after casting while the steam treated UHPC exhibited over 400 microstrain of shrinkage during the treatment but was then effectively stabilized (Graybeal 2007).

2.3.5 Creep

Collepardi *et al.* (2007) presented results from creep tests performed on UHPC, and reported that the creep strain of the UHPC specimens under a stress of 7.69 ksi (53.0 MPa), with a stress-strength ratio of 0.33 at the time of loading, was greater than that of NSC with compressive strength ranging from 4.35 to 5.8 ksi (30.0 to 40.0 MPa). However, the ultimate specific creep including elastic strain was 2.41 x 10^{-10} ksi^{-1} (1.7 x 10^{-9} MPa^{-1}) regardless of the stress-strength ratio and aggregate to cement ratio of the original or modified UHPC. It was also reported that the specific creep of autoclaved UHPC specimens was lower than that of specimens cured at room temperature, and the creep of UHPC specimens cured at room temperature was the same as that of normal strength concrete.

2.4 DURABILITY ISSUES

UHPC tends to exhibit advanced mechanical and durability properties when compared to HPC. Some characteristics of UHPC include: compressive strength greater than 22.0 ksi (150.0 MPa), internal fiber reinforcement to ensure non-brittle behavior, and high binder content with special aggregates. The strength of heat treated UHPC is approximately 15% greater than non-heat treated, durability properties are also improved. The use of heat treatment is optional and depends on the application (Rebentrost and Cavil 2006). Because of a push to extend the life expectancy of existing and planned infrastructure, the durability of concrete has become increasingly important in recent years (Graybeal and Tanesi 2007).

2.4.1 Water Absorption

Excessive water absorption by concrete leads to scaling of material when the concrete is exposed to freezing and thawing. This scaling can eventually lead to corrosion of reinforcement due to penetration of chloride ions, particularly in tidal areas (Roux *et al.* 1996). Roux *et al.* (2006) studied the water absorption of UHPC 200 and UHPC 200c in which UHPC 200 was table vibrated and UHPC 200c was produced with a pre-setting pressure of 8.7 ksi (60.0 MPa). Two reference concretes C30 (low cement content) and C80 (high cement content) were used for comparison. The diameter and height of C30 and C80 specimens were 4.33 in. (110 mm) and 8.66 in. (220 mm), respectively. In their experimental

program, the authors conducted tests on 1.2 in. (30 mm) thick cylindrical specimens that were 2.8 in. (70 mm) in diameter, cured for 28 days in water at 68°F (20°C) and then stored in air at 68°F (20°C) with a relative humidity of 50%. The concrete slices were placed on a water-saturated sponge, immersed in water to a depth of 0.2 in. (5 mm) and the specimens were weighed at specific time intervals. The results were presented as the amount of water absorbed per unit surface area as a function of the square root of the elapsed time.

Water absorption of UHPC 200 was observed to be less than 0.0003 lb/in^2 (0.2 kg/m^2) and no point of inflection was detected which indicates the absence of capillary porosity. The absence of capillary porosity was also observed using mercury porosimetry. Due to the absence of capillary porosity, ingress of aggressive agents is strongly resisted and superior durability characteristics are achieved. The water absorption of C30 specimens was approximately 0.00412 lb/in^2 (2.75 kg/m^2) while the water absorption for C80 specimens was approximately 0.00045 lb/in^2 (0.3 kg/m^2). The water absorption values for UHPC 200 and UHPC 200c were smaller than 0.00045 lb/in^2 (0.3 kg/m^2).

Dili and Santhanam (2004) compared the water absorption rate of UHPC and HPC and observed a similar trend of decreasing water absorption with age. However, it was reported that the percentage water absorption of UHPC is low compared to that of HPC. The authors commented on the marginal increase of water absorption for fiber reinforced specimens that were heat cured. They stated two reasons for this marginal increase in water absorption: incorporation of fibers leads to the formation of channels at the paste-fiber interface and the heat treatment encourages the development of an open microstructure. This reasoning seems to be the probable explanation for the increase in water absorption of fiber reinforced concrete specimens. Another possibility for the increase in water absorption is the development of micro cracks upon release of the applied pre-setting load (Matte and Moranville 1999).

2.4.2 Chloride Penetration

The presence of chloride ions near the reinforcing steel in concrete structures is a major cause of corrosion. If the chloride ion concentration exceeds the threshold value, the passivating layer for the reinforcing steel becomes ineffective and corrosion of the steel occurs. Hence, the study of chloride ion concentration and the impermeable nature of the concrete is of importance.

Roux *et al.* (1996) conducted experiments on UHPC 200 and two reference concretes C30 and C80 for comparison. The authors performed two kinds of tests: measurement of simple diffusion and measurement of migration under steady-state chloride flow conditions based on differences in the electrical potential. Specimens were sealed in an epoxy resin coating and equipped with a reservoir containing 0.5 M NaCl on top keeping the chloride concentration constant throughout the testing period (1 year) and the apparent diffusion coefficient was evaluated. It was observed that the chloride ion concentration was approximately 3.5% for C30 specimens, 0.75% for C80 specimens, and zero for UHPC 200 specimens.

The other method used by the authors (Roux *et al.* 1996) to calculate the effective diffusion coefficient, was measurement of migration under steady-state chloride flow conditions based on differences in the electrical potential (12 Volts). In this method, the authors did not consider the chemical interaction between chloride ions and the material. A 0.196 in. (5.0 mm) thick concrete disc was inserted between a cathodic cell containing 0.5 M NaCl solution and an anodic cell containing distilled water. The chloride content of the two cells was observed over a period of time from the instant when steady-state migration was reached. The effective diffusion coefficients of C30, C80, and UHPC 200c specimens were reported as 1.7 x 10^{-9} in^2/second (sec) (1.1 x 10^{-12} m^2/sec), 9.3 x 10^{-10} in^2/sec (0.6 x 10^{-12} m^2/sec), and 3.1 x 10^{-11} in^2/sec (0.02 x 10^{-12} m^2/sec), respectively. This indicates that chloride impermeability of UHPC 200c concrete was superior compared to the other two concretes.

Wen-Yu *et al.* (2007) conducted experiments on six specimens to investigate the chloride impermeability of UHPC by applying pressure to the specimens at a rate of 0.0145 ksi/8 hours (h) (0.1 MPa/8h) with the pressure increasing from 0.0145 to 0.232 ksi (0.1 to 1.6 MPa). Upon removal of hydraulic pressure, only 0.106 in. (2.7 mm) penetration was observed which lead to the conclusion that UHPC has excellent chloride impermeability.

Dili and Santhanam (2004) presented the results of rapid chloride permeability tests conducted after 28 days. The authors reported that the chloride ion penetration was greater when the UHPC and HPC specimens were heat cured. The data presented in their paper (2004), reveals that the chloride penetration was due to the incorporation of fibers in the specimens, and the reason stated for it is the increased conductance of concrete. However, it was reported that the resistance to chloride ion penetration of UHPC was superior to that of HPC.

Graybeal and Tanesi (2007) tested UHPC's ability to resist chloride ion penetration. A high resistance to ingress of aggressive chemicals was reported after noticing a very low level of water absorption. There was a discontinuous capillary porosity resulting in decreased permeability. Testing for scaling and abrasions resistance indicated that UHPC was not susceptible to either problem.

2.4.3 Freeze-Thaw Durability

Wen-yu *et al.* (2007) developed UHPC that was used in the construction of a railway bridge built on frozen earth (Qinghai-Tibet railway, China). The bridge was built in harsh climate conditions: low air temperature, concentrated rain and snow, and heavy sandstorms. These conditions required the concrete used for the bridge to have superior freeze-thaw durability. The authors conducted freezing and thawing tests for investigating the frost resistance of UHPC on two series of test specimens. The size of the specimens used for the test was 4.0 in. x 4.0 in. x 16.0 in. (100 mm x 100 mm x 400 mm). The temperature range for the specimens was from -30.6°F (-17°C) to 46.4°F (8°C). ASTM C-666 specifies that freezing-and-thawing cycles should consist of lowering the temperature of specimens from 40°F (4°C) to 0°F (-18°C) and then raising the temperature from 0°F (-18°C) to 40°F (4°C) in not less than 2 hours nor more than 5 hours. No decrease in relative dynamic modulus or loss of mass after

800 cycles of freezing and thawing was reported. The relative dynamic modulus was 100%. Therefore, the authors concluded that the UHPC had excellent resistance to freezing and thawing.

Shaheen and Shrive (2006) investigated resistance to freezing and thawing (according to ASTM C-666) on pre-cracked specimens that were 3.0 in. x 3.0 in. x 14.0 in. (76 mm x 76 mm x 357 mm). Unlike the earlier research, the authors used specimens with grooves on each side to simulate cracks. Specimens were placed in a tempering tank for 24 hours with the temperature ranging from -30.0°F (1.1°C) to 35.9°F (2.2°C). The specimens were then immersed in the freeze-thaw chamber to begin testing on the thawing phase of a freeze-thaw cycle. After the completion of every 36 cycles, fundamental transverse frequency, mass, and average length were recorded. The test was continued through the completion of 300 cycles. It was reported that there was no significant length change or mass loss. Relative dynamic modulus and durability factors were calculated and were found to be 100% which indicated good resistance to freezing and thawing. According to ASTM C-666 relative dynamic modulus is calculated as:

$$E_{rel}(c) = \left(\frac{n_1^2}{n^2}\right) 100 \qquad \text{Equation 2.8}$$

where, $E_{rel}(c)$ is the relative dynamic modulus after c cycles of freezing and thawing (percent); n is the fundamental transverse frequency (Hz) at zero cycles of freezing and thawing; and n_1 is the fundamental transverse frequency (Hz) after c cycles of freezing and thawing. The durability factor is computed as:

$$DF = \frac{E_{rel} N}{M} \qquad \text{Equation 2.9}$$

where, DF is the durability factor of the test specimen; E_{rel} is the relative dynamic modulus after N cycles (percent); N is the number of cycles at which E_{rel} reaches the specified minimum value for discontinuing the test or the specified number of cycles at which the exposure is to be terminated (whichever is less); and M is the specified number of cycles at which the exposure is to be terminated.

Testing was also conducted by Graybeal and Tanesi (2007) to determine the durability properties of UHPC. Results indicate that UHPC is very resistant to deterioration caused by freezing and thawing. In Graybeal's study, 3.0 in. x 4.0 in. x 16.0 in. (76 mm x 102 mm x 406 mm) UHPC prisms were produced. Three prisms were cast for each curing regiment. After casting, curing treatments were applied, then freeze/thaw testing began between 5 and 6 weeks later. In the following two days after the cast, the prisms were submerged in 39.9°F (4.4°C) water to prepare them for the initial test measurement. The specified lower and upper temperature targets for the freezing and thawing environments were 0°F and 40°F (−18°C and 4.4°C), respectively. The automated equipment used in this test program allowed for five cycles of freezing and thawing to be completed per day (Graybeal 2006a). It was found that the relative dynamic modulus (RDM) changed very little when the specimens were either

delayed steam treated or tempered steam regimes, decreased slightly in the steam-treated regime, and increased significantly in the untreated regime (Graybeal 2006b).

2.4.4 Alkali Silica Reaction

Alkali-silica reaction (ASR) testing was also performed by Graybeal and Tanesi (2007). The results indicated that there should be no concern of ASR problems with the concrete after steam-based curing. Free water must be present for ASR to occur in any concrete. Because UHPC has a low permeability, it is unlikely that ASR would be an issue under any curing regime, additionally UHPC is not susceptible to ASR due to its high silica fume content.

2.5 DUCTAL®

Ductal®, a product developed by Lafarge, is currently the only UHPC commercially available in the United States. Currently, there are six different chemical formulations available in North America, all under the Ductal® brand name. Ductal® is stronger than normal concrete in compressive and flexural strengths and also performs better in terms of abrasion, freezing and thawing, carbonation, and chloride ion penetration. Due to the optimization of Ductal's® gradation of the raw material components, Ductal® is 10% denser than normal concrete. Other durability properties are shown in Table 2.3.

Ductal® is able to bend and carry large loads without brittle or sudden failure. The ductile failure of Ductal® more closely resembles the failure mode of steel rather than concrete. Ductal's® failure is gradual versus concrete's sudden, brittle failure. Because of its combination of strength with ductility, Ductal® can often be designed without the use of reinforcing steel which can result in smaller sized members and faster construction times (Lafarge 2009).

Ductal® is significantly stronger than normal concrete and has strength characteristics comparable to some metals. Its compressive strength is in the range of 22.0 to 30.0 ksi (152.0 to 207.0 MPa) compared to 3.0 to 7.0 ksi (20.0 to 50.0 MPa) for normal concrete. Ductal's® flexural strength range is between 5.0 to 7.0 ksi (35.0 and 50.0 MPa). Flexural strength for normal concrete is typically in the range of 0.5 to 1.0 ksi (3.0 to 7.0 MPa) (21). CS1000 is the type of Ductal® used for bridge decks, marine docks/walls, troughs, piles, and stay in place forms. The physical properties of CS1000 are shown in Table 2.4. To obtain the compressive strength of this concrete, 3.0 in. x 6.0 in. (8.0 cm x 15.0 cm) cylinders were tested.

TABLE 2.3 Durability of Ductal® (Lafarge 2009a).

	HPC 8.7 ksi (60.0 MPa)	Ductal® 2% steel fibers 90°C (194°F) - curing
Slump Flow (ASTM shock-table) in. (mm)	8.0 (> 200)	8.0 (>200)
Abrasion:(relative volume loss) Index I	2.75	1.2
Freeze-thaw: (residual E-mod after 300 cycles), %	90	100
Carbonation: (depth of penetration) in. (mm)	0.08 (2.0)	0 (0)
Chloride ion diffusion: 10^{-12} ft^2/s (10^{-12} m^2/s)	5.0 (0.5)	0.2 (0.02)
Post-curing shrinkage:10^{-6}	300	0

TABLE 2.4 Physical Properties of Ductal® CS1000 (2009b).

	Test Data					
	Mean		Standard Deviation		Design Values	
	MPa	ksi	MPa	ksi	MPa	ksi
Compression	140.0	20.0	10.0	1.40	100.0	14.5
Flexural	30.0	4.3	5.0	0.7	-	-
Direct Tension, f_{tj}	8.0	1.16	1.0	0.145	5.0	0.725
Young's Modulus	MPa	ksi	MPa	ksi	MPa	ksi
	50,000	7,200	2,000	3.0	45,000	6,500

A typical composition for a Ductal® mixture is shown in Table 2.5. The mixture proportions used in Graybeal's (2006b) study included:

- Premix 3,700 lb/yd^3 (2,195 kg/m^3) of concrete
- Water 184 lb/yd^3 (109 kg/m^3) of concrete
- HRWRA 51.9 lb/yd^3 (30.8 kg/m^3) of concrete
- Accelerator 50.6 lb/yd^3 (30.0 kg/m^3) of concrete
- Steel Fibers 263 lb/yd^3 (156 kg/m^3) of concrete

TABLE 2.5 Typical Composition of Ductal® (Graybeal 2006b).

Material	Amount, lb/yd^3 (kg/m^3)	Percent by Weight
Portland Cement	1,200 (712)	28.5
Fine Sand	1,720 (1,020)	40.8
Silica Fume	390 (231)	9.3
Ground Quartz	355 (211)	8.4
Superplasticizer (Glenium 3000NS)	51.8 (30.7)	1.2
Accelerator (Rheocrete CNI)	50.5 (30)	1.2
Steel Fibers	263 (156)	6.2
Water	184 (109)	4.4

When used in optimum dosages, the high range water reducing admixture (HRWRA) reduces the water-to-cementitious materials ratio (w/cm) while improving the workability of concrete. The addition of microsilica enhances the mechanical properties of the paste by filling voids, enhancing rheology, and producing secondary hydrates. The quartz powder is useful for its reactivity during heat treatment (Dili and Santhanam 2004). The fluidity of fresh concrete increases with decreased carbon content of the silica fume.

2.6 UHPC STRUCTURES

Several countries are using UHPC, including Ductal®, in experimental or pilot projects. In China, a high-durability panel entirely made of UHPC was used for railway bridge walkways in Qinghai-Tibet. In Korea, a pedestrian bridge with a 430.0 ft (130.0 m) arch has been constructed. Portugal has used UHPC for seawall anchors, Australia has used UHPC in a vehicular bridge, France has used it in building power plants and Canada has used it in several projects. In all of these cases, the material was chosen for its ability to stand up to high stresses both environmental and load related (Gao *et al.* 2005).

The bridge over Shepherds Creek in Australia was the constructed using UHPC for normal highway traffic. This bridge is approximately 93 miles (150 kilometers) north of Sydney, Australia and replaced an existing timber bridge. It has four traffic lanes and a footway. The bridge is a single span of 49.0 ft (15.0 m) in length and has a width of 69.0 ft (21.0 m) with a 16° skew. The substructure is composed of driven steel piles with a cast-in-place capping beam. The superstructure consists of sixteen precast, pre-tensioned UHPC beams and an in-situ reinforced concrete deck slab. The I-beams have a total depth of 20.0 in. (60.0 cm) a weight of 190.0 lb/ft (280.0 kg/m) and are spaced at 4.3 ft (1.3 m) (Rebentrost and Cavill 2006).

The first bridge to utilize UHPC in the United States was the Mars Hill Bridge in Wapello County, Iowa. This three-girder bridge spans 110.0 ft (33.83 m) and has 3.5 ft (1.1 m) deep

prestressed girders. The designer modified the girders from the standard Iowa bulb-tee design by using thinner flanges and a narrower web. Normal steel shear reinforcement was eliminated after testing demonstrated that the UHPC, with its steel-fiber reinforcement, was sufficient to carry the design loads (Bierwagen 2005).

According to Norm McDonald, director of the Iowa Department of Transportation Office of Bridges and Structures, "Two of the biggest challenges with the Wapello County Bridge were the lack of a U.S. design specification and limited experience working with UHPC," (Bierwagen 2005). Design guidelines developed in France were used for the design capacities for the bridge beams. These design capacities were verified by testing a 71.0 ft (22.0 m) long large-scale beam (Graybeal and Tanesi 2007). Fiber optic gauges were installed inside the final beam that was cast to allow researchers the ability to measure strains at strand release, during construction, and under dead and live loads (Bierwagen 2005). Construction of this bridge began on August 17, 2005. The bridge was open to traffic on February 20, 2007.

The Cat Point Creek Bridge in Richmond County, Virginia opened to traffic in October 2008 as the second UHPC Bridge in the United States. The 10-span bridge contains one UHPC span of 81.4 ft (24.8 m) with five 3.7 ft (1.1 m) deep girders. The girders were prestressed and include a one-for-one replacement of conventional concrete with UHPC. Traditional mild steel shear reinforcement was eliminated due to the tensile properties of UHPC. A local pre-cast plant in southeastern Virginia fabricated the girders (Graybeal 2009).

After the completion of the Wapello County Bridge in Iowa in 2006, another project was set to begin in Buchanan County, Iowa. The dimensions of the bridge are as follows: 24.25 ft (7.39 m) wide by 112.33 ft (34.2 m) long, the center span will be 51.08 ft (15.9 meters) from center-to-center of the pier caps, and plain neoprene bearing seats will be provided for the 50.0 ft (15 m) simple span PI (π) section (Keierleber *et al.* 2007). An example of a π girder cross section is shown in Figure 2.2. Design work conducted for the bridge project in Wapello County was used along with the testing that was performed by Turner-Fairbank Laboratory on UHPC concrete and the PI section (Keierleber *et al.* 2007).

The main difference between the Wapello County Bridge and the Buchanan County Bridge is the design of the girders. The Wapello County Bridge has modified bulb-tee girders where as the Buchanan County Bridge has π girders. Figure 2.3 is the Buchanan County Bridge. The design started with the π section that was developed by the Federal Highway Administration's (FHWA) Turner-Fairbank Laboratory and Massachusetts Institute of Technology (MIT). During testing of the section at Turner-Fairbank, some problems were found with the initial shape. These problems were addressed during the design process, and changes to the section were made. Transverse strength of deck, live load distribution between beams, and fiber distribution in web areas were the problems addressed (Keierleber *et al.* 2007).

Initial design of the deck did not meet the requirements for a service loading of 16.0 kip (71.0 kN) wheel load with 33% impact (Keierleber *et al.* 2007). After many options were

considered, a decision was made to use a constant 4.0 in. (102 mm) deck with transverse post-tensioning. This change was intended to keep the changes as simple as possible and limit the cost of modifying the beam forms to keep the research budget within allowable limits (Keierleber *et al.* 2007).

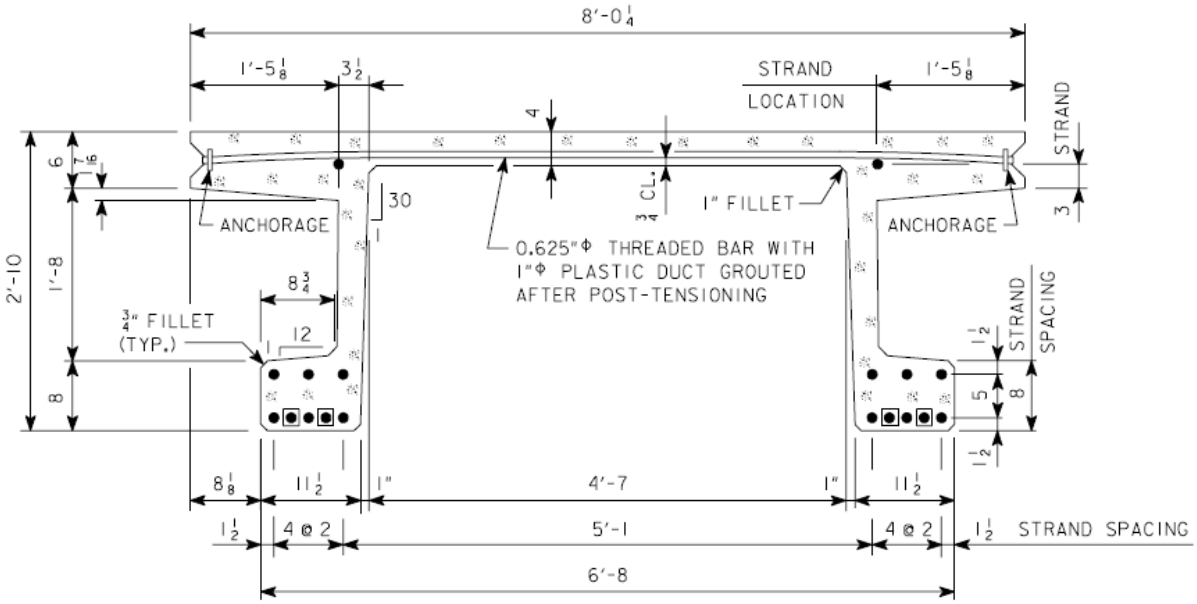

FIGURE 2.2 Example of PI Girder (Keierleber *et al.* 2007).

FIGURE 2.3 PI-Girder Bridge in Buchanan County Iowa.

Testing revealed poor live load distribution between the beam sections. It is possible that this was due to the flexibility of the beams, the connection between the beam sections, and the lack of diaphragms. To improve distribution, steel diaphragms were added to the bottom of the section (Keierleber *et al.* 2007).

The last problem addressed was fiber distribution in the web area. According to Keierleber *et al.* (2007), it was found that testing wires were disrupting the proper flow of fibers through the web and may have caused planes of weakness in the web sections where the shear failures took place. To resolve this problem, the webs were thickened by 0.5 in. (13 mm) to improve the flow of the steel fiber in case, testing wires were cast in the web. Construction began in spring 2008, and the bridge was open for traffic in November 2008.

2.7 DESIGN

A rectangular stress block approximation for the compressive behavior of concrete in flexure provides a simplified means to predict the flexural behavior of prestressed concrete girders. This relationship is an accurate approximation for the nonlinear stress-strain behavior of conventional concrete and is widely used in flexural provisions of reinforced concrete design specifications. However, two of the assumptions inherent in United States design codes (AASHTO 2007; ACI 2008) are violated by the behavior of UHPC. First, UHPC exhibits a compressive stress-strain response that more closely resembles a triangular stress distribution than the familiar parabolic distribution of conventional concrete. Although this behavior could be accounted for through a modification of the parameters of the rectangular stress block, design codes currently do not contain provisions allowing the proper modifications to be used. Second, UHPC exhibits tensile capacity after cracking. Code-based ultimate flexural capacity calculations assume that the concrete carries no tensile force, thus these calculations may be significantly in error if applied to UHPC. After testing, it was concluded that UHPC I-girders will display flexural capacities greater than those of conventional concrete girders with similar cross-sectional geometry (Graybeal 2008).

The positive and negative moment capacity was determined from the experimentally observed behavior of UHPC in bending, stress-strain compatibility, and basic principles of mechanics. The moment capacity analysis can be completed through an iterative process by assuming the neutral axis depth and perform a stress-strain analysis on the cross-section. Internal forces are resolved from the stress-strain analysis and equilibrium of the cross-section is verified (Garcia and Graybeal 2007).

At the serviceability limit state, the French recommendations, AFGC/SETRA, (2002) in section 2.3 proposes to keep the shear stress limits of the French code for prestressed concrete. These limits tend to avoid cracks in prestressed structures and should not be changed for UHPC. At the ultimate limit state, the recommendations introduce fiber shear strength that compliments resistance of the concrete and the potential active or passive reinforcements. Concrete shear strength of UHPC must be treated differently than for traditional concrete because of the lack of aggregate interlock (Resplendino and Petijean 2003).

Design of the UHPC two-way ribbed deck first consisted of defining an element and then determining the live, dead, and collision design loads on the UHPC deck for different limit states. The design followed the 2006 AASHTO LRFD Bridge Design Specifications where appropriate. Composite action between the girders and the deck was assured via shear

connectors that extended from the girders into pockets created between webs of the deck panel, which are then filled with grout (Garcia and Graybeal 2007).

The results from the material characterization study and the structural testing (performed at Turner Fairbank) indicated that the use of UHPC in conventionally shaped highway bridge girders was not efficient. Prestressed I-girder shapes were traditionally designed for normal strength concretes that required an internal mild steel reinforcing cage to carry secondary tensile forces (Graybeal and Hartmann 2004).

2.8 RAPID CONSTRUCTION

The ability to rapidly construct highway bridges has become increasingly important in recent years due to the congested nature of our nation's highways. FHWA has established a research program to alleviate this problem. FHWA's research has included an extensive material characterization study as well as full scale structural testing of bridge girders. To date, the UHPC bridge girder structural testing has focused on the flexural and shear behavior of prestressed UHPC girders that do not contain mild steel reinforcement.

Results from the material characterization study and the structural testing (performed at Turner Fairbank) indicated that the use of UHPC in conventionally shaped highway bridge girders is not efficient. This led FHWA to work with researchers at MIT to develop an optimized highway bridge girder design for UHPC. This work resulted in the π section previously mentioned and shown in Figure 2.2.

The design of this element includes numerous aspects that are relevant to the rapid construction of highway bridges. The most important aspect is its manageable size, shape, and weight. The 70.0 ft (21.34 m) long, 8.0 ft (2.35 m) wide optimized girder only weighed 23 tons (21,000 kg) allowing for easy transport. The size also makes it easy to erect. The stable design of the girder allows for placement of any number of girders across the bridge width without the need for temporary bracing (Graybeal and Hartmann 2004).

Another design aspect that allows for rapid construction is the connection mechanism between parallel girders. Bolt holes were cast into the thickened portion of the deck so that a bolt could pass through the connection. The positive connection occurred every 3.0 ft (0.91 m) along the length of the bridge. The connection was easily completed from the underside of the deck. The third aspect of the rapid constructability is the longitudinal shear key that runs the length of the length of the bridge between any two girders. Grout is placed in the female-female key after the bottom of the key was filled with a backer rod. The shear key can be placed quickly, depending on the grout and grout placement machinery used (Graybeal and Hartmann 2004).

2.9 ONGOING RESEARCH

The recent development of concrete having extremely high compressive and tensile strengths has made possible new and exciting applications for concrete. However, its use is limited due to the current cost associated with the mixing and curing procedures. Therefore, research projects have been initiated to develop a concrete mixture using readily available local materials that have comparable performance to the currently existing products. The hope is that this ongoing research will potentially produce a mixture with greatly reduced cost as well as more practical mixing and curing procedures, allowing a wider range of applications for UHPC (Kleymann *et al.* 2006).

The Nebraska University (NU) UHPC research project is one of these research projects. The objective is to develop a concrete mixture using readily available local materials that has comparable performance to the currently available products. This mixture will need to achieve extremely high compressive strength, adequate flowability, and practical mixing and curing procedures. In addition, the mixture will have a significantly reduced cost due to the use of local materials and will be able to be produced or modified by designers (Kleymann *et al.* 2006).

The mixture proportions for NU UHPC are similar to those of many of the available UHPC products. However, the constituent materials used in typical UHPC were replaced by local materials. The study attempted to maintain a particle gradation similar to that of typical UHPC. The most notable difference between the products currently available and the experimental mixtures is the elimination of steel fibers. Although this negates the greatly increased tensile strength, it significantly reduces the cost while comparable compressive strengths can still be achieved (Kleymann *et al.* 2006). Table 2.6 shows the estimated costs of the different NU UHPC mixtures.

TABLE 2.6 Estimated Cost of NU UHPC Mixtures (Kleymann *et al.* 2006).

Mixture	Estimated $ per yd^3 ($ per m^3)
NU UHPC #2	$380 ($497)
NU UHPC #3	$441 ($578)
NU UHPC #5	$652 ($853)
NU UHPC #6	$433 ($566)
NU UHPC #7	$385 ($504)

3 CASE STUDIES

3.1 MARS HILL BRIDGE, WAPELLO COUNTY, IOWA

3.1.1 Introduction

An aging bridge was identified to be replaced in Wapello County, Iowa. The bridge was a relic of a past generation when labor and materials were cheap, it was a steel truss with a timber deck and timber abutments. Bridge engineers saw this bridge replacement as an opportunity to use ultra high performance concrete (UHPC) and started planning this project in 2003.

Wapello County was awarded partial funding through Transportation Equity Act for the 21st Century (TEA-21) Innovative Bridge Construction Program (IBRC). The goal of this legislation as stated on the FHWA bridge technology website is: IBRC is an initiative by the FHWA to provide direction and funding to help state, county, and local bridge owners incorporate innovative materials and materials technologies in their bridge projects. This program is intended to "increase productivity by lowering the life-cycle costs of bridges, to keep Americans and America's commerce moving, and to enhance safety" (IBRC 2009). UHPC is an ideal material for this program as it has a lower life-cycle cost and is much more durable than NSC or even HPC.

3.1.2 Bridge Description

The Mars Hill Bridge (Figure 3.1) crosses Little Soap Creek in the south-central, rural part of Wapello County, Iowa. The new bridge utilizing UHPC is a single, simple span structure with a clear span of 110.0 ft (33.83 m). There is no curvature in either the horizontal or vertical direction and there is no skew. Three modified bulb-tee Iowa Department of Transportation (IDOT) Type C girders (BTCIIO), spaced at 9.58 ft (2.92 m), with 0.5 in. (13 mm) haunches compose the cross section of the superstructure (Figures 3.2 and 3.3) along with a composite, 8.0 in. (203 mm), cast-in-place deck of conventional, normal weight 150 pcf (23.6 kN/m^3) concrete with a compressive strength of 4.5 ksi (31.0 MPa). The deck is 27.1 ft (8.28 m) wide with a 2% crown on either side of the centerline of the bridge. The travel way dimension is 24.5 ft (7.47 m), allowing for two lanes of traffic. The deck overhang is 4.0 ft (1.22 m) (Figure 3.4). The beams are braced by a single diaphragm in each bay at the midpoint by a steel C-section. Supporting the superstructure is a conventional Iowa Department of Transportation (IDOT) integral abutment at each end of the three beams with wingwalls. The traffic barrier is an open, concrete guard rail (Degen 2005). Table 3.1 summarized the bridge geometry.

FIGURE 3.1 Mars Hill Bridge: The First UHPC Bridge Constructed in the United States.

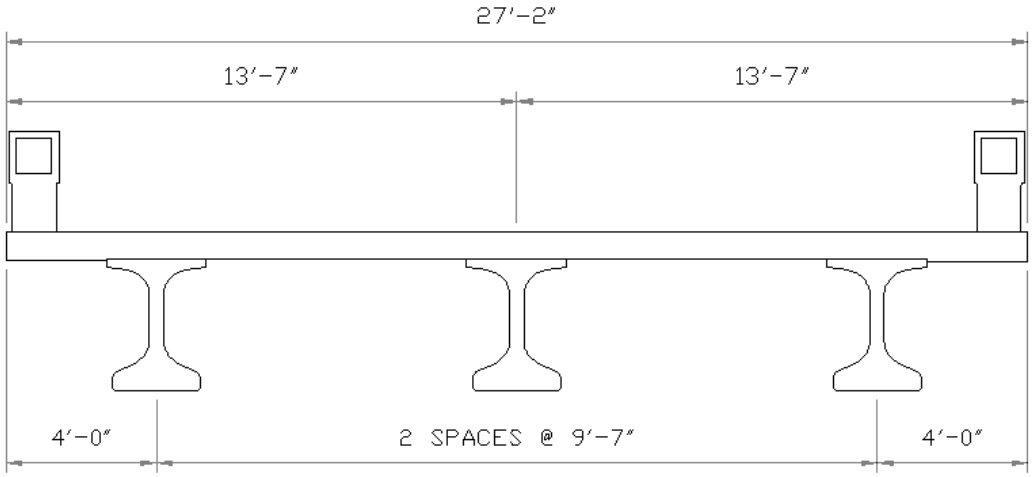

FIGURE 3.2 Mars Hill Bridge Cross-Section.

FIGURE 3.3 Underside of Mars Hill Bridge.

FIGURE 3.4 Girder and Deck Overhang, Mars Hill Bridge.

TABLE 3.1 Mars Hill Bridge Geometry.

Parameter	Description
Span Type	1 single span
Clear Span	110'-0" (33.83 m)
Curvature	None
Number of Girders	3
Type of Girder	modified BT-45" (1.14 m)
Girder Spacing	9'-7" (2.92 m)
Width of Deck	27'-2" (8.28 m)

3.1.3 Beam Description

The prestressed beams utilize UHPC that is marketed as Ductal® from the company LaFarge North America based in Canada. The modified BTCIIO beams [the BTCIIO girder is itself a modification of the traditional Iowa 45.0 in. (1.14 m) bulb tee girder] were modified to take advantage of the material properties of UHPC, namely its high compressive strength and significant tensile strength. The modifications included reducing the web width 2.0 in. (51 mm) to 4.5 in. (114 mm), the top flange thickness by 1.0 in. (25 mm) to 2.8 in. (71 mm); the bottom flange thickness by 2.0 in. (51 mm) to 5.5 in. (140 mm). These changes resulted in an overall beam depth of 42.0 in. (1.06 m) instead of 45.0 in. (1.14 m). Reducing the geometry resulted in less required concrete material, and thus, a more cost effective and structurally efficient member. The beams have a total length of 111.0 ft (33.83 m), with a clear span of 110.0 ft (33.53 m). Figure 3.5 shows a cross-sectional comparison of a typical IDOT BTCIIO bulb tee and the modified BTCIIO bulb tee. The difference in the BTCIIO girders is illustrated in Figure 3.6 with the modified shape superimposed on the typical shape. The shaded region is the area of the typical bulb tee that was eliminated by using the more efficient modified shape.

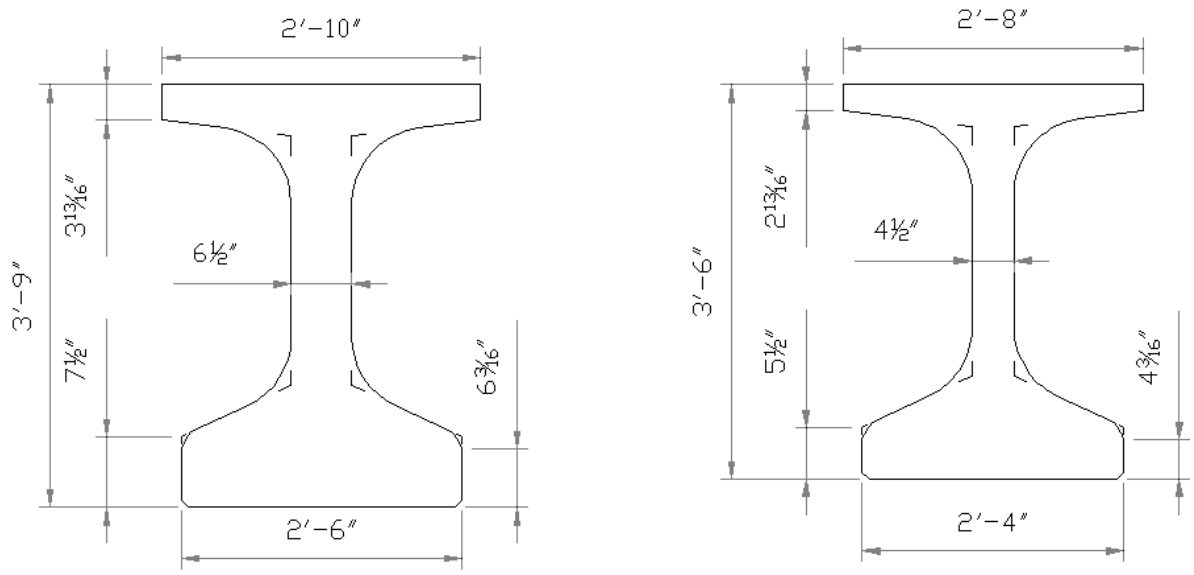

(a) **(b)**

FIGURE 3.5 IDOT BTCIIO 45 in. (1.14 m) Girder: (a) Typical (b) Modified.

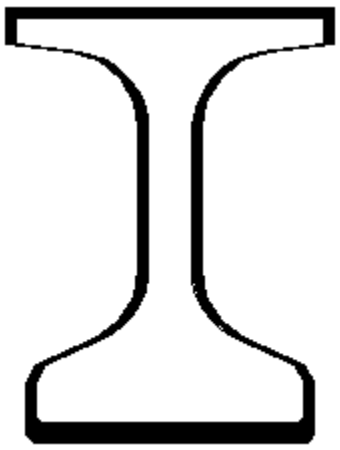

FIGURE 3.6 Modified BTCIIO Girder Superimposed on a Typical BTCIIO.

A comparison of the Iowa girder's cross-sectional area and volume is shown in Table 3.2. The table compares the respective cross-sectional areas and the required volume of concrete per girder. It is evident that there was a significant reduction in the cross-sectional area and in the overall volume of concrete needed to cast the 111.0 ft (33.83 m) beams. Overall the modified shape resulted in the saving of 40% of concrete material in the girders, compared to the typical BTCIIO beam.

TABLE 3.2 Comparison of the BTCIIO and Modified BTCIIO Girders.

Girder	Cross-Sectional Area ft^2 (m^2)	Volume for Bridge ft^3 (m^3)
BTCIIO	4.79 (0.445)	531.5 (15.0)
Modified BTCIIO	3.41 (0.317)	378.5 (10.72)

An interesting feature is the behavior of UHPC with regards to creep and shrinkage. At the time the bridge was designed, there was limited research on UHPC's behavior in creep and shrinkage. Due to the fact that UHPC contains more cementitious material than conventional concrete, the overall creep and shrinkage was estimated to be significantly greater than NSC and HPC. To provide for the higher expected shrinkage and creep an additional 1.15 in. (29.1 mm) was added to the overall beam length, as specified in the design plans, to account for the creep, shrinkage and elastic shortening (Bierwagen and McDonald 2005).

Prestressing was provided by 49 - 0.6 in. (15 mm) Grade 270 - low relaxation strands, stressed to 72.6% of ultimate strength, per beam (see Figure 3.8). No mild steel reinforcement (i.e., shear, confining, or temperature and shrinkage reinforcement) is used in the beam. Harped and debonded strands are used to control end stresses. The reasoning behind the decision to harp and debonded strands was concern that the improved bond strength of UHPC would create a concentration of release forces at the junction of the flange and the bottom web (Bierwagen and McDonald 2005). The final decision to control the release forces was provided for in three ways:

1. harping five strands;
2. debonding a total of 16 strands in two groups at 3.0 ft (0.91 m) increments; and
3. two partial length bonded strands in the top flange.

Due to the geometry restrictions of the web the five harped strands are all in a single column as they move into the web from the bottom flange. Strands were debonded in the bottom flange in two groups (Figure 3.7). The first group, at 6.5 ft (1.98 m) from the end of the beam, eight strands were debonded in a symmetric pattern. Then at 3.5 ft (1.07 m) from the end of the beam an additional eight strands were debonded. The final result was 16 debonded strands at the end of the beam out of the total 26 strands in the bottom bulb. Finally, in the top flange two strands are bonded from the end of the beam out to a distance of approximately 6.5 ft (1.98 m) and then cut. This is a common practice to help control end stresses.

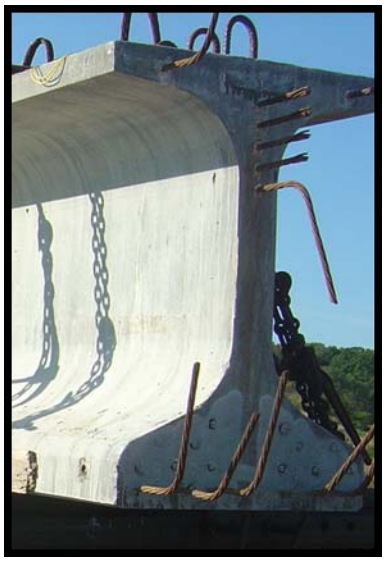

FIGURE 3.7 Strands and Lifting Devices for BTCIIO.

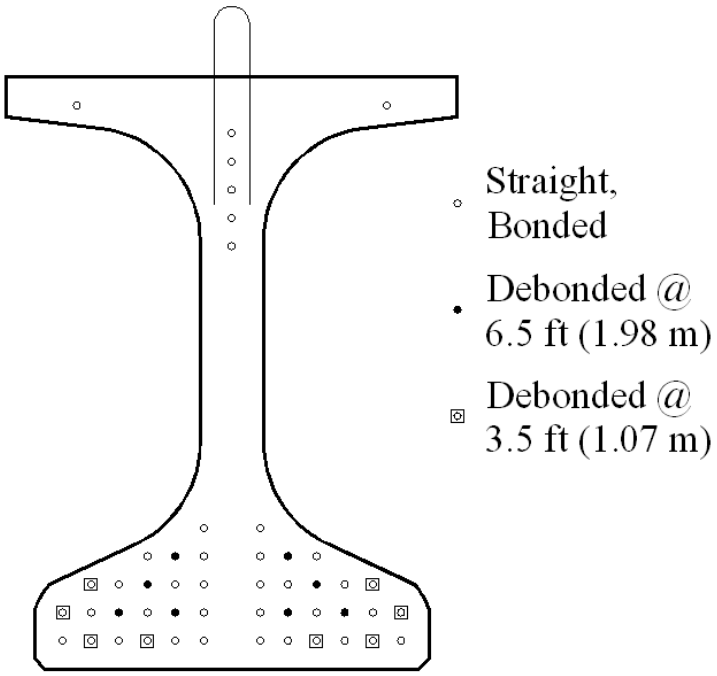

FIGURE 3.8 Strand Layout and Mild Steel Reinforcement of the Modified BTCIIO Girder.

3.1.4 Specifications

Construction specifications used are from the IDOT and the design specifications are AASHTO LRFD, 2nd edition (1998), with modifications. The design stresses are in accordance with the AASHTO LRFD Bridge Design Specifications for Highway Bridges, 2nd edition (1998) and the concrete stresses in accordance with UHPC special provisions for this project.

In a phone conversation, Dean Bierwagen, the designer of the bridge from IDOT, said that the French *Interim Recommendations* produced by the Service d`études techniques des routes et autoroutes of the Association Française de Génie Civil (SETRA/AFGC) (2002), was looked at as a design guide, but the specification is specific to the French Code which made it difficult for him to use. He found that the *Design Guidelines for UHPC Prestressed Concrete Beam* (2000) by N. Gowripalan and R.I. Gilbert by the University of South Wales was more useful to him as he designed the UHPC beams. He also mentioned that the *Recommendations for Design and Construction of Ultra High Strength Fiber Reinforced Concrete Structures (Draft)* (2006) from Japan were useful to him as well. These guidelines provided suggested design formulas and limit states for UHPC.

3.1.5 Project Timeline

The Mars Hill Bridge is the first bridge in the United States constructed with UHPC. Because UHPC has different characteristics the design process is not typical of normal or high strength concrete design. The IDOT incorporated several new design steps in the process of designing the bridge beams, which are listed below (Bierwagen and McDonald 2005):

1. UHPC design seminar
2. Test batching
3. Review of precasting plants
4. More test batching
5. Casting of beams to test flexure and shear
6. Testing of beams
7. Construction of bridge
8. Two year evaluation of beam after construction completed

To initiate the project experts in the area of UHPC gave presentations to explain design issues, material testing, and precasting topics to familiarize the people on this project with UHPC (Bierwagen and McDonald 2005).

Precasting plants in Iowa were certified by LaFarge to produce UHPC. These plants had a number of concerns about using Ductal® cement, including:

1. High cost of the material
2. Longer mixing time

3. Possible damage to mixing equipment
4. Proper placement in the forms and producing the complete batch at one time
5. Inadequate forms to compensate for expected large shrinkage values of UHPC
6. Long setting and curing times, resulting in lost production time in the casting beds
7. Lack of testing equipment

These concerns resulted in higher than expected bids from the precastors in Iowa (Bierwagen and McDonald 2005), thus, LaFarge in Winnipeg, Canada was selected to produce the test beams and production beams.

3.1.6 Testing of Materials and Testing of Experimental Beams

The IDOT and the Center for Transportation Research and Education at Iowa State University tested concrete cubes and test beams of various sizes to determine the compressive strength and better understand flexural and shear resistance behavior of UHPC.

Ductal® was used for this project. Table 3.3 shoes the material identity card for this concrete.

TABLE 3.3 Materials Identity Card of Ductal® (Bierwagen and McDonald 2005).

Parameter	Value
Release Compressive Strength	12.0 ksi (100.0 MPa)
Release Modulus of Elasticity	5,700 ksi (40.0 MPa)
Final Design Compressive Strength	28.0 ksi (165.5 MPa)
Final Modulus of Elasticity	7,820 ksi (55.2 MPa)
Allowable Tension Stress at Service	0.6 ksi (4.1 MPa)
Allowable Compression Stress at Service	14.4 ksi (99.3 MPa)
Unit Weight of UHPC Concrete	156 pcf (2499 kgcm)

3.1.6.1 Material Testing

Uniaxial compression tests were performed on concrete cubes with a side length of 2.0 in. (51 mm). The cubes have uniform, smooth surfaces which facilitate the gathering of accurate data from the compression tests. Cubes were cast and cured with the experimental beams and under two other curing conditions (see Table 3.4). The uniaxial tests are described by ASTM C-109 *Standard Test Method for Compressive Strength of Hydraulic Cement Mortars [using 50 mm (2 in.)] Cube Specimens* because of the high compressive strength the specimens were loaded at a rate of 300 lb/sec (1.33 kN/sec) which is above the described standard (Degen 2005).

TABLE 3.4 Results from UHPC Cubes (Degen 2005).

Curing Method	Average f'_c ksi (MPa)	Standard Deviation ksi (MPa)
194°F (90°C)	25.12 (173.2)	4.32 (29.8)
Cured with Beam	24.56 (169.34)	2.91 (20.1)
Room Temperature	21.5 (148.2)	3.98 (27.4)

Results of the uniaxial compression tests show that curing methods have a significant effect on the compressive strength of the concrete, as seen in Table 3.4. The cubes cured with the beam averaged 24.56 ksi (169.3 MPa) with a standard deviation of 2.91 ksi (20.1 MPa) which is the most consistent data.

Prism flexure tests were also performed on UHPC test samples that were cast and cured with the test beams. Prisms had dimensions 1.57 in. x 1.57 in. x 6.30 in. (40 mm x 40 mm x 160 mm) according to ASTM C-78 *Standard Test Method for Flexural Strength of Concrete (Using Simple Beam with Third Point Loading)*. This guideline is for conventional concrete and had to be modified for this experiment. The cracking load of conventional concrete is different than the cracking load of UHPC. Thus, for the UHPC a cracking load was defined as the point when the data of load versus displacement diagram was no longer linear, this was determined to happen at a load of 0.9 kips (4.0 kN), which corresponds well to published data (Degen 2005). Table 3.5 summarizes the results that were determined from the prism testing.

TABLE 3.5 Results from Prism Flexural Testing (Degen 2005).

Curing Method	Average Flexural Cracking Tensile ksi (MPa)	Standard Deviation ksi (MPa)
194°F (90°C)	1.16 (8.0)	0.21 (1.4)
Cured with Beam	1.04 (7.20)	0.12 (0.8)
Room Temperature	0.930 (0.64)	0.12 (0.8)

FIGURE 3.9 Test Prism from Flexural Testing of Mars Hill Bridge.

FIGURE 3.10 Close View of Crack Bridging Fibers in Test Prism.

FIGURE 3.11 Sample of 0.5 in. (12 mm) Steel Fibers Used in UHPC Mix for Mars Hill Bridge.

3.1.6.2 Large Scale Testing: Single Experimental Beam with 71.0 ft (21.64 m) Length

A single 71.0 ft (22.0 m) test beam was cast that had an identical strand layout and design to the production beams. This test beam was used to verify design assumptions of the production beams (Bierwagen and McDonald 2005) and "to collect information about the structural performance of UHPC" (Degen 2005), through flexure and flexure-shear testing. A total of five fiber optic strain gages were attached to the bottom prestressing stands during casting (Bierwagen and McDonald 2005). In addition, 19 strain gages were attached to the beam to monitor its behavior during testing (Degen 2005).

The flexure test consisted of applying four point loads near the near midspan. The beam was loaded with a total of 243.0 kips (1,081 kN) and then inspected for cracks. After inspection the load was increased to 265.0 kips (1,139 kN), approximately equal to the service load conditions (Degen 2005). In order to allow for shear testing, the beam was not loaded to the ultimate load condition to prevent damage and allowing for subsequent testing.

According to Degen, "the primary purpose of the flexure test was to provide reassurance to the design engineer that the beam had sufficient capacity for implementation in the first

United States UHPC bridge" (2005). Results showed no cracking under service loads. Furthermore, the beam had sufficient strength to bear the service loads without the benefit of composite action with the effective area of the deck.

Table 3.6 compares the flexural capacity of the beams determined from analytical methods. Note that there is no data for the ultimate level of experimental capacity because the beam was not loaded to failure. The experimental moment is the moment the beam resisted from external forces during testing up to a measured non-linearity in the of the stress-strain diagram. The analytical moment is the expected capacity of the bridge beam when the effective area of the deck is used in composite computations. The applied moment on the bridge beam is the expected loading on the actual bridge beams during service.

Results show that the analytical methods used to determine the moment capacity are sufficient to predict the capacity of the beam. As expected the capacity of the bridge beam is larger due to the composite action between the beam and the deck.

TABLE 3.6 Moment of Test and Bridge Beams (Degen 2005).

Limit State	Experimental Moment Capacity of Test Beam kip-ft (kN-m)	Analytical Moment Capacity of Bridge Beam kip-ft (kN-m)	Applied Moment on Bridge Beam kip-ft (kN-m)
Service	3730 (5,057)	4760 (6,454)	4624 (6,269)
Ultimate	-	7620 (10,330)	7350 (9,965)

According to Degen, "the primary purpose of the shear testing was to assess the shear behavior of UHPC in a full scale specimen and also the shear strength of the beam was of interest to insure sufficient capacity of the UHPC girders for the Wapello County bridge." In addition, data gathered was used to develop a model for shear design.

The shear test used the same point load configuration as the flexure tests with the loads applied at 7.5 ft (2.3 m) (approximately 10% of beam length) from the end of the beam. Loads were applied in three increments of 369.8 kips (1,645 kN), 397.6 kips (1,762 kN), and 594 kips (2,642 kN). At each of these three loads cracking was heard and the beam was inspected for cracks (Degen 2005). The beam was supported in such a way that arching and deep beam actions were reduced. Ultimately, tensile failure in the web was the failure mode of the test beam.

Results show that the capacity of the beam was greater than the applied forces (see Table 3.7), indicating that the design of the bridge was safe (Degen 2005). Because UHPC is a new material and its behavior in shear is still under research the analytical shear capacity was taken to be the same as the experimental shear capacity. The applied shear on the bridge beam is the expected force as a result of dead and live loads. For UHPC beams it is important

to be capable of predicting the initiation of cracking because cracking is not allowed at the service limit state. Knowing the service capacity allows the design engineer to have confidence that the structure will perform as desired.

TABLE 3.7 Shear Capacities of the Test Beam and the Bridge Beam (Degen 2005).

Limit State	Experimental Shear Capacity of Test Beam kip (kN)	Analytical Shear Capacity of Bridge Beam kip (kN)	Applied Shear on Bridge Beam kip (kN)
Service	312 (1,388)	312 (1,388)	210 (934)
Ultimate	497 (2,211)	497 (2,211)	301 (1,339)

Degen further determined from the experimental data and analytical data that cracking in the beam can be accurately predicted by using the modified field compression theory (MFCT) (Degen 2005).

Finally, a shear-flexure test was performed. The purpose of this test was to "determine the behavior of UHPC under combined flexure and shear loading" (Degen 2005). The four point loads were applied to the beam in a different pattern than that of the flexure and shear test. The configuration and placement optimized the effects of shear and flexure in the test. The beam was loaded near failure as indicated by the increase in deflection without increased loading. One finding showed that experimental deflection correlated well with the analytical solution.

3.1.6.3 Small-Scale Testing: Experimental Beams with length 4 ft 6 in. (1.37 m) to 6 ft 4 in. (1.63 m)

Additional shear behavior data was gathered through the testing of fifteen, small scale, prestressed beams (see Table 3.8). These small beams were designed in such a way that the flexural capacity was twice the capacity in shear in order to ensure shear failure would be the controlling failure mode (Degen 2005).

The small beams had externally attached strain gages to measure the response of the beams under loading. It was hoped that these experiments would result in greater knowledge of shear behavior, however, the small scale testing experiments "did not provide extensive information about the shear behavior of UHPC" (Degen 2005). This is attributed to the fact that the failure modes of the small beams were not considered to be "pure shear failures" (Degen 2005).

TABLE 3.8 Summary of Small Scale Test Beams.

Section	Depth in. (mm)	Length in. (m)
A	8 (203)	54 (1.37)
B	8 (203)	54 (1.37)
C	8 (203)	54 (1.37)
D	10 (254)	64 (1.63)
E	10 (254)	64 (1.63)

3.1.7 Design and Analysis Methods Used in the Design the UHPC Bridge Girders

Part of the challenge of designing the first UHPC beams in the United States was a lack of American design guidelines that could be used to determine design parameters. There have been several foreign documents produced to give guidance on the design of UHPC structures. The foremost are the *Interim Recommendations* (SETRA/AFGC 2002); *Design Guidelines for UHPC Prestressed Concrete Beam* by N. Gowripalan and R.I. Gilbert of the University of South Wales (2000) and the *Recommendations for Design and Construction of Ultra High Strength Fiber Reinforced Concrete Structures* (2006) from Japan as well as the research model developed by Dr. Franz Josef-Ulm of MIT (2004). These documents were used to determine design values of important parameters which are summarized in Table 3.9. Dr. Ulm was asked to review the design because of his research in the field of UHPC mechanics and analysis. Dr. Ulm reviewed the design and checked the capacities of the modified beam in bending and shear.

TABLE 3.9 Design Parameters Used in the Design of the Mars Hill Bridge (Degen 2005).

Parameter	Mean Value ksi (MPa)
Compressive Strength, f'_c	28.0 (193)
Initial Stiffness, K_o	7820 (19,512)
Postcracking Stiffness, K_1	233 (1,607)
Cracking Strength, Σ_1^-	1.1 (7.6)
Postcracking Strength, Σ_1^+	1.0 (6.9)
Ductile Strength, Σ_2	1.67 (11.5)
Fiber Length, L_f	0.5 in. (12.7mm)

The following design method was taken from the design review performed by Dr. Ulm. The design of the bridge beams is very similar to the design of any conventional slab on concrete girder bridge by the LRFD convention. The loads, both dead and live, are computed by

traditional methods of tributary area and the HL-93 live load was a given condition. In the design brief prepared by Dr. Ulm the service limit state was based on the factored loads "corresponding to the LRFD Service III state for tensile stresses in prestressed concrete component" (Ulm 2004). The equation for Service III load effects is:

$$1.0\ (DC + DW) + 0.8\ (\delta \times LL + IM) \qquad \text{Equation 3.1}$$

where, DC is the dead load of the structural components and non structural attachments; DW is the future wearing surface; δ x LL is the design truck or the design tandem with dynamic allowance; and IM is the design lane load of 0.64 kip/ft (9.4 kN/m) without dynamic allowance.

The only modification for this limit state is described by stating that the beam is not allowed to crack at service loads, in mathematical terms:

$$[[\omega]] = 0 \qquad \text{Equation 3.2}$$

where, ω is the crack dimension in inches. Thus the "characteristic resistance (R) in the Service Limit State (SLS)" for UHPC is,

$$(\phi R)^{SLS} = \phi R([[\omega]] = 0) \qquad \text{Equation 3.3}$$

where, ϕ is the strength reduction factor. At the ultimate limit state the loading effects are calculated according to LRFD Strength I as:

$$1.25DC + 1.50DW + 1.75\ (\delta \times LL + IM) \qquad \text{Equation 3.4}$$

At the Ultimate Limit State (ULS) cracking is allowed and is limited according to the AFGC/SETRA recommendations. The characteristic resistance is described by:

$$(\phi R)^{ULS} = \phi R([[\omega]] = [[\omega]]^{limit}) \qquad \text{Equation 3.5}$$

The crack width limit, $[[\omega]]^{limit}$, is determined based on the presence of reinforcement in the UHPC component. For instance, the web of the Mars Hill beams is unreinforced, thus the allowable crack opening for the UHPC is:

$$[[\omega]]^{limit}_{unreinforced} = 0.01 \text{ in. } (0.3 \text{ mm}) \qquad \text{Equation 3.6}$$

In the bottom flange where there are prestressing strands, and thus, the component is reinforced, the allowable crack opening is:

$$[[\omega]]^{limit}_{reinforced} = \text{minimum of } \frac{L_f}{4} \text{ or } \frac{h}{100} \qquad \text{Equation 3.7}$$

where, L_f is the length of the fibers used in the UHPC matrix and h is the height of the non-composite UHPC section. Steel fibers in the Ductal® mix were 0.5 in. (13 mm) in length (Degen 2005) and the height of the modified BTCIIO beams is 42.0 in. (1.14 m). Thus, the crack width limit for this bridge is the minimum of:

$$\frac{0.5\ \text{in}}{4} = 0.13\ \text{in.}(3.3\ \text{mm}) \qquad \text{Equation 3.8}$$

or

$$\frac{42\ \text{in}}{100} = 0.42\ \text{in.}\ (10.7\ \text{mm}) \qquad \text{Equation 3.9}$$

Therefore, for this bridge the crack width was limited to 0.01 in. (0.3 mm) in the web and 0.13 in. (3.3 mm) in the bottom flange.

The concrete material properties and the beam geometry was assumed to be fixed, thus the focus of the design was on the prestressing strands to support the loads.

The maximum, number of 0.5 in. (13 mm) and 0.6 in. (15 mm) strands was determined based on the modified BTCIIO girder geometry. Knowing the number of strands allows for the total prestressing force on the section to be determined. To analyze the composite section capacity, the section was decritized into rectangular elements of equal widths to simplify the analysis. The prestress force, γ, was taken as 80% of ultimate stress. It is at this point that the section capacity can be determined. In order to meet the design moment criteria the following equations must both be satisfied simultaneously:

$$M_{SLS}(x_M) \leq \phi_M M_R^{SLS} \qquad \text{Equation 3.10}$$

$$M_{ULS}(x_M) \leq \phi_M M_R^{ULS} \qquad \text{Equation 3.11}$$

where, M_{SLS} is the design moment at the service limit state at position x_M from the end of the beam; ϕ_M=0.85 is the strength reduction factor used specifically for Ductal®; and M_R^{SLS} is the moment capacity of the section as a function of the prestressing force and the distance of the prestressing strands from the bottom of the beam.

It was found that a prestressing force at the service limit of 2,140 kips (9,519 kN) and a prestressing force at the ultimate limit state of 2,490 kips (11,076 kN) is required. The prestressing force at the ultimate limit state is the largest and therefore governs the design prestressing force. This is a high level of prestressing. This level of prestressing could possibly lead to excessive deformation of the strand at transfer, during transport to the construction site, and during construction (Ulm 2004).

The prestress losses were calculated according to procedure given in LRFD 5.9.5. The prestress losses by this method take into account the initial relaxation, elastic shortening, shrinkage, and creep. With regards to the prestressing force in the strands the experimental

results revealed that there were approximately 27.2% losses of the prestressing force and the analytical result from AASHTO of 30.4% losses shows that AASHTO methods of calculating loss are conservative by 11.8%. This demonstrates that the AASHTO LRFD method is a conservative and viable way to calculate prestress losses in UHPC.

The shear design considers criteria for both the service limit state and the ultimate limit state.

At the service limit state the stress component must be less than the cracking strength of the UHPC, $\Sigma_1^- = 1{,}100$ ksi (7,600 MPa). Symbolically, that is:

$$\sigma = \frac{\sigma}{2} + \sqrt{\left(\frac{\sigma}{2}\right)^2 + \tau^2} \leq \Sigma_1^- \qquad \text{Equation 3.12}$$

where, σ is the longitudinal stress near the support from the prestressing strands and τ is the shear stress in the section. By rearranging the above equation the maximum admissible shear stress can be determined as:

$$\tau_{lim} = \Sigma_1^- \sqrt{1 - \frac{\sigma}{\Sigma_1^-}} \qquad \text{Equation 3.13}$$

The mean strength of the section can be determined by multiplying the allowable shear stress by the effective web area, represented by:

$$\phi_v V_R^{SLS} = A_w^{eff} \Sigma_1^- \sqrt{1 - \frac{\sigma}{\Sigma_1^-}} \qquad \text{Equation 3.14}$$

where, ϕ_M=0.85 is the strength reduction factor for Ductal®; V_R^{SLS} is the capacity of the section in shear; and A_w^{eff} is the effective shear area of the web which is approximately the width of the web multiplied by the height of the web. By this calculation the proposed web thickness originally submitted by IDOT was determined to be approximately 10% under capacity. It was recommended to increase the web thickness, and thus, the effective web area to a minimum of 5.0 in. (127 mm) (Ulm 2004).

The ultimate limit state of shear is "based on the premise that crack-bridging fibers, after cracking of the UHPC, carry a part of the shear load; very similar to shear reinforcement" (Degen 2005).

Without traditional mild steel shear reinforcement (stirrups) the ultimate limit state shear capacity is represented by:

$$\phi_V V_R^{ULS} = \phi_c V_c + V_p + \phi_f V_f \qquad \text{Equation 3.15}$$

where, V_R^{ULS} is the design strength of the section at the ultimate limit state, Φ_c=0.66; V_c is the contribution of the UHPC, according to AFGC/SETRA recommendations. The equation in terms of English units is expressed below (Ulm 2004).

$$\Phi_c V_c = 0.09\sqrt{f_c'}\, b_w\, z \qquad \text{Equation 3.16}$$

where, b_w is the web thickness; z is the effective height-within the UHPC section (between the prestressing cable and the compression flange); V_p is the contribution of the inclined prestressing tendons (Ulm 2004); and V_f is the contribution of the crack-bridging 0.5 in. (13 mm) steel fibers and calculated as:

$$V_f = \frac{A_w^{eff}\,\sigma_p}{\tan(\beta_u)} \qquad \text{Equation 3.17}$$

The strength reduction factor, ϕ_M, is set at a lower value of 0.66 to account for the random orientation of the fibers and the variability of UHPC material.

The effective fiber area is calculated as $A_w = b_w\, z$, and σ_p is the residual UHPC tensile strength related to the strain at the ultimate and service limit state of the UHPC. β_u is the angle of inclination of the compression strut with a lower bound of 30° (Ulm 2004).

It is interesting to note that the contribution of the concrete and the fibers have sufficient capacity to carry the shear loading. The inclined strands were ignored in the strength calculations except that the web was considered reinforced by the inclined strands, thereby increasing the allowable crack width.

Degen analyzed the beam in shear using the modified compression field theory (MCFT) and it was found that MCFT was conservative and therefore appropriate for predicting the shear strength of the UHPC beam.

In the final hardened state the UHPC has sufficient strength to resist high levels of compression due to prestressing, however, at transfer care must be taken with due consideration as the UHPC has not attained its high strength. The anchorage zone may need to be reinforced to "ensure a smooth stress transfer from the bottom flange into the beam" (Ulm 2004).

For composite section capacity, the deck was transformed into an equivalent area of UHPC concrete using the traditional equation for the modular ratio:

$$n = \frac{E_{UHPC}}{E_{slab}} \qquad \text{Equation 3.18}$$

This bridge is unique though in the load reduction factors, η. The ductility factor is typically taken to be 1.0 for normal ductility, but the behavior of the designed UHPC beams allowed have a load reduction factor of 0.95 instead. The redundancy factor was taken as 1.0 which is

typical. Finally, the location of the Mars Hill Bridge is in a rural part of Wapello County and the importance factor was taken as 0.95 for low importance instead of the traditional 1.0 (Degen 2005).

A final note on the design of this bridge, the UHPC allowed for a smaller beam cross section to carry the service and ultimate loads more efficiently than a typical BTCTIIO girder. However, a more efficient use "of the UHPC material would consist of replacing the concrete slab by an integrated UHPC slab" (Degen 2005). It is clear that the new π – shaped girder developed by MIT makes a better use of the UHPC material characteristics.

3.1.8 Conclusion

The work done by Degen has shown that the procedures used in the design of the beams are sufficient to provide adequate levels of flexural capacity at the service level and the ultimate level. The proposed design procedure by Degen and Ulm showed that the beams were conservatively designed as indicated by the lower predicted design strengths using material mechanics than the experimental strengths.

3.2 CAT POINT CREEK BRIDGE, RICHMOND COUNTY, VIRGINIA

3.2.1 Introduction

The Cat Point Creel Bridge in Richmond County, Virginia, the second bridge in the U.S. to utilize UHPC, opened in 2008 (Figure 3.12). The Cat Point Creek Bridge has ten spans, with one span designed with UHPC girders to support traffic. The purpose of this was to allow a local precast beam fabricator to gain experience with the new concrete product. The goal was to have a fabricator comfortable in the production of UHPC so that in the future UHPC can be more fully implemented into the Commonwealth of Virginia's bridge inventory.

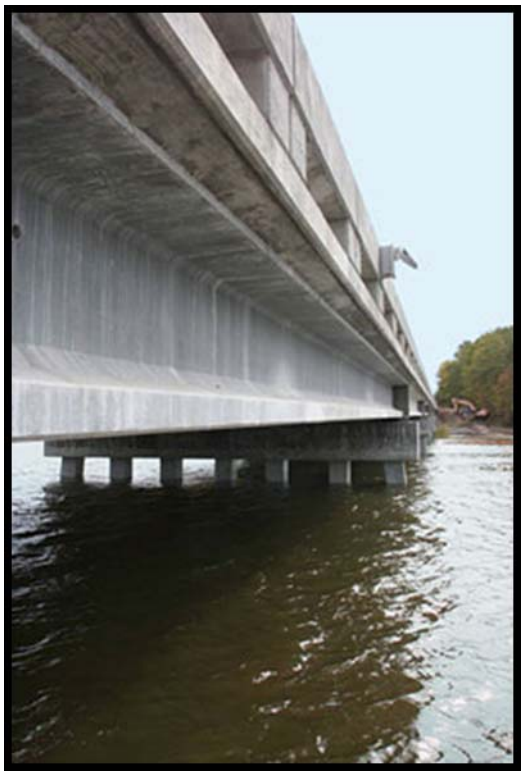

FIGURE 3.12 Second Bridge Built with UHPC in Richmond County, Virginia.

3.2.2 Bridge Description

The bridge is ten spans continuous for live load. The second span utilizes UHPC with a 28-day compressive strength of 23.0 ksi (158.6 MPa); the other spans (i.e., spans 1 and 3 through 10) use HPC with a compressive strength of 8.0 ksi (55.2 MPa). All spans from centerline-to-centerline of supports measure 81.5 ft (24.8 m). The bridge has no vertical or horizontal curvature, nor is it skewed. All spans use five BT-45 in. (1.14 m) spaced at 9.08 ft (2.8 m), with variable haunches to account for the crown at the centerline of the bridge of 0.25 in. per foot (21 mm per meter). The deck uses conventional concrete with a 28-day

minimum compressive strength of 4.0 ksi (27.6 MPa) and has a minimum dimension of 8.5 in. (216 mm) and has an overhang of 2.83 ft (0.86 m). The width of the deck is 42.3 ft (12.9 m) out-to-out and the travel way width is 40.0 ft (12.2 m) to accommodate three traffic lanes. Concrete barrier rails are used. The beams are braced by C15 channels in each bay at the midpoint of each span. Supporting the structure are integral abutments and intermediate bents on driven piles (Bridge Plans). Figure 3.14 shows the bridge cross-section and Table 3.10 summarizes the bridge geometry.

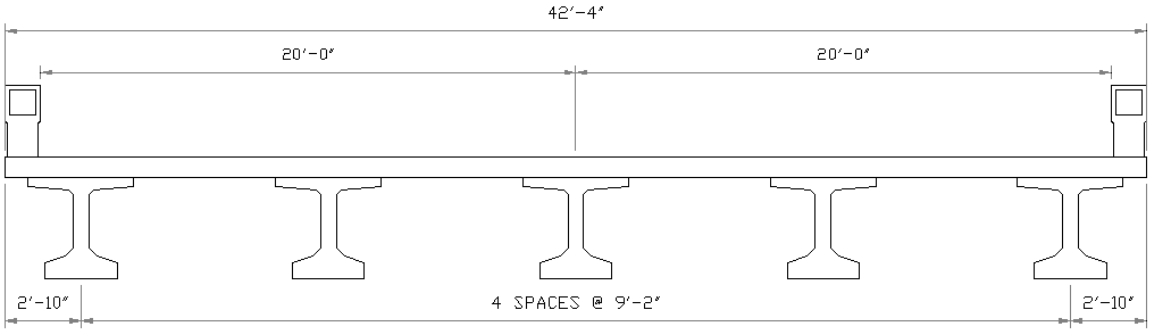

FIGURE 3.13 Cross-Section of Cat Point Creek Bridge.

TABLE 3.10 Cat Point Creek Bridge Geometry.

Parameter	Description
Span Type	10 span continuous
Clear Span	81'-6" (24.84 m)
Curvature	None
No. of Girders per Span	5
Type of Girder	BT-45" (1.14m)
Girder Spacing	9'-2" (2.79 m)
Width of Deck	42'-4" (12.9 m)

3.2.3 UHPC Beam Description

With constructability in mind, it was decided that a standard AASHTO girder [precast bulb tee (PCBT)-45 Virginia Department of Transportation (VDOT), see Figure 3.14] would be used in the design of this bridge. As shown in Figure 3.15, all beams (both UHPC and high strength concrete) have 40 - 0.5 in. (12 mm) Grade 270-low relaxation strands. Six strands are linearly harped from the top of the beam to the harp point 7.83 ft (2.39 m) from the centerline of the beam, about which the beam is symmetrical. An additional quarter-length strand is used at the beam ends in each of the top flanges of the UHPC beams to control end stresses. Note that these additional strands are not placed in the HSC beams. No traditional mild steel reinforcement is placed within the UHPC beams. From a phone discussion with Bryan Silvis, the VDOT bridge engineer on this project, the original intent was to retain the stirrups in place a means of precaution and the risk adverse policies of the state. But it was shown by Dr. Ulm (2004) that the tensile strength of the UHPC and the steel fibers provided

sufficient strength to resist the shear forces produced by dead and live loads. However, confining reinforcement is still used in the bottom bulb surrounding the prestressing strands. There are three loops of mild steel across the top flange to resist the horizontal shear and to provide composite action between the beams and deck (see Figure 3.16). The connection is the same in the HPC spans as this is a standard practice of VDOT.

It should be noted that the prestressing force in each strand is the same in the UHPC beams and the HPC beams.

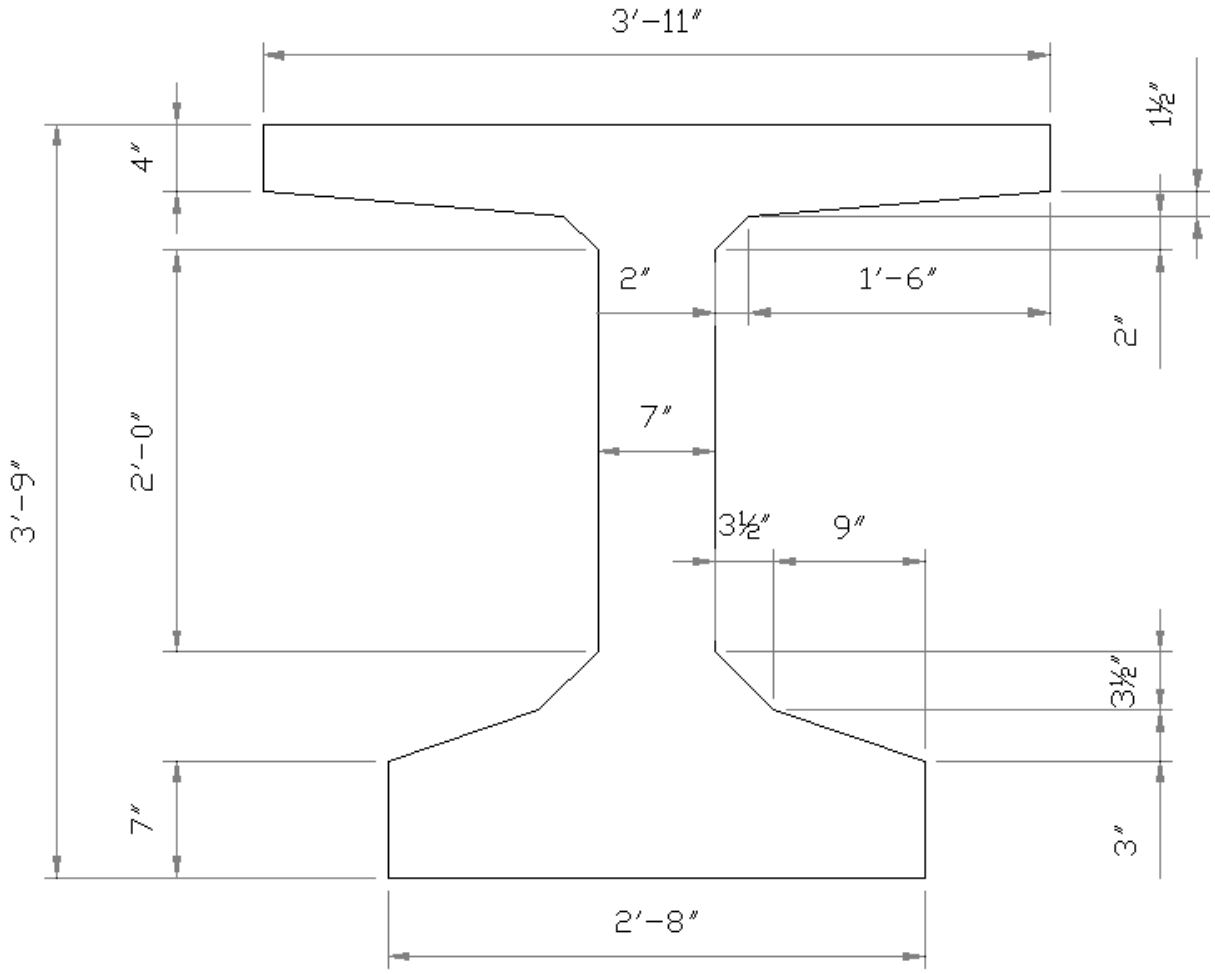

FIGURE 3.14 Dimensions of the VDOT PCBT-45 (1.14 m).

3.2.4 Specifications

The construction specifications used were the VDOT Road and Bridge Specification, 2002. The design specifications included the AASHTO Standard Specifications for Highway Bridges, 1996; 1997 and 1998 Interim Specifications; and VDOT Modifications. In addition, MIT provided guidance on limits for UHPC beams at the service and ultimate limit states. The aim of these limits is to ensure that UHPC fails in a ductile manner, deflections are

limited, and bond rupture does not occur in the prestressing strands (Ulm 2004). It is important to note that the goal of the project was to gain experience with UHPC, not to optimize the beam design.

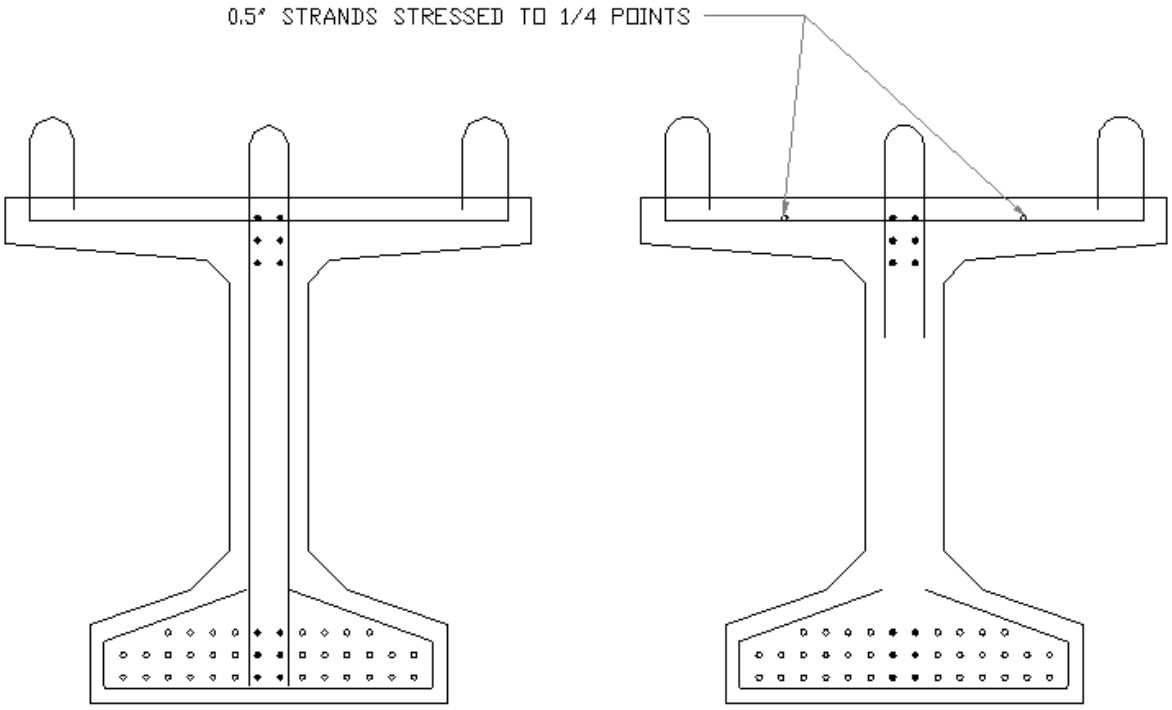

(a) **(b)**

FIGURE 3.15 VDOT PCBT Strand Layout and Mild Steel Reinforcement: (a) HPC (b) UHPC.

3.2.5 Analysis Methods

The second span of this bridge is unique in the world in its design and analysis as it is the first to use the MIT recommendations (Ulm 2004). The MIT recommendations are a conglomerate of the SETRA/AFGC cracking guidelines and shear criterion, LRFD design philosophy and design factors and a stress-strain diagram developed by MIT for UHPC (Ulm 2004). It should be noted that since the design and construction of the Cat Point Creek Bridge new MIT recommendations have been developed that are similar to what is described but are more efficient (Ulm 2004).

The design of the bridge beams for the Cat Point Creek Bridge is essentially the same as the Mars Hill Bridge and the design procedure is not repeated here.

Because the same sections are used for the HPC and the UHPC the strands play an important role in the determination of the section capacity. From the bridge plans provided by Bryan Silvis of the VDOT a comparison was made between the HPC and the UHPC girders. It is

quickly noticed that the deflection are very similar in value. Also the UHPC has two additional strands in the top flange of the beam (see Figure 3.15). These two strands are straight and bonded up to the quarter points of the beam. These two strands are only stressed to 1.0 kip (4.4 kN). Traditionally, this type of layout helps to control end stresses. End stress control is a consideration in UHPC because the improved bond of the concrete to the strands and creates a concentration of forces at the end of the beam.

The approach used by MIT to determine the number of prestressing strands is to divide the beam into discrete rectangular sections and the strands are assumed to be grouped into single rows at the same height. From this point it is possible to determine the required prestressing force that is required to resist flexure at the service and ultimate limit states (Ulm 2004). This type of analysis determines the prestressing force that is required for flexural strength at the service and ultimate limit states.

The maximum, and thus conservative, number of 0.5 in. (13 mm) and 0.6 in. (15 mm) strands was determined based on the VDOT PCBT-45 girder geometry. From this quantity the total prestressing force was determined. Prestress force is assumed to be 80% of the ultimate capacity.

It was found that a prestressing force at the ultimate limit state (the governing limit state) of 2,100 kips (9,341 kN) is required. Similar to the Mars Hill Bridge, this is a high level of prestressing, which could possibly lead to excessive deformation of the strand at transfer, during transport to the construction site, and during construction (Ulm 2004).

To determine the moment capacity of the section the loads are calculated according to standard practice. Equilibrium and plane section remain plane are still valid for UHPC. The tensile strains in the bottom flange for simply supported members must be limited at the service and ultimate limits as stated before. The stress-strain behavior is different than NSC or HPC, thus it is defined differently. Whereas in NSC and HPC the tensile strength of the concrete is neglected, the stress-strain model for UHPC accounts for elastic tensile behavior and post-cracking tensile behavior (Ulm 2004).

The MIT recommendations for shear are similar to the AFGC/SETRA recommendations with regards to the fact that shear capacity is calculated differently for the service and the ultimate limit states. At the service limit state the beams are not allowed to crack. Therefore the stresses produced by loads must be less than the cracking strength (Ulm 2004).

For the ultimate limit state it is assumed that the "matrix has cracked and that the fibers bonded to the matrix carry part of the shearing load" (Ulm 2004). Because of the short fiber length typically used, about 2.0 in. (51 mm), the maximum crack width criteria is in place to ensure that the fibers will remain bonded to the concrete and not pull out of the matrix.

The UHPC beams used at Cat Point Creek have sufficient shear resistance to carry all loads at the service and ultimate limit state without using mild steel stirrups to provided additional strength to the section.

3.2.6 Conclusion

The prestress UHPC girders differ from the HPC only in the fact that the tensile strength of the UHPC allowed for the shear stirrups to be removed from the UHPC beams. The UHPC beams are a "one-to-one replacement of conventional concrete with UHPC" (Graybeal 2009). This project did not garner the attention that the Iowa bridge did because it was the second bridge constructed and only a single span utilizes UHPC.

It is apparent from the bridge plans that the section was not optimized to take advantage of UHPC material properties. Also the cross sections have almost identical cross-sections, which leads to the conclusion that the UHPC girder must have significantly greater moment resistance than the HPC girder. For this bridge there are several optimization possibilities. First, the web could be reduced from the typical dimension of 7.0 in. (178 mm) to 6.0 in. (152 mm) (Ulm 2004). Second, the top flange was highly overdesigned. It fact, it "could be eliminated, if not required for other purposes" (Ulm 2004). Similar to the Iowa bridge, Dr. Ulm recommended that an integrated UHPC deck would be an ideal optimization.

4 UHPC PARAMETRIC STUDY: FLEXURE

Three types of typical prestressed bridges used predominantly in New Mexico were identified. These three structure types are:

1. Single simple spans
2. Two-span continuous for dead and live loads
3. Three-span continuous for dead and live loads

A representative structure was identified for each of these three bridge types. The single simple span representative is the pair of bridges at the I-25/Doña Ana Interchange. The continuous representative was found in one structure, the Sunland Park River Crossing Bridge, which as a two-span continuous unit and a three span continuous unit.

These bridges were designed HPC. In this parametric flexure study comparisons are based on these as-designed/as-built bridges with HPC and an equivalent bridge that employs UHPC. The goal of this flexure parametric study is to optimize the usage of UHPC, resulting in a reduced required volume of girder concrete by reducing the number and size of the girders. This study will use girder cross-sections that are standard in the state of New Mexico.

Several UHPC material characteristics were identified from literature that are important to prestressed concrete girder design. These characteristics include: modulus of elasticity, modulus of rupture (i.e., allowable tensile stress), creep, and shrinkage. Both the modulus of elasticity and modulus of rupture were considered in this task based on literature findings related to UHCP properties. Creep and shrinkage are calculated by the current AASHTO specifications because without specific material testing, modified design values cannot be accurately used (AASHTO 2007).

4.1 PARAMETRIC FLEXURE STUDY I-25/DOÑA ANA INTERCHANGE

The I-25/Doña Ana Interchange Bridge (Figure 4.1) is a simple span structure with a length of 112.5 ft (34.29 m). There is no curvature in the horizontal direction and a slight vertical curve; there is no skew. Each span has six typical New Mexico Department of Transportation (NMDOT) BT-63 girders, spaced at 7.25 ft (2.21 m) (Figure 4.2), which compose the cross-section of the superstructure along with an 7.5 in. (191 mm) cast-in-place deck of conventional concrete with a compressive strength of 4.0 ksi (27.6 MPa). The deck is 43.0 ft (13.11 m) wide with a 2% grade. The travel way dimension is 40.0 ft (12.19 m), allowing two travel lanes to cross the bridge. The deck overhang is 3.38 ft (1.03 m). The beams are braced by intermediate 0.325 in. (9.53 mm) steel bent plate diaphragms at every third point of the span. Supporting the superstructure is an abutment at each end of the six beams with wingwalls. The traffic barrier is a 42.0 in. (1.07 m) concrete guard rail.

This bridge was designed according to AASHTO Standard Specifications 17th edition and the interims of 2002.

FIGURE 4.1 North Bound Structure of I-25/Doña Ana Interchange.

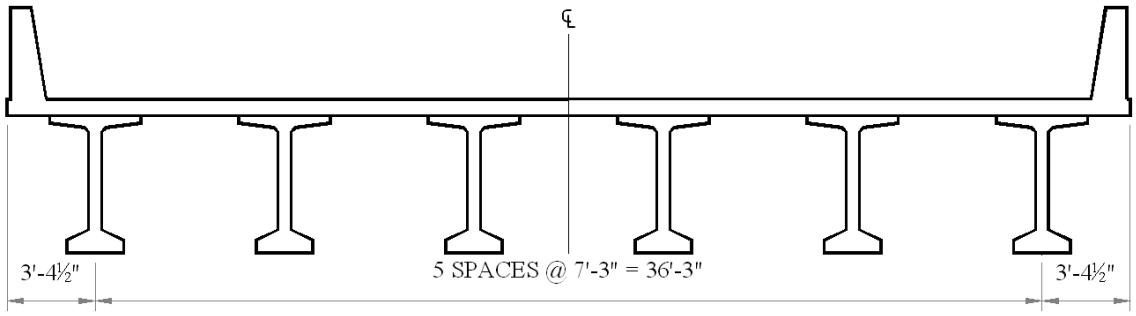

FIGURE 4.2 Cross-Section of I-25/Doña Ana Interchange, as Modeled in CONSPAN®.

4.1.1 CONSPAN® Flexure Analysis for I-25/Doña Ana Interchange

CONSPAN®, a commercially available, comprehensive design and analysis software for precast and prestressed beams, is used in this study for the design and analysis of the structure. Table 4.1 shows the design matrix developed to guide the comparison between HPC and UHPC bridge girders. The design matrix considers various parameters. Parameters that were considered constant included: deck width; ratio of deck overhang to girder-to-girder spacing (46.6%); deck compressive strength; harped strand pattern; and girder length. Variable parameters included: number of girder lines; deck thickness; release and final

compressive strengths; modulus of elasticity; modulus of rupture (i.e., allowable tensile stress); and diameter of prestressing strands. The BT-63 in the design plans has modified dimensions based on the NMDOT standard drawings; however, the BT-54, Type III, Type II and Type I girder options were based on NMDOT standard dimensions. The I-25/Doña Ana Interchange was designed based on Load Factor Design (LFD); thus, comparisons made with UHPC are made using the LFD design methodology.

TABLE 4.1 Design Matrix for I-25/Doña Ana Interchange.

Number of Girders	Types of Girders				
	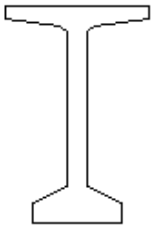 BT - 63	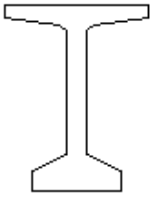 BT - 54	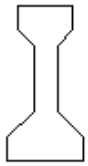 Type III	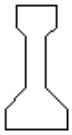 Type II	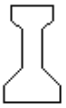 Type I
6	I	II	III	IV	V
5	VI	VII	VII	IX	X
4	XI	XII	XIII	XIV	XV

The roman numerals in Table 4.1 represent the different bridge cross-sections considered. For example, cross-section I consists of six BT-63 girders, cross-section XII consists of four BT-54 girders, etc.

For each cross-sectional configuration, final compressive strengths of 9.5, 15.0, 17.5, 20.0 and 22.5 ksi (65.5, 103.4, 120.7, 137.9 and 155.1 MPa) are used. For each compressive strength, the required number of 0.6 in. (15 mm) and 0.7 in. (18 mm) strands were determined based on the modulus of elasticity calculated by the AASHTO code, AFGC/SETRA equation, and Graybeal equation. In addition, the modulus of rupture is calculated by the AASHTO code and then prestressing strands are manually removed so that tensile stress limits from the literature control the number of strands.

4.1.2 Effects of Modulus of Elasticity

Three design equations from the literature were selected to predict the values of modulus of elasticity for UHPC: (1) AASHTO; (2) AFGC/SETRA; and (3) Graybeal (see Section 2.3.3). Separate equations were considered in order to compare the influence of the modulus of elasticity on the design of the UHPC beams. The AASTHO equation has been shown to overestimate the modulus of elasticity for UHPC. The AFGC/SETRA equation has been shown to most accurately predict the modulus of elasticity based on the least squares method

(Alborn *et al.* 2008). The Graybeal equation conservatively underestimates the modulus of elasticity (i.e., predicted values are lower than measured values).

Using the AFGC/SETRA and Graybeal equations to predict the modulus of elasticity, the required number of strands is similar, with the Graybeal equation occasionally requiring fewer strands. The AFGC/SETRA equation predicts larger values for the modulus of elasticity than Graybeal's equation; therefore, the fewer strands required using the Graybeal equation can be attributed to the smaller modular ratio between the normal strength concrete deck and the UHPC girder.

Due to the conservative nature of the Graybeal equation compared to the AFGC/SETRA equation, live load deflections are greater in magnitude than the former equation. It has been shown in this study that live load deflections are not a controlling limit state for any of the viable bridge cross-sections. Thus, the Graybeal equation was adopted for final design values of modulus of elasticity for the UHPC in this study. This equation requires the fewest strands provides adequate stiffness to control live load deflections. Additionally, the Graybeal equation is applicable over a large range of compressive strengths, 4.0 to 28.0 ksi (27.6 to 193.1 MPa), and has the best fitting scalar coefficient compared to other equations found in literature (Graybeal 2005).

4.1.3 Effects of Modulus of Rupture

To date, there have been no equations presented in the literature to accurately predict the modulus of rupture in UHPC. Therefore, to analyze the effects of the UHPC's increased strength in tension, limiting values for tension reported in the literature are used. Tension stress limits of 1.16 ksi (8.0 MPa) (Gowripalan and Gilbert 2000), 1.3 ksi (9.0 MPa) (Graybeal 2008), 2.0 ksi (13.8 MPa) and 2.4 ksi (16.5 MPa) (AFGC/SETRA 2002) were used to evaluate the influence on the number of strands required. For the range of compressive strengths considered herein, Gowripalan and Gilbert (2000) suggest the lower bound value for tensile strength of 1.16 ksi (8.0 MPa). Graybeal (2008) uses 1.3 ksi (9.0 MPa) as a limiting value for tensile strength. Since the difference in stress between 1.16 ksi (8.0 MPa) and 1.3 ksi (9 MPa) is small, a value of 1.5 ksi (10.3 MPa) was used to aid in generating a trend relating the required number of prestressing strands to the service tensile stress in the girders. An additional limit of 2.0 ksi (13.8 MPa) was also considered in this study, and the upper bound was taken to be 2.4 ksi (16.5 MPa) (Ahlborn *et al.* 2008). It is important to note that in much of the literature, UHPC is considered to have a range of compressive strengths from 21.7 to 31.9 ksi (150.0 to 220.0 MPa) (Ahlborn *et al.* 2008, Graybeal 2008, Gowripalan and Gilbert 2000), which is higher than the range of compressive strengths considered in this study [ranging from 15.0 to 22.5 ksi (103.4 to 137.9 MPa)].

It should be noted, however, that the limiting value of 1.16 ksi (8.0 MPa) is a characteristic value for flexural tensile strength that has a factor of safety of 4 (Gowripalan and Gilbert 2000). Because of the conservative nature of this characteristic value and the additional factors of safety in design (i.e., load factors, strength reduction factors) it is reasonable to

assume that this limiting value is applicable to all the final compressive strengths used in this study.

4.1.4 Prestressing Strand Dimensions

Two sizes of prestressing strands are used in this study, 0.6 in. (15 mm) diameter and 0.7 in. (18 mm) diameter. Table 4.2 compares the properties of the two strands. The primary difference is the cross-sectional area. The 0.7 in. (18 mm) strands provide 35% more cross-sectional area than the 0.6 in. (15 mm) strands, with only a 17% increase in diameter. The advantage of the larger prestressing strands is the labor savings and the increased prestressing force available using fewer strands (Schuler 2009).

TABLE 4.2 Comparison of Prestressing Strand Properties.

Strand ID	Type	Ultimate Strength, f_{pu} ksi (MPa)	Diameter in. (mm)	Area $in.^2$ (mm^2)
6/10-270K-LR	Low Relaxation	270 (1,800)	0.6 (15)	0.217 (140)
7/10-270K-LR	Low Relaxation	270 (1,800)	0.7 (18)	0.294 (190)

4.1.5 Results of I-25/Doña Ana Interchange Utilizing 0.6 in. (15 mm) Diameter Strands

The as-designed bridge has 36 - 0.6 in (15 mm) strands; 24 straight, 6 harped, and 6 debonded-partial length strands in the top flange to control stresses and provide the required flexural moment capacity. For the parametric study, only harped strands were used to obtain consistent comparisons. Harped strand patterns were developed in a two step process. First the auto design feature of CONSPAN® was used to have an initial strand pattern. This initial pattern was modified by hand by adding and removing strands and adjusting the harped strand pattern to ensure that the final strand pattern was a sound design. In this manner a straight/harped only strand pattern was generated for the as-designed bridge. The resulting pattern required a total of 28 - 0.6 in. (15 mm) strands; 26 straight and 2 harped strands. The difference in strands between the as-designed and baseline bridge occurs at two locations. There are two less straight strands in the bottom bulb for the baseline bridge girder. Also the as-designed bridge girder plans call out 6 debonded-partial length strands in the top flange. For the purpose of the parametric study six BT-63 girders with 28 (26 straight and 2 harped) - 0.6 in. (15 mm) diameter strands is considered to be the baseline design of the I-25/Doña Ana Interchange Bridge. All bridge configurations are compared to the baseline design.

The design matrix (see Table 4.1) was followed sequentially until it was determined that a certain cross-section configuration was not a viable design according to the LFD specifications. Table 4.3 shows the results obtained from CONSPAN® using the Graybeal equation to estimate the modulus of elasticity and limiting the modulus of rupture to AASHTO provisions (i.e., the tensile strength of UHPC reported in literature is not considered in Table 4.3). Under LFD, the number of girder lines and the girder size decrease

from six BT-63 girders to five BT-54 girders, for a total savings of 23% in girder concrete volume. This concrete volume reduction can be realized with a 64-71% increase in the required number of 0.6 in. (15 mm) strands for UHPC compressive strengths of 15.0 to 22.5 ksi (103.4 to 155.1 MPa), respectively. The deck thickness is increased by 13.3%.

Table 4.4 shows the results obtained from CONSPAN® using the Graybeal equation to estimate the modulus of elasticity and limiting the modulus of rupture to 1.16 ksi (8 MPa). The use of the higher tensile stress decreases the number of girder lines and the girder size from six BT-63 girders to four BT-63 girders, for a total savings of 33% in girder concrete volume. This concrete volume reduction can be realized with a 50% increase in the required number of 0.6 in. (15 mm) strands and a 26.7% increase in the deck thickness.

Figure 4.3 is a comparison of the results from Tables 4.3 and 4.4. By increasing the compressive strength and the allowable tensile stress, savings in the number of prestressing strands ranges from 7-29%. Additionally, the increased tensile stress limit allows for an additional bridge configuration to be considered viable, namely four BT-63 girders. This configuration saves an additional concrete volume of 11% compared to five BT-54 girders that are viable under the LFD code. Table 4.5 shows the savings of each configuration.

These comparisons show with the increase in compressive strength and the improved tensile strength of UHPC, greater concrete savings are possible in the girders that are not possible with HPC. Live load deflections were checked for all designs. An allowable deflection is given by L/800 or 1.7 in. (43 mm). All deflections reported in Tables 4.3 and 4.4 satisfy this serviceability requirement.

TABLE 4.3 I-25/Doña Ana Interchange Using 0.6 in. (15 mm) Strands According to LFD Code.

Viable Cross-Section Config-urations	Final Strength of UHPC, ksi (MPa)	Deck Thickness in. (mm)	Total Number of Strands	Straight & Harped		Live Load Deflections, in. (mm)	
I (6 BT-63 Girder Lines)	9.5 (65.5)	7.5 (191)	28	26	2	0.771	(20)
	15.0 (103.4)		26	24	2	0.749	(19)
	17.5 (120.7)		26	24	2	0.713	(18)
	20.0 (137.9)		26	24	2	0.683	(17)
	22.5 (155.1)		26	24	2	0.658	(17)
II (6 BT-54 Girder Lines)	9.5 (65.5)	7.5 (191)	36	30	6	1.074	(27)
	15.0 (103.4)		34	28	6	1.036	(26)
	17.5 (120.7)		34	28	6	0.989	(25)
	20.0 (137.9)		34	28	6	0.949	(24)
	22.5 (155.1)		34	28	6	0.915	(23)
V (5 BT-63 Girder Lines)	9.5 (65.5)	8.5 (216)	36	30	6	0.825	(21)
	15.0 (103.4)		34	28	6	0.799	(20)
	17.5 (120.7)		34	28	6	0.761	(19)
	20.0 (137.9)		34	28	6	0.73	(19)
	22.5 (155.1)		32	26	6	0.706	(18)
VII (5 BT-54 Girder Lines)	9.5 (65.5)	8.5 (216)	-	-	-	-	-
	15.0 (103.4)		48	38	10	1.104	(28)
	17.5 (120.7)		48	42	6	1.054	(27)
	20.0 (137.9)		46	40	6	1.103	(28)
	22.5 (155.1)		46	40	6	0.977	(25)

- Non-viable design

TABLE 4.4 I-25/Doña Ana Interchange Using 0.6 in. (15 mm) Strands According to a Tensile Stress Limit of 1.16 ksi (8 MPa).

Viable Cross-Section Config-urations	Final Strength of UHPC, ksi (MPa)	Deck Thickness, in. (mm)	Total Number of Strands	Straight & Harped		Live Load Deflections, in. (mm)	
I (6 BT-63 Girder Lines)	9.5 (65.5)*	7.5 (191)	28	26	2	0.771	(20)
	15.0 (103.4)		22	20	2	0.756	(19)
	17.5 (120.7)		22	20	2	0.719	(18)
	20.0 (137.9)		22	20	2	0.689	(18)
	22.5 (155.1)		22	20	2	0.663	(17)
II (6 BT-54 Girder Lines)	9.5 (65.5)*	7.5 (191)	36	30	6	1.074	(27)
	15.0 (103.4)		30	24	6	1.046	(27)
	17.5 (120.7)		30	24	6	0.997	(25)
	20.0 (137.9)		30	24	6	0.956	(24)
	22.5 (155.1)		30	24	6	0.921	(23)
VI (5 BT-63 Girder Lines)	9.5 (65.5)*	8.5 (216)	36	30	6	0.825	(21)
	15.0 (103.4)		28	22	6	0.81	(21)
	17.5 (120.7)		30	24	6	0.768	(20)
	20.0 (137.9)		30	24	6	0.736	(19)
	22.5 (155.1)		30	24	6	0.708	(18)
VII (5 BT-54 Girder Lines)	9.5 (65.5)*	8.5 (216)	-	-	-	-	-
	15.0 (103.4)		42	32	10	1.117	(28)
	17.5 (120.7)		40	34	6	1.066	(27)
	20.0 (137.9)		40	34	6	1.021	(26)
	22.5 (155.1)		40	34	6	0.985	(25)
XI (4 BT-63 Girder Lines)	9.5 (65.5)*	9.5 (241)	-	-	-	-	-
	15.0 (103.4)		42	32	10	0.897	(23)
	17.5 (120.7)		42	36	6	0.852	(22)
	20.0 (137.9)		42	36	6	0.815	(21)
	22.5 (155.1)		42	36	6	0.785	(20)

* Utilizes AASHTO LFD tensile stress limit
- Non-viable design

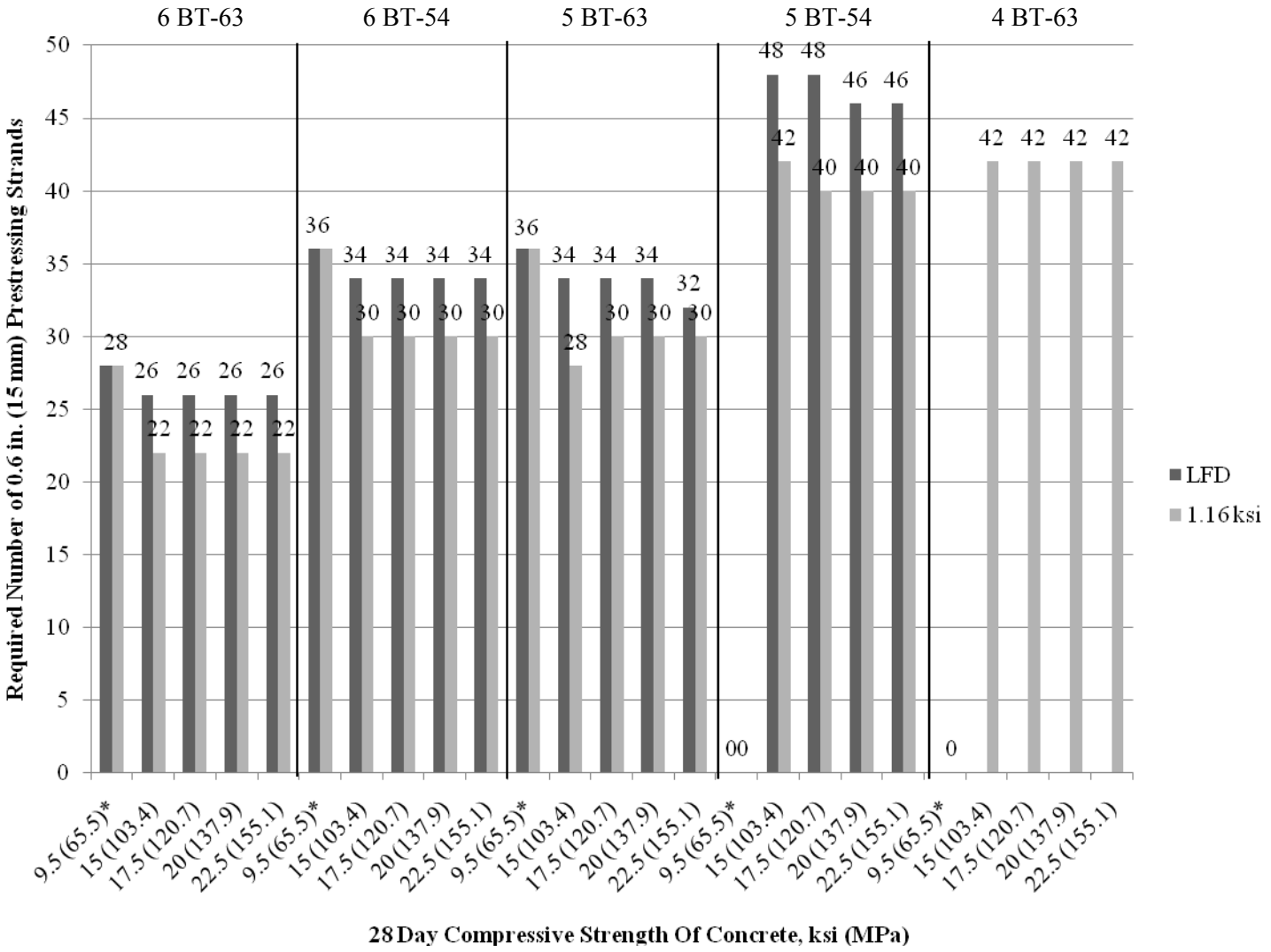

FIGURE 4.3 Comparison of the Required Number of 0.6 in. (15 mm) Prestressing Strands based on Different Allowable Service Tensile Stress Limits for I-25/Doña Ana Interchange.

TABLE 4.5 Comparison of Tensile Stress Limits Results for I-25/Doña Ana Interchange Using 0.6 in. (15 mm) Strands To the Baseline Design.

		Tensile Stress Limit according to LFD			Tensile Stress Limit of 1.16 ksi (8 MPa)		
Viable Cross-Section Configurations	Final Strength of UHPC, ksi (MPa)	Change in Deck Thickness, %	Savings of Concrete Volume in Girders, %	Increase in Number of Strands, %	Change in Deck Thickness, %	Savings of Concrete Volume in Girders, %	Increase in Number of Strands, %
I (6 BT-63 Girder Lines)	9.5 (65.5)	0.0%	0%	0%	0.0%	0%	0%
	15.0 (103.4)			-7%			-21%
	17.5 (120.7)			-7%			-21%
	20.0 (137.9)			-7%			-21%
	22.5 (155.1)			-7%			-21%
II (6 BT-54 Girder Lines)	9.5 (65.5)	0.0%	8%	29%	0.0%	8%	29%
	15.0 (103.4)			21%			7%
	17.5 (120.7)			21%			7%
	20.0 (137.9)			21%			7%
	22.5 (155.1)			21%			7%
VI (5 BT-63 Girder Lines)	9.5 (65.5)	13.3%	17%	29%	13.3%	17%	29%
	15.0 (103.4)			21%			0%
	17.5 (120.7)			21%			7%
	20.0 (137.9)			21%			7%
	22.5 (155.1)			14%			7%
VII (5 BT-54 Girder Lines)	9.5 (65.5)	13.3%	23%	-	13.3%	23%	-
	15.0 (103.4)			71%			50%
	17.5 (120.7)			71%			43%
	20.0 (137.9)			64%			43%
	22.5 (155.1)			64%			43%
XI (4 BT-63 Girder Lines)	9.5 (65.5)*	N/A	N/A	-	26.7%	33%	-
	15.0 (103.4)			-			50%
	17.5 (120.7)			-			50%
	20.0 (137.9)			-			50%
	22.5 (155.1)			-			50%

- Non-viable design

4.1.6 Results of I-25/Doña Ana Interchange Utilizing 0.7 in. (18 mm) Diameter Strands

For the purpose of the parametric study six BT-63 girders with 22 (20 straight and 2 harped) 0.7 in. (18 mm) diameter strands is considered to be the baseline design of the I-25/Doña Ana Interchange.

The design matrix in Table 4.1 was followed sequentially until it was determined that a certain cross-section configuration was not a viable design according to the LFD specifications. Table 4.6 shows the results obtained from CONSPAN® using the Graybeal equation to estimate the modulus of elasticity and limiting the modulus of rupture to AASHTO provisions (i.e., the tensile strength of UHPC is not considered in Table 4.6). Under LFD, the number of girder lines and the girder size decreases from six BT-63 girders to four BT-63 girders using UHPC, for a total savings of 33% in girder concrete volume. This concrete volume reduction can be realized with a 55% increase in the required number of 0.7 in. (18 mm) strands and 26.7% increase in the deck thickness.

Table 4.7 shows the results obtained from CONSPAN® using the Graybeal equation to estimate the modulus of elasticity and limiting the modulus of rupture to 1.16 ksi (8 MPa). The use of higher tensile stress decreases the number of girder lines and the girder size from six BT-63 girders to four BT-54 girders, for a total savings of 38% in girder concrete volume. This concrete volume reduction can be realized with a 109% increase in the required number of 0.7 in. (18 mm) strands and 26.7% increase in the deck thickness.

Figure 4.4 is a comparison of the results from Tables 4.6 and 4.7. By increasing the compressive strength and tensile stress, savings in the number of prestressing strands ranges from 9-18%. Additionally, the increased tensile stress limit allows for an additional bridge configuration to be considered viable, namely four BT-54 girders. This configuration saves an additional concrete volume of 5% compared to four BT-63 girders that are viable under the LFD code. Table 4.8 shows the savings of each configuration.

This comparisons show that the improved girder compressive and tensile strength of UHPC in combination with 0.7 in. (18 mm) strands, will yield greater concrete savings that are not possible with HPC and 0.6 in. (15 mm) strands. Live load deflections were checked for all designs. An allowable deflection is given by L/800 or 1.7 in. (43 mm). All deflections reported in Tables 4.6 and 4.7 satisfy this serviceability requirement.

TABLE 4.6 Results for I-25/Doña Ana Interchange Using 0.7 in. (18 mm) Strands According to LFD Code.

Viable Cross-Section Configurations	Final Strength of UHPC, ksi (MPa)	Deck Thickness in. (mm)	Total Number of Strands	Straight & Harped		Live Load Deflections, in. (mm)
I (6 BT-63 Girder Lines)	9.5 (65.5)	7.5 (191)	22	20	2	0.767 (19)
	15.0 (103.4)		20	18	2	0.745 (19)
	17.5 (120.7)		20	18	2	0.710 (18)
	20.0 (137.9)		20	18	2	0.680 (17)
	22.5 (155.1)		20	18	2	0.655 (17)
II (6 BT-54 Girder Lines)	9.5 (65.5)	7.5 (191)	26	22	4	1.071 (27)
	15.0 (103.4)		26	22	4	1.029 (26)
	17.5 (120.7)		24	20	4	0.988 (25)
	20.0 (137.9)		24	20	4	0.948 (24)
	22.5 (155.1)		24	20	4	0.914 (23)
VI (5 BT-63 Girder Lines)	9.5 (65.5)	8.5 (216)	26	22	4	0.824 (21)
	15.0 (103.4)		24	20	4	0.799 (20)
	17.5 (120.7)		24	20	4	0.761 (19)
	20.0 (137.9)		24	20	4	0.730 (19)
	22.5 (155.1)		24	20	4	0.703 (18)
VII (5 BT-54 Girder Lines)	9.5 (65.5)	8.5 (216)	-	-	-	- -
	15.0 (103.4)		32	26	6	1.094 (28)
	17.5 (120.7)		32	26	6	1.044 (27)
	20.0 (137.9)		32	26	6	1.003 (25)
	22.5 (155.1)		32	26	6	0.968 (25)
XI (4 BT-63 Girder Lines)	9.5 (65.5)	9.5 (241)	-	-	-	- -
	15.0 (103.4)		34	24	10	0.874 (22)
	17.5 (120.7)		34	24	10	0.834 (21)
	20.0 (137.9)		34	24	10	0.800 (20)
	22.5 (155.1)		34	24	10	0.772 (20)

- Indicates non-viable bridge

TABLE 4.7 Results for I-25/Doña Ana Interchange Using 0.7 in. (18 mm) Strands According to Tensile Stress Limit of 1.16 ksi (8.0 MPa).

Viable Cross-Section Config-urations	Final Strength of UHPC, ksi (MPa)	Deck Thickness in. (mm)	Total Number of Strands	Straight & Harped		Live Load Deflections, in. (mm)	
I (6 BT-63 Girder Lines)	9.5 (65.5)	7.5 (191)	22	20	2	0.767	(19)
	15.0 (103.4)		16	14	2	0.756	(19)
	17.5 (120.7)		16	14	2	0.719	(18)
	20.0 (137.9)		16	14	2	0.689	(18)
	22.5 (155.1)		16	14	2	0.663	(17)
II (6 BT-54 Girder Lines)	9.5 (65.5)	7.5 (191)	26	22	4	1.071	(27)
	15.0 (103.4)		22	18	4	1.043	(26)
	17.5 (120.7)		22	18	4	0.994	(25)
	20.0 (137.9)		22	18	4	0.954	(24)
	22.5 (155.1)		22	18	4	0.919	(23)
VI (5 BT-63 Girder Lines)	9.5 (65.5)	8.5 (216)	26	22	4	0.824	(21)
	15.0 (103.4)		22	18	4	0.804	(20)
	17.5 (120.7)		22	18	4	0.766	(19)
	20.0 (137.9)		22	18	4	0.734	(19)
	22.5 (155.1)		22	18	4	0.707	(18)
VII (5 BT-54 Girder Lines)	9.5 (65.5)	8.5 (216)	-	-	-	-	-
	15.0 (103.4)		28	22	6	1.107	(28)
	17.5 (120.7)		28	22	6	1.056	(27)
	20.0 (137.9)		28	22	6	1.014	(26)
	22.5 (155.1)		28	22	6	0.978	(25)
XI (4 BT-63 Girder Lines)	9.5 (65.5)	9.5 (241)	-	-	-	-	-
	15.0 (103.4)		30	20	10	0.886	(23)
	17.5 (120.7)		30	20	10	0.844	(21)
	20.0 (137.9)		30	20	10	0.810	(21)
	22.5 (155.1)		30	20	10	0.780	(20)
XII (4 BT-54 Girder Lines)	9.5 (65.5)	9.5 (241)	-	-	-	-	-
	15.0 (103.4)		-	-	-	-	-
	17.5 (120.7)		-	-	-	-	-
	20.0 (137.9)		46	38	8	1.057	(27)
	22.5 (155.1)		46	38	8	1.104	(28)

- Indicates non-viable design

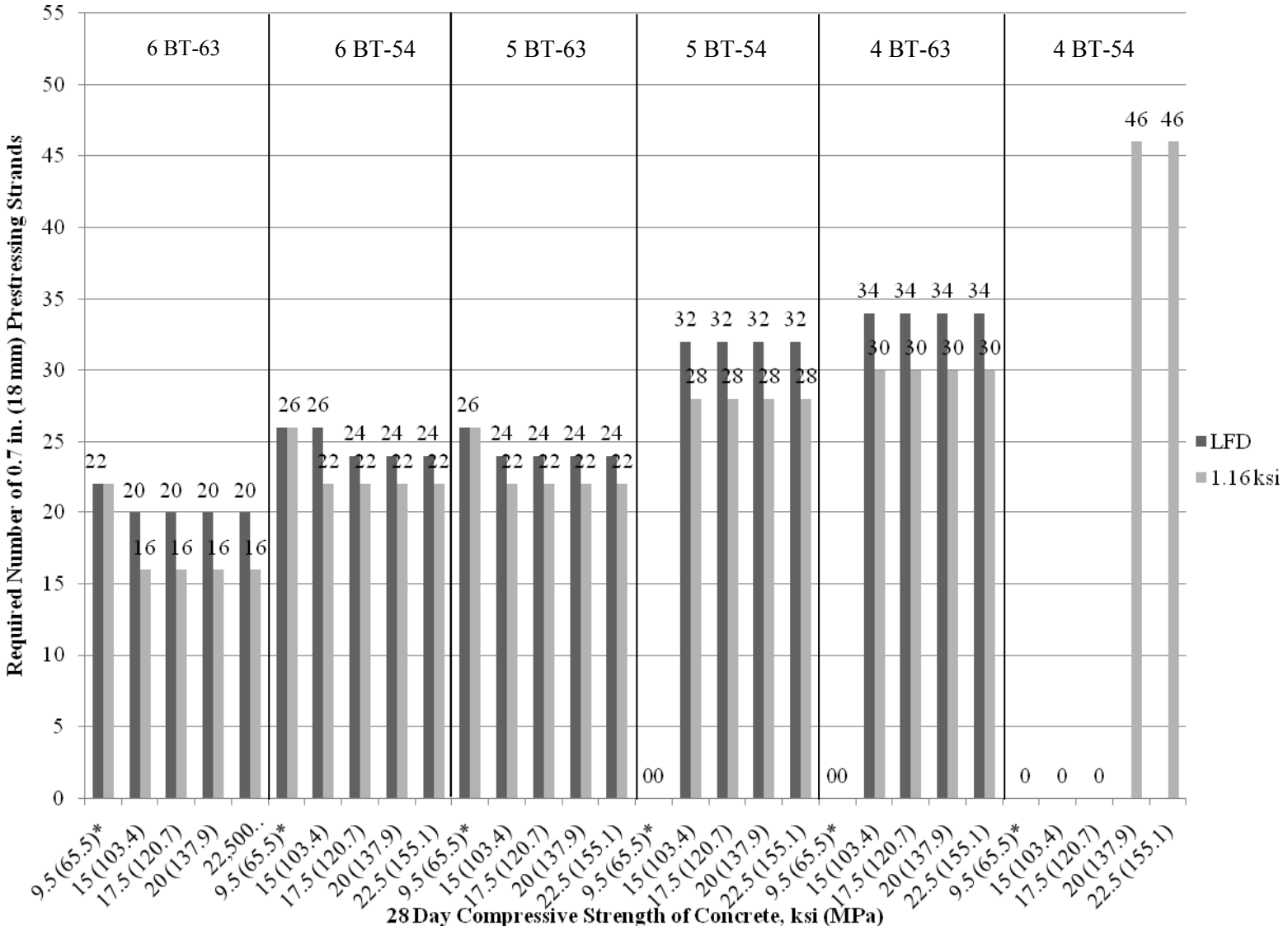

FIGURE 4.4 Comparison of the Required Number of 0.7 in. (18 mm) Prestressing Strands based on Different Tensile Stress Limits.

TABLE 4.8 Comparison of Materials with Different Allowable Tensile Stress Limits for I-25/Doña Ana Interchange Using 0.7 in. (18 mm) Strands.

		LFD CODE			1.16 ksi (8.0 MPa)		
Viable Cross-Section Config-urations	Final Strength of UHPC, ksi (MPa)	Change in Deck Thickness %	Savings of Concrete Volume in Girders, %	Increase in Number of Strands, %	Change in Deck Thickness %	Savings of Concrete Volume in Girders, %	Increase in Number of Strands, %
I (6 BT-63 Girder Lines)	9.5 (65.5)	0.0%	0%	0%	0.0%	0%	0%
	15 (103.4)			-9%			-27%
	17.5 (120.7)			-9%			-27%
	20 (137.9)			-9%			-27%
	22.5 (155.1)			-9%			-27%
II (6 BT-54 Girder Lines)	9.5 (65.5)	0.0%	8%	18%	0.0%	8%	18%
	15 (103.4)			18%			0%
	17.5 (120.7)			9%			0%
	20 (137.9)			9%			0%
	22.5 (155.1)			9%			0%
VI (5 BT-63 Girder Lines)	9.5 (65.5)	13.3%	117%	18%	13.3%	17%	18%
	15 (103.4)			9%			0%
	17.5 (120.7)			9%			0%
	20 (137.9)			9%			0%
	22.5 (155.1)			9%			0%
VII (5 BT-54 Girder Lines)	9.5 (65.5)	13.3%	23%	-	13.3%	23%	-
	15 (103.4)			45%			27%
	17.5 (120.7)			45%			27%
	20 (137.9)			45%			27%
	22.5 (155.1)			45%			27%
XI (4 BT-63 Girder Lines)	9.5 (65.5)	26.7%	33%	-	26.7%	33%	-
	15 (103.4)			55%			36%
	17.5 (120.7)			55%			36%
	20 (137.9)			55%			36%
	22.5 (155.1)			55%			36%
XII (4 BT-54 Girder Lines)	9.5 (65.5)	N/A	N/A	-	26.7%	38%	-
	15 (103.4)			-			-
	17.5 (120.7)			-			-
	20 (137.9)			-			109%
	22.5 (155.1)			-			109%

-non-viable design

4.2 SUNLAND PARK BRIDGE – TWO-SPAN CONTINUOUS AND THREE-SPAN CONTINUOUS UNITS

The Sunland Park River Crossing Bridge has seven spans (2 span continuous, 3 span continuous, and 2 span continuous) (see Figure 4.5 and 4.6) with span lengths of 121.92 ft (37.16 m). Each span has ten modified BT-54 prestressed concrete girders, spaced at 6.8 ft (2.1 m) (Figure 4.7), with average haunch dimensions of 4.5 in. (114 mm), compose the cross-section of the superstructure along with an 8.0 in. (203 mm), stay in place deck of conventional concrete with a compressive strength of 4.0 ksi (27.6 MPa). The deck is 70.0 ft (21.3 m) wide with a 2% crown on each side from the centerline. The travel way dimension is 58.5 ft (17.8 m) wide, allowing two travel lanes in each direction. The deck overhang is 4.0 ft (1.2 m). The steel reinforcement used in the superstructure is the No. 4 (M13) horizontal shear/composite action bars at the beam slab interface and the longitudinal and transverse deck reinforcement. The beams are braced by intermediate steel bent plate diaphragms at every third point of the span. Supporting the superstructure is an abutment at each end of the beams with wingwalls. The traffic barrier is a 42.0 in. (1.07 m) concrete guard rail.

FIGURE 4.5 Two Span Unit of Sunland Park River Crossing.

FIGURE 4.6 Three-Span Unit of Sunland Park River Crossing.

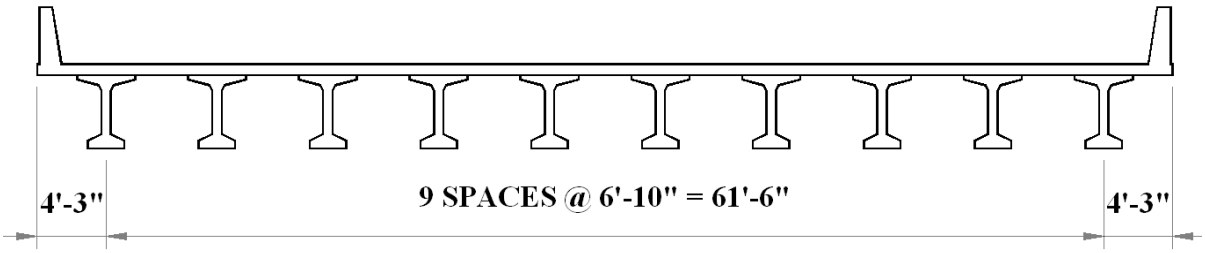

FIGURE 4.7 Cross-Sectional Geometry of Sunland Park River Crossing Two-Span and Three-Span Units.

4.2.1 CONSPAN® Flexure Analysis for Sunland Park Two-Span Unit

The methodology used for the two-span continuous and the three-span continuous units of the Sunland Park Bridge is essentially the same as the I-25/Doña Ana Interchange described previously. The primary difference is the design matrix shown in Table 4.9 and the ratio of the deck overhang to girder spacing varies [i.e., the overhang dimension of 4.25 ft (1.30 m) was kept constant].

The design matrix allows six girder lines to be considered. According the NMDOT Bridge Procedures and Design Guide section 4.3.1, the effective deck span between girders will control the design of the bridge superstructure if fewer than six girder lines are used.

TABLE 4.9 Design Matrix for Sunland Park Bridge.

Number of Girders	Type of Girders				
	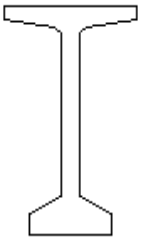 BT-63	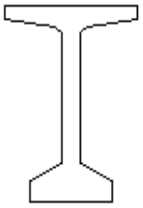 BT-54	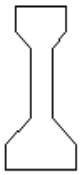 Type III	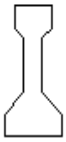 Type II	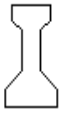 Type I
10	N/A	I	II	III	IV
9	N/A	V	VI	VII	VIII
8	N/A	IX	X	XI	XII
7	N/A	XIII	XIV	XV	XVI
6	XVII-b	XVII-a	XVIII	XIX	XX

Note, the AASHTO Type I, II and III were found to be unsatisfactory girder types for this structure.

4.2.2 Results of Sunland Park Bridge Two-Span Continuous Unit Utilizing 0.6 in. (15 mm) Diameter Strands

The as-designed bridge has 40 - 0.6 in. (15 mm) strands; 32 straight and 8 harped strands to control stresses and provide the required flexural moment capacity. For the purpose of the parametric study ten modified BT-54 girders with 40 (32 straight and 8 harped) - 0.6 in. (15 mm) diameter strands is considered to be the baseline design of the Sunland Park Bridge two-span continuous unit.

The design matrix in Table 4.9 was followed sequentially until it was determined that a certain cross-section configuration was not a viable design according to the LFD specifications. Table 4.10 shows the results obtained from CONSPAN® using the Graybeal equation to estimate the modulus of elasticity and limiting the modulus of rupture to AASHTO provisions (i.e., the tensile strength of UHPC reported in literature is not considered in Table 4.10).

Under LFD, the number of girder lines decreases from ten modified BT-54 girders to eight modified BT-54 girders using UHPC, for a total savings of 20% in girder concrete volume; this is similar to the finding in the I-25/Doña Ana Interchange of 23%. This concrete volume reduction can be realized with a 20-30% increase in the required number of 0.6 in. (15 mm) strands and a 6.3% increase in the deck thickness.

Table 4.11 shows the results obtained from CONSPAN® using the Graybeal equation to estimate the modulus of elasticity and limiting the modulus of rupture to 1.16 ksi (8.0 MPa).

The use of the higher tensile stress decreases the number of girder lines from ten modified BT-54 girders to eight modified BT-54 girders, the difference observed by allowing the tensile stress to increase results in a savings in the required amount of prestressing strands. Eight modified BT-54 girders can be designed with a 5% increase in the required number of strands instead of 20-30% required by LFD. Table 4.12 is a summary of the material savings.

Figure 4.8 is a comparison of the results from Tables 4.10 and 4.11. The use of the higher tensile stress creates a savings in the number of prestressing strands ranges from 5-25%. Live load deflections were checked for all designs. A limiting deflection is given by L/800 or 1.8 in. (46 mm). All deflections reported in Tables 4.10 and 4.11 satisfy this serviceability requirement.

TABLE 4.10 Sunland Park Bridge Two-Span Unit Using 0.6 in. (15 mm) Strands According to LFD Code.

Viable Cross-Section Configurations	Final Strength of UHPC, ksi (MPa)	Deck Thickness in. (mm)	Total Number of Strands	Straight & Harped		Live Load Deflections, in. (mm)	
I (10 BT-54 Girder Lines)	9.5 (65.5)	8 (203)	40	32	8	0.877	(22)
	15.0 (103.4)		36	30	6	0.868	(22)
	17.5 (120.7)		36	30	6	0.829	(21)
	20.0 (137.9)		36	30	6	0.796	(20)
	22.5 (155.1)		36	30	6	0.768	(20)
II (9 BT-54 Girder Lines)	9.5 (65.5)	8 (203)	46	26	20	0.775	(20)
	15.0 (103.4)		42	36	6	0.937	(24)
	17.5 (120.7)		42	36	6	0.895	(23)
	20.0 (137.9)		40	34	6	0.861	(22)
	22.5 (155.1)		40	34	6	0.830	(21)
VI (8 BT-54 Girder Lines)	9.5 (65.5)	8.5 (216)	-	-	-	-	-
	15.0 (103.4)		52	42	10	0.999	(25)
	17.5 (120.7)		50	44	6	0.954	(24)
	20.0 (137.9)		50	44	6	0.916	(23)
	22.5 (155.1)		48	42	6	0.884	(22)

- Non-viable design

TABLE 4.11 Sunland Park Bridge Two-Span Unit Using 0.6 in. (15 mm) Strands According to a Limit Tensile Strength of 1.16 ksi (8 MPa).

Viable Cross-Section Configurations	Final Strength of UHPC, ksi (MPa)	Deck Thickness, in. (mm)	Total Number of Strands	Straight & Harped		Live Load Deflections, in. (mm)	
I (10 BT-54Girder Lines)	9.5 (65.5)*	8 (203)	40	26	14	0.877	(22)
	15.0 (103.4)		32	20	12	0.875	(22)
	17.5 (120.7)		32	20	12	0.835	(21)
	20.0 (137.9)		32	20	12	0.801	(20)
	22,500 (155.1)		30	20	10	0.775	(20)
V (9 BT-54 Girder Lines)	9.5 (65.5)*	8 (203)	46	30	16	0.775	(20)
	15.0 (103.4)		36	24	12	0.943	(24)
	17.5 (120.7)		36	24	12	0.9	(23)
	20.0 (137.9)		36	24	12	0.864	(22)
	22,500 (155.1)		36	24	12	0.834	(21)
IX (8 BT-54 Girder Lines)	9.5 (65.5)*	8.5 (216)	-	-	-		-
	15.0 (103.4)		40	22	18	0.864	(22)
	17.5 (120.7)		42	24	18	0.834	(21)
	20.0 (137.9)		42	24	18	0.919	(23)
	22.5 (155.1)		42	24	18	0.886	(23)

* Indicates that values utilize AASHTO LFD tensile stress limit.
- Non-viable design.

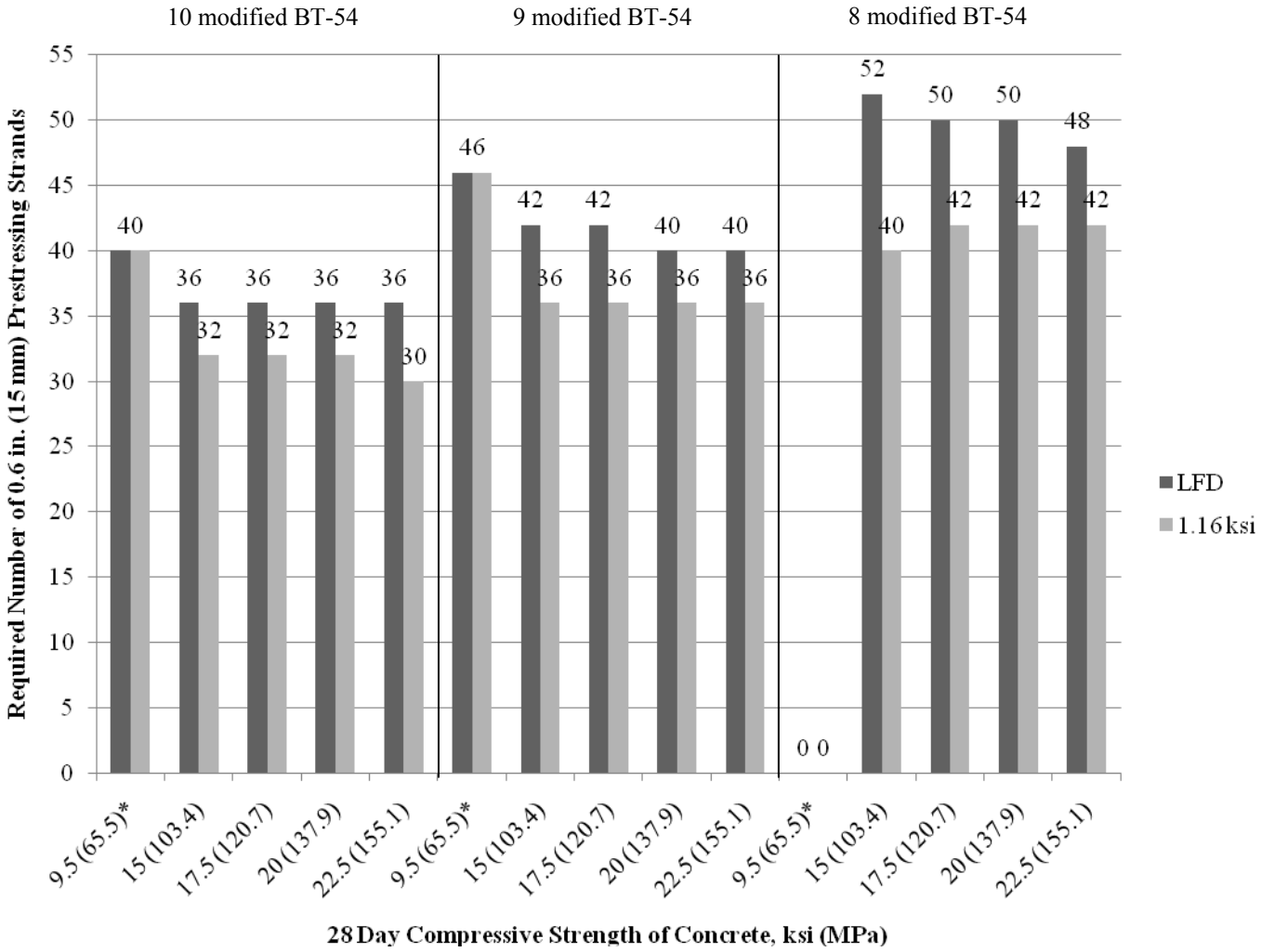

FIGURE 4.8 Comparison of the Required Number of 0.6 in. (15 mm) Prestressing Strands Based on Different Tensile Stress Limits for Sunland Park Bridge Two-Span Unit.

TABLE 4.12 Comparison of Allowable Tensile Stress Limits for Sunland Park Bridge Two-Span Unit Using 0.6 in. (15 mm) Stands.

		Tensile Stress Limit according to LFD			Tensile Stress Limit of 1.16 ksi (8 MPa)		
Viable Cross-Section Config-urations	Final Strength of UHPC, ksi (MPa)	Change in Deck Thickness, %	Savings of Concrete Volume in Girders, %	Increase in Number of Strands, %	Change in Deck Thickness, %	Savings of Concrete Volume in Girders, %	Increase in Number of Strands, %
I (10 BT-54 Girder Lines)	9.5 (65.5)	0.0%	0%	0%	0.0%	0%	0%
	15.0 (103.4)			-10%			-20%
	17.5 (120.7)			-10%			-20%
	20.0 (137.9)			-10%			-20%
	22.5 (155.1)			-10%			-25%
II (9 BT-54 Girder Lines)	9.5 (65.5)	0.0%	10%	15%	0.0%	10%	15%
	15.0 (103.4)			5%			-10%
	17.5 (120.7)			5%			-10%
	20.0 (137.9)			0%			-10%
	22.5 (155.1)			0%			-10%
VI (8 BT-54 Girder Lines)	9.5 (65.5)	6.3%	20%	-	6.3%	20%	-
	15.0 (103.4)			30%			0%
	17.5 (120.7)			25%			5%
	20.0 (137.9)			25%			5%
	22.5 (155.1)			20%			5%

4.2.3 Results of Sunland Park Bridge Two-Span Continuous Unit Utilizing 0.7 in. (18 mm) Diameter Strands

For the purpose of the parametric study ten modified BT-54 girders with 26 – 0.7 in. (18 mm) strands; 20 straight and 6 harped, is considered to be the base line design of the Sunland Park Bridge.

The design matrix in Table 4.9 was followed sequentially until it was determined that a certain cross-section configuration was not a viable design according to the LFD specifications. Table 4.13 shows the results obtained from CONSPAN® using the Graybeal equation to estimate the modulus of elasticity and limiting the modulus of rupture to AASHTO provisions (i.e., the tensile strength of UHPC reported in literature is not considered in Table 4.13). Under LFD, the number of girder lines and the girder size decreases from ten modified BT-54 girders to seven modified BT-54 girders, for a total savings of 30% in girder concrete volume. This concrete volume reduction can be realized with a 62-69% increase in the required number of 0.7 in. (18 mm) strands and a 20% increase in the deck thickness.

Table 4.14 shows the results obtained from CONSPAN® using the Graybeal equation to estimate the modulus of elasticity and limiting the modulus of rupture to 1.16 ksi (8 MPa). The use of the higher tensile stress decreases the number of girder lines from ten modified BT-54 girders to six BT-63 girders, for a total savings of 40% in girder concrete volume. This concrete volume reduction can be realized with a 38-46% increase in the required number of 0.7 in. (18 mm) strands and a 40% increase in the deck thickness.

Figure 4.9 and Table 4.15 are comparisons of the results from Tables 4.13 and 4.14. By increasing the allowable tensile stress, savings in the number of prestressing strands ranges from 13-81%. Additionally, the increased tensile stress limit allows for an additional bridge configuration to be considered viable, namely, six BT-63 girders. This configuration saves an additional concrete volume of 13% compared to seven modified BT-54 girders that are viable under the LFD code.

Live load deflections were checked for these viable designs. A limiting deflection is given by L/800 or 1.8 in. (46 mm). All deflections reported in Tables 4.13 and 4.14 satisfy this serviceability requirement.

TABLE 4.13 Sunland Park Bridge Two-Span Unit Using 0.7 in. (18 mm) Strands According to LFD code.

Viable Cross-Section Config-urations	Final Strength of UHPC, ksi (MPa)	Deck Thickness, in. (mm)	Total Number of Strands	Straight & Harped		Live Load Deflections, in. (mm)	
I (10 BT-54 Girder Lines)	9.5 (65.5)*	8 (203)	26	20	6	0.878	(22)
	15.0 (103.4)		22	20	2	0.876	(22)
	17.5 (120.7)		22	20	2	0.835	(21)
	20.0 (137.9)		22	20	2	0.801	(20)
	22.5 (155.1)		22	20	2	0.773	(20)
V (9 BT-54 Girder Lines)	9.5 (65.5)*	8 (203)	32	24	8	0.966	(25)
	15.0 (103.4)		26	24	2	0.942	(24)
	17.5 (120.7)		26	24	2	0.899	(23)
	20.0 (137.9)		26	24	2	0.862	(22)
	22.5 (155.1)		26	24	2	0.832	(21)
IX (8 BT-54 Girder Lines)	9.5 (65.5)*	8.5 (216)	-	-	-	-	-
	15.0 (103.4)		28	26	2	1.002	(25)
	17.5 (120.7)		28	26	2	0.956	(24)
	20.0 (137.9)		30	28	2	0.913	(23)
	22.5 (155.1)		30	28	2	0.881	(22)
XIII (7 BT-54 Girder Lines)	9.5 (65.5)*	9 (229)	-	-	-	-	-
	15.0 (103.4)		36	30	6	1.067	(27)
	17.5 (120.7)		36	32	4	0.925	(23)
	20.0 (137.9)		36	32	4	0.98	(25)
	22.5 (155.1)		36	34	2	0.946	(24)
XVII-b (6 BT-63 Girder Lines)	9.5 (65.5)*	10.5 (267)	-	-	-	-	-
	15.0 (103.4)		36	32	4	0.869	(22)
	17.5 (120.7)		38	32	6	0.808	(21)
	20.0 (137.9)		38	32	6	0.775	(20)
	22.5 (155.1)		38	34	4	0.748	(19)

* Indicates that values utilize AASHTO LFD tensile stress limit
- Non-viable design

TABLE 4.14 Sunland Park Bridge Two-Span Unit Using 0.7 in. (18 mm) Strands According to Tensile Limit of 1.16 ksi (8.0 MPa).

Viable Cross-Section Config-urations	Final Strength of UHPC, ksi (MPa)	Deck Thickness in. (mm)	Total Number of Strands	Straight & Draped		Live Load Deflections, in. (mm)	
I (10 BT-54 Girder Lines)	9.5 (65.5)*	8 (203)	26	20	6	0.878	(22)
	15.0 (103.4)		22	20	2	0.876	(22)
	17.5 (120.7)		22	20	2	0.835	(21)
	20.0 (137.9)		22	20	2	0.801	(20)
	22.5 (155.1)		22	20	2	0.773	(20)
V (9 BT-54 Girder Lines)	9.5 (65.5)*	8 (203)	32	24	8	0.966	(25)
	15.0 (103.4)		26	24	2	0.942	(24)
	17.5 (120.7)		26	24	2	0.899	(23)
	20.0 (137.9)		26	24	2	0.862	(22)
	22.5 (155.1)		26	24	2	0.832	(21)
IX (8 BT-54 Girder Lines)	9.5 (65.5)*	8.5 (216)	-	-	-	-	-
	15.0 (103.4)		28	26	2	1.002	(25)
	17.5 (120.7)		28	26	2	0.956	(24)
	20.0 (137.9)		30	28	2	0.913	(23)
	22.5 (155.1)		30	28	2	0.881	(22)
XIII (7 BT-54 Girder Lines)	9.5 (65.5)*	9 (229)	-	-	-	-	-
	15.0 (103.4)		36	30	6	1.067	(27)
	17.5 (120.7)		36	32	4	0.925	(23)
	20.0 (137.9)		36	32	4	0.98	(25)
	22.5 (155.1)		36	34	2	0.946	(24)
XVII-b (6 BT-63 Girder Lines)	9.5 (65.5)*	10.5 (267)	-	-	-	-	-
	15.0 (103.4)		36	32	4	0.869	(22)
	17.5 (120.7)		38	32	6	0.808	(21)
	20.0 (137.9)		38	32	6	0.775	(20)
	22.5 (155.1)		38	34	4	0.748	(19)

* Indicates that values utilize AASHTO LFD tensile stress limit
- Non-viable design

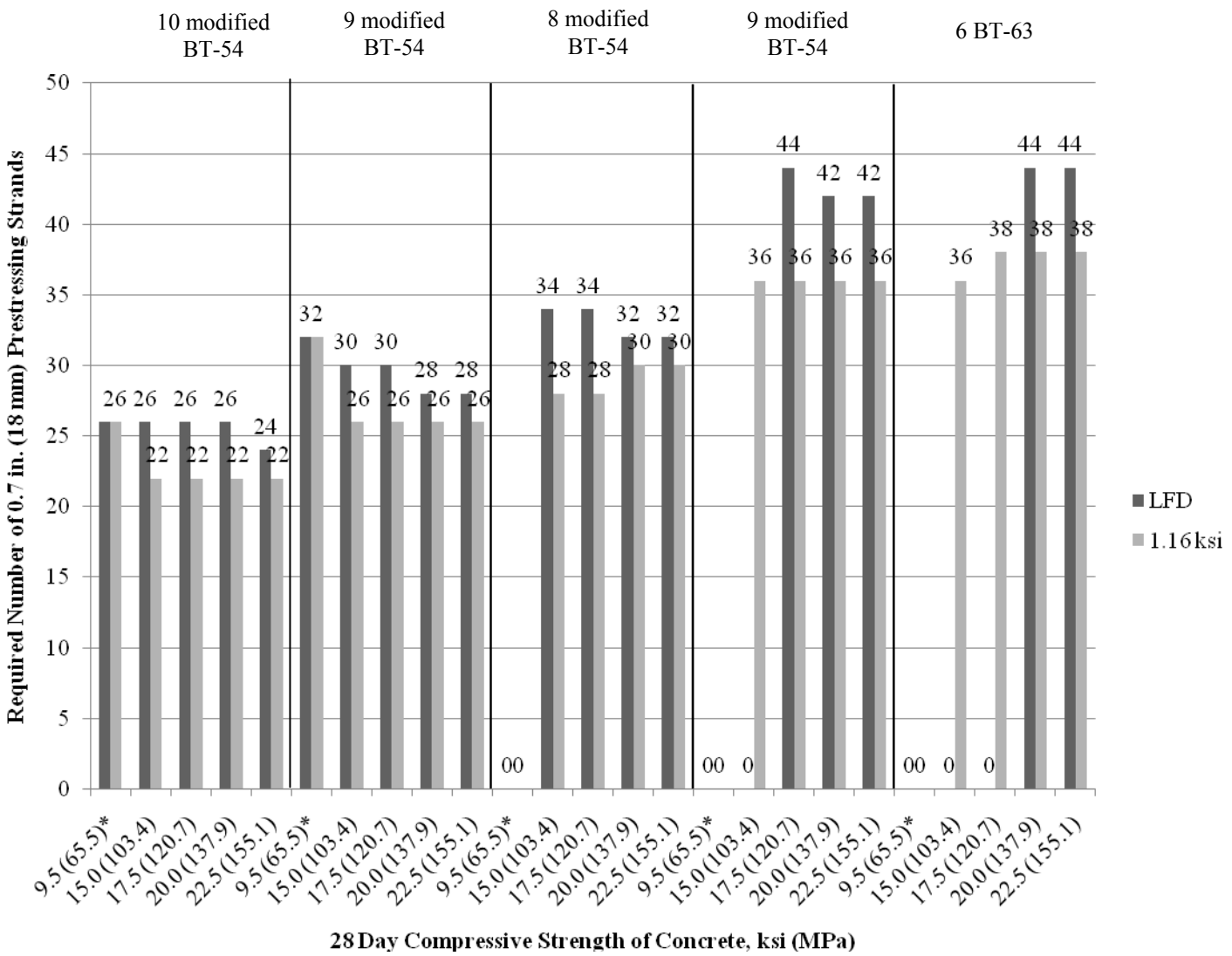

FIGURE 4.9 Comparison of the Required Number of 0.7 in. (18 mm) Prestressing Strands Based on Different Service Tensile Stress Limits for Sunland Park Bridge Two-Span Unit.

TABLE 4.15 Comparison of Allowable Tensile Stress Limits for Sunland Park Bridge Two-Span Unit Using 0.7 in. (18 mm) Strands.

		Tensile Stress Limit according to LFD			Tensile Stress Limit of 1.16 ksi (8.0 MPa)		
Viable Cross-Section Config-urations	Final Strength of UHPC, ksi (MPa)	Change in Deck Thickness, %	Savings of Concrete Volume in Girders, %	Increase in Number of Strands, %	Change in Deck Thickness %	Savings of Concrete Volume in Girders,%	Increase in Number of Strands,%
I (10 BT-54 Girder Lines)	9.5 (65.5)	6.7%	0%	0%	6.7%	0%	0%
	15.0 (103.4)			0%			-15%
	17.5 (120.7)			0%			-15%
	20.0 (137.9)			0%			-15%
	22.5 (155.1)			-8%			-15%
V (9 BT-54 Girder Lines)	9.5 (65.5)	6.7%	10%	23%	6.7%	10%	23%
	15.0 (103.4)			15%			0%
	17.5 (120.7)			15%			0%
	20.0 (137.9)			8%			0%
	22.5 (155.1)			8%			0%
IX (8 BT-54 Girder Lines)	9.5 (65.5)	13.3%	20%	-	13.3%	20%	-
	15.0 (103.4)			31%			8%
	17.5 (120.7)			31%			8%
	20.0 (137.9)			23%			15%
	22.5 (155.1)			23%			15%
XIII (7 BT-54 Girder Lines)	9.5 (65.5)	20.0%	30%	-	20.0%	30%	-
	15.0 (103.4)			-			38%
	17.5 (120.7)			69%			38%
	20.0 (137.9)			62%			38%
	22.5 (155.1)			62%			38%
XVII-b (6 BT-63 Girder Lines)	9.5 (65.5)*	N/A	N/A	-	40.0%	43%	-
	15.0 (103.4)			-			38%
	17.5 (120.7)			-			46%
	20.0 (137.9)			-			46%
	22.5 (155.1)			-			46%

- Non-viable design

4.2.4 CONSPAN® Flexure Analysis for Sunland Park Three-Span Unit

4.2.4.1 Sunland Park Bridge Three-Span Continuous Unit: Spans 3 and 5 with 0.6 in. (15 mm) Strands

The three-span continuous unit of the Sunland Park Bridge has two distinct girder cross-sections: span 3 and 5 have identical strand layouts and span 4 has a separate strand layout. Spans 3 and 5 have girders designed with 40 - 0.6 in. (15 mm) strands; 30 straight and 10 harped strands, to control stresses and provide the required flexural moment capacity. This configuration will be considered to be the baseline design.

The design matrix in Table 4.9 was followed sequentially until it was determined that a certain cross-section configuration was not a viable design according to the LFD specifications. Table 4.16 shows the results obtained from CONSPAN® using the Graybeal equation to estimate the modulus of elasticity and limiting the modulus of rupture to AASHTO provisions (i.e., the tensile strength of UHPC reported in literature is not considered in Table 4.16). Under LFD, in spans 3 and 5 UHPC allows the number of girder lines to be decreased from ten modified BT-54 girders to eight modified BT-54 girders, for a total savings of 20% in girder concrete volume; This concrete volume reduction can be realized with a 15-20% increase in the required number of 0.6 in. (15 mm) strands and 6.3% increase in the deck thickness. Table 4.17 summarizes the material savings.

Table 4.17 shows the results obtained from CONSPAN® using the Graybeal equation to estimate the modulus of elasticity and limiting the modulus of rupture to 1.16 ksi (8 MPa) for spans 3 and 5. The use of the higher tensile stress decreases the number of girder lines from ten modified BT-54 girders to eight modified BT-54 girders as well, the difference between the using the tensile strength of UHPC and LFD is savings in concrete volume can be realized with an 0% increase in the required number of strands. This is compared to 15-20% increase in the required number of strands under LFD provisions.

Figure 4.10 is a comparison of the results from Tables 4.16 and 4.17. By increasing the limit on allowable tensile stress savings in the number of prestressing strands ranges from 6-17%. Live load deflections were checked for these viable designs. A limiting deflection is given by L/800 or 1.8 in. (46 mm). All deflections reported in Tables 4.16 and 4.17 satisfy this serviceability requirement.

TABLE 4.16 Sunland Park Bridge Spans 3 & 5 Using 0.6 in. (15 mm) Strands According to LFD Code.

Viable Cross-Section Configurations	Final Strength of UHPC, ksi (MPa)	Deck Thickness in. (mm)	Total Number of Strands	Straight & Harped		Live Load Deflections, in. (mm)	
I (10 BT-54 Girder Lines)	9.5 (65.5)	8 (203)	36	26	10	0.875	(22)
	15.0 (103.4)		34	28	6	0.866	(22)
	17.5 (120.7)		34	28	6	0.826	(21)
	20.0 (137.9)		34	28	6	0.793	(20)
	22.5 (155.1)		32	26	6	0.767	(19)
II (9 BT-54 Girder Lines)	9.5 (65.5)	8 (203)	42	26	16	0.945	(24)
	15.0 (103.4)		40	26	14	0.791	(20)
	17.5 (120.7)		38	32	6	0.892	(23)
	20.0 (137.9)		38	32	6	0.857	(22)
	22.5 (155.1)		36	30	6	0.828	(21)
V (8 BT-54 Girder Lines)	9.5 (65.5)	8.5 (216)	-	-	-	-	-
	15.0 (103.4)		48	40	10	0.993	(25)
	17.5 (120.7)		48	42	6	0.948	(24)
	20.0 (137.9)		46	40	6	0.911	(23)
	22.5 (155.1)		46	40	6	0.879	(22)

- Non-viable design

TABLE 4.17 Sunland Park Bridge Span 3 & 5 Using 0.6 in. (15 mm) Strands According Tensile Limit Strength of 1.16 ksi (8 MPa).

Viable Cross-Section Configurations	Final Strength of UHPC, ksi (MPa)	Deck Thickness, in. (mm)	Total Number of Strands	Straight & Harped		Live Load Deflections, in. (mm)	
I (10 BT-54 Girder Lines)	9.5 (65.5)*	8 (203)	36	26	10	0.875	(22)
	15.0 (103.4)		30	28	2	0.873	(22)
	17.5 (120.7)		30	28	2	0.832	(21)
	20.0 (137.9)		30	28	2	0.798	(20)
	22.5 (155.1)		30	28	2	0.769	(20)
V (9 BT-54 Girder Lines)	9.5 (65.5)*	8 (203)	42	26	16	0.000	()
	15.0 (103.4)		34	32	2	0.796	(20)
	17.5 (120.7)		34	32	2	0.897	(23)
	20.0 (137.9)		34	32	2	0.861	(22)
	22.5 (155.1)		34	32	2	0.830	(21)
IX (8 BT-54 irder Lines)	9.5 (65.5)*	8.5 (216)	-	-	-	-	-
	15.0 (103.4)		40	36	4	0.998	(25)
	17.5 (120.7)		40	36	4	0.952	(24)
	20.0 (137.9)		40	36	4	0.914	(23)
	22.5 (155.1)		40	36	4	0.882	(22)

* Indicates that values utilize AASHTO LFD tensile stress limit
- Non-viable design

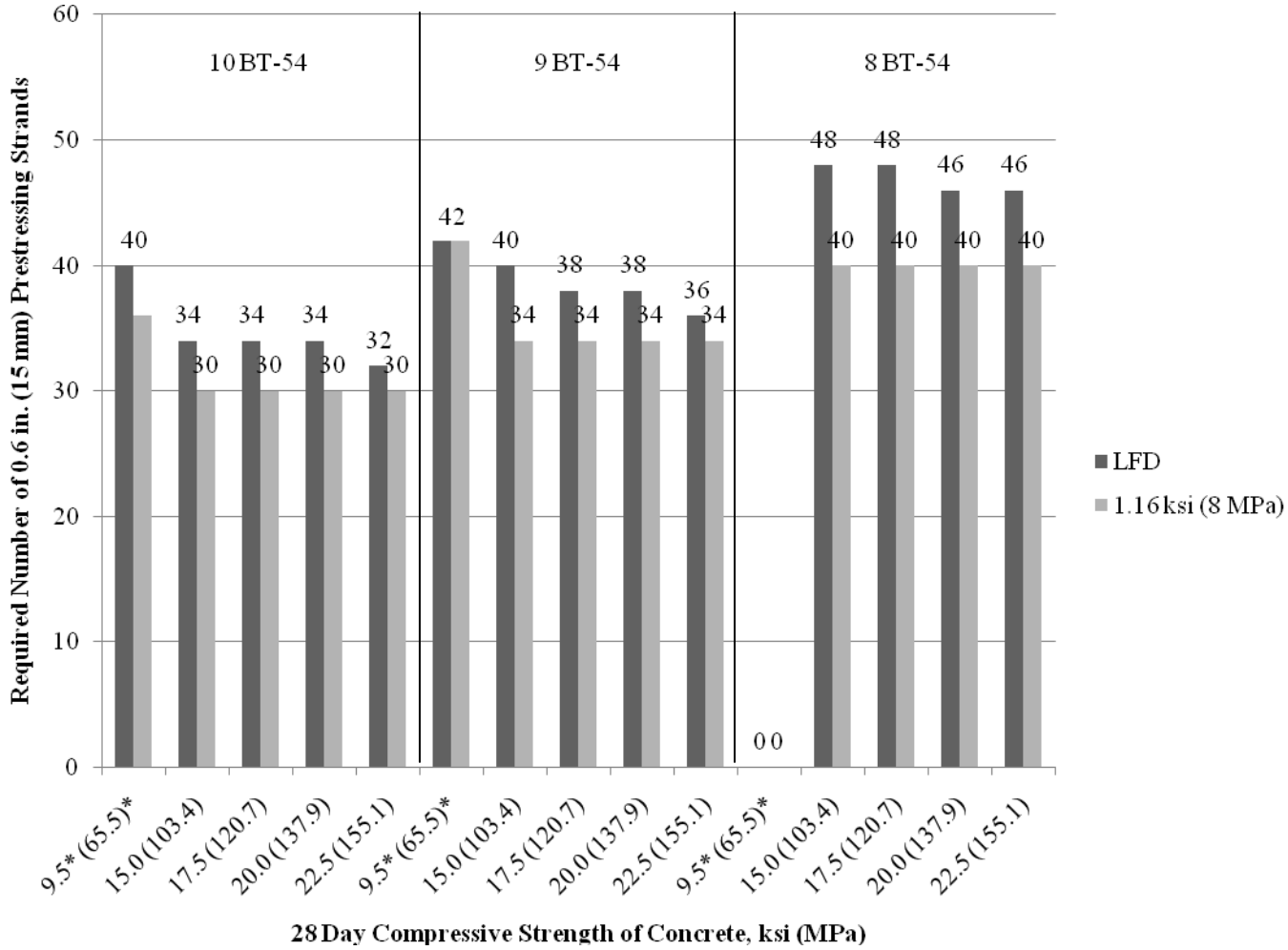

FIGURE 4.10 Comparison of the Required Number of 0.7 in. (18 mm) Prestressing Based on Different Service Tensile Stress Limits for Sunland Park Bridge Span 3 and 5.

TABLE 4.18 Comparison of Allowable Tensile Stress Limits for Sunland Park Bridge Spans 3 & 5 Using 0.6 in. (15 mm) Strands.

		Tensile Stress Limit according to LFD			Tensile Stress Limit of 1.16 ksi (8 MPa)		
Viable Cross-Section Config-urations	Final Strength of UHPC, ksi (MPa)	Change in Deck Thickness, %	Savings of Concrete Volume in Girders, %	Increase in Number of Strands, %	Change in Deck Thickness %	Savings of Concrete Volume in Girders, %	Increase in Number of Strands, %
I (10 BT-54 Girder Lines)	9.5 (65.5)	0.0%	0%	0%	0.0%	0%	-10%
	15.0 (103.4)			-15%			-25%
	17.5 (120.7)			-15%			-25%
	20.0 (137.9)			-15%			-25%
	22.5 (155.1)			-20%			-25%
II (9 BT-54 Girder Lines)	9.5 (65.5)	0.0%	10%	5%	0.0%	10%	5%
	15.0 (103.4)			0%			-15%
	17.5 (120.7)			-5%			-15%
	20.0 (137.9)			-5%			-15%
	22.5 (155.1)			-10%			-15%
VI (8 BT-54 Girder Lines)	9.5 (65.5)	6.3%	20%	-	6.3%	20%	-
	15.0 (103.4)			20%			0%
	17.5 (120.7)			20%			0%
	20.0 (137.9)			15%			0%
	22.5 (155.1)			15%			0%

4.2.4.2 Sunland Park Bridge Three-Span Continuous Unit: Span 4 with 0.6 in. (15 mm) Strands

Span 4 has 34 - 0.6 in. (15 mm) strands; 28 straight and 6 harped. This configuration will be considered to be the baseline design.

The design matrix in Table 4.9 was followed sequentially until it was determined that a certain cross-section configuration was not a viable design according to the LFD specifications. Table 4.19 shows the results obtained from CONSPAN® using the Graybeal equation to estimate the modulus of elasticity and limiting the modulus of rupture to AASHTO provisions (i.e., the tensile strength of UHPC reported in literature is not considered in Table 4.19). Under LFD, in spans 3 and 5 UHPC allows the number of girder lines to be decreased from ten modified BT-54 girders to eight modified BT-54 girders, for a total savings of 20% in girder concrete volume; This concrete volume reduction can be realized with a 15-20% increase in the required number of 0.6 in. (15 mm) strands and 6.3% increase in the deck thickness.

Table 4.20 shows the results obtained from CONSPAN® using the Graybeal equation to estimate the modulus of elasticity and limiting the modulus of rupture to 1.16 ksi (8 MPa) for spans 3 and 5. The use of the higher tensile stress decreases the number of girder lines from ten modified BT-54 girders to eight modified BT-54 girders as well, the difference between the using the tensile strength of UHPC and LFD is savings in concrete volume can be realized with a 0% increase in the required number of strands. This is compared to 15-20% increase in the required number of strands under LFD.

Figure 4.4 is a comparison of the results from Tables 4.19 and 4.20. By increasing the limit on allowable tensile stress savings in the number of prestressing strands ranges from 6-17%. Live load deflections were checked for all designs. A limiting deflection is given by L/800 or 1.8 in. (46 mm). All deflections reported in Tables 4.19 and 4.20 satisfy this serviceability requirement.

Table 4.21 is a summary of material savings.

TABLE 4.19 Sunland Park Bridge Span 4 Using 0.6 in. (15 mm) Strands According to LFD Code.

Viable Cross-Section Configurations	Final Strength of UHPC, ksi (MPa)	Deck Thickness in. (mm)	Total Number of Strands	Straight & Harped		Live Load Deflections, in. (mm)
I (10 BT-54 Girder Lines)	9.5 (65.5)	8 (203)	32	24	8	0.683 (17)
	15.0 (103.4)		30	26	4	0.676 (17)
	17.5 (120.7)		30	26	4	0.645 (16)
	20.0 (137.9)		30	26	4	0.619 (16)
	22.5 (155.1)		28	24	4	0.599 (15)
II (9 BT-54 Girder Lines)	9.5 (65.5)	8 (203)	36	26	10	0.737 (19)
	15.0 (103.4)		34	26	8	0.617 (16)
	17.5 (120.7)		32	26	6	0.698 (18)
	20.0 (137.9)		32	26	6	0.670 (17)
	22.5 (155.1)		32	26	6	0.646 (16)
VI (8 BT-54 Girder Lines)	9.5 (65.5)	8.5 (216)	-	-	-	- -
	15.0 (103.4)		40	34	6	0.774 (20)
	17.5 (120.7)		40	34	6	0.739 (19)
	20.0 (137.9)		38	32	6	0.71 (18)
	22.5 (155.1)		38	32	6	0.685 (17)

- Non-viable design

TABLE 4.20 Sunland Park Bridge Span 4 Using 0.6 in. (15 mm) Strands According to Tensile Stress Limit of 1.16 ksi (8 MPa).

Viable Cross-Section Configurations	Final Strength of UHPC, ksi (MPa)	Deck Thickness in. (mm)	Total Number of Strands	Straight & Harped		Live Load Deflections, in. (mm)	
I (10 BT-54 Girder Lines)	9.5 (65.5)*	8 (203)	32	24	8	0.683	(17)
	15.0 (103.4)		26	24	2	0.683	(17)
	17.5 (120.7)		26	24	2	0.651	(17)
	20.0 (137.9)		26	24	2	0.624	(16)
	22.5 (155.1)		26	24	2	0.601	(15)
V (9 BT-54 Girder Lines)	9.5 (65.5)*	8 (203)	36	26	10	0.737	(19)
	15.0 (103.4)		28	26	2	0.622	(16)
	17.5 (120.7)		28	26	2	0.704	(18)
	20.0 (137.9)		28	26	2	0.675	(17)
	22.5 (155.1)		28	26	2	0.650	(17)
IX (8 BT-54 Girder Lines)	9.5 (65.5)*	8.5 (216)	-	-	-	-	-
	15.0 (103.4)		34	30	4	0.781	(20)
	17.5 (120.7)		34	30	4	0.744	(19)
	20.0 (137.9)		34	30	4	0.714	(18)
	22.5 (155.1)		34	30	4	0.688	(17)

* Indicates that values utilize AASHTO LFD tensile stress limit
- Non-viable design

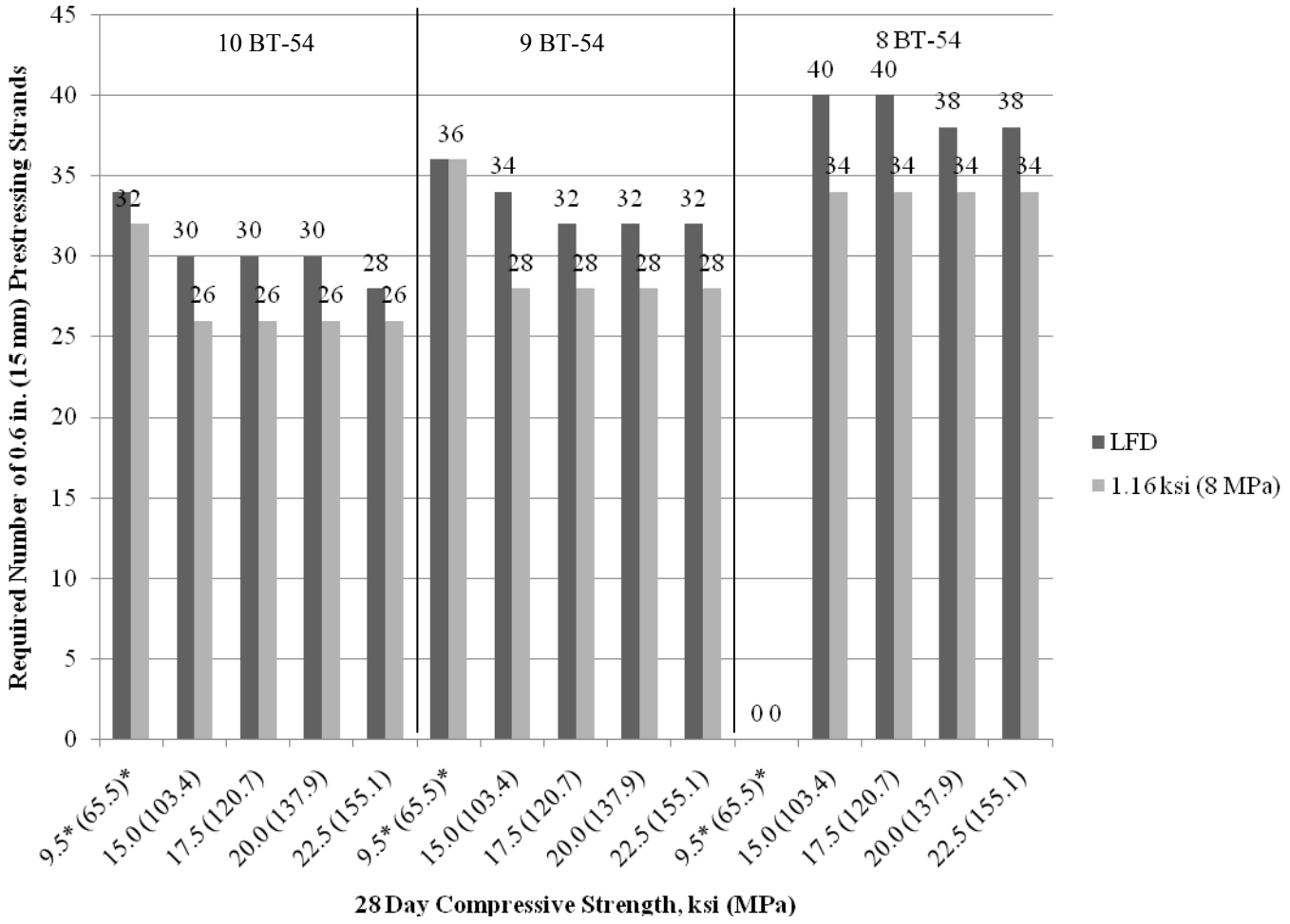

FIGURE 4.11 Comparison of the Required Number of 0.6 in. (18 mm) Prestressing Strands for Span 4 Based on Different Service Tensile Stress Limits for Sunland Park Bridge Span 4.

TABLE 4.21 Comparison of Allowable Tensile Stress Limits for Sunland Park Bridge Span 4 Using 0.6 in. (15 mm) Strands.

		Tensile Stress Limit according to LFD			Tensile Stress Limit of 1.16 ksi		
Viable Cross-Section Config-urations	Final Strength of UHPC, ksi (MPa)	Change in Deck Thickness, %	Savings of Concrete Volume in Girders, %	Increase in Number of Strands, %	Change in Deck Thickness, %	Savings of Concrete Volume in Girders, %	Increase in Number of Strands, %
I (10 BT-54 Girder Lines)	9.5 (65.5)	0.0%	0%	0%	0.0%	0%	-10%
	15.0 (103.4)			-15%			-25%
	17.5 (120.7)			-15%			-25%
	20.0 (137.9)			-15%			-25%
	22.5 (155.1)			-20%			-25%
II (9 BT-54 Girder Lines)	9.5 (65.5)	0.0%	10%	5%	0.0%	10%	5%
	15.0 (103.4)			0%			-15%
	17.5 (120.7)			-5%			-15%
	20.0 (137.9)			-5%			-15%
	22.5 (155.1)			-10%			-15%
VI (8 BT-54 Girder Lines)	9.5 (65.5)	6.3%	20%	-	6.3%	20%	-
	15.0 (103.4)			20%			0%
	17.5 (120.7)			20%			0%
	20.0 (137.9)			15%			0%
	22.5 (155.1)			15%			0%

- Non-viable design

4.2.5 Results of Sunland Park Bridge Three-Span Continuous Unit Utilizing 0.7 in. (18 mm) Strands

4.2.5.1 Sunland Park Bridge Three-Span Continuous Unit: Spans 3 and 5 with 0.7 in. (18 mm) Strands

The Three-Span continuous unit of the Sunland Park Bridge has two distinct cross-sections: span 3 and 5 have identical strand layouts and span 4 has separate strands layout. The base line for spans 3 and 5 will have 26 - 0.7 in. (18 mm) strands with a combination of 20 straight and 6 harped strands to control stresses and provide the required flexural moment capacity. For span 4 the base line will be considered to have 24 – 0.7 in. (18 mm) stands with a combination of 18 straight and 6 harped strands.

The design matrix in Table 4.9 was followed until it was determined that a certain cross-section configuration was not a viable design according to the LFD specifications. Table 4.22 shows the results obtained from CONSPAN® using the Graybeal equation to estimate the modulus of elasticity and limiting the modulus of rupture to AASHTO provisions (i.e., the tensile strength of UHPC is not considered in Table 4.22).

Table 4.23 shows the results obtained from CONSPAN® using the Graybeal equation to estimate the modulus of elasticity and limiting the modulus of rupture to 1.16 ksi (8 MPa). Figure 4.7 is a comparison of the results from Tables 4.22 and 4.23. By increasing the limit on allowable tensile stress savings in the number of prestressing strands ranges from 5-25%. Contrary to the I-25/Doña Ana Interchange, the increased tensile stress limit does not allow for any additional bridge configurations to be considered viable under the LFD code with 0.6 in. (15 mm) strands. The positive moment stresses for 7 modified BT-54 girders are too large to be considered feasible.

However, under AASHTO LFD, UHPC allows the number of girder lines and girder size to be decreased from 10 modified BT-54 girders to 8 modified BT-54 girders, for a total savings of 20% in girder concrete volume; this is similar to the finding in the I-25/Doña Ana Interchange of 23%. This concrete volume reduction can be realized with a 28-33% increase in the required number of 0.6 in. (15 mm) strands and a 6.3% increase in the deck thickness. Table 4.24 summarizes the material savings.

The use of UHPC tensile stress allows the number of girder lines and girder size to be decreased from 10 modified BT-54 girders to 8 modified BT-54 girders as well, the difference between the codes is this savings in concrete volume can be realized with an 11% increase in the required number of strands. This is compared to 20-30% increase in the required number of strands under AASHTO LFD.

Live load deflections were checked for these viable designs. A limiting deflection is given by L/800 or 1.8 in. (46 mm). All deflections reported in Tables 4.23 and 4.24 satisfy this serviceability requirement.

TABLE 4.22 Sunland Park Bridge Spans 3 and 5 Using 0.7 in. (18 mm) Strands According to LFD Code.

Viable Cross-Section Config-urations	Final Strength of UHPC, ksi (MPa)	Deck Thickness, in. (mm)	Total Number of Strands	Straight & Harped		Live Load Deflections, in. (mm)	
I (10 BT-54 Girder Lines)	9.5 (65.5)	8 (203)	26	20	6	0.873	(22)
	15.0 (103.4)		22	20	2	0.870	(22)
	17.5 (120.7)		22	20	2	0.830	(21)
	20.0 (137.9)		22	20	2	0.796	(20)
	22.5 (155.1)		22	20	2	0.768	(20)
V (9 BT-54 Girder Lines)	9.5 (65.5)	8 (203)	-	-	-	-	-
	15.0 (103.4)		24	22	2	0.795	(20)
	17.5 (120.7)		24	22	2	0.897	(23)
	20.0 (137.9)		24	22	2	0.861	(22)
	22.5 (155.1)		24	22	2	0.830	(21)
IX (8 BT-54 Girder Lines)	9.5 (65.5)	8.5 (216)	-	-	-	-	-
	15.0 (103.4)		28	26	2	0.995	(25)
	17.5 (120.7)		28	26	2	0.950	(24)
	20.0 (137.9)		28	26	2	0.912	(23)
	22.5 (155.1)		28	26	2	0.879	(22)
XIII (7 BT-54 Girder Lines)	9.5 (65.5)	9 (229)	-	-	-	-	-
	15.0 (103.4)		34	34	4	1.100	-
	17.5 (120.7)		34	34	4	1.018	(26)
	20.0 (137.9)		36	34	2	0.973	(25)
	22.5 (155.1)		36	34	2	0.940	(24)
XVII-b (6 BT-63 Girder Lines)	9.5 (65.5)	10.5 (267)	-	-	-	-	-
	15.0 (103.4)		-	-	-	-	-
	17.5 (120.7)		36	32	4	0.808	(21)
	20.0 (137.9)		36	32	4	0.775	(20)
	22.5 (155.1)		36	32	4	0.747	(19)

- Non-viable design

TABLE 4.23 Sunland Park Bridge Spans 3 and 5 Using 0.7 in Strands According to Allowable Tensile Stress of 1.16 ksi (8 MPa).

Viable Cross-Section Configurations	Final Strength of UHPC, ksi (MPa)	Deck Thickness, in. (mm)	Total Number of Strands	Straight & Harped		Live Load Deflections, in. (mm)	
I (10 BT-54 Girder Lines)	9.5* (65.5)*	8 (203)	26	18	6	0.680	(17)
	15.0 (103.4)		20	20	16	0.679	(17)
	17.5 (120.7)		20	20	16	0.647	(16)
	20.0 (137.9)		20	20	16	0.621	(16)
	22.5 (155.1)		20	20	16	0.598	(15)
V (9 BT-54 Girder Lines)	9.5* (65.5)*	8 (203)	-	-	-	-	-
	15.0 (103.4)		22	18	2	0.619	(16)
	17.5 (120.7)		20	18	2	0.703	(18)
	20.0 (137.9)		20	18	2	0.675	(17)
	22.5 (155.1)		20	18	2	0.650	(17)
IX (8 BT-54 Girder Lines)	9.5* (65.5)*	8.5 (216)	-	-	-	-	-
	15.0 (103.4)		24	22	2	0.781	(20)
	17.5 (120.7)		24	22	2	0.745	(19)
	20.0 (137.9)		24	22	2	0.714	(18)
	22.5 (155.1)		24	22	2	0.689	(18)
XIII (7 BT-54 Girder Lines)	9.5* (65.5)*	9 (229)	-	-	-	-	-
	15.0 (103.4)		30	28	2	0.862	(22)
	17.5 (120.7)		30	28	2	0.798	(20)
	20.0 (137.9)		30	28	2	0.766	(19)
	22.5 (155.1)		30	28	2	0.738	(19)
XVII-b (6 BT-63 Girder Lines)	9.5* (65.5)*	10.5 (267)	-	-	-	-	-
	15.0 (103.4)		-	-	-	-	-
	17.5 (120.7)		30	24	6	0.637	(16)
	20.0 (137.9)		32	26	6	0.606	(15)
	22.5 (155.1)		32	26	6	0.584	(15)

* Indicates that values utilize AASHTO LFD tensile stress limit
- Non-viable design

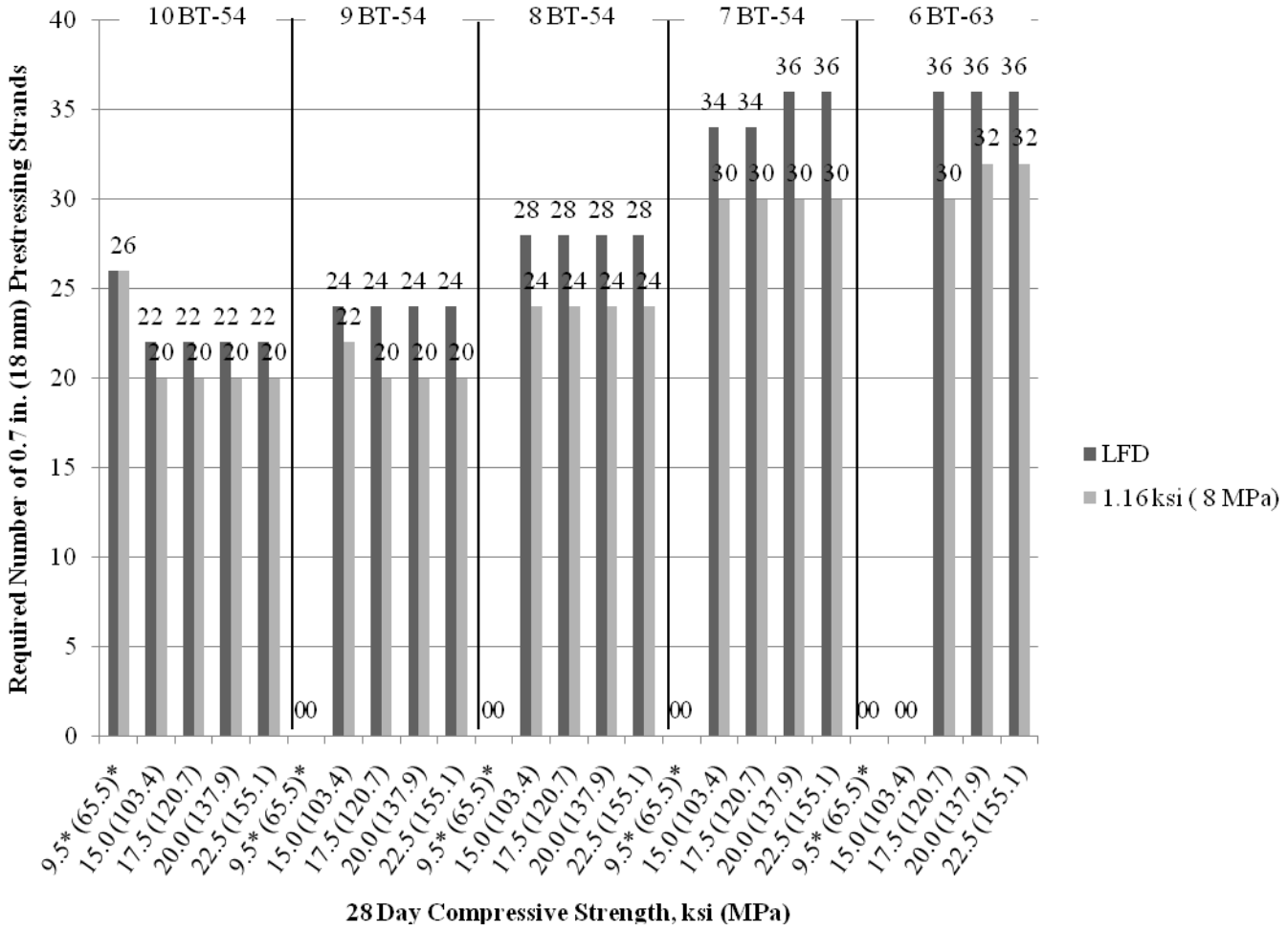

FIGURE 4.12 Comparison of the Required Number of 0.7 in. (18 mm) Prestressing Strands Based on Different Service Tensile Stress. Limits for Sunland Park Bridge Spans 3 and 5.

TABLE 4.24 Comparison of Allowable Tensile Stress Limits for Sunland Park Bridge Spans 3 & 5 Using 0.7 in. (18 mm) Strands.

		Tensile Stress Limit according to LFD			Tensile Stress Limit of 1.16 ksi (8 MPa)		
Viable Cross-Section Config-urations	Final Strength of UHPC, ksi (MPa)	Change in Deck Thickness, %	Savings of Concrete Volume in Girders, %	Increase in Number of Strands, %	Change in Deck Thickness ,%	Savings of Concrete Volume in Girders, %	Increase in Number of Strands, %
I (10 BT-54 Girder Lines)	9.5 (65.5)	6.7%	0%	0%	6.7%	0%	0%
	15.0 (103.4)			-15%			-23%
	17.5 (120.7)			-15%			-23%
	20.0 (137.9)			-15%			-23%
	22.5 (155.1)			-15%			-23%
V (9 BT-54 Girder Lines)	9.5 (65.5)	6.7%	10%	-	6.7%	10%	-
	15.0(103.4)			-8%			-15%
	17.5 (120.7)			-8%			-23%
	20.0 (137.9)			-8%			-23%
	22.5 (155.1)			-8%			-23%
IX (8 BT-54 Girder Lines)	9.5 (65.5)	13.3%	20%	-	13.3%	20%	-
	15.0 (103.4)			8%			-8%
	17.5 (120.7)			8%			-8%
	20.0 (137.9)			8%			-8%
	22.5 (155.1)			8%			-8%
XIII (7 BT-54 Girder Lines)	9.5 (65.5)	20.0%	30%	-	20.0%	30%	-
	15.0 (103.4)			-			15%
	17.5 (120.7)			31%			15%
	20.0 (137.9)			38%			15%
	22.5 (155.1)			38%			15%
XVII-b (6 BT-63 Girder Lines)	9.5 (65.5)*	N/A	N/A	-	40.0%	43%	-
	15.0 (103.4)			-			-
	17.5 (120.7)			-			15%
	20.0 (137.9)			-			23%
	22.5 (155.1)			-			23%

- Non-viable design

4.2.5.2 Sunland Park Bridge Three-Span Continuous Unit: Span 4 with 0.7 in. (18 mm) Strands

Span 4 has 34 0.6 in. (15 mm) strands; 28 straight and 6 harped. This configuration will be considered to be the baseline design.

The design matrix in Table 4.9 was followed sequentially until it was determined that a certain cross-section configuration was not a viable design according to the LFD specifications. Table 4.25 shows the results obtained from CONSPAN® using the Graybeal equation to estimate the modulus of elasticity and limiting the modulus of rupture to AASHTO provisions (i.e., the tensile strength of UHPC reported in literature is not considered in Table 4.25). Under LFD, in span 4 UHPC allows the number of girder lines to be decreased from ten modified BT-54 girders to eight modified BT-54 girders, for a total savings of 20% in girder concrete volume. This concrete volume reduction can be realized with a 15-20% increase in the required number of 0.6 in. (15 mm) strands and a 6.3% increase in the deck thickness.

Table 4.26 shows the results obtained from CONSPAN® using the Graybeal equation to estimate the modulus of elasticity and limiting the modulus of rupture to 1.16 ksi (8 MPa) for span 4. The use of the higher tensile stress decreases the number of girder lines from ten modified BT-54 girders to eight modified BT-54 girders as well, the difference between the using the tensile strength of UHPC and LFD is savings in concrete volume can be realized with a 0% increase in the required number of strands. This is compared to 15-20% increase in the required number of strands under LFD.

Figure 4.13 is a comparison of the results from Tables 4.25 and 4.26. By increasing the limit on allowable tensile stress savings in the number of prestressing strands ranges from 6-17%. Live load deflections were checked for all designs. A limiting deflection is given by L/800 or 1.8 in. (46 mm). All deflections reported in Tables 4.25 and 4.26 satisfy this serviceability requirement.

Table 4.27 summarizes the material savings.

TABLE 4.25 Sunland Park Bridge Span 4 Using 0.7 in. (18 mm) Strands According to LFD Code.

Viable Cross-Section Configurations	Final Strength of UHPC, ksi (MPa)	Deck Thickness in. (mm)	Total Number of Strands	Straight & Harped		Live Load Deflections, in. (mm)	
I (10 BT-54 Girder Lines)	9.5 (65.5)	8 (203)	24	18	6	0.680	(17)
	15.0 (103.4)		22	18	4	0.675	(17)
	17.5 (120.7)		22	18	4	0.643	(16)
	20.0 (137.9)		20	16	4	0.592	(15)
	22.5 (155.1)		20	16	4	0.598	(15)
V (9 BT-54 Girder Lines)	9.5 (65.5)	8 (203)	-	-	-	-	-
	15.0 (103.4)		24	18	6	0.616	(16)
	17.5 (120.7)		24	20	4	0.695	(18)
	20.0 (137.9)		24	20	4	0.667	(17)
	22.5 (155.1)		24	20	4	0.849	(22)
IX (8 BT-54 Girder Lines)	9.5 (65.5)	8.5 (216)	-	-	-	-	-
	15.0 (103.4)		28	24	4	0.771	(20)
	17.5 (120.7)		28	24	4	0.736	(19)
	20.0 (137.9)		28	24	4	0.707	(18)
	22.5 (155.1)		28	22	6	0.682	(17)
XIII (7 BT-54 Girder Lines)	9.5 (65.5)	9 (229)	-	-	-	-	-
	15.0 (103.4)		34	28	6	0.852	(22)
	17.5 (120.7)		34	28	6	0.789	(20)
	20.0 (137.9)		34	28	6	0.758	(19)
	22.5 (155.1)		34	28	6	0.731	(19)
XVII-b (6 BT-63 Girder Lines)	9.5 (65.5)	10.5 (267)	-	-	-	-	-
	15.0 (103.4)		-	-	-	-	-
	17.5 (120.7)		36	30	6	0.625	(16)
	20.0 (137.9)		34	30	4	0.603	(15)
	22.5 (155.1)		34	30	4	0.581	(15)

- Non-viable design

TABLE 4.26 Sunland Park Bridge Span 4 Using 0.7 in Strands According to Allowable Tensile Stress of 1.16 ksi (8 MPa).

Viable Cross-Section Configurations	Final Strength of UHPC, ksi (MPa)	Deck Thickness in. (mm)	Total Number of Strands	Straight & Harped		Live Load Deflections, in. (mm)	
I (10 BT-54 Girder Lines)	9.5 (65.5)*	8 (203)	24	18	6	0.680	(17)
	15.0 (103.4)		20	16	4	0.679	(17)
	17.5 (120.7)		20	16	4	0.647	(16)
	20.0 (137.9)		20	16	4	0.621	(16)
	22.5 (155.1)		20	16	4	0.598	(15)
V (9 BT-54 Girder Lines)	9.5 (65.5)*	8 (203)	-	-	-	-	-
	15.0 (103.4)		22	18	2	0.619	(16)
	17.5 (120.7)		20	18	2	0.703	(18)
	20.0 (137.9)		20	18	2	0.675	(17)
	22.5 (155.1)		20	18	2	0.650	(17)
IX (8 BT-54 Girder Lines)	9.5 (65.5)*	8.5 (216)	-	-	-	-	-
	15.0 (103.4)		24	22	2	0.781	(20)
	17.5 (120.7)		24	22	2	0.745	(19)
	20.0 (137.9)		24	22	2	0.714	(18)
	22.5 (155.1)		24	22	2	0.689	(18)
XIII (7 BT-54 Girder Lines)	9.5 (65.5)*	9 (229)	-	-	-	-	-
	15.0 (103.4)		30	28	2	0.862	(22)
	17.5 (120.7)		30	28	2	0.798	(20)
	20.0 (137.9)		30	28	2	0.766	(19)
	22.5 (155.1)		30	28	2	0.738	(19)
XVII-b (6 BT-63 Girder Lines)	9.5 (65.5)*	10.5 (267)	-	-	-	-	-
	15.0 (103.4)		-	-	-	-	-
	17.5 (120.7)		30	24	6	0.637	(16)
	20.0 (137.9)		32	26	6	0.606	(15)
	22.5 (155.1)		32	26	6	0.584	(15)

* Indicates that values utilize AASHTO LFD tensile stress limit.
- Non-viable design

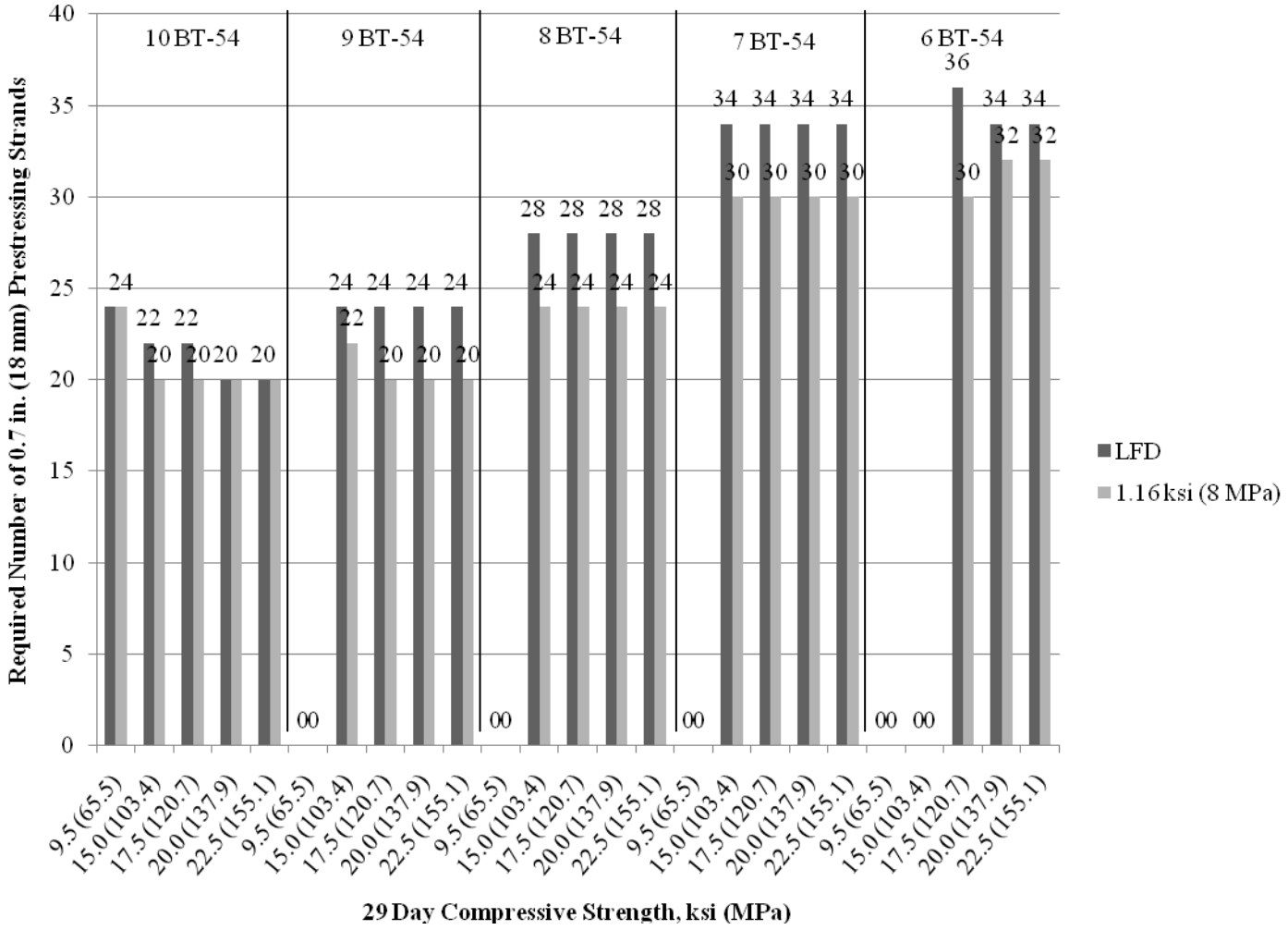

FIGURE 4.13 Comparison of the Required Number of 0.7 in. (18 mm) Prestressing Strands Based on Different Service Tensile Stress Limits for Sunland Park Bridge Span.

TABLE 4.27 Comparison of Allowable Tensile Stress Limits for Sunland Park Bridge Span 4 Using 0.7 in. (18 mm) Strands.

		Tensile Stress Limit according to LFD			Tensile Stress Limit of 1.16 ksi (8 MPa)		
Viable Cross-Section Configurations	Final Strength of UHPC, ksi (MPa)	Change in Deck Thickness, %	Savings of Concrete Volume in Girders, %	Increase in Number of Strands, %	Change in Deck Thickness, %	Savings of Concrete Volume in Girders, %	Increase in Number of Strands, %
I (10 BT-54 Girder Lines)	9.5 (65.5)	6.7%	0%	-8%	6.7%	0%	-8%
	15.0 (103.4)			-15%			-23%
	17.5 (120.7)			-15%			-23%
	20.0 (137.9)			-23%			-23%
	22.5 (155.1)			-23%			-23%
V (9 BT-54 Girder Lines)	9.5 (65.5)	6.7%	10%	-	6.7%	10%	-
	15.0 (103.4)			-8%			-15%
	17.5 (120.7)			-8%			-23%
	20.0 (137.9)			-8%			-23%
	22.5 (155.1)			-8%			-23%
IX (8 BT-54 Girder Lines)	9.5 (65.5)	13.3%	20%	-	13.3%	20%	-
	15.0 (103.4)			8%			-8%
	17.5 (120.7)			8%			-8%
	20.0 (137.9)			8%			-8%
	22.5 (155.1)			8%			-8%
XIII (7 BT-54 Girder Lines)	9.5 (65.5)	20.0%	30%	-	20.0%	30%	-
	15.0 (103.4)			-			-
	17.5 (120.7)			31%			15%
	20.0 (137.9)			31%			15%
	22.5 (155.1)			31%			15%
XVII-b (6 BT-63 Girder Lines)	9.5 (65.5)	N/A	N/A	-	40.0%	43%	-
	15.0 (103.4)			-			-
	17.5 (120.7)			-			15%
	20.0 (137.9)			-			23%
	22.5 (155.1)			-			23%

- Non-viable design

5 UHPC PARAMETRIC STUDY: SHEAR

The shear design of UHPC girders differs significantly from the design of HPC girders. The steel fibers that are contained in a steel fiber reinforced (SFR) UHPC mix design contribute to the shear capacity of the section at the ultimate limit state (i.e., after the girder section cracks). The combined contribution of the concrete and steel fibers to shear capacity can be sufficient to carry factored shear forces without the need for the traditional, transverse mild steel stirrups; thus, the mild steel reinforcement may be reduced or eliminated according to AFGC/SETRA 7.3.2 (2002).

5.1 DESIGN SHEAR STRENGTH PROCEDURE FOR STEEL FIBER REINFORCED UHPC

The shear strength procedure described in this section is based on the Recommendations for the Design of UHPC by MIT. This procedure uses the French based AFGC/SETRA recommendations and the research conducted at MIT on Ductal®. The formalized procedure is found in the white paper produced by Dr. Franz-Josef Ulm of MIT for the Mars Hill Bridge built in Wapello County, Iowa (Ulm 2004).

For the shear portion of this study shear loads and forces were calculated using the AASHTO LRFD specifications. Justification for using LRFD methods is twofold. First, LRFD uses state of the art methods for determining the anticipated shear failure angle, θ, based on the Modified Compression Field Theory. Secondly, the procedures developed used by Dr. Ulm of MIT use the LRFD load factors to determine the factored shear force on the UHPC girder.

The ultimate limit state (ULS) for shear is based on the premise that crack-bridging (steel) fibers carry a part of the shear load, very similar to shear reinforcement. The design strength of the section is expressed as:

$$\varphi_V V_R^{ULS} = \varphi_c V_c + V_p + \varphi_f V_f + \varphi_s V_s \qquad \text{Equation 5.1}$$

where, $\varphi_v V_R^{ULS}$ is the characteristic shear capacity (referred to as the design capacity for the remainder of this report); φ_c is a strength reduction factor, taken as 0.66 to account for material variability; V_c is the contribution of the concrete; V_p is the contribution of the harped prestressing strands; φ_f is a strength reduction factor taken as 0.66 to account for non-ideal randomization of the fibers; V_f is the contribution of the steel fibers; $\varphi_s$is the LRFD strength reduction factor for shear and is taken as 0.9; and V_s is contribution of the mild steel stirrup. For prestressed concrete applications, the concrete contribution to shear strength is expressed as:

$$V_c = 0.09\sqrt{f'_c}\, b_w z \qquad \text{Equation 5.2}$$

where, f'_c is the 28 day design compressive strength of the concrete; b_w is the web width; and z is the lever arm at the ultimate moment equal to the distance between the centroid of the

compression block and the centroid of the prestressing strands (Graybeal 2006). The term V_p represents the vertical force component of the harped prestressing strands after losses and the steel fiber contribution to shear strength is given as:

$$V_f = \frac{A\sigma_p}{\tan(\beta_u)} \quad \text{Equation 5.3}$$

where, A is the area of the shear plane (i.e., area of fiber effect), and is computed as 90% of the web width multiplied by the lever arm at ultimate moment (i.e., $A = 0.9b_w z$). The term σ_p is the residual tensile strength carried across the shear crack from the time of cracking until a limiting strain is achieved. According to Graybeal (2006), the value for residual tensile stress is determined experimentally from tension tests. In the absence of experimental data for the UHPC and the girders of this parametric study typical values from literature were examined and a conservative value of 1.0 ksi (6.9 MPa) was used in this study. This is a reasonable value to assume without experimental testing because it is below the expected tensile cracking limit of the UHPC. The final term is tan(β_u), which is the tangent of the compression strut angle in the shear area measured from the horizontal (β_u has a lower bound of 30°). In the AASHTO LRFD specifications θ is identical to the term β_u. For the remainder of this study, the angle of the compression strut will be referred to as θ. Under the LRFD code option in CONSPAN®, θ is calculated directly and is given as output data. The method used by CONSPAN®, to calculate θ is specified in LRFD Art. 5.8.3.4.2.

Finally, if mild steel stirrups are required then V_s is computed according to LRFD Equation 5.8.3.3-4.

$$V_s = \frac{A_v f_y (\cot\theta + \cot\alpha)\sin\alpha}{s} \quad \text{Equation 5.4}$$

where, A_v is the area of the transverse reinforcement (i.e., stirrups); f_y is the yield strength of the mild steel [equal to 60 ksi (414 MPa)]; θ is as described above; α is the angle of the transverse reinforcement (taken as 90°); and s is the spacing of the stirrups.

5.1.1 Shear Analysis for I-25/Doña Ana Interchange

In the flexure portion of this study, two final bridge configurations were obtained:

1. Four BT-63 girders using 0.6 in. (15 mm) strands.
2. Four BT-54 girders using 0.7 in. (18 mm) strands.

These configurations were obtained based on flexure using the AASHTO LFD specifications. The CONSPAN® program was used to generate the ultimate shear forces for these two bridge configurations based on the AASHTO LRFD specifications.

5.1.1.1 Results for Four BT-63 Girders with 0.6 in. (15 mm) Strands

The final bridge configuration based on LFD for flexure employed four typical NMDOT BT-63 girders with design compressive strengths of 15.0 to 22.5 ksi (103.4 to 155.1 MPa). Table 5.1 provides a summary of the shear findings at the critical section located 5.17 ft (1.58 m) from the face of the support. Note that all design compressive strengths used in the flexure portion of this study produced adequate shear capacity without the need for shear stirrups. The excess capacity ranges from 5.7% to 11% for 15.0 to 22.5 ksi (103.4 to 155.1 MPa), respectively.

The computed shear failure angle at the critical section was below the limiting value of 30°; thus, the angle used to determine the steel fiber contribution to the strength of the section was taken as 30°. Note that the fiber contribution is constant for all design compressive strengths. Recall that the fiber contribution is not related to the compressive or tensile strength of the concrete, but is a function of the shear failure plane and residual tensile stress in the fibers after the concrete cracks. It should further be noted that the fiber contribution to the shear capacity is much larger compared to the concrete and the harped strand contribution. The fiber contribution represents approximately 77.2% of the design shear strength of the girder section. Also note that the harped contribution is greatest for the 15.0 ksi (103.4 MPa) concrete due to the increase in the number of required harped strands to meet the stress at release requirements.

The girder section has sufficient capacity to carry the ultimate shear forces with no change to the cross-sectional geometry. Figure 5.1 represents shear envelopes based on the design compressive strength of the UHPC. The figure is an envelope for half the girder length and is symmetrical about the centerline.

In Figure 5.1 the design strength increases slightly from the critical section to the $3/10^{th}$ point. This is the result of the lever arm length (z) increase due to the lower center of gravity of the prestressing strand group. This increase in lever arm increases the fiber and concrete contribution to the design strength, while the strand contribution remains constant.

The apparent sudden decrease in design strength between the $3/10^{th}$ and $4/10^{th}$ point is a result of a greater predicted angle, θ, (thus, reducing the fiber contribution), and the lack of harped strands in this region of the girder.

Notice the difference in the slope of the capacity line of the 15.0 ksi (103.4 MPa) design compressive strength and the remaining design compressive strengths between the critical section and the $3/10^{th}$ point. The cause for the lower design shear strength is the increased number of harped prestressing strands. The higher number of harped strands causes the center of gravity of the strands to be higher in the beam, resulting in a smaller lever arm, z.

As a final note for Figure 5.9, notice the relatively flat trend of the design strength. Such behavior is expected because the fiber content of the UHPC mix is constant throughout the girder. For comparison, traditionally reinforced girder with mild steel stirrups has a design

capacity that is primarily dependant on the spacing of the stirrups. These stirrups vary in spacing throughout the length of the girder and the general shape of the design capacity graph is stepped.

TABLE 5.1 Shear Results for I-25/Doña Ana Interchange with Four BT-63 Girders Using 0.6 in. (15 mm) Prestressing Strands.

	f'_c = 22.5 ksi (155.1 MPa)	f'_c = 20.0 ksi (137.9 MPa)	f'_c = 17.5 ksi (120.7 MPa)	f'_c = 15.0 ksi (103.4 MPa)
Typical Web Width, in. (mm)	6 (150)	6 (150)	6 (150)	6 (150)
Modified Web Width, in. (mm)	N/A	N/A	N/A	N/A
Computed Shear Failure Plane Angle, θ, degrees	27.9	27.8	27.7	27.8
Fiber Contribution, V_f @ critical section kips (kN)	515.8 (2,294)	515.8 (2,294)	515.8 (2,294)	515.8 (2,294)
Concrete Contribution, V_c @ critical section kips (kN)	135.7 (603.1)	128.0 (569.4)	119.8 (532.9)	107.0 (476.0)
Strand Contribution, V_p @ critical section kips (kN)	6.5 (28.9)	6.5 (28.9)	6.5 (28.9)	12.3 (54.7)
Design Shear Strength, $\varphi_v V_R^{ULS}$ kips (kN)	440.9 (1,961)	435.7 (1,938)	430.0 (1,918)	415.9 (1,850)
Factored Shear, V_u @ critical section kips (kN)	392.5 (1,746)	392.5 (1,746)	392.5 (1,746)	392.5 (1,746)
Excess Capacity, %	11.0%	9.9%	8.7%	5.7%

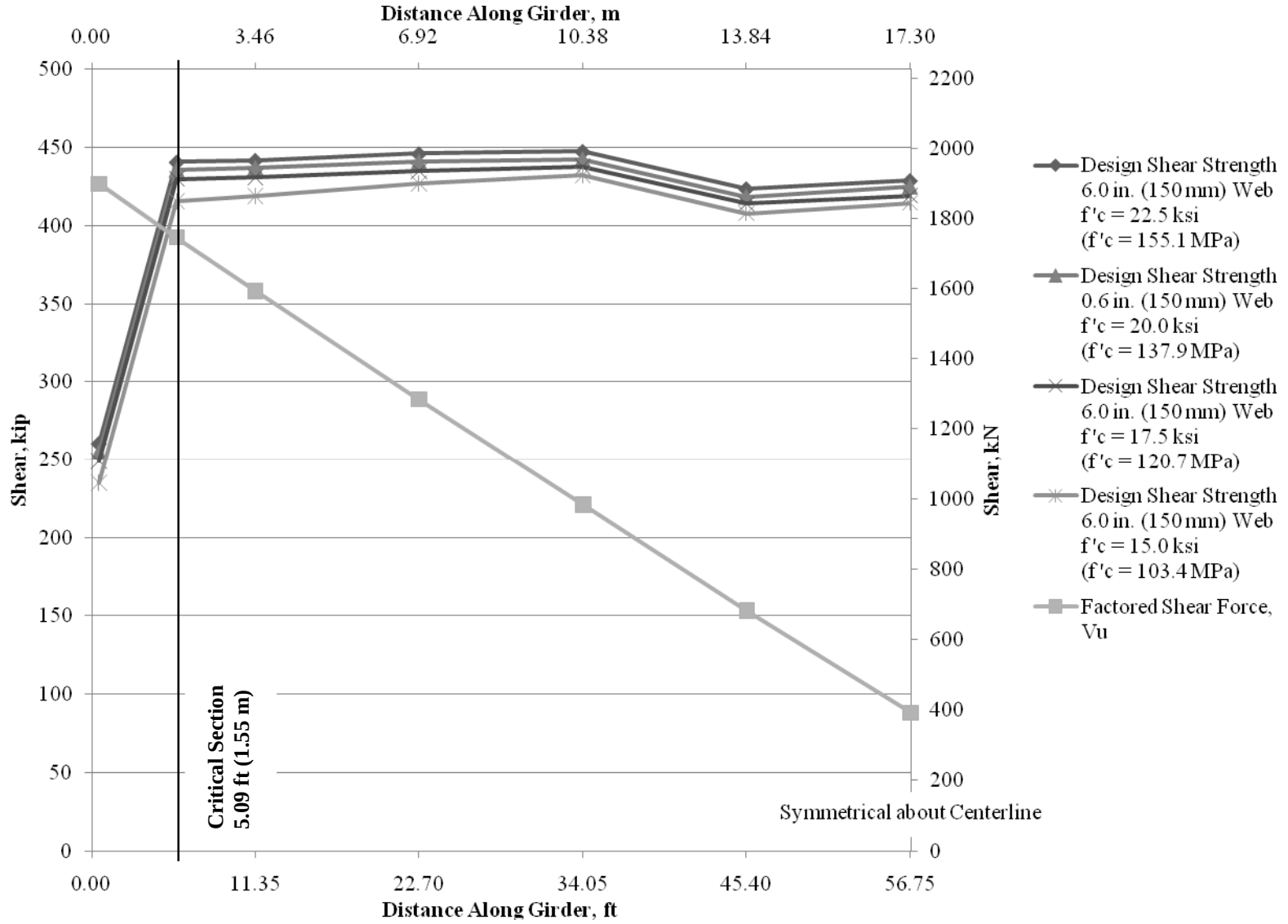

FIGURE 5.1 Shear Envelopes for I-25/Doña Ana Interchange with Four BT-63 Girders Using 0.6 in. (15 mm) Strands.

5.1.1.2 Results for Four BT-54 Girders Using 0.7 in. (18 mm) Strands

The final bridge configuration based on LFD for flexure employed four typical NMDOT BT-54 girders with design compressive strengths of 20.0 to 22.5 ksi (120.7 to 155.1 MPa).

At the critical section, located 5.11 ft (1.56 m) from the face of the support, note that both design compressive strengths used in the flexure portion of this study produced viable shear designs when the web thickness was increased to 7.0 in. (180 mm), Table 5.2 is a summary of the shear findings. The typical BT-54 girders have a 6.0 in. (150 mm) web thickness and have insufficient capacity at the critical section. The increase of width did not change the amount of prestressing strands required for flexure. The excess capacity ranges from 10.3% to 11.2% for 20.0 to 22.5 ksi (137.9 to 155.1 MPa), respectively, for the BT-54 girders with 7.0 in. (180 mm).

Note that to meet shear capacity requirements the width of the web was increased; however, another alternative would be to add traditional mild steel stirrups in the critical section of the girder to satisfy capacity requirements. Table 5.3 provides a summary of the shear findings at the critical section. Figure 5.3 is the shear envelope that illustrates that No. 5 (M16) shear stirrups placed at 24.0 in. (610.0 mm) on-center (o.c.) meets the design capacity requirements.

TABLE 5.2 Shear Results for I-25/Doña Ana Interchange Using 0.7 in. (18 mm) Prestressing Strands.

	f'_c = 22.5 ksi (155.1 MPa)	f'_c = 20.0 ksi (137.9 MPa)
Typical Web Width, in. (mm)	6 (150)	6 (150)
Modified Web Width, in. (mm)	7 (180)	7 (180)
Computed Shear Failure Plane Angle, θ, degrees	27.6	27.6
Fiber Contribution, V_f @ critical section kips (kN)	503.0 (2,238)	503.0 (2,238)
Concrete Contribution, V_c @ critical section kips (kN)	129.2 (574.7)	122.0 (542.7)
Strand Contribution, V_p @ critical section kips (kN)	22.4 (99.6)	22.4 (99.6)
Design Shear Strength, $\varphi_v V_R^{ULS}$ kips (kN)	443.9 (1,961)	439.1 (1,953)
Factored Shear, V_u @ critical section kips (kN)	394.0 (1,753)	394.0 (1,753)
Excess Capacity, %	11.2%	10.3%

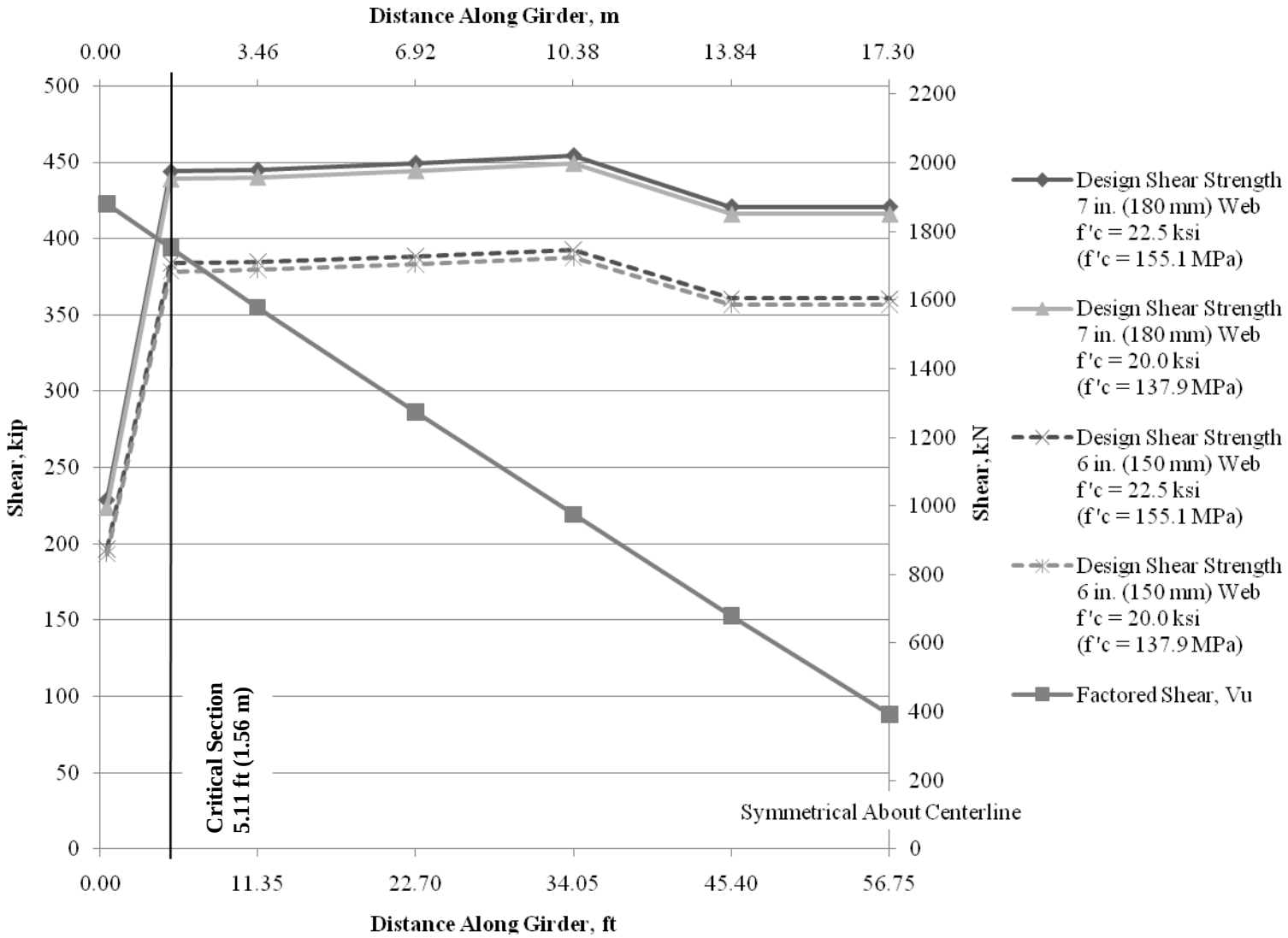

FIGURE 5.2 Shear Envelopes for I-25/Doña Ana Interchange with Four Modified BT-54 Girders Using 0.7 in. (18 mm) Strands.

TABLE 5.3 Shear Results for I-25/Doña Ana Interchange Using 0.7 in. (18 mm) Prestressing Strands with No. 5 (M16) Mild Steel Stirrups.

	f'_c = 22.5 ksi (155.1 MPa)	f'_c = 20.0 ksi (137.9 MPa)
Typical Web Width, in. (mm)	6 (150)	6 (150)
Modified Web Width, in. (mm)	N/A	N/A
Computed Shear Failure Plane Angle, θ, degrees	27.6	27.6
Fiber Contribution, V_f @ critical section kips (kN)	503.0 (2,238)	503.0 (2,238)
Stirrup Contribution, V_s @ critical Section kips (kN)	114.2 (508.0)	114.2 (508.0)
Concrete Contribution, V_c @ critical section kips (kN)	110.8 (492.9)	104.6 (465.3)
Strand Contribution, V_p @ critical section kips (kN)	22.4 (99.6)	22.4 (99.6)
Design Shear Strength, $\varphi_v V_R^{ULS}$ kips (kN)	486.5 (2,164.0)	481.4 (2,141.0)
Factored Shear, V_u @ critical section kips (kN)	394.0 (1,753)	394.0 (1,753)
Excess Capacity, %	19.0%	18.5%

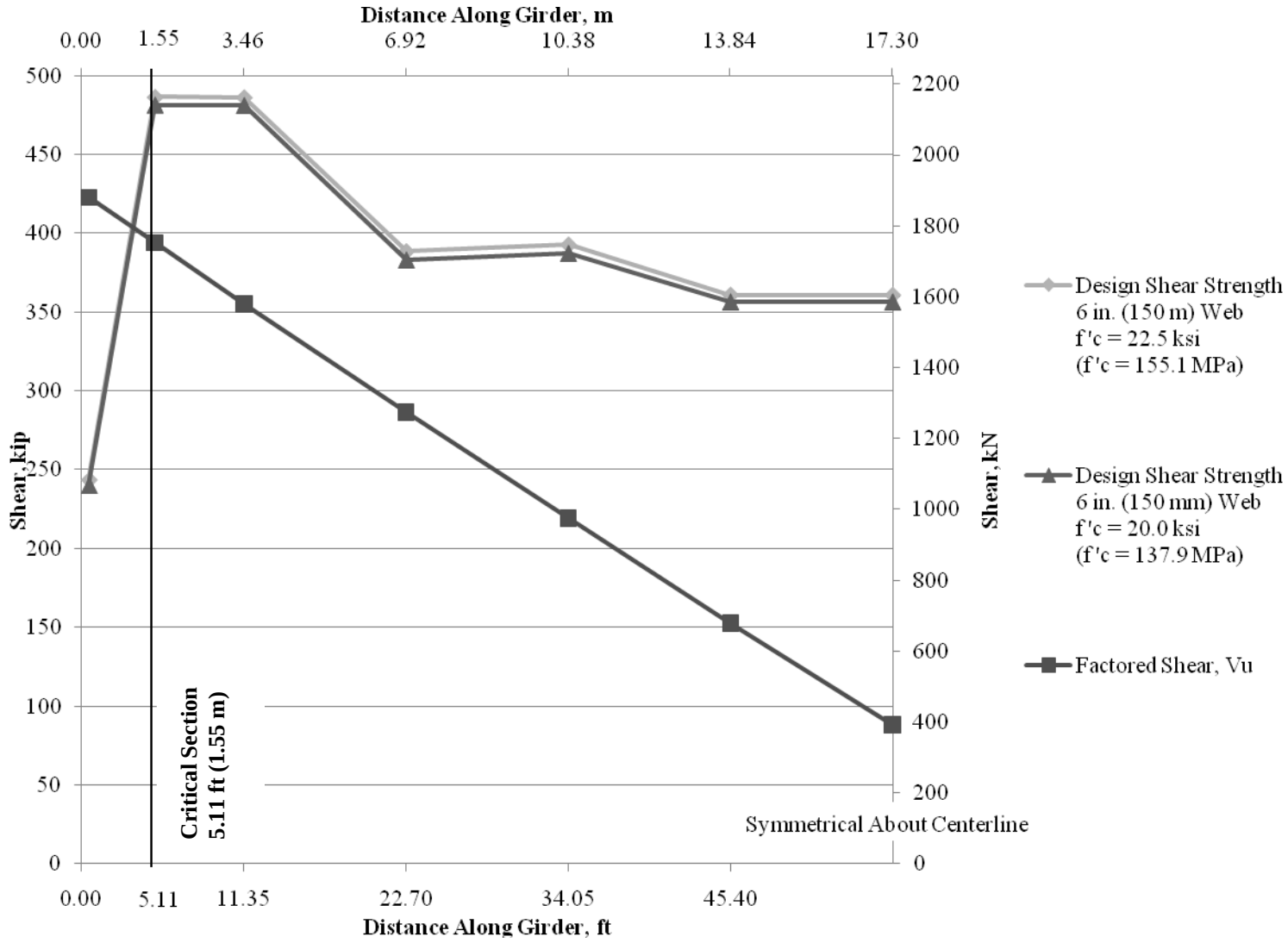

FIGURE 5.3 Shear Envelopes for I-25/Doña Ana Interchange with Four Modified BT-54 Girders Using 0.7 in. (18 mm) Strands and Traditional Mild Steel Stirrups.

5.1.2 Shear Analysis of Sunland Park Bridge

In the flexure portion of this study, the two-span continuous unit and three-span continuous unit of the Sunland Park Bridge were treated separately. For both units two final bridge configurations were obtained.

1. Eight modified BT-54 girders with 0.6 in. (15 mm) strands.
2. Six BT-63 girders with 0.7 in. (18 mm) strands.

These configurations were obtained based on flexure using the AASHTO LFD specifications. The CONSPAN® program was used to generate the ultimate shear forces for these two bridge configurations based on the AASHTO LRFD specifications.

5.1.2.1 Results for Two-Span Continuous Unit with Eight BT-54 Girders Using 0.6 in. (15 mm) Strands

The final bridge configuration based on LFD for flexure results employed eight modified NMDOT BT-54 girders with design compressive strengths of 15.0 to 22.5 ksi (103.4 to 155.1 MPa). Table 5.4 provides a summary of the shear findings at the critical section near the interior support located at 117.61 ft (35.85 m), note that all design compressive strengths used in the flexure portion of this study produced adequate shear capacity without the need for shear stirrups when the web width was increased 1.0 in. (25 mm) to 8.0 in. (203 mm). The excess capacity ranges from 6.9% to 11.2% for 15.0 to 22.5 ksi (103.4 to 155.1 MPa) UHPC, respectively, at the interior support. The excess capacity at critical sections near the exterior supports range from 27.5% to 30.2% for 15.0 to 22.5 ksi (103.4 to 155.1 MPa) concrete, respectively.

The computed shear failure angles at the critical section near the interior support was above the limiting value of 30° The angles, θ are larger at the interior support than the exterior support. This is a result of the combined effects of shear and flexure at the interior support.

Figure 5.4 represents shear envelopes based on the design compressive strength. As shown in the figure, at the critical section near the interior support, the computed design strength is lower than the design strength at the exterior support. This is due to the larger computed shear failure crack of approximately 33.9°, compared to the 30° angle at the exterior support. Note the large excess capacity at the exterior support, which suggests that a more refined design may provide greater material savings.

Similar to the I-25/Doña Ana Interchange shear design, an alternative to web width increase is to add mild steel stirrups in the critical shear regions. Table 5.5 provides a summary of the shear findings when No. 5 (M16) stirrups at 24 in. (610 mm) o.c. are used. The excess capacity ranges from 2.6% to 6.5% for 15.0 to 22.5 ksi (103.4 to 155.1 MPa) concrete, respectively, at the interior support. The stirrups were placed at 24.0 in. (610 mm) for a distance of $1/10^{th}$ the span [12.29 ft (3.75 m)] from the supports. Figure 5.5 represents shear envelopes based on the design compressive strength.

TABLE 5.4 Shear Results for Sunland Park Bridge Two-Span Unit with Eight BT-54 Girders Using 0.6 in. (15 mm) Prestressing Strands.

	f'_c = 22.5 ksi (155.1 MPa)	f'_c = 20.0 ksi (137.9 MPa)	f'_c = 17.5 ksi (120.7 MPa)	f'_c = 15.0 ksi (103.4 MPa)
Typical Web Width, in. (mm)	7 (180)	7 (150)	7 (150)	7 (150)
Modified Web Width, in. (mm)	8 (203)	8 (203)	8 (203)	8 (203)
Computed Shear Failure Plane Angle, θ, degrees	33.9	33.9	33.9	33.9
Fiber Contribution, V_f @ critical section kips (kN)	481.4 (2,141)	481.4 (2,141)	481.4 (2,141)	481.4 (2,141)
Concrete Contribution, V_c @ critical section kips (kN)	148.5 (660.6)	140.0 (622.8)	131.0 (582.7)	121.2 (539.1)
Strand Contribution, V_p @ critical section kips (kN)	9.6 (42.7)	9.6 (42.7)	9.6 (42.7)	9.6 (42.7)
Design Shear Strength, $\varphi_v V_R^{ULS}$ kips (kN)	430.8 (1,916)	423.9 (1,886)	417.9 (1,859)	411.0 (1,828)
Factored Shear, V_u @ critical section kips (kN)	382.6 (1,702)	382.6 (1,702)	382.6 (1,702)	382.6 (1,702)
Excess Capacity, %	11.2%	9.7%	8.4%	6.9%

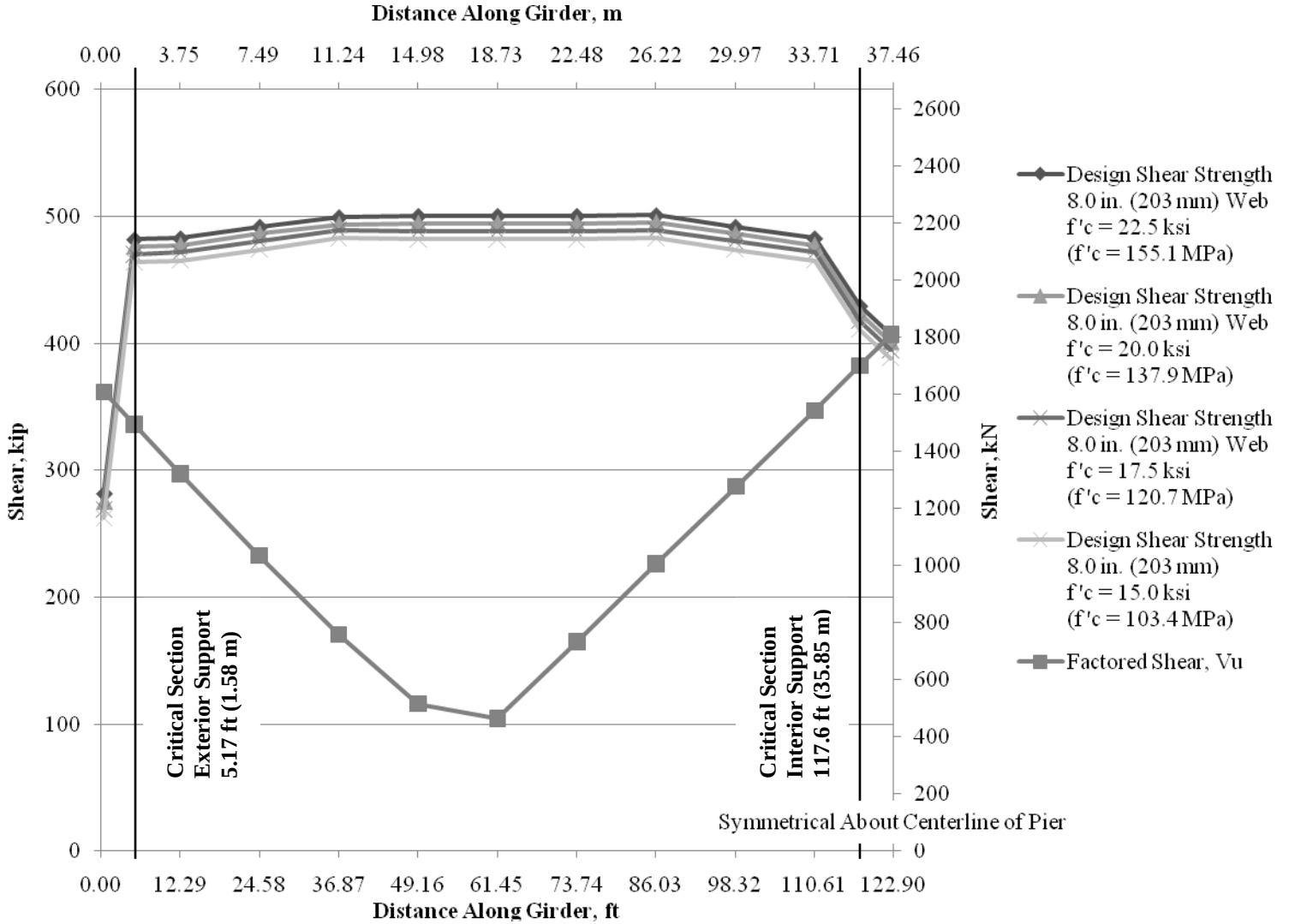

FIGURE 5.4 Shear Envelopes for Sunland Park Bridge Two-Span Unit with Eight Modified BT-54 Girders Using 0.6 in. (15 mm) Strands.

TABLE 5.5 Shear Results for Sunland Park Bridge Two-Span Unit with Eight BT-54 Girders Using 0.6 in. (15 mm) Prestressing Strands with Stirrups.

	f'_c = 22.5 ksi (155.1 MPa)	f'_c = 20.0 ksi (137.9 MPa)	f'_c = 17.5 ksi (120.7 MPa)	f'_c = 15.0 ksi (103.4 MPa)
Typical Web Width, in. (mm)	7 (180)	7 (150)	7 (150)	7 (150)
Modified Web Width, in. (mm)	N/A	N/A	N/A	N/A
Computed Shear Failure Plane Angle, θ, degrees	33.9	33.9	33.9	33.9
Fiber Contribution, V_f @ critical section kips (kN)	421.2 (1,874)	421.2 (1,874)	421.2 (1,874)	421.2 (1,874)
Stirrup Contribution, V_s @ critical section kips (kN)	35.6 (158.4)	35.6 (158.4)	35.6 (158.4)	35.6 (158.4)
Concrete Contribution, V_c @ critical section kips (kN)	129.9 (577.8)	122.5 (544.9)	114.6 (509.8)	106.1 (472.0)
Strand Contribution, V_p @ critical section kips (kN)	9.6 (42.7)	9.6 (42.7)	9.6 (42.7)	9.6 (42.7)
Design Shear Strength, $\varphi_v V_R^{ULS}$ kips (kN)	409.1 (1,820)	404.1 (1,798)	398.9 (1,774)	392.8 (1,747)
Factored Shear, V_u @ critical section kips (kN)	382.6 (1,702)	382.6 (1,702)	382.6 (1,702)	382.6 (1,702)
Excess Capacity, %	6.5%	5.3%	4.1%	2.6%

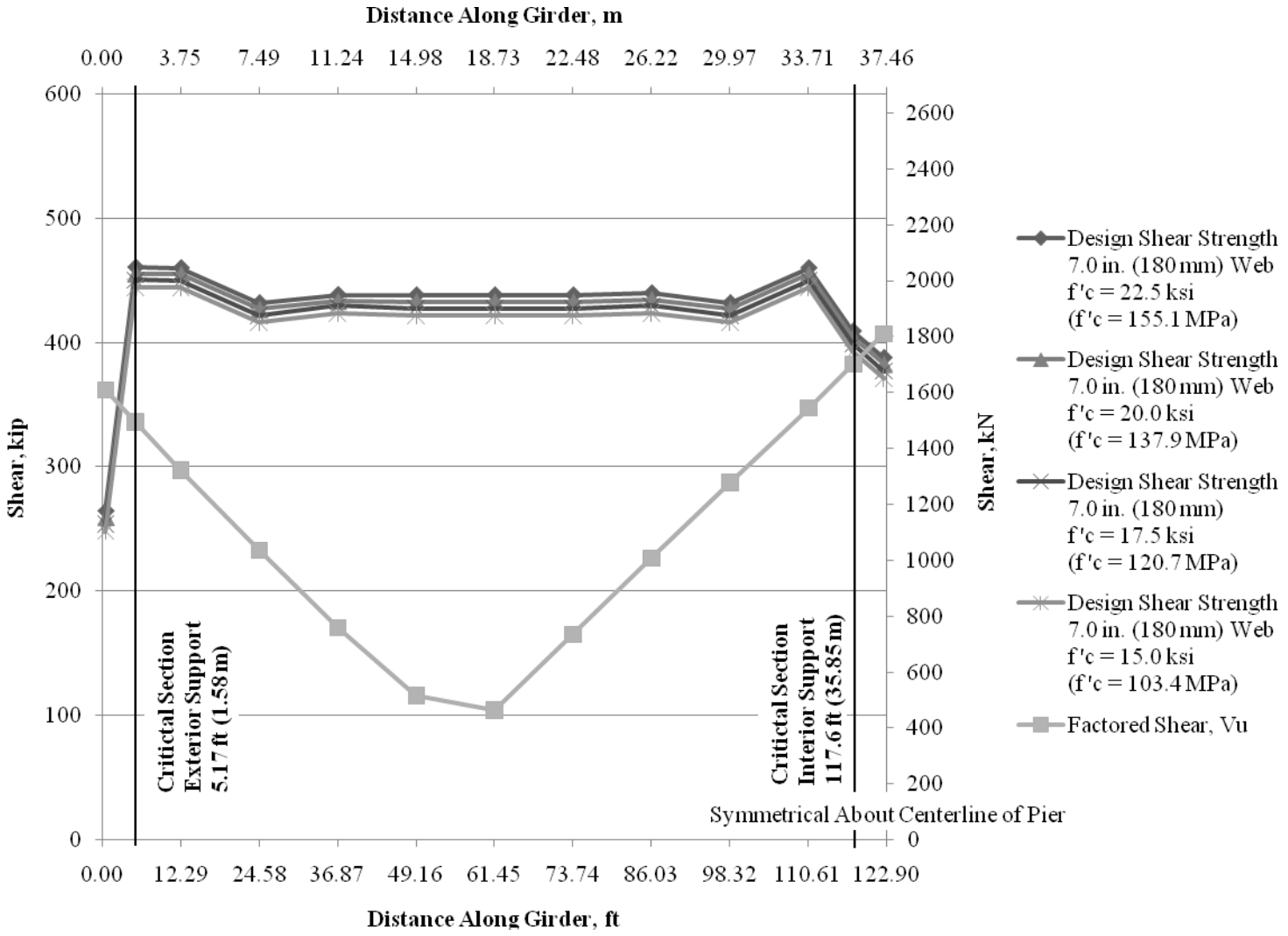

FIGURE 5.5 Shear Envelopes for Sunland Park Bridge Two-Span Unit with Eight Modified BT-54 Girders Using 0.6 in. (18 mm) Strands and No. 5 (M16) Mild Steel Stirrups.

5.1.2.2 Results for Two-span Continuous Unit with Six BT-63 Girders Using 0.7 in. (18 mm) Strands

The final bridge configuration based on LFD for flexure results employed six BT-63 girders with final design compressive strengths of 20.0 to 22.5 ksi (137.9 to 155.1 MPa). Table 5.6 provides a summary of the shear findings at the critical section near the interior support located at 117.61 ft (35.85 m). Note that all design compressive strengths used in the flexure portion of this study produced inadequate shear designs when mild steel stirrups are excluded. Even an increase of up to 2.0 inches (51 mm) in the web width will not produce satisfactory designs; therefore, the best option is to include stirrups in the design. Figure 5.6 illustrates the design strength of the girders for each of the three possible web widths.

TABLE 5.6 Shear Results for Sunland Park Bridge Two-Span Unit with Six BT-63 Girders Using 0.7 in. (18 mm) Prestressing Strands.

	f'_c = 22.5 ksi (155.1 MPa)	f'_c = 20.0 ksi (137.9 MPa)
6.0 in. (150 mm) Web Excess Capacity, %	-22.7%	-26.7%
7.0 in. (180 mm) Web Excess Capacity, %	-10.0%	-13.4%
8.0 in. (203 mm) Web Excess Capacity, %	0.3%	-2.7%

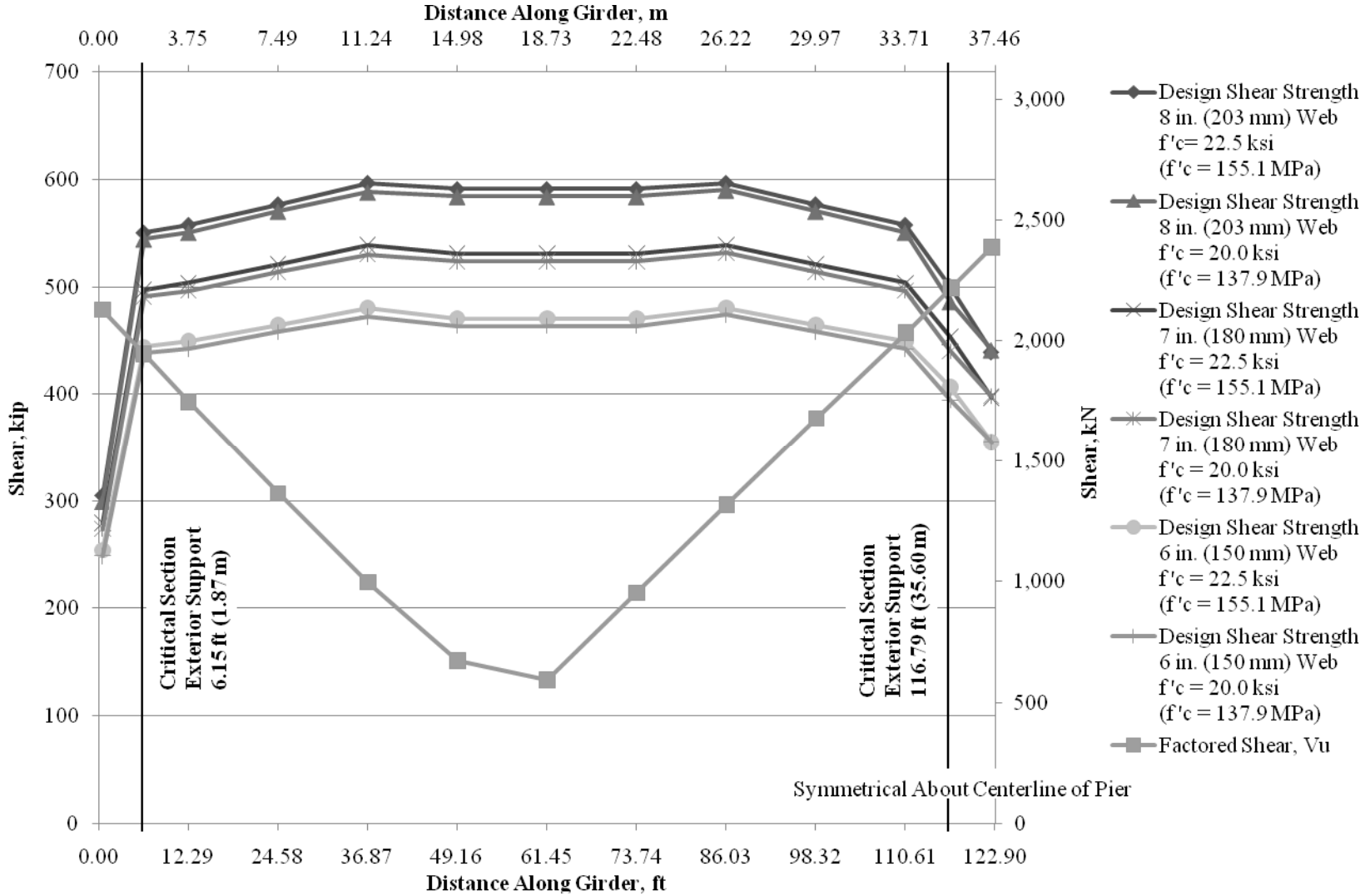

FIGURE 5.6 Shear Envelope for Sunland Park Bridge Two-Span Unit with Six BT-63 Girders Using 0.7 in. (18 mm) Strands.

To provide adequate design shear strength, No. 5 (M16) mild steel stirrups are placed at 24 in. (610 mm) up to the first $1/10^{th}$ point from the face of the support. This is a large reduction of stirrups compared to the as-designed bridge. Table 5.7 is a summary of the shear findings. Figure 5.7 is the shear envelope that illustrates the design shear strength. Note the design strength for f'_c = 20.0 ksi (137.9 MPa) is within 2% of the required capacity.

TABLE 5.7 Shear Results for Sunland Park Bridge Two-span Continuous Unit Using 0.7 in. (18 mm) Prestressing Strands and No. 5 (M16) Mild Steel Stirrups.

	f'_c = 22.5 ksi (155.1 MPa)	f'_c = 20.0 ksi (137.9 MPa)
Typical Web Width, in. (mm)	6 (150)	6 (150)
Modified Web Width, in. (mm)	N/A	N/A
Computed Shear Failure Plane Angle, θ, degrees	33.2	33.8
Fiber Contribution, V_f @ critical section kips (kN)	422.3 (1,879)	412.8 (1,836)
Stirrup Contribution, V_s @ critical section kips (kN)	116.2 (516.9)	113.3 (504.0)
Concrete Contribution, V_c @ critical section kips (kN)	149.1 (663.2)	140.1 (632.2)
Strand Contribution, V_p @ critical section kips (kN)	25.7 (114)	25.7 (114)
Characteristic Shear Strength, $\varphi_v V_R^{ULS}$ kips (kN)	511.2 (2,274)	496.3 (1,949)
Factored Shear, V_u @ critical section kips (kN)	499.0 (2,220)	499.0 (2,220)
Excess Capacity, %	2.4%	-0.5%

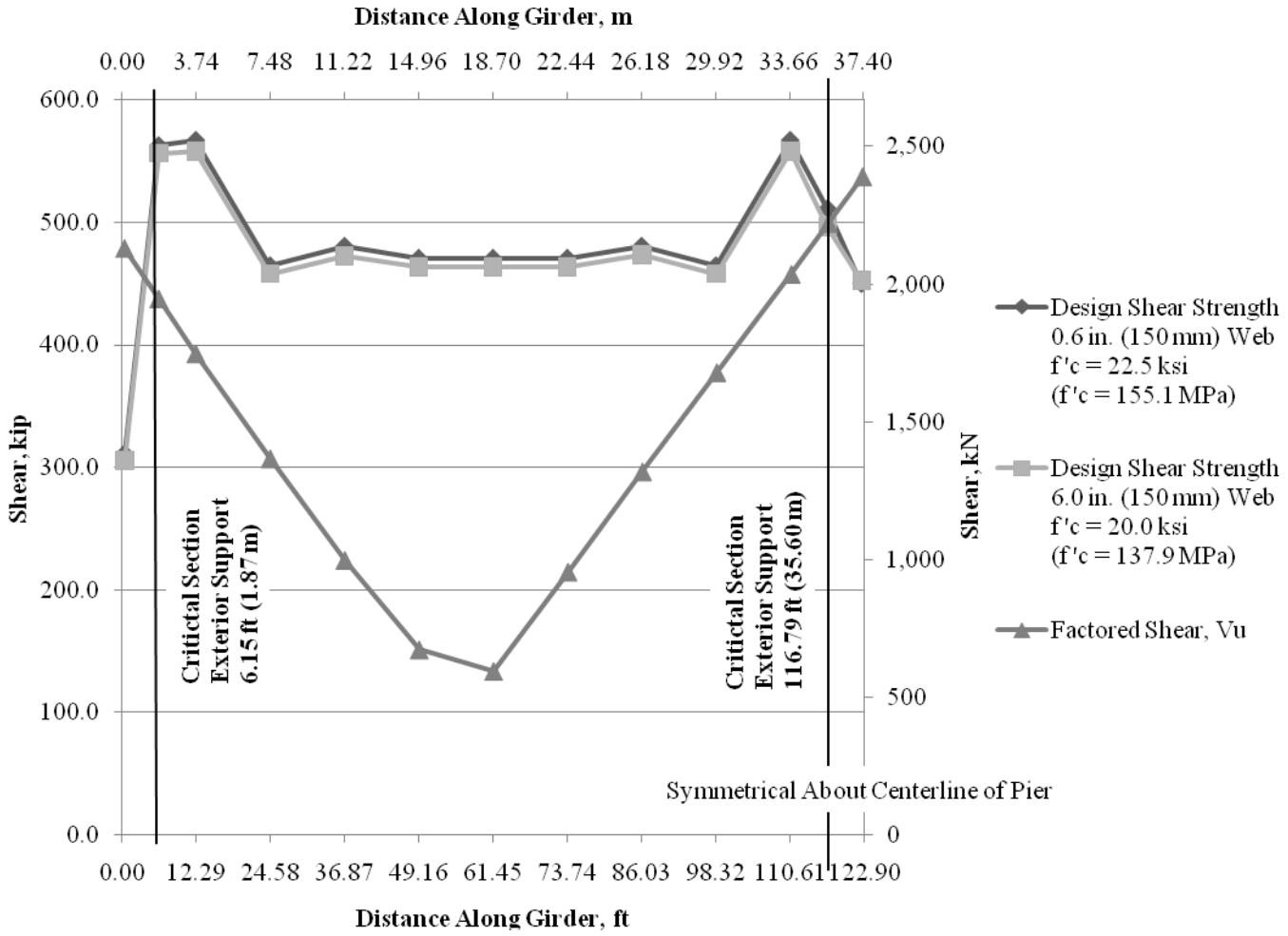

FIGURE 5.7 Shear Envelope for Sunland Park Bridge Two-Span Unit for Six BT-63 Girders Using 0.7 in. (18 mm) Strands and No. 5 (M16) Stirrups.

5.1.2.3 Results for Three-span Continuous Unit with Eight BT-54 Girders Using 0.6 in. (15 mm) Strands

The final bridge configuration based on flexure results employed eight modified NMDOT BT-54 girders with final compressive strengths of 15.0 to 22.5 ksi (103.4 to 155.1 MPa). Table 5.8 provides a summary of the shear findings for the exterior span at the interior support and 5.9 is a summary of the shear findings for the interior span.

For the exterior spans, at the critical sections near the interior supports located at 117.61 ft (35.85 m) from the exterior support, all design compressive strengths that produced a viable design in the flexure portion of this study produced adequate capacity without the need for shear stirrups when the web width was increased 1.0 in. (25 mm) to 8.0 (203 mm), similar to the two-span unit results. The excess capacity range from 4.9% to 8.3% for 15.0 to 22.5 ksi (103.4 to 155.1 MPa) concrete, respectively. The predicted angle of the shear crack was found to be approximately 35° from horizontal.

For the interior span, at the critical section located at 5.17 ft (1.58 m) from the interior support, all design compressive strengths that produced a viable design in the flexure portion of this study produced viable shear designs when the web width is increased 1.0 in. (25 mm) to 8.0 in. (203 mm), similar to the exterior results. The excess capacity range from 10.2% to 14.4% for 15.0 to 22.5 ksi (103.4 to 155.1 MPa) concrete, respectively. The predicted angle of the shear crack was found to be approximately 35° from horizontal.

Figure 5.8 represents the shear envelopes based on the design compressive strength with eight modified BT-54 girders with 8.0 in. (203 mm) webs. Notice the shear capacity of the exterior midspan. The sudden drop in capacity is directly related the lower computed shear failure angle, θ. This is different compared to the other shear envelopes in this study which have relatively constant capacity in this region of the beam.

An alternative to increasing the width of the web is to add mild steel stirrups in the critical shear regions. Tables 5.10 and 5.11 provide a summary of the shear findings when No. 3 (M8) stirrups are used at 24 in. (610 mm). The excess capacity ranges from 14.9% to 17.9% for 15.0 to 22.5 ksi (103.4 to 155.1 MPa) concrete, respectively, for the exterior span and 14.9% to 17.9% for 15.0 to 22.5 ksi (103.4 to 155.1 MPa) concrete, respectively for the interior span. The stirrups are placed at 24.0 in. (610 mm) o.c. up to a distance of $1/10^{th}$ the span [12.29 ft (3.75 m)] from the supports. Figure 5.9 represents shear envelopes based on the design compressive strength.

TABLE 5.8 Shear Results for Sunland Park Bridge Three-Span Unit with Eight Modified BT-54 Girders Using 0.6 in. (15 mm) Prestressing Strands Exterior Spans.

	f'_c = 22.5 ksi (155.1 MPa)	f'_c = 20.0 ksi (137.9 MPa)	f'_c = 17.5 ksi (120.7 MPa)	f'_c = 15.0 ksi (103.4 MPa)
Typical Web Width, in. (mm)	7 (180)	7 (150)	7 (150)	7 (150)
Modified Web Width, in. (mm)	8 (203)	8 (203)	8 (203)	8 (203)
Computed Shear Failure Plane Angle, θ, degrees	35.2	35.2	35.2	35.2
Fiber Contribution, V_f @ critical section kips (kN)	477.7 (2,125)	477.7 (2,125)	477.7 (2,125)	477.7 (2,125)
Concrete Contribution, V_c @ critical section kips (kN)	135.7 (603.6)	127.9 (568.9)	119.7 (532.5)	110.8 (492.9)
Strand Contribution, V_p @ critical section kips (kN)	5.2 (23.1)	5.2 (23.1)	5.2 (23.1)	5.2 (23.1)
Design Shear Strength, $\varphi_v V_R^{ULS}$ kips (kN)	414.1 (1,842)	410.1 (1,824)	403.4 (1,794)	397.5 (1,768)
Factored Shear, V_u @ critical section kips (kN)	379.7 (1,689)	379.7 (1,689)	379.7 (1,689)	379.7 (1,689)
Excess Capacity, %	8.3%	7.8%	6.3%	4.9%

TABLE 5.9 Shear Results for Sunland Park Bridge Three-Span Unit With Eight BT-54 Girders Using 0.6 in. (18 mm) Prestressing Strands Interior Span.

	f'_c = 22.5 ksi (155.1 MPa)	f'_c = 20.0 ksi (137.9 MPa)	f'_c = 17.5 ksi (120.7 MPa)	f'_c = 15.0 ksi (103.4 MPa)
Typical Web Width, in. (mm)	7 (180)	7 (150)	7 (150)	7 (150)
Modified Web Width, in. (mm)	8 (203)	8 (203)	8 (203)	8 (203)
Computed Shear Failure Plane Angle, θ, degrees	35.0	35.0	35.0	35.0
Fiber Contribution, V_f @ critical section kips (kN)	486.7 (2,169)	486.7 (2,169)	486.7 (2,169)	486.7 (2,169)
Concrete Contribution, V_c @ critical section kips (kN)	138.5 (616.1)	130.5 (579.6)	122.1 (540.0)	113.0 (497.3)
Harped Strand Contribution, V_p @ critical section kips (kN)	6.0 (26.7)	6.0 (26.7)	6.0 (26.7)	6.0 (26.7)
Design Shear Strength, $\varphi_v V_R^{ULS}$ kips (kN)	422.8 (1,881)	417.5 (1,857)	411.9 (1,832)	405.8 (1,805)
Factored Shear, V_u @ critical section kips (kN)	366.2 (1,629)	366.2 (1,629)	366.2 (1,629)	366.2 (1,629)
Excess Capacity, %	13.4%	12.4%	11.5%	10.2%

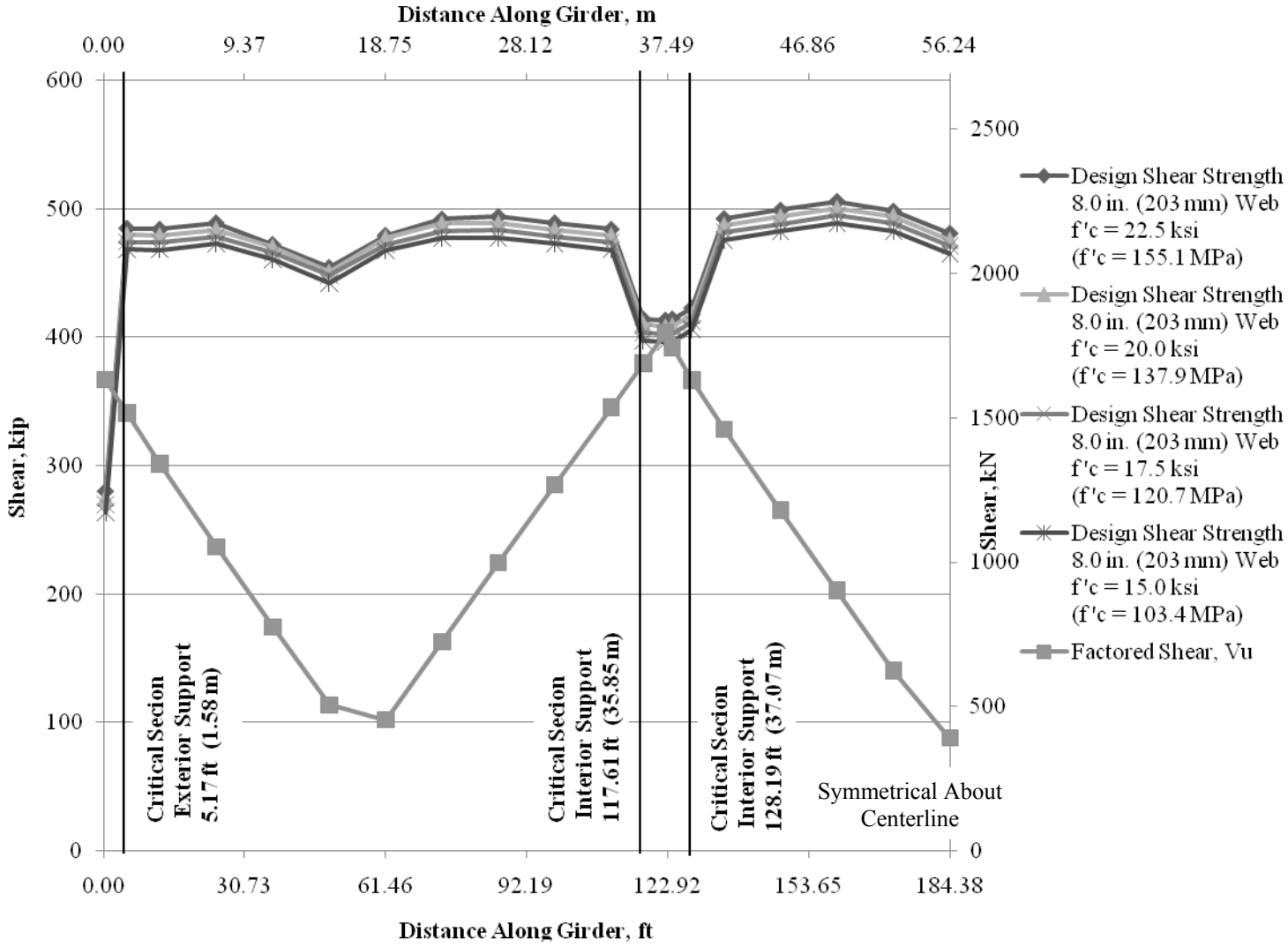

FIGURE 5.8 Shear Envelopes for Sunland Park Bridge Three-Span Continuous Unit Using 0.6 in. (15 mm) Strands.

TABLE 5.10 Shear Results for Sunland Park Bridge Three-Span Unit with BT-54 Girders Using 0.6in. (15 mm) Prestressing Strands Exterior Spans with Stirrups.

	f'_c = 22.5 ksi (155.1 MPa)	f'_c = 20.0 ksi (137.9 MPa)	f'_c = 17.5 ksi (120.7 MPa)	f'_c = 15.0 ksi (103.4 MPa)
Typical Web Width, in. (mm)	7 (180)	7 (150)	7 (150)	7 (150)
Modified Web Width, in. (mm)	N/A	N/A	N/A	N/A
Computed Shear Failure Plane Angle, θ, degrees	35.1	35.1	35.1	35.1
Fiber Contribution, V_f @ critical section kips (kN)	418.0 (1,859)	418.0 (1,859)	418.0 (1,859)	418.0 (1,859)
Stirrup Contribution, V_s @ critical section kips (kN)	35.5 (157.9)	35.5 (157.9)	35.5 (157.9)	35.5 (157.9)
Concrete Contribution, V_c @ critical section kips (kN)	135.7 (603.6)	127.9 (568.9)	119.7 (532.5)	110.8 (492.9)
Strand Contribution, V_p @ critical section kips (kN)	5.2 (23.1)	5.2 (23.1)	5.2 (23.1)	5.2 (23.1)
Design Shear Strength, $\varphi_v V_R^{ULS}$ kips (kN)	407.3 (1,812)	402.1 (1,789)	395.5 (1,759)	389.5 (1,733)
Factored Shear, V_u @ critical section kips (kN)	378.0 (1,681)	378.0 (1,681)	378.0 (1,681)	378.0 (1,681)
Excess Capacity, %	6.9%	6.0%	4.4%	3.0%

TABLE 5.11 Shear Results for Sunland Park Bridge Three-Span Unit with Eight BT-54 Girders Using 0.6in. (15 mm) Prestressing Strands Exterior Spans with Stirrups.

	f'_c = 22.5 ksi (155.1 MPa)	f'_c = 20.0 ksi (137.9 MPa)	f'_c = 17.5 ksi (120.7 MPa)	f'_c = 15.0 ksi (103.4 MPa)
Typical Web Width, in. (mm)	7 (180)	7 (150)	7 (150)	7 (150)
Modified Web Width, in. (mm)	N/A	N/A	N/A	N/A
Computed Shear Failure Plane Angle, θ, degrees	35.0	35.0	35.0	35.0
Fiber Contribution, V_f @ critical section kips (kN)	425.9 (1,895)	425.9 (1,895)	425.9 (1,895)	425.9 (1,895)
Concrete Contribution, V_c @ critical section kips (kN)	138.5 (616.1)	130.3 (579.6)	121.4 (540.0)	111.8 (497.3)
Stirrup Contribution, V_s @ critical section kips (kN)	36.4 (161.9)	36.4 (161.9)	36.4 (161.9)	36.4 (161.9)
Strand Contribution, V_p @ critical section kips (kN)	5.8 (25.8)	5.8 (25.8)	5.8 (25.8)	5.8 (25.8)
Design Shear Strength, $\varphi_v V_R^{ULS}$ kips (kN)	414.8 (1,845)	409.2 (1,820)	403.3 (1,794)	396.7 (1,765)
Factored Shear, V_u @ critical section kips (kN)	364.5 (1,621)	364.5 (1,621)	364.5 (1,621)	364.5 (1,621)
Excess Capacity, %	12.1%	10.9%	9.6%	8.1%

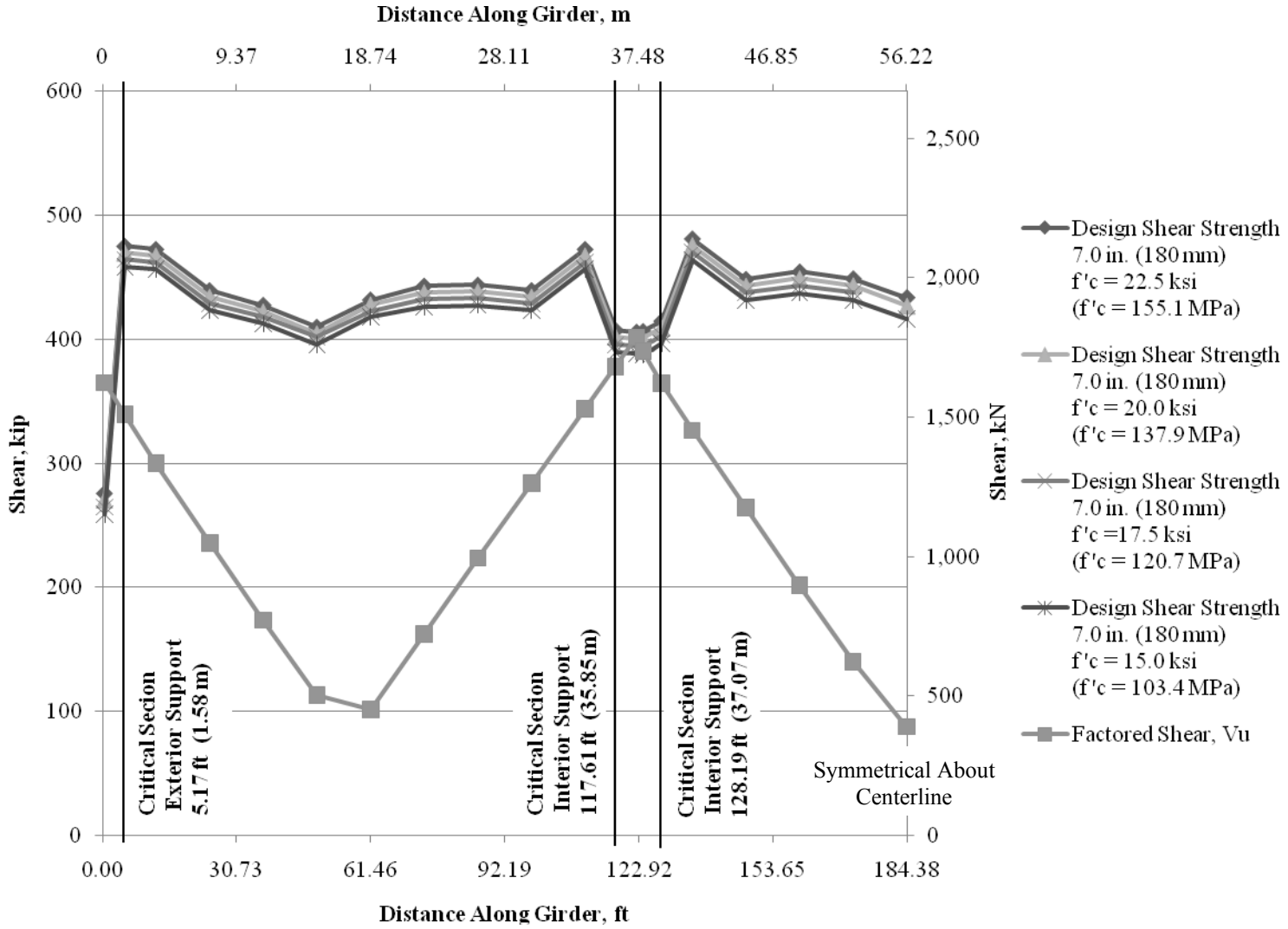

FIGURE 5.9 Shear Envelopes for Sunland Park Bridge Three-Span Unit for Eight BT-54 Girders Using 0.6 in. (15 mm) Strands and No. 3 (M8 Stirrups).

5.1.2.4 Results for Three-Span Continuous Unit with Six BT-63 Girders Using 0.7 in. (18 mm) Strands

The final bridge configuration based on flexure results employed six NMDOT BT-63 girders with final compressive strengths of 17.5 to 22.5 ksi (120.7 to 155.1 MPa).

It is important to note that at the critical section near the interior supports, for both the exterior and interior spans that even an increase of 2.0 in. (25 mm) does not provide sufficient design shear capacity. Therefore, mild steel stirrups must be included in this design. The 2.0 in. (25 mm) increase would make the web width 8.0 in. (203 mm) and is the maximum width that Coreslab in Albuquerque can cast this beam with its current casting beds.

Tables 5.12 and 5.13 provide a summary of the shear findings at the critical section near the interior support when No. 5 (M16) stirrups spaced at 18 in. (460 mm) o.c. are employed. The excess capacity ranges from 0.9% to 2.9% for 17.5 to 22.5 ksi (120.7 to 155.1 MPa) concrete, respectively for the exterior span and 4.7% to 6.7% for 17.5 to 22.5 ksi (120.7 to 155.1 MPa) concrete, respectively for the interior span.

Figure 5.10 is a comparison of how the section capacity varies with the compressive strength of the UHPC.

TABLE 5.12 Shear Results for Sunland Park Bridge Three-span Unit Using 0.7 in. (18 mm) Prestressing Strands Exterior Spans.

	f'_c = 22.5 ksi (155.1 MPa)	f'_c = 20.0 ksi (137.9 MPa)	f'_c = 17.5 ksi (120.7 MPa)
Typical Web Width, in. (mm)	6 (150)	6 (150)	6 (150)
Modified Web Width, in. (mm)	N/A	N/A	N/A
Computed Shear Failure Plane Angle, θ, degrees	35.3	35.3	35.3
Fiber Contribution, V_f @ critical section kips (kN)	406.2 (1,807)	406.2 (1,807)	406.2 (1,807)
Stirrup Contribution, V_s @ critical section kips (kN)	149.2 (663.7)	149.2 (663.7)	149.2 (663.7)
Concrete Contribution, V_c @ critical section kips (kN)	133.1 (592.1)	125.6 (558.7)	117.5 (522.7)
Strand Contribution, V_p @ critical section kips (kN)	18.5 (82.3)	18.5 (82.3)	18.5 (82.3)
Design Shear Strength, $\varphi_v V_R^{ULS}$ kips (kN)	512.4 (2,279)	507.5 (2,258)	502.1 (2,234)
Factored Shear, V_u @ critical section kips (kN)	497.5 (2,213)	497.5 (2,213)	497.5 (2,213)
Excess Capacity, %	2.9%	2.0%	0.9%

TABLE 5.13 Shear Results Sunland Park Bridge Three-Span Unit Using 0.7 in. (18 mm) Prestressing Strands Interior Span.

	f'_c = 22.5 ksi (155.1 MPa)	f'_c = 20.0 ksi (137.9 MPa)	f'_c = 17.5 ksi (120.7 MPa)
Typical Web Width, in. (mm)	6 (150)	6 (150)	6 (150)
Modified Web Width, in. (mm)	N/A	N/A	N/A
Computed Shear Failure Plane Angle, θ, degrees	33.8	33.8	33.8
Fiber Contribution, V_f @ critical section kips (kN)	403.9 (1,797)	403.9 (1,797)	403.9 (1,797)
Stirrup Contribution, V_s @ critical section kips (kN)	148.3 (659.7)	148.3 (659.7)	148.3 (659.7)
Concrete Contribution V_c @ critical section kips (kN)	125.0 (603.1)	117.9 (569.4)	109.9 (509.8)
Strand Contribution, V_p @ critical section kips (kN)	27.8 (124)	27.8 (124)	27.8 (124)
Design Shear Strength, $\varphi_v V_R^{ULS}$ kips (kN)	513.8 (2,286)	509.1 (2,265)	503.4 (2,239))
Factored Shear, V_u @ critical section kips (kN)	479.5 (2,133)	479.5 (2,133)	479.5 (2,133)
Excess Capacity, %	6.7%	5.8%	4.7%

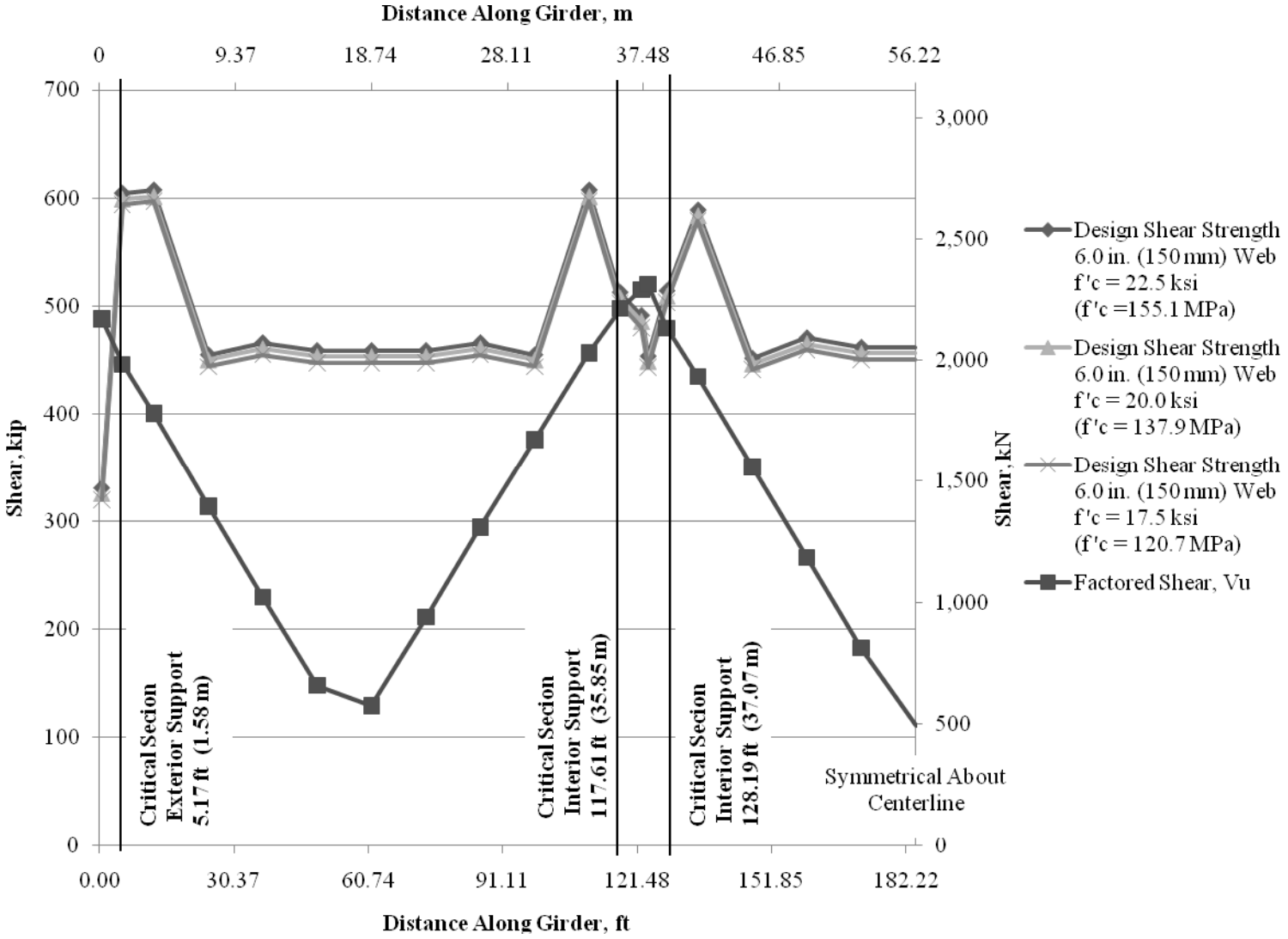

FIGURE 5.10 Shear Envelopes for Sunland Park Bridge Three-Span Unit for Six BT-63 Girder Using 0.7 in. (18 mm) Strands.

6 PARAMETRIC STUDY: NEGATIVE MOMENT REINFORCEMENT IN THE SUNLAND PARK BRIDGE

An important design issue for to the Sunland Park Bridge is the non-prestressed mild steel reinforcement in the negative moment region over the intermediate piers. As the number of required girders decreases, the moment forces at the pier increase; thus, the required amount of mild steel reinforcement in the deck must also increase.

According to LFD Article 9.7.2.3.2, the ultimate negative resisting moment shall be calculated using the compressive strength of the girder concrete regardless of the strength of the diaphragm concrete. The LFD provisions are valid for concrete having compressive strengths up to 15.0 ksi (103.4 MPa). Recall that the concrete strengths considered in this study range from 15.0 to 22.5 ksi (103.4 to 155.1 MPa). Thus, the concrete strength exceeds the compressive limit for which the LFD specification is valid.

An analysis was performed that considered two scenarios:

1. The diaphragm strength was limited to 15.0 ksi (103.4 MPa) for each girder compressive strength.
2. The diaphragm strength was considered to have the same compressive strength as the girder concrete.

Subsequently, the amount of mild deck steel was determined according to the LFD code.

6.1.1 Results: Two-span Continuous Unit

The required amount of mild deck steel was calculated assuming that the steel was placed at mid-depth of the deck. As anticipated, the required amount of steel varies directly with the number of girders and the girder depth.

The results in Table 6.1 is a summary of the required amount of mild deck steel required at each compressive strength of girder concrete. It is interesting to note that a 15% difference in concrete strength from 15.0 ksi (65.5 MPa) to 22.5 ksi (155.1 MPa) results only in a 1% decrease in the required amount of steel. This finding shows that the LFD specification can be assumed valid for compressive strengths up to 22.5 ksi (155.1 MPa).

TABLE 6.1 Required Amount of Mild Steel Reinforcement in the Deck in the Maximum Negative Moment Region.

	Final Compressive Strength of Concrete, f'_c ksi (MPa)	Max $M_{u,\ required}$ kip-ft (kN-m)	$1.2M_{cr}$ kip-ft (kN-m)	Required Steel in Deck in^2 (mm^2)	Increase from As-designed
10 BT-54 Girders (As-designed)	9.5 (155.1)	-4,114.9 (-5,584.9)	-1,681.3 (-2,279.5)	16.4 (10,580)	0%
8 BT-54 Girders [Configuration with 0.6 in. (15 mm) Strands]	15.0 (103.4)	-5262.2 (-7134.6)	-1,995.4 (-2,705.4)	20.72 (13,370)	21%
	17.5 (120.7)		-2,050.2 (-2,779.7)	20.62 (13,300)	20%
	20.0 (137.9)		-2,100.1 (-2,847.4)	20.55 (12,260)	20%
	22.5 (155.1)		-2,146.1 (-2,909.7)	20.49 (13,220)	20%
6 BT-63 Girders [Configuration with 0.7 in. (18 mm) Strands]	15.0 (103.4)	-7301.9 (-9,900.0)	-3,371.8 (-4,571.5)	24.57 (15,850)	33%
	17.5 (120.7)		-3,455.5 (-4,685.0)	24.45 (15,770)	33%
	20.0 (137.9)		-3,530.2 (-4,786.3)	24.36 (15,720)	33%
	22.5 (155.1)		-3,669.3 (-4,974.9)	24.28 (15,660)	32%

Figure 6.1 is a schematic of steel in the effective width of the as-designed bridge use No. 8 bars (M25) at 6.0 in. (150 mm) on-center (o.c.) in the top of the 8 in. (203 mm) deck. For comparison, Figure 6.2 is a schematic for eight BT-54 girders and uses No. 8 bars (M25) at 6.0 in. (150 mm) o.c. in the top of the 8.5 in. (216 mm) deck and Figure 6.3 is a schematic for six BT-63 girders and uses No. 8 bars (M32) at 6 in. (150 mm) o.c. in the top of the 10.5 in. (267 mm) deck. Figures 6.1, 6.2 and 6.3 have the same mild deck steel layout as the as-designed bridge.

It is important to note that there was no increase in the overall required amount of steel. The additional steel requirement is met because the effective width of the deck increases proportionally to the required amount of steel.

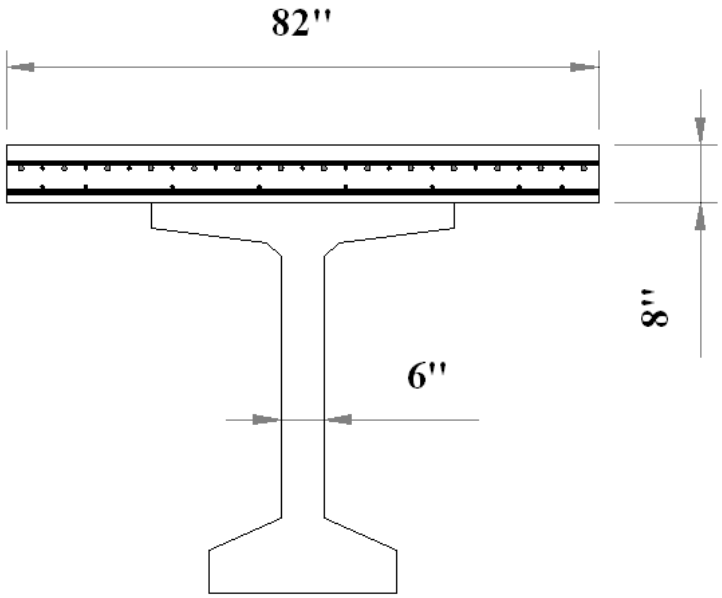

FIGURE 6.1 Negative Moment Reinforcement for Ten Modified BT-54 Girders.

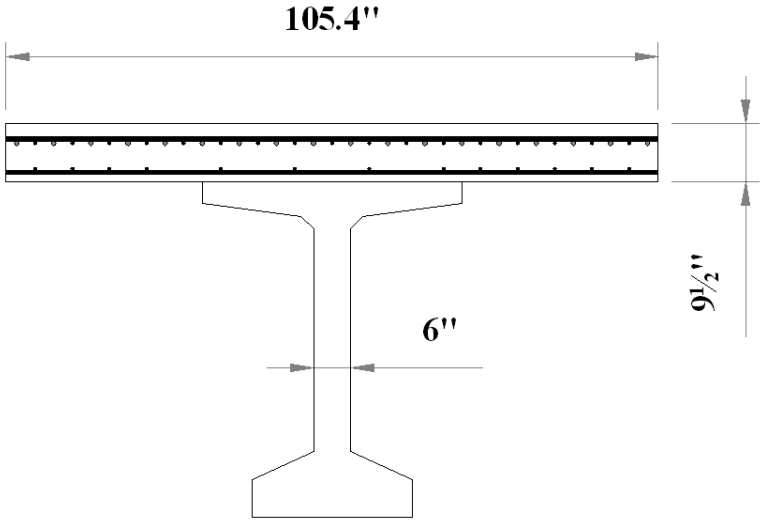

FIGURE 6.2 Negative Moment Reinforcement for Eight Modified BT-54 Girders.

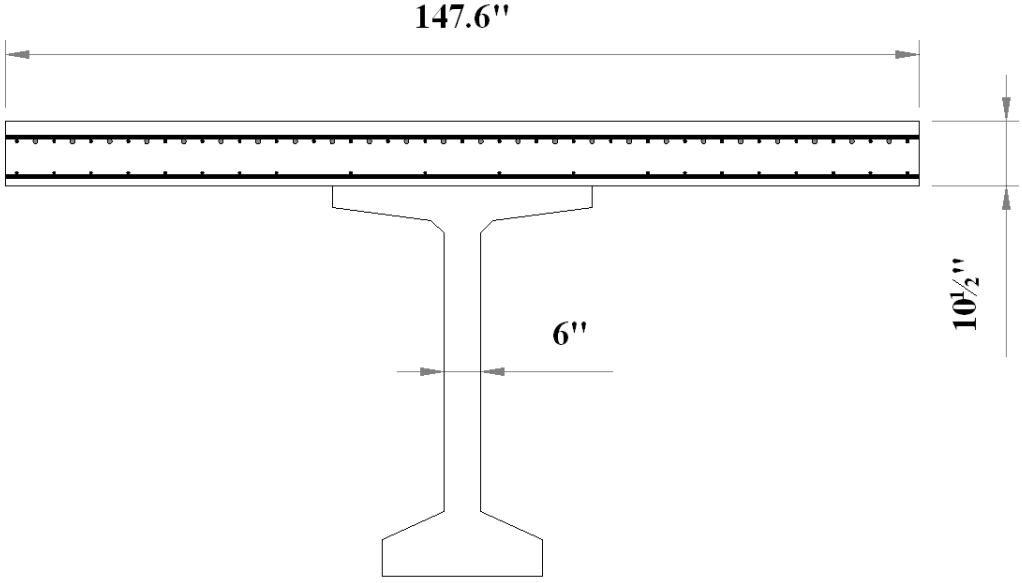

FIGURE 6.3 Negative Moment Reinforcement for Six BT-63 Girders.

6.1.2 Results for Sunland Park Bridge: Three-Span Continuous Unit

The three-span continuous unit has similar results to the two-span continuous unit. Table 6.2 summarizes the results.

Reinforcement layout is the same as the layout of the two-span continuous unit.

TABLE 6.1 Required Amount of Mild Steel Reinforcement in the Deck in the Maximum Nega

	Final Compressive Strength of Concrete, f'_c ksi (MPa)	Max $M_{u,\ required}$ kip-ft (kN-m)	$1.2M_{cr}$ kip-ft (kN-m)	Required Steel in Deck in^2 (mm^2)	Increase from As-designed
10 BT-54 Girders (As-designed)	9.5 (155.1)	-3,756.4 (-5,093.0)	-1,681.3 (-2,279.5)	14.70 (9,480)	0%
8 BT-54 Girders [Configuration with 0.6 in. (15 mm) Strands]	15.0 (103.4)	-4,831.0 (-6,550.0)	-1,995.4 (-2,705.4)	19.97 (12,880)	28%
	17.5 (120.7)		-2,050.2 (-2,779.7)	18.89 (12,190)	24%
	20.0 (137.9)		-2,100.1 (-2,847.4)	18.83 (12,150)	24%
	22.5 (155.1)		-2,146.1 (-2,909.7)	18.69 (12,060)	23%
6 BT-63 Girders [Configuration with 0.7 in. (18 mm) Strands]	15.0 (103.4)	-6,709.6 (-9,097.0)	-3,371.8 (-4,571.5)	22.52 (14,530)	36%
	17.5 (120.7)		-3,455.5 (-4,685.0)	22.42 (14,460)	36%
	20.0 (137.9)		-3,530.2 (-4,786.3)	22.34 (12,410)	36%
	22.5 (155.1)		-3,669.3 (-4,974.9)	22.18 (14,310)	35%

7 SUMMARY OF PARAMETRIC STUDY

This summary shows the final results for the final bridge configurations using 0.6 in. (15 mm) and 0.7 in. (18 mm) prestressing strands based on the flexure and shear parametric study presented in Sections 5 and 6. The results show the change in the material required when UHPC is used instead of HPC.

7.1.1 Summary of I-25/Doña Ana Interchange Final Results

7.1.1.1 Summary of I-25/Doña Ana Interchange Baseline Design

The base line design had a bridge configuration of six BT-63 girders using 28 - 0.6 in. (15 mm) prestressing strands, shown in Figure 7.1. The deck thickness is 7.5 in. (191 mm).

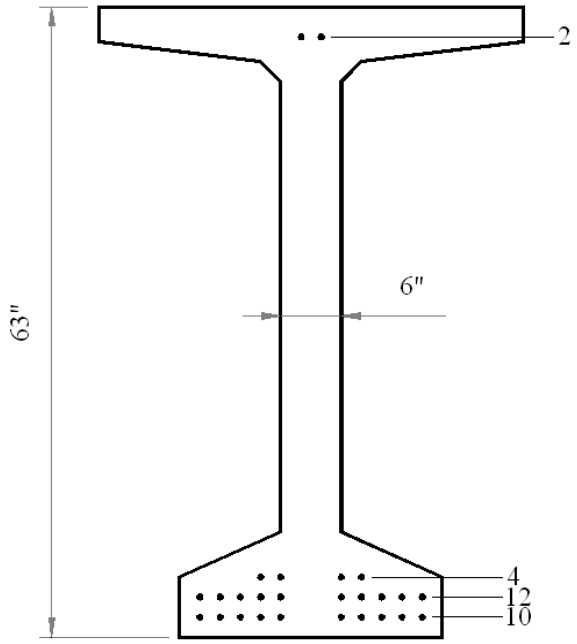

FIGURE 7.1 End View Cross-Section of Baseline Design (BT-63 Girders) with 28 - 0.6 in. (15 mm) Strands Employing HPC.

7.1.1.2 Summary Final Results Using 0.6 in. (15 mm) Prestressing Strands

When 0.6 in. (15 mm) prestressing strands are used a final bridge configuration of four BT-63 girders can be used, shown in Figure 7.2. This configuration is available for UHPC compressive strengths of 15.0 to 22.5 ksi (103.4 to 155.1 MPa). This configuration has a 26.7% increase in deck thickness, 33% reduction in required amount of girder concrete and a 50% increase in the number of required prestressing strands per girder compared to the baseline design. For each flexure design there is a corresponding shear design that provides adequate shear capacity with no change to the section geometry or the use mild steel stirrups.

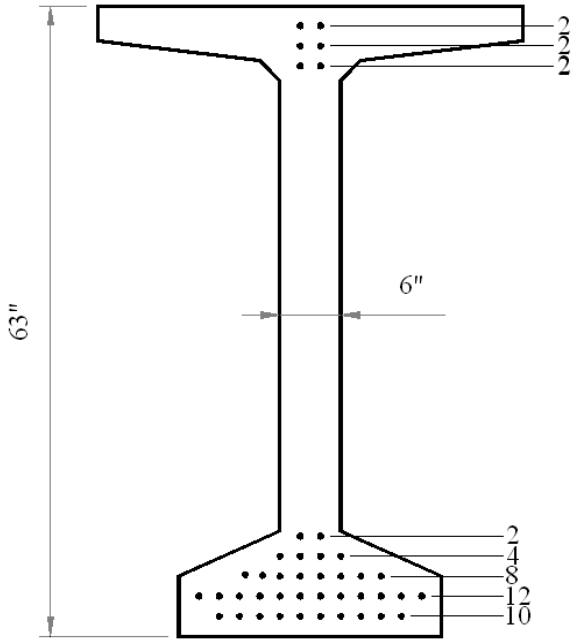

FIGURE 7.2 End View Cross-Section of Four BT-63 Girders with 42 - 0.6 in. (15 mm) Strands Employing UHPC.

7.1.1.3 Summary Final Results Using 0.7 in. (18 mm) Prestressing Strands

When 0.7 in. (18 mm) prestressing strands are used a final bridge configuration of four BT-54 girders can be used, shown in Figure 7.3. This configuration is available for UHPC compressive strengths of 22.0 to 22.5 ksi (137.9 to 155.1 MPa). This configuration has a 26.7% increase in deck thickness and a 109% increase in the number of required prestressing strands per girder compared to the baseline design. For each flexure design there is a corresponding shear design that provides adequate shear capacity. There are two primary options of providing shear strength:

1. Increase the web width 1.0 in. (25 mm), see Figure 7.3. If this option is selected there will be a reduction of 33% of girder concrete.

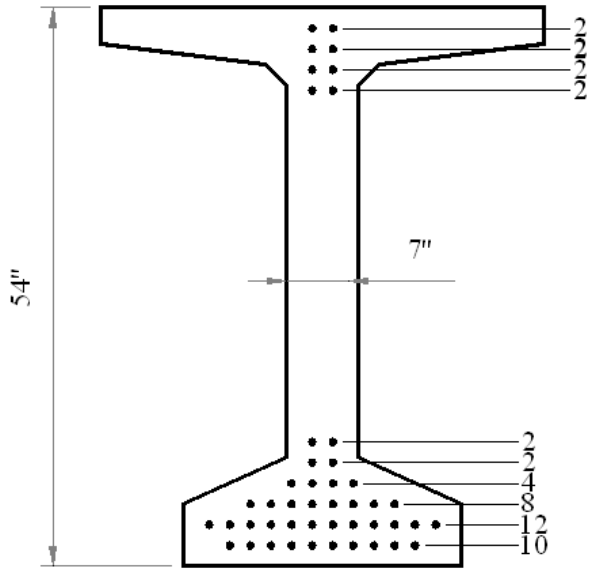

FIGURE 7.3 End View Cross-Section of Four BT-54 Girders with 48 - 0.7 in. (18 mm) Strands Employing UHPC.

2. Use No. 5 (M16) mild steel stirrups at 24 in. (610 mm) o.c. shown in Figure 7.4. If this option is selected there will be a 38% reduction in required amount of girder concrete.

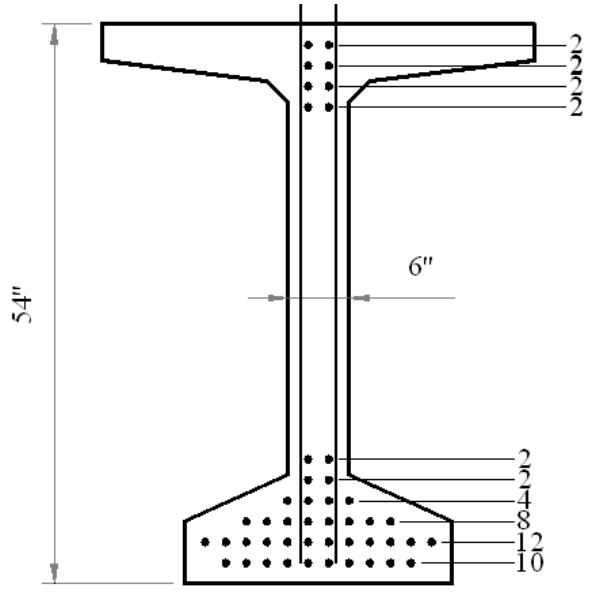

FIGURE 7.4 End View Cross-Section of Four BT-54 Girders with 48 - 0.7 in. (18 mm) Strands Employing UHPC.

7.1.2 Summary of Sunland Park Bridge Two-span Continuous Unit Results

7.1.2.1 Summary of Sunland Park Two-Span Unit As-Designed Bridge

The as-designed bridge had a bridge configuration of two spans with ten BT-54 girders in each span. Each beam uses 40 - 0.6 in. (15 mm) strands, as shown in Figure 7.5 and has an 8.0 in. (18 mm) thick deck.

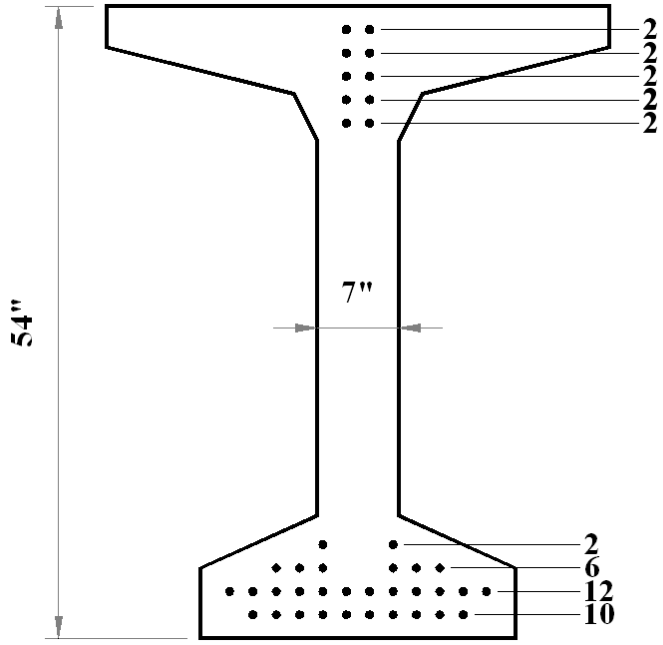

FIGURE 7.5 End View Cross-Section of Ten BT-54 Girder with 40-15 mm (0.6 in.) Strands Employing HPC.

7.1.2.2 Summary Final Results Using 0.6 in. (15 mm) Prestressing Strands

When 0.6 in. (15 mm) prestressing strands are used a final bridge configuration of eight modified BT-54 girders can be used. This configuration is available for UHPC compressive strengths of 15.0 to 22.5 ksi (103.4 to 155.1 MPa). This configuration has a 6.3% increase in deck thickness and a 0 to 5% increase in the number of required prestressing strands per girder compared to the as-designed bridge. For each flexure design there is a corresponding shear design that provides adequate shear capacity. There are two primary options of providing shear strength:

1. Increase the web width 1.0 in. (25 mm), as shown in Figure 7.6. If this option is selected there will be a reduction of 5.8% of girder concrete.

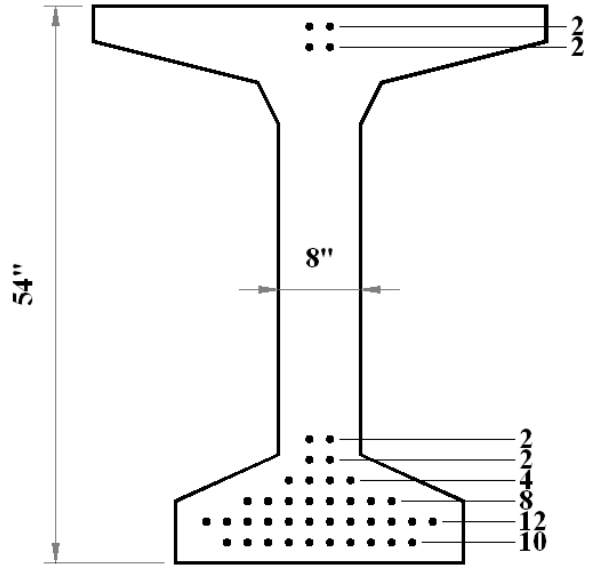

FIGURE 7.6 End View Cross-Section of Eight BT-54 Girders with 42-0.6 in. (15 mm) Strands Employing UHPC.

2. Use No. 5 (M16) mild steel stirrups at 24 in. (610 mm) o.c. If this option is selected there will be a 20% reduction in required amount of girder concrete.

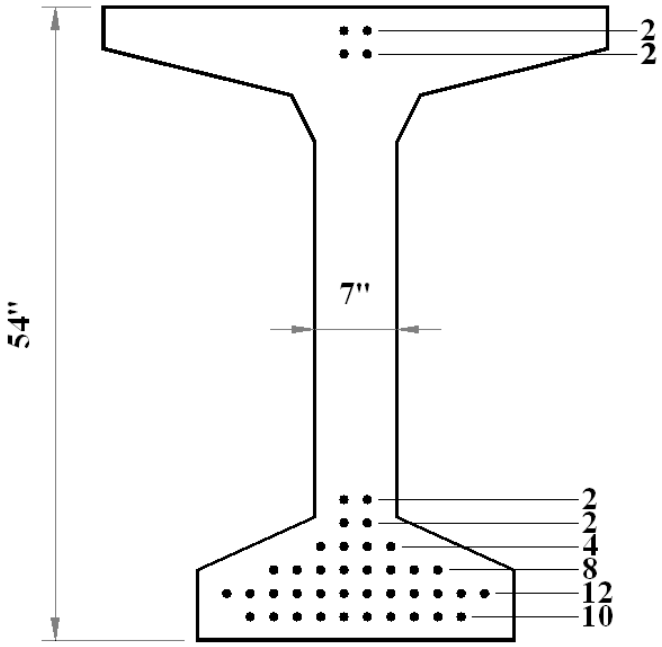

FIGURE 7.7 End View Cross-Section of Eight BT-54 Girders with 42-0.6 in. (15 mm) Strands Employing UHPC.

The amount of required deck steel in the negative moment region over the pier does not change compared to the as-designed bridge.

7.1.2.3 Summary Final Results Using 0.7 in. (18 mm) Prestressing Strands

When 0.7 in. (18 mm) prestressing strands are used a final bridge configuration of six BT-63 girders can be used. This configuration is available for UHPC compressive strengths of 15.0 to 22.5 ksi (103.4 to 155.1 MPa). This configuration has a 31.3% increase in deck thickness, 43% reduction in required amount of girder concrete, and a 28 to 46% increase in the number of required prestressing strands per girder compared to the as-designed bridge. Increasing the width of the web was not a viable option for this bridge configuration. The amount of required deck steel in the negative moment region over the pier does not change compared to the as-designed bridge.

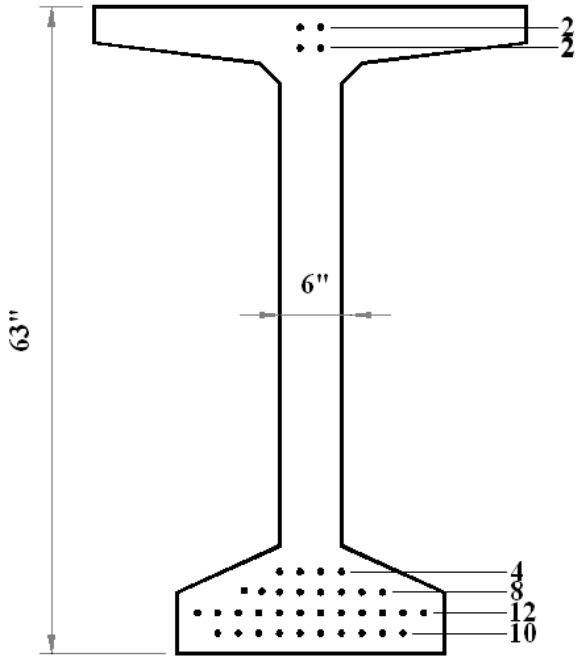

FIGURE 7.8 End View Cross-Section of Six BT-63 Girders with 38-0.6 in. (15 mm) Strands Employing UHPC.

7.1.3 Summary of Sunland Park Bridge Three-Span Continuous Unit Results

7.1.3.1 Summary of Sunland Park As-Designed Bridge

The as-designed bridge had a bridge configuration of three spans with ten BT-54 girders in each span. Each beam in the exterior spans uses 40 - 0.6 in. (15 mm) strands and the interior span use 32 – 0.6 in. (15 mm) strands, as shown in Figure 7.9 and has an 8.0 in. (18 mm) thick deck.

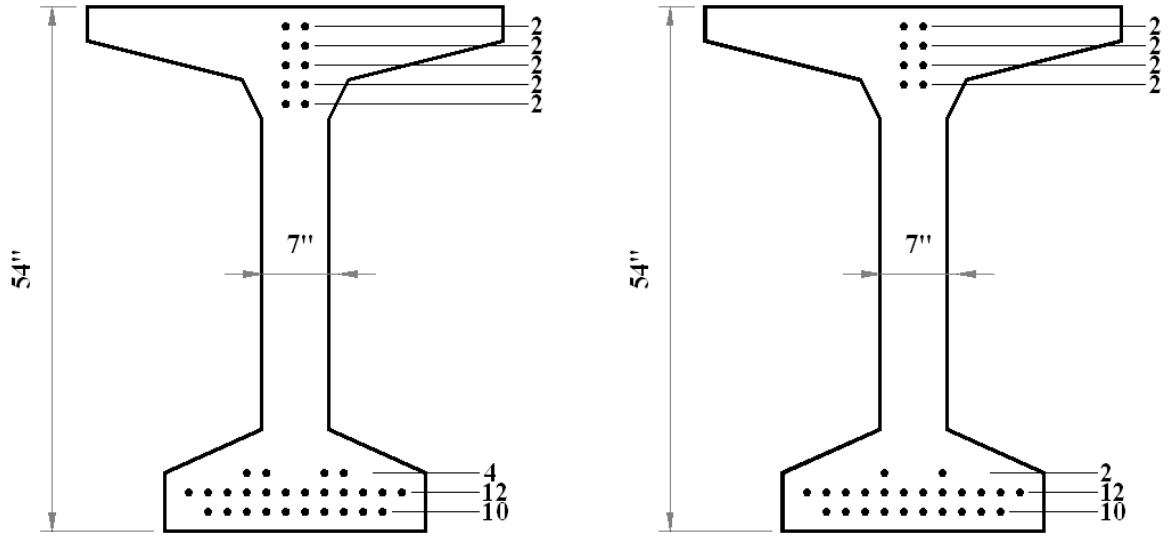

FIGURE 7.9 End View Cross-Section of Ten BT-54 Girders with 32- 0.6 in. (15 mm) Strands Employing HPC.

7.1.3.2 Summary Final Results Using 0.6 in. (15 mm) Prestressing Strands

When 0.6 in. (15 mm) prestressing strands are used a final bridge configuration of eight modified BT-54 girders can be used for both the exterior and interior spans. This configuration is available for UHPC compressive strengths of 15.0 to 22.5 ksi (103.4 to 155.1 MPa). This configuration has a 6.3% increase in deck thickness, 20% reduction in required amount of girder concrete, and an increase the number of required prestressing strands per girder of 0% for the exterior spans and a 15% decrease in the interior span, compared to the as-designed bridge. Similar to the Dona Ana results there are two primary options of providing shear strength:

1. Increase the web width 1.0 in. (25 mm). If this option is selected there will be a reduction of 5.8% of girder concrete, the same result as the two-span unit.

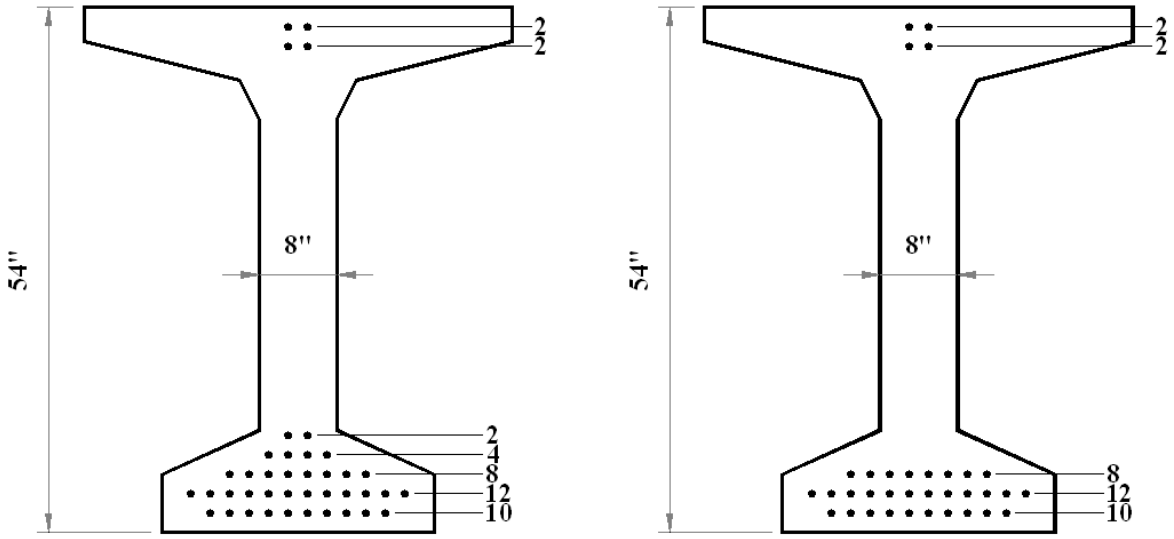

FIGURE 7.10 End View Cross-Section of BT-54 Girder with 8 in. (203 mm) and 42 - 0.6 in. (15 mm) Strands Employing UHPC.

2. Use No. 3 (M8) mild steel stirrups at 24 in. (610 mm) o.c. If this option is selected there will be a 20% reduction in required amount of girder concrete. This is a smaller bar size that the two-span unit.

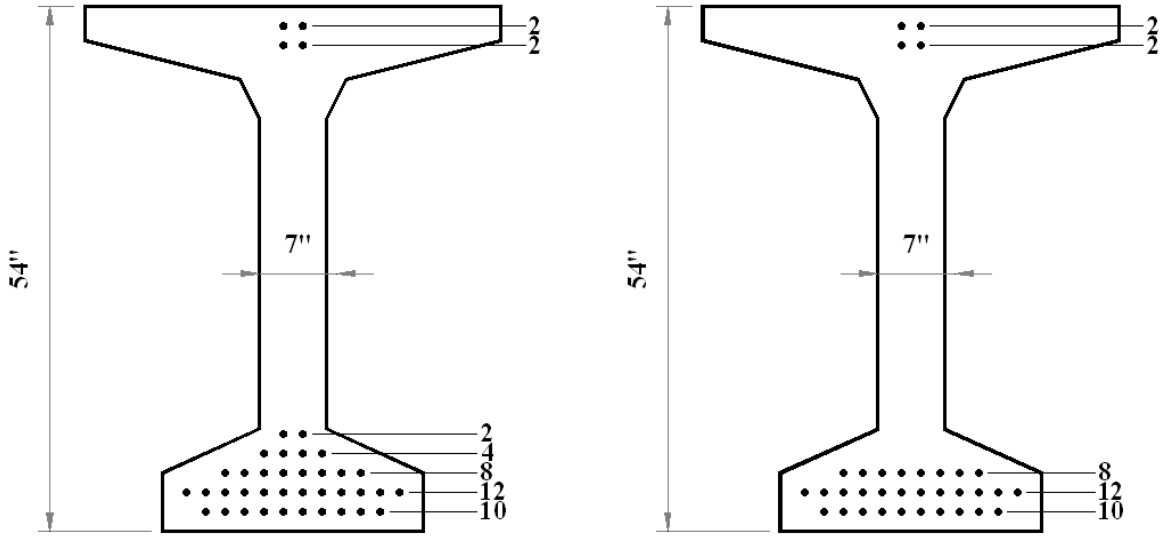

FIGURE 7.11 End View Cross-Section of BT-54 Girder with 7 in. (180 mm) 34 - 0.6 in. (15 mm) Strands Employing UHPC.

The amount of required deck steel in the negative moment region over the piers does not change compared to the as-designed bridge.

7.1.3.3 Summary Final Results Using 0.7 in. (18 mm) Prestressing Strands

When 0.7 in. (18 mm) prestressing strands are used a final bridge configuration of six BT-63 girders can be used for both the exterior and interior spans. This configuration is available for UHPC compressive strengths of 17.5 to 22.5 ksi (137.9 to 155.1 MPa). This configuration has a 31.3% increase in deck thickness, 43% reduction in required amount of girder concrete, and an increase in the required number of prestressing strands of 15 to 23% in the exterior spans and a 25 to 33% increase for the interior span compared to the as-designed bridge. Like the two-span unit results, increasing the web width is not a viable option. No. 5 (M16) must be used at 18 in. (460 mm) o.c.

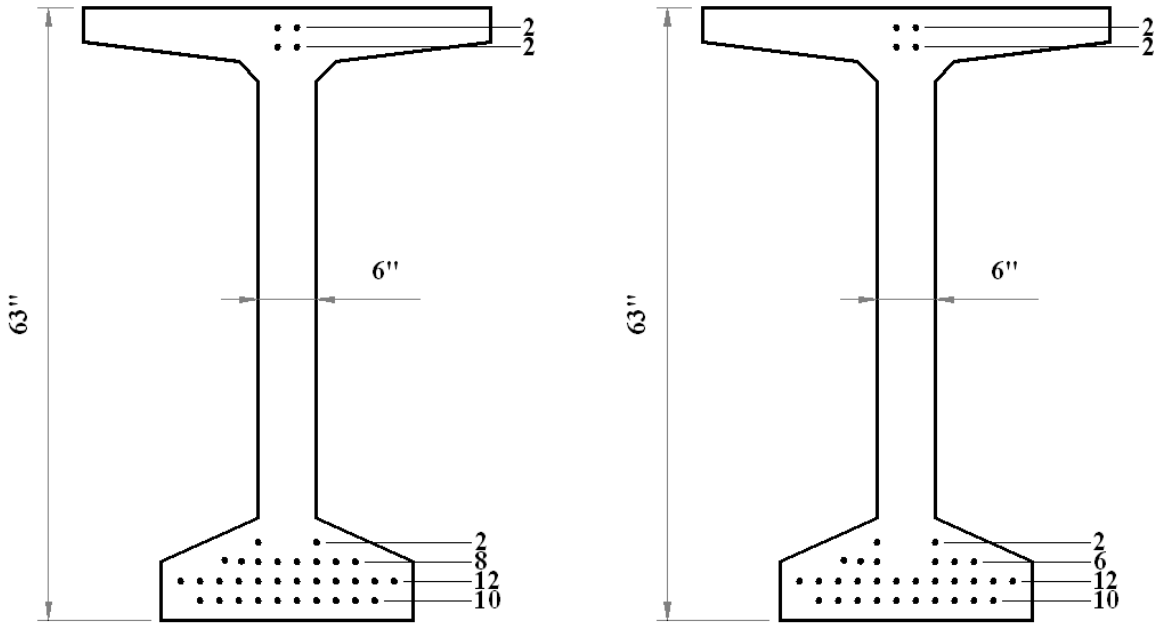

FIGURE 7.12 End View Cross-Section of BT-63 Girder with 34 - 0.7 in. (18 mm) Strands Employing UHPC.

The amount of required deck steel in the negative moment region over the piers does not change compared to the as-designed bridge.

7.1.4 Hold-Down Forces

All girder cross-sections in the flexure parametric study have hold-down forces less than 40 kips (178 kN). This is the capacity of the hold-down mechanism as the Coreslab plant in Albuquerque.

7.1.5 Prestressing Steel Requirement

7.1.5.1 Minimum Steel Requirement

All girder cross-sections meet the minimum amount of prestressed reinforcement to develop adequate moment at the critical section as least 120% of the cracking moment specified in LFD Art. 9.18.2.

7.1.5.2 Maximum Prestressing Steel

The maximum amount of prestressing steel is specified in LFD Art. 9.18.1. Every final cross-section that employs UHPC has a reinforcement index greater than the limit of $0.36\beta_1$, therefore, the design flexural strength is calculated according to equation 9-23 in LFD Art. 9.18.1 instead of LFD Art. 9.17.3.

THIS PAGE LEFT BLANK INTENTIONALLY

8 CONFINEMENT STEEL

Chapter 2 presented a case study on the Mars Hill Bridge in Wapello County, Iowa. Unique to this bridge was the removal of mild steel reinforcement for shear, temperature and shrinkage, and confinement steel in the transfer region.

The bursting force effect is addressed in LFD Art. 9.22. According to this article stirrups and nominal reinforcement should be placed at least a distance d from the end of the beam. If 0.7 in. (18 mm) strands are used the final bridge configurations typically required stirrups in this region of the beam and the inclusion of confinement steel would be a simple task and would not add significantly to the total overall cost of a UHPC beam (see Section 9 of this report).

However, if 0.6 in. (15 mm) strands are used the final bridge configurations do not require stirrups to provide adequate shear strength. In these UHPC girders the effects of bursting are considered. According to LFD Art. 9.21.6.3 the magnitude of the bursting force, T_{burst}, can be estimated according to equation 8.1.1 as:

$$T_{burst} = 0.25 \sum P_u \left(1 - \frac{a}{h}\right) + 0.5 P_u \sin \alpha \qquad \text{Equation 8.1}$$

where, ΣP_u is the sum of the total factored tendon loads; a is the lateral dimension of the anchorage device in the direction considered; h is the lateral dimension of the cross-section in the direction considered; P_u is the factored tendon force; and α is the angle of inclination of the resultant of the tendon forces with respect to the centerline of the member. Since the bursting force is a tensile force it is divided by the area of the bottom bulb to determine the stress in the bottom bulb, this is then compared to the tensile stress limit to determine if confinement steel is required.

The most heavily reinforced section is a BT-54 girder with 38 - 0.7 in. (18 mm) strands in the bottom bulb. The estimated bursting stress is 0.94 ksi (6.4 MPa), which is less than the allowable tensile limit of 1.16 ksi (8 MPa), therefore confinement steel in the bottom bulb is not required.

THIS PAGE LEFT BLANK INTENTIONALLY

9 ECONOMIC ANALYSIS

9.1 INTRODUCTION

The first UHPC bridge built in Iowa used a modified Iowa 45 in. (1.14 m) bulb tee. To save material in the beam section, the web width, the thickness of the top flange and the thickness of the bottom flange were reduced. In this study, rather than modifying an existing shape, the beam sizes were reduced using existing NMDOT standard girder sections. For the economic analysis the as-designed girder is compared to the design of a girder with a design compressive strength of 22.5 ksi (155.1 MPa). The greatest material savings are found with the highest compressive strength in this study and therefore produce the greatest economic benefit.

9.2 COST COMPARISON OF UHPC GIRDERS BY REDUCING GIRDER SIZE

9.2.1 Concrete Costs for I-25/Doña Ana Interchange

The compressive strength of the baseline design was modified from 9.5 ksi (65.5 MPa) to 22.5 ksi (155.1 MPa). The cost of one BT-63 girder with HPC is approximately $2,602. For one BT-63 girder with UHPC the cost is approximately $14,260. This cost can be reduced by choosing a smaller section (e.g., BT-54) which reduces the volume of concrete needed. The cost of one BT-54 girder with UHPC is $13,180. The sections that were modeled are shown in Table 9.1 along with the cost estimate for each.

Figures of the final cross-section are shown in Section 7, Figures 7.1-7.4. The lowest number of girders possible was found to be four BT-54 girders. This design was only possible with the use of 0.7 in. (18 mm.) strands. If it is not possible to use 0.7 in. (18 mm) strands, five BT-54 girders is the best choice.

In Section 5 of this report it was shown that when 0.7 in. (18 mm) strands are used that the design shear capacity was insufficient when a section with a 6.0 in. (150 mm) web was used. To have adequate shear capacity either the web thickness of the BT-54 girder would have to be increased in width by 1.0 in. (25 mm) or use mild steel stirrups. Based on the total cost of concrete in Table 9.1 if the web thickness is increased the cost of the girder concrete increases by approximately $1,080. This suggests that using mild steel stirrups would be a lower cost option.

TABLE 9.1 I-25/Doña Ana Interchange Concrete Volumes and Costs.

	Base Line Design, 9.5 ksi (65.5 MPa)	4 BT-63 Girders, 22.5 ksi (155.1 MPa)	4 BT-54 Girders, 22.5 ksi (155.1 MPa)	4 Modified BT-54 Girders, 22.5 ksi (155.1 MPa)
Cross-Sectional Area of One Girder, in^2 (cm^2)	713 (4600)	713 (4600)	659 (4250)	713 (4600)
Total Volume of Concrete for All Girders, yd^3 (m^3)	124.89 (95.49)	83.26 (63.66)	76.95 (58.83)	83.26 (63.66)
Cost of Concrete for One Girder	$2,602	$14,260	$13,180	$14,260
TOTAL cost of Concrete	$15,610	$57,040	$52,720	$57,031

9.2.2 Concrete Costs for Sunland Park River Crossing Bridge

The two-span unit and three-span unit are treated separately in this economic analysis just as in the parametric study. The primary difference is the additional span in the three-span unit.

9.2.2.1 Concrete Costs for Sunland Park Bridge Two-Span Unit

The compressive strength of the baseline design was modified from 9.5 ksi (65.5 MPa) to 22.5 ksi (155.1 MPa). The cost of one BT-54 girder with HPC is approximately $2,818. For one BT-54 girder with UHPC and a web with of 7.0 in. (180 mm) the cost is approximately $15,441. The cost of one BT-63 girder with UHPC is $15,441. Because the sections have the same cross-sectional area the savings in cost are not realized until the number of required girders decreases from eight BT-54 girders to six BT-63 girders. Table 9.2 shows cost estimates for the beams modeled for both the spans along with the cost estimate for each.

The end view cross-section of the as-designed bridge is shown in Section 7 Figures 7.4-7.8. The lowest number of girders possible was found to be six BT-63 girders. This design was only possible with the use of 0.7 in. (18 mm) strands. If it is not possible to use 0.7 in. (18 mm) strands, eight BT-54 girders is the best choice. This design requires more strands than the eight BT-54 girders, but the fact that there are two less girders results in a significant reduction in the total cost.

TABLE 9.2 Sunland Park Two-Span Unit Concrete Volumes and Costs.

	As-Designed, 10 BT-54 Girders 9.5 ksi (65.5 MPa)	8 BT-54 Girders, 22.5 ksi (155.1 MPa)	8 Modified BT-54 Girders, 22.5 ksi (155.1 MPa)	6 BT-63 Girders, 22.5 ksi (155.1 MPa)
Cross-Sectional Area of One Girder, in^2 (cm^2)	713 (4,600)	713 (4,600)	767 (4,950)	713 (4,600)
Total Volume of Concrete for All Girders, yd^3 (m^3)	450.83 (344.69)	360.67 (275.75)	387.98 (296.63)	270.5 (206.81)
Cost of Concrete for One Girder	$2,818	$15,441	$16,610	$15,441
TOTAL cost of Concrete	$56,350	$247,100	$265,810	$185,320

9.2.2.2 Concrete Costs for Sunland Park Bridge Three-Span Unit

The compressive strength of the baseline design was modified from 9.5 ksi (65.5 MPa) to 22.5 ksi (155.1 MPa). The cost of one BT-54 girder with HPC is approximately $2,820. For one BT-54 girder with UHPC and a web with of 7.0 in. (180 mm) the cost is approximately $15,440. The cost of one BT-63 girder with UHPC is $15,440. Because the sections have the same cross-sectional area the savings in cost are not realized until the number of required girders decreases from eight BT-54 girders to six BT-63 girders. Table 9.3 shows cost estimates for the beams modeled for both the spans along with the cost estimate for each.

The end view cross-section of the as-designed bridge is shown in Section 7, Figures 7.9-7.13. The lowest number of girders possible was found to be six BT-63 girders. This design was only possible with the use of 0.7 in. (18 mm) strands. If it is not possible to use 0.7 in. (0.18 mm) strands, eight BT-54 girders is the best choice. This design requires more strands than the eight BT-54 girders, but the fact that there are two less girders results in a significant reduction in the total cost.

TABLE 9.3 Sunland Park Three-Span Unit Concrete Volumes and Costs.

	As-Designed, 10 BT-54 Girders 9.5 ksi (65.5 MPa)	8 BT-54 Girders, 22.5 ksi (155.1 MPa)	8 Modified BT-54 Girders, 22.5 ksi (155.1 MPa)	6 BT-63 Girders, 22.5 ksi (155.1 MPa)
Cross-Sectional Area of One Girder, in^2 (cm^2)	713 (4,600)	713 (4,600)	767 (4,950)	713 (4,600)
Total Volume of Concrete for All Girders, yd^3 (m^3)	675.25 (344.69)	541 (275.75)	581.97 (296.63)	405.75 (206.81)
Cost of Concrete for One Girder	$2,820	$15,440	$16,610	$15,440
TOTAL cost of Concrete	$84,531	$370,650	$398,720	$277,984

9.3 PRESTRESSING STRAND COMPARISON

Strand size greatly affects the overall design which in turn affects the cost. In this case, using 0.7 in. (18 mm) strands requires an additional $150,000 initial cost because new stressing rams will have to be acquired by Coreslab in Albuquerque and the strands themselves are almost twice as expensive as the 0.6 in. (15 mm) strands.

This cost was developed based on a strand unit cost of $0.36/ft ($1.18/m) for 0.6 in. (15 mm) stands and $0.65/ft ($2.13/m) for 0.7 in. (18 mm) stands.

9.3.1 I-25/Doña Ana Interchange Strand Comparison

The cost of the 0.6 in. (15 mm) strands in the baseline bridge is $6,860. The total cost of 0.6 in. (15 mm) strands in a bridge configuration with four BT-63 girders is $6,680, which is a 0% increase compared to the baseline design. The total cost of 0.7 in. (18 mm) strands in a bridge configuration with four BT-54 girders is $13,570, which is a 49.4% increase over the baseline design. Table 9.4 provides a summary of the costs.

TABLE 9.4 Dona Ana Strand Costs.

	Baseline Design, 9.5 ksi (65.5 MPa)	4 BT-63 Girders, 22.5 ksi (155 MPa)	4 BT-54 Girders, 22.5 ksi (155 MPa)
Number of 0.6 in. (15 mm) Strands Per Girder	28	42	-
Number of 0.7 in. (18 mm) Strands Per Girder	22	30	46
Cost of 0.6 in. (15 mm) Strands Per Bridge	$6,860	$6,860	-
Cost of 0.7 in. (18 mm) Strands Per Bridge	$9,740	$8,853	$13,570

9.3.2 Sunland Park River Crossing Strand Comparison

9.3.2.1 Sunland Park Two-Span Unit Strand Comparison

The cost of the 0.6 in. (15 mm) strands in the as-designed bridge is $35,400. The total cost of the 0.6 in. (15 mm) strands in a bridge configuration with eight BT-54 girders is $29,740, which is a 16% decrease compared to the as-designed bridge. The total cost of the 0.7 in. (18 mm) strands in a bridge configuration with six BT-63 girders is $36,430 which is a 2.8% increase compared to the baseline. Table 9.5 provides a summary of the total cost of prestressing strands per bridge configuration.

TABLE 9.5 Sunland Park Two-Span Unit Strand Costs.

	As-Designed, 9.5 ksi (65.5 MPa)	8 BT-54 Girders, 22.5 ksi (155 MPa)	6 BT-63 Girders, 22.5 ksi (155 MPa)
Number of 0.6 in. (15 mm) Strands Per Girder	40	42	-
Number of 0.7 in. (18 mm) Strands Per Girder	26	30	38
Cost of 0.6 in. (15 mm) Strands Per Bridge	$35,400	$29,740	-
Cost of 0.7 in. (18 mm) Strands Per Bridge	$41,550	$38,350	$36,430

9.3.2.2 Sunland Park Three-Span Unit Strand Comparison

The cost of the 0.6 in. (15 mm) strand in the as-designed bridge is $46,020. The total cost of 0.6 in. (15 mm) strands in a bridge configuration with eight BT-54 girders is $44,610, which is a 3.1% decrease compared to the as-designed bridge. The total cost of 0.7 in. (18 mm) strands is a bridge configuration with six BT-63 girders is $46,020, which is the same cost as the as-designed bridge. Table 9.6 provides a summary of the prestressing strand costs.

TABLE 9.6 Sunland Park Three-Span Unit Strand Costs.

	As-Designed, 9.5 ksi (65.5 MPa)	8 BT-54 Girders, 22.5 ksi (155 MPa)	6 BT-63 Girders, 22.5 ksi (155 MPa)
Number of 0.6 in. (15 mm) Strands Exterior Spans Per Girder	36	40	-
Number of 0.6 in. (15 mm) Strands Interior Span Per Girder	32	34	-
Number of 0.7 in. (18 mm) Strands Exterior Spans Per Girder	26	24	32
Number of 0.7 in. (18 mm) Strands Interior Span Per Girder	24	24	32
Cost of 0.6 in. (15 mm) Strands Exterior Spans Per Bridge	$31,860	$29,740	-
Cost of 0.6 in. (15 mm) Strands Interior Span Per Bridge	$14,160	$14,870	-
Cost of 0.7 in. (18 mm) Strands Exterior Spans Per Bridge	$41,550	$30,680	$30,680
Cost of 0.7 in. (18 mm) Strands Interior Span Per Bridge	$19,180	$15,340	$15,340

9.4 STEEL FIBERS CONSTITUENT COSTS

The steel fibers are the most expensive constituent in UHPC. To reduce this cost, the possibility of reducing the steel fibers content from 2% to 1% by volume has been explored. In previous studies, all mild reinforcement has been removed. In this study, a cost analysis was performed for a beam that has steel fibers at 2% by volume with minimal mild reinforcement that is only used for composite action versus a beam that has steel fibers at 1% by volume and typical mild steel reinforcement (i.e., confinement, steel shear stirrups, temperature and shrinkage).

The total material cost for a single BT-63 girder is $14,680 with 2% fiber content (see Table 9.7). The total material cost is $12,710 for the same girder with only 1% fiber content (see

Table 9.8) if the fiber are completely eliminated, the cost is $9,810 (see Table 9.9). Further testing will have to be performed to ensure that this is a possibility. Such a possibility could significantly affect the flexure and shear results, namely the allowable tensile stress and the fiber contribution to shear capacity.

TABLE 9.7 Material Costs for a BT-63 Girder with Minimal Mild Steel Reinforcement and Steel Fibers at 2% Volume.

	Unit	Cost/unit	Amount Needed for 1 Girder	Total Cost
Fine Sand	ton (metric ton)	$40.00 ($44.09)	22 (20)	$880
Cement	sacks (kg)	9.00 (0.21)	266 (11,342)	$2,390
Silica Fume	lb (kg)	$0.40($ 0.88)	8,118 (3,682)	$3,250
Steel Fibers	lb (kg)	$1.10 ($2.43)	5,475 (2,484)	$6,020
Mild Reinforcement	lb (kg)	$0.40 ($0.88)	813 (369)	$330
HRWRA	gal. (L)	$13.42 ($3.55)	135 (512)	$1,810
Total				$14,680

TABLE 9.8 Material Costs for a BT-63 Girder with Typical Mild Steel Reinforcement and Steel Fibers at 1% Volume.

	Unit	Cost/unit	Amount Needed for 1 Girder	Total Cost
Fine Sand	ton (metric ton)	$40.00 ($44.09)	22 (20)	$880
Cement	sacks (kg)	$9.00 ($0.21)	11,342 (266)	$2,390
Silica Fume	lb (kg)	$0. 40 ($0. 88)	8,118 (3,682)	$3,250
Steel Fibers	lb (kg)	$1.10 ($2.43)	2,632 (1,194)	$2,900
Mild Reinforcement	lb (kg)	$0.40 ($0.88)	3,689 (1,674)	$1,480
HRWRA	gal. (L)	$13.42 ($3.55)	135 (512)	$1,810
Total				$12,710

TABLE 9.9 Material Costs for a BT-63 Girder with Typical Mild Steel Reinforcement Without Steel Fibers.

	Unit	Cost/unit	Amount Needed for 1 Girder	Total Cost
Fine Sand	ton (metric ton)	$40.00 ($44.09)	20 (22)	$880
Cement	sacks (kg)	$9.00 ($0.21)	11,342 (266)	$2,390
Silica Fume	lb (kg)	$0.40 ($0.88)	8,118 (3,682)	$3,250
Steel Fibers	lb (kg)	$1.10 ($2.43)	0 (0)	$0
Mild Reinforcement	lb (kg)	$0.40 ($0.88)	3,689 (1,674)	$1,480
HRWRA	gal. (L)	$13.42 ($3.55)	135 (512)	$1,810
Total				$9,810

9.5 MILD STEEL COSTS

When developing the costs for UHPC girder designs, some assumptions had to be made. It was assumed that all mild reinforcement could be removed for the UHPC girders except for the hoops on top of the beam that ensure composite action based on the design of the Mars Hill Bridge. Another assumption was that the amount of reinforcing needed for the BT-54 girders was the same as the amount needed for the BT-63 girders. This is justified because the difference in the amount of mild steel is small, approximately 1.5 lb (0.7 kg).

The cost of the mild reinforcement was determined based on a unit cost of $0.40 per lb ($0.88 per kg).

9.5.1 I-25/Doña Ana Interchange Mild Steel Costs

Figure 9.1 shows the minimum requirements of NMDOT. The amount of mild reinforcement needed was found in the plans of the I-25/Doña Ana Bridge as listed in Table 9.10. In Section 8 of this report it was shown that the steel marked #4H and #7E1 were not necessary and the cost is not included in Tables 9.11 and 9.12. The total cost of mild steel for the baseline design is $1,475. The only cost of steel for the four BT-63 girders is $45, this is the hoops [No. 4S1 (No. 13S1) in the top flange to provide horizontal shear capacity for the composite connection with the NSC deck. The total cost of mild steel for the four BT-54 girders is $75, this is for bars No. 4S1 (No. 13S1) and No. 5S2 (No.16S2). Recall from Table 9.1 that the cost of UHPC required to provide sufficient shear capacity by increasing the web thickness was $1,170. It is clear for this bridge that using mild steel stirrups is much more cost effective.

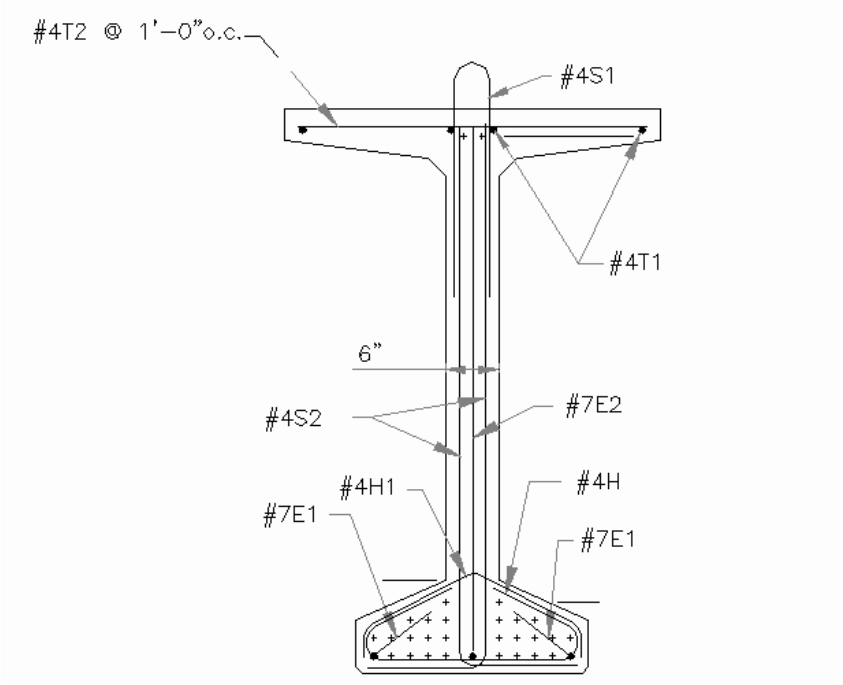

FIGURE 9.1 NMDOT Mild Steel Reinforcement Requirements for a BT-63 Girder.

TABLE 9.10 Reinforcing Bar Requirements for As-Designed BT-63 Girders for the I-25/Doña Ana Bridge.

Size and Type	Length, ft (m)	Quantity	Total Length Needed, ft (m)	Unit Weight, lb/ft (kg/m)	Total Weight, lb (kg)	Cost
#7E1	5.67 (1.73)	4	22.7 (6.91)	2.044 (3.042)	11.1 (5.03)	$4.00
#8E2	8.00 (2.44)	28	224 (68.3)	2.67 (3.973)	83.90 (38.06)	$34.00
#4S1	5.13 (1.56)	106	543.25 (165.58)	0.668 (0.994)	813.25 (368.88)	$325.00
#5S2	5.92 (1.80)	212	1,254.3 (382.32)	1.043 (1.552)	1,202.62 (545.50)	$481.00
#4H	4.13 (1.26)	56	231 (70.4)	0.668 (0.994)	345.81 (156.86)	$138.00
#4T1	113.2 (34.49)	4	452.67 (137.97)	0.668 (0.994)	677.64 (307.37)	$271.00
#4T2	3.25 (0.99)	114	370.50 (112.93)	0.668 (0.994.)	554.64 (251.58)	$222.00
Cost Per Girder						$1,475.00
Total Cost Per Bridge						$8,850.00

TABLE 9.11 Reinforcing Bar Requirements for Four BT-63 Girders for the I-25/Doña Ana Bridge.

Size and Type	Length, ft (m)	Quantity	Total Length Needed, ft (m)	Unit Weight, lb/ft (kg/m)	Total Weight, lb (kg)	Cost
#4S1	2.8 (0.85)	60	168 (51.2)	0.668 (0.994)	112 (51)	$45.00
Cost Per Girder						$45.00
Total Cost Per Bridge						$180.00

TABLE 9.12 Reinforcing Bar Requirements for Four BT-54 Girders for the I-25/Doña Ana Bridge.

Size and Type	Length, ft (m)	Quantity	Total Length Needed, ft (m)	Unit Weight, lb/ft (kg/m)	Total Weight, lb (kg)	Cost
#4S1	2.8 (0.85)	60	168 (51.2)	0.668 (0.994)	112 (51)	$45.00
#5S2	5.2 (1.6)	14	72.8 (22.4)	1.043 (1.552)	76 (35)	$30.00
Cost Per Girder						$75.00
Total Cost Per Bridge						$300.00

9.5.2 Mild Steel Costs for Sunland Park Bridge Two-Span Unit

The amount of mild steel reinforcement needed for the as-designed bridge was found in the plans for the Sunland Park River Crossing and is similar to Figure 9.12. Table 9.13 provides a summary of the as-designed mild steel with a total cost of $943. Tables 9.14 and 9.15 provide summaries of the required amount of steel for the eight BT-54 girders configuration and six BT-63 girders configuration. Note that the amount of steel required for both this bridges is the same. This is due to the fact that the BT-63 has a larger shear capacity than the BT-54, thus, as the shear loading increases so does the girder capacity.

TABLE 9.13 Reinforcing Bar Requirements for As-Designed BT-54 Girders for Sunland Park Two-Span Unit.

Size and Type	Length, ft (m)	Quantity	Total Length Needed, ft (m)	Unit Weight, lb/ft (kg/m)	Total Weight, lb (kg)	Cost
#7E1	8.66 (2.64)	4	34.6 (10.56)	2.044 (3.042)	69.6 (32.1)	$28.00
#8E2	12.17 (3.71)	2	24.3 (4.72)	2.67 (3.973)	64.9 (18.8)	$26.00
#4S1	2.79 (0.85)	60	167.4 (51)	0.668 (0.994)	111.8 (50.7)	$45.00
#5S2	5.18 (1.58)	224	1,160.3 (382.32)	1.043 (1.552)	1,210.2 (593.4)	$484.00
#5S3	4.10 (1.58)	24	98.4 (37.9)	1.043 (1.552)	102.6 (58.8)	$41.00
#4H	4.13 (1.25)	34	140.4 (42.5)	0.668 (0.994)	93.8 (42.2)	$38.00
#4H1	2.66 (0.81)	34	90.4 (27.6)	0.668 (0.994)	60.4 (27.4)	$24.00
#4T1	34.71 (10.58)	16	555.4 (169.3)	0.668 (0.994)	371.0 (168.3)	$148.00
#4T2	3.25 (0.99)	126	409.5 (124.7)	0.668 (0.994.)	273.5 (124.0)	$109.00
Cost Per Girder						$943.00
Total Cost Per Bridge						$18,860.00

TABLE 9.14 Reinforcing Bar Requirements for Eight BT-54 Girders for Sunland Park Two-Span Unit.

Size and Type	Length, ft (m)	Quantity	Total Length Needed, ft (m)	Unit Weight, lb/ft (kg/m)	Total Weight, lb (kg)	Cost
#4S1	2.79 (0.85)	60	167.4 (51)	0.668 (0.994)	111.8 (50.7)	$45.00
#5S2	5.18 (1.58)	16	82.9 (25.3)	1.043 (1.552)	86.5 (39.3)	$37.00
Total Cost						$82.00
Total Cost Per Bridge						$1,640.00

TABLE 9.15 Reinforcing Bar Requirements for Six BT-63 Girders for Sunland Park Two-Span Unit.

Size and Type	Length, ft (m)	Quantity	Total Length Needed, ft (m)	Unit Weight, lb/ft (kg/m)	Total Weight, lb (kg)	Cost
#4S1	2.79 (0.85)	60	167.4 (51)	0.668 (0.994)	111.8 (50.7)	$45.00
#5S2	5.18 (1.58)	16	82.9 (25.3)	1.043 (1.552)	86.5 (39.3)	$37.00
Cost per Girder						$82.00
Total Cost Per Bridge						$1,640.00

9.5.3 Mild Steel Costs for Sunland Park Bridge Three-Span Unit

The amount of mild steel reinforcement needed for the as-designed bridge was found in the plans for the Sunland Park River Crossing. Table 9.16 provides a summary of the as-designed mild steel with a total cost of $943. Tables 9.17 and 9.18 provide summaries of the required amount of steel for the eight BT-54 girders configuration and six BT-63 girders configuration. Note that the amount of steel required for both this bridges is slightly different. The eight BT-54 girders require No. 5 (M16) stirrups at 24 in. (610 mm) while the six BT-63 girders require No. 5 (M16) stirrups at 18 in. (460 mm).

TABLE 9.16 Reinforcing Bar Requirements for As-Designed BT-54 Girders for Sunland Park Three-Span Unit.

Size and Type	Length, ft (m)	Quantity	Total Length Needed, ft (m)	Unit Weight, lb/ft (kg/m)	Total Weight, lb (kg)	Cost
#7E1	8.66 (2.64)	4	34.6 (10.56)	2.044 (3.042)	69.6 (32.1)	$28.00
#8E2	12.17 (3.71)	2	24.3 (4.72)	2.67 (3.973)	64.9 (18.8)	$26.00
#4S1	2.79 (0.85)	60	167.4 (51)	0.668 (0.994)	111.8 (50.7)	$45.00
#5S2	5.18 (1.58)	224	1,160.3 (382.32)	1.043 (1.552)	1,210.2 (593.4)	$484.00
#5S3	4.10 (1.58)	24	98.4 (37.9)	1.043 (1.552)	102.6 (58.8)	$41.00
#4H	4.13 (1.25)	34	140.4 (42.5)	0.668 (0.994)	93.8 (42.2)	$38.00
#4H1	2.66 (0.81)	34	90.4 (27.6)	0.668 (0.994)	60.4 (27.4)	$24.00
#4T1	34.71 (10.58)	16	555.4 (169.3)	0.668 (0.994)	371.0 (168.3)	$148.00
#4T2	3.25 (0.99)	126	409.5 (124.7)	0.668 (0.994.)	273.5 (124.0)	$109.00
Cost Per Girder						$943.00
Cost Per Bridge						$28,290.00

TABLE 9.17 Reinforcing Bar Requirements for Eight BT-54 Girders for Sunland Park Three-Span Unit.

Size and Type	Length, ft (m)	Quantity	Total Length Needed, ft (m)	Unit Weight, lb/ft (kg/m)	Total Weight, lb (kg)	Cost
#4S1	2.79 (0.85)	60	167.4 (51)	0.668 (0.994)	111.8 (50.7)	$45.00
#5S2	5.18 (1.58)	16	82.9 (25.3)	1.043 (1.552)	86.5 (39.3)	$37.00
Cost Per Girder						$82.00
Total Cost Per Bridge						$2,460.00

TABLE 9.18 Reinforcing Bar Requirements for Six BT-63 Girders for Sunland Park Three-Span Unit.

Size and Type	Length, ft (m)	Quantity	Total Length Needed, ft (m)	Unit Weight, lb/ft (kg/m)	Total Weight, lb (kg)	Cost
#4S1	2.79 (0.85)	60	167.4 (51)	0.668 (0.994)	111.8 (50.7)	$45.00
#5S2	5.18 (1.58)	18	93.2 (25.3)	1.043 (1.552)	97.2 (39.3)	$39.00
Cost Per Girder						$84.00
Total Cost Per Bridge						$2,520.00

9.6 NORMAL STRENGTH CONCRETE DECK COST

The NMDOT has standard concrete deck details specified in section 4.3.1 of the NMDOT Bridge Procedures and Design Guide (2005). The thickness of the normal strength concrete deck varies with the effective span beam girders, while the spacing and amount of mild steel deck reinforcement remains constant, as the spacing increases between girders, the thickness of the deck increases, thus increasing in volume. The cost of NSC was estimated to be $\$100/yd^3$ ($\$131/m^3$).

9.6.1 I-25/Doña Ana Interchange Deck Cost

The deck of the as-designed I-25/Doña Ana Interchange Bridge has a thickness of 7.5 in. (190 mm), width of 43.0 ft (13.11 m) and a length of 113.5 ft (34.60 m). The cost of the as-designed deck is $11,447, shown in Table 9.19. The increase in cost for a four BT-54 or four BT-63 girders is 13.3%.

TABLE 9.19 I-25/Doña Ana Interchange Deck Costs.

	Deck Thickness, in. (mm)	Volume of Concrete, yd^3 (m^3)	Cost of Concrete Deck
6 BT-63 Girders	7.5 (190)	114.5 (87.54)	$11,447
4 BT-63 Girders	9.5 (240	145.0 (110.9)	$14,499
4 BT-54 Girders	9.5 (240	145.0 (110.9)	$14,499

9.6.2 Sunland Park Two-Span Unit Deck Cost

The deck of the as-designed Sunland Park Bridge has a thickness of 8.0 in. (203 mm), width of 70.0 ft (21.34 m) and a length of 122.92 ft (137.47 m). The cost of the as-designed deck is $42,491, shown in Table 9.20. The increase in cost for eight BT-54 girders is 6.2% and six BT-63 girders is 31.2%. This is a higher percent increase compared to the I-25/Doña Ana Interchange Bridge because a higher percentage of girders were eliminated in the Sunland Park Bridge.

TABLE 9.20 Sunland Park Two-Span Unit Deck Costs.

	Deck Thickness, in. (mm)	Volume of Concrete, yd^3 (m^3)	Cost of Concrete Deck
10 BT-54 Girders	8.0 (203)	11472.5 (8,771.4)	$42,491
8 BT-54 Girders	8.5 (216)	12189.57 (9,320.0)	$45,147
6 BT-54 Girders	10.5 (267)	15057.70 (11,512.4)	$55,769

9.6.3 Sunland Park Three-Span Unit Deck Cost

The deck of the as-designed Sunland Park Bridge has a thickness of 8.0 in. (203 mm), width of 70.0 ft (21.34 m) and a length of 122.92 ft The cost of the as-designed deck is $63,736, shown in Table 9.21. The increase in cost for eight BT-54 girders is 6.2% and six BT-63 girders is 31.2%. The percent increase is the same as the two-span unit, but the cost is higher due to the additional span.

TABLE 9.21 Sunland Park Three-Span Unit Deck Costs.

	Deck Thickness, in. (mm)	Volume of Concrete, yd^3 (m^3)	Cost of Concrete Deck
10 BT-54 Girders	8 (203)	637.4 (487.3)	$63,736
8 BT-54 Girders	8.5 (216)	677.2 (517.8)	$67,720
6 BT-54 Girders	10.5 (267)	836.5 (639.6)	$83,654

9.7 TOTAL PRESENT COST COMPARISON

9.7.1 Total Cost for I-25/Doña Ana Interchange

An overall cost comparison table was developed as shown in Table 9.22. From this table, it is evident that the four BT-63 girders design is the least expensive design that uses UHPC with a total cost of $120,014. The total cost for four BT-54 girders is $124,030, this is 3.3% more cost than the four BT-63 girder design. This price leaves out the $150,000 setup fee required to use 0.7 in. (18 mm) strands.

The best design based on present cost is six BT-63 girders.

TABLE 9.22 I-25/Doña Ana Interchange Comparison Final Costs.

	6 HPC BT-63 Girders [0.6 in. (15 mm) strands]	4 UHPC BT-63 Girders [0.6 in. (15 mm) strands]	4 BT-54 Girders [0.7 in. (18 mm) strands]	4 Modified BT-54 Girders [0.7 in. (18 mm) strands)]
Cost of Girder Concrete	$15,610	$57,040	$52,720	$57,030
Cost of Strands	$6,860	$6,860	$13,570	$13,570
Mild Reinforcement	$8,850	$180	$300	$300
Labor Cost	$38,817	$43,130	$43,130	$43,130
Cost of Deck Concrete	$11,297	$12,804	$14,310	$14,310
Total Cost	$81,434	$120,014	$124,030	$128,340

9.7.2 Total Cost for Sunland Park Bridge Two-Span Unit

An overall cost comparison table was developed as shown in Table 9.23. From this table, it is evident that the six BT-63 girders design is the least expensive design that uses UHPC with a total cost of $419,288. The total cost for eight BT-54 girders is $510,465, this is 21.7% more cost than the six BT-63 girder design. This price leaves out the $150,000 setup fee required to use 0.7 in. (18 mm) strands.

TABLE 9.23 Sunland Park Two-Span Unit Comparison Final Costs.

	10 HPC BT-54 Girders 0.6 in. (15 mm) strands	8 UHPC BT-54 Girders 0.6 in. (15 mm) strands	8 Modified BT-54 Girders 0.7 in. (18 mm) strands	6 BT-63 Girders 0.7 in. (18 mm) strands
Cost of Girder Concrete	$56,350	$247,100	$265,810	$185,320
Cost of Strands	$35,400	$29,740	$29,740	$36,430
Mild Reinforcement	$18,860	$1,640	$1,640	$1,640
Labor Cost	$140,129	$186,838	$186,838	$140,129
Cost of Deck Concrete	$42,491	$45,147	$45,147	$55,769
Total Cost	$293,230	$510,465	$529,175	$419,288

9.7.3 Total Cost for Sunland Park Bridge Three-Span Unit

An overall cost comparison table was developed as shown in Table 9.24. From this table, it is evident that the six BT-63 girders design is the least expensive design that uses UHPC with a total cost of $620,371. The total cost for eight BT-54 girders is $763,567, this is 23.1% more cost than the six BT-63 girder design. This price leaves out the $150,000 setup fee required to use 0.7 in. (18 mm) strands. It is clear that stirrups provide a less expensive approach to achieve the required shear capacity as compared to modifying the web width.

TABLE 9.24 Sunland Park Three-Span Unit Comparison Final Costs.

	10 HPC BT-54 Girders 0.6 in. (15 mm) strands	8 UHPC BT-54 Girders 0.6 in. (15 mm) strands	8 Modified UHPC BT-54 Girders 0.7 in. (18 mm) strands	6 BT-63 Girders 0.7 in. (18 mm) strands
Cost of Girder Concrete	$84,531	$370,650	$398,720	$277,984
Cost of Strands	$47,790	$42,480	$42,480	$46,020
Mild Reinforcement	$28,290	$2,460	$2,460	$2,520
Labor Cost	$210,193	$280,258	$280,258	$210,193
Cost of Deck Concrete	$63,736	$67,720	$67,720	$83,654
Total Cost	$434,540	$763,567	$791,638	$620,371

9.8 FUTURE WORTH

The typical life span of New Mexico bridge girders is designed for 75 years. In this study it was assumed that the life span of the UHPC girders would be twice as long as that of the HPC girders. This was determined based on the Ahlborn *et al.* (2008) study in Michigan. Based on the life spans stated above, the current bridges will need girder replacements in 75 years. Consideration of the life-cycle cost is important in this study. If the only financial parameter considered is present value it is clear that HPC is the least expensive. However the economic interests of New Mexico's citizens may be best served by considering the life-cycle costs of HPC and UHPC.

The present worth of both HPC and UHPC bridge designs are considered in Tables 9.22, 9.23, and 9.24 for I-25/Doña Ana Interchange and Sunland Park bridges. The future worth of these bridges is determined by Equation 9.1:

$$F = P(1+i)^n \qquad \text{Equation 9.1}$$

where, F is the future worth after n years; P is the present worth; i is the inflation rate taken as 3.85% (based on 2009 inflation rate); and n is the life span of the bridge, taken as n for the HPC girders and 150 for the UHPC girders.

The future worth is then adjusted to a net present value (NPV) and is determined by Equation 9.2:

$$NPV = F(1+r)^{-n}$$ Equation 9.2

where, F is the future worth calculated by Equation 9.1; r is the discount rate, taken as 3.85% and n and described previously.

9.8.1 I-25/Doña Ana Interchange Future Worth

Table 9.25 provides a summary of the future worth analysis. Figures 9.3, 9.4, and 9.5 are cash flow diagrams that illustrate the life-cycle costs. The upward arrows on Figure 9.3 represent the present value of the HPC bridge and the future value. The downward arrow is the present cost of constructing an HPC bridge today. The value $162,868 is twice the present value of the bridge. The reasoning behind this is that if the HPC were to be built today the initial cost would be $81,434 to construct the bridge and $81,434 would have to be set aside in savings. This money, set aside at an interest rate of 3.85% will generate the future cost of the HPC bridge in 75 years. The downward arrows in Figure 9.4 and 9.5 are present costs of constructing the bridges with four BT-63 girders and four BT-54 girders, respectively. Within a 75 year life span there will be no cost to rebuild the UHPC bridges.

Note the last row of normalized NPV's. This value is a normalized to the Net Present Value. Based on the interest and discount this value must be less than 2.0 for there to be an economic benefit. The value 2.0 represents the total initial cost of building the HPC bridge. The designs that use UHPC each have values less than 2.0. Therefore, there is life-cycle cost benefits to using UHPC for the I-25/Doña Ana Interchange. The lease expensive option is four UHPC BT-63 girders with 0.6 in. (15 mm) strands.

The last column of Table 9.25 shows the cost of four modified BT-54 girder. This cross-section is required to provide adequate shear strength if mild steel stirrups are excluded. Compared to the cost of four typical BT-54 girders it is 3.5% more expensive to increase the web width than to use mild steel stirrups.

TABLE 9.25 I-25/Doña Ana Interchange Future Worth Results.

	6 HPC BT-63 Girders 0.6 in. (15 mm) strands	4 UHPC BT-63 Girders 0.6 in. (15 mm) strands	4 BT-54 Girders 0.7 in. (18 mm) strands	4 Modified BT-54 Girders 0.7 in. (18 mm) strands
Present Value	$81,434	$120,014	$124,030	$128,340
Future Worth	$1,384,509	$34,690,156	$35,851,130	$37,096,892
Net Present Value	$81,434	$120,014	$124,030	$128,340
Normalized NPV	1.00	1.47	1.52	1.58

FIGURE 9.2 Cash Flow Diagram for Six HPC BT-63 Girders.

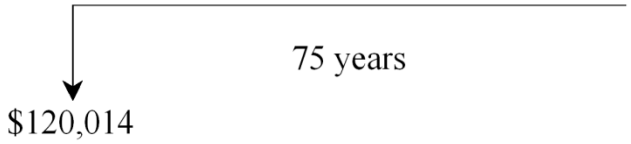

FIGURE 9.3 Cash Flow Diagram for Four UHPC BT-63 Girders.

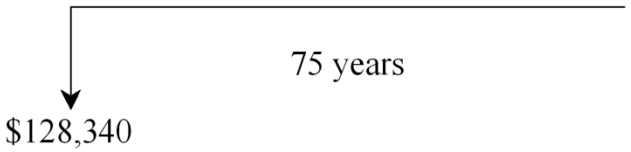

FIGURE 9.4 Cash Flow Diagram for Four UHPC BT-54 Girders.

9.8.2 Sunland Park Two-Span Unit Future Worth

Table 9.26 provides a summary of the future worth analysis. Notice the last row of normalized NPV's. The designs that use UHPC each have values less than 2.0 and the design that uses six BT-63 girders has a value of 1.43. The Figures 9.6, 9.7, and 9.8 are cash flow diagrams that illustrate the life-cycle costs. The initial outlay of the six UHPC BT-63 girders is the least expensive, therefore, there is an economic benefit in the employment of 0.7 in. (18 mm) strands and UHPC.

TABLE 9.26 Sunland Park Two-Span Unit Future Worth Results.

	10 HPC BT-54 Girders 0.6 in. (15 mm) strands	8 UHPC BT-54 Girders 0.6 in. (15 mm) strands	8 Modified BT-54 Girders 0.7 in. (18 mm) strands	6 BT-63 Girders 0.7 in. (18 mm) strands
Present Value	$293,230	$510,465	$529,175	$419,288
Future Worth	$4,985,348	$147,550,625	$152,958,777	$121,195,815
Net Present Value	$293,230	$510,465	$529,175	$419,288
Normalized NPV	1.00	1.74	1.80	1.43

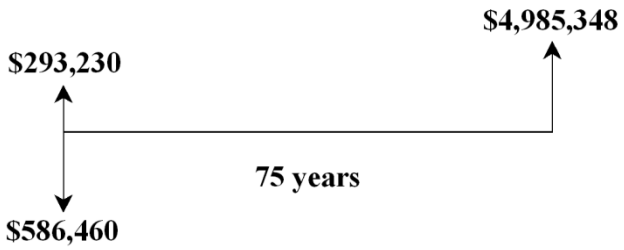

FIGURE 9.5 Cash Flow Diagram for Ten HPC BT-54 Girders.

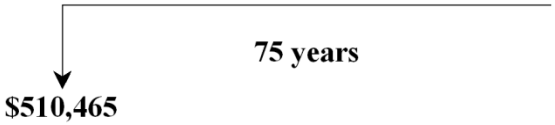

FIGURE 9.6 Cash Flow Diagram for Eight UHPC BT-54 Girders.

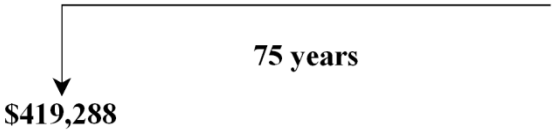

FIGURE 9.7 Cash Flow Diagram for Six UHPC BT-63 Girders.

9.8.3 Sunland Park Three-Span Unit Future Worth

Table 9.27 provides a summary of the future worth analysis. Notice the last row of normalized NPV's. The designs that use UHPC each have values less than 2.0 and the design that uses six BT-63 girders has a value of 1.43. The Figures 9.9, 9.10, and 9.11 are cash flow diagrams that illustrate the life-cycle costs. The initial outlay of the six UHPC BT-63 girders is the least expensive; therefore, there is an economic benefit in the employment of 0.7 in. (18 mm) strands and UHPC.

TABLE 9.27 Sunland Park Three-Span Unit Future Worth Results.

	10 HPC BT-54 Girders 0.6 in. (15 mm) strands	8 UHPC BT-54 Girders 0.6 in. (15 mm) strands	8 Modified BT-54 Girders 0.7 in. (18 mm) strands	6 BT-63 Girders 0.7 in. (18 mm) strands
Present Value	$434,540	$763,567	$791,638	$620,371
Future Worth	$7,387,846	$220,710,257	$228,823,985	$179,319,154
Net Present Value	$434,540	$763,567	$791,638	$620,371
Normalized NPV	1.00	1.76	1.82	1.43

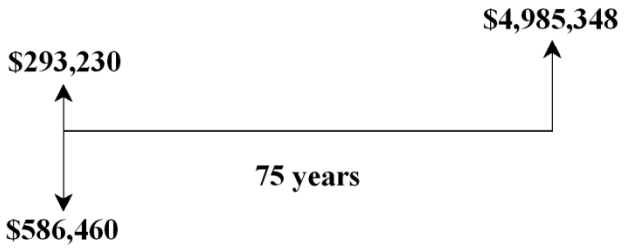

FIGURE 9.8 Cash Flow Diagram for Ten HPC BT-54 Girders.

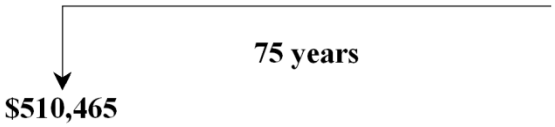

FIGURE 9.9 Cash Flow Diagram for Eight UHPC BT-54 Girders.

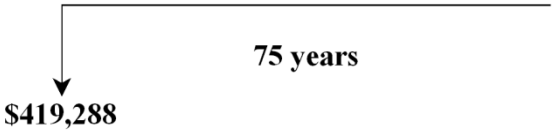

FIGURE 9.10 Cash Flow Diagram for Six UHPC BT-63 Girders.

9.9 SUMMARY OF ECONOMIC ANALYSIS

There are many variables that influence the cost of UHPC. Mixture proportions, the curing regimen, the percent volume are all factors that can be optimized to lower the cost of UHPC. However, further research is needed to investigate these different parameters. In addition,

design standards and specifications are not readily available for using UHPC. Thus, many of the properties of UHPC are not taken advantage of fully. Once additional research and more design applications using UHPC have been constructed, a better understanding of this material will exist, in which we can fully optimize the manner in which we use this material. This will once again lower the cost.

From the two bridges analyzed in this economic analysis, it can be seen that the initial cost of implementing UHPC is high. However, if the lifecycle costs are included, in the long run, UHPC has the potential to save money.

THIS PAGE LEFT BLANK INTENTIONALLY

10 CONCLUSIONS AND RECOMMENDATIONS

10.1 PROPERTIES AND CHARACTERISTICS OF UHPC

Ultra high performance concrete has the potential to offer many advantages for structural design applications. These properties enable the design and construction of bridges with longer spans, improved durability, and smaller structural members. The improved durability properties also improve the longevity of bridges, potentially doubling the service life of the structure.

Some of the properties identified from literature are listed below:

- Increased strength and ductile behavior (due to the addition of steel fibers) allow the concrete to deform and support flexural and tensile forces, well beyond initial cracking.
- Compared with conventional concrete, UHPC beams without reinforcement have a high load capacity particularly for shear.
- Compressive strengths:15.0 to 29.0 ksi (103.4 to 200.0 MPa)
- Flexural capacity: 4.0 to 8.0 ksi (27.6 to 55.2 MPa)
- Modulus of elasticity: 7,200 ksi – 8,000 ksi (49.6 to 55.2 GPa)
- The durability characteristics of the material are similar to those of an impermeable material reducing the effects of corrosion. This is an ideal material for joint applications.
- UHPC demonstrates a higher resistance to abrasion than that of normal strength concrete.
- UHPC exhibits almost no shrinkage or creep, which makes the material very suitable for applications in prestressed concrete.
- Due to addition of steel fibers, the failure of UHPC beams is plastic (i.e., improved ductility).
- Properties are greatly influenced by the curing regimen.

Due to these improved material properties, UHPC has the potential to greatly influence many structural applications. UHPC continues to be used throughout the world, including the United States, in many different applications. The three UHPC bridges constructed in the United States have shown good performance and as researchers, engineers, and precasters become more familiar with the material, it is expected that the number of UHPC structures will continue to grow. Iowa State University is continuing research on bridge applications including incorporating UHPC into bridge decks. In New York, UHPC is being used for bridge joints due to its low permeability.

It is noted that the only readily available UHPC at this time is Ductal®, which is proprietary and thus, information on the mixture proportions characteristics and properties are limited. Also note that the properties identified above are for Ductal®. It is expected that other UHPC mixture proportions have similar properties, but further research needs to be conducted in this area. Due to the high cost of Ductal®, it is recommended that mixture proportions for a UHPC using materials local to New Mexico be developed as a continuation of this research project.

10.2 CONCLUSIONS FROM THE PARAMETRIC BRIDGE STUDY

Based on the results of the parametric study, the following conclusions were drawn:

- UHPC girders with traditional 0.6 in. (15 mm) diameter strands allow for fewer girder lines and less required concrete material as compared to high strength concrete.
- Larger diameter prestressing strands [i.e., 0.7 in. (18 mm)] strands can further reduce the member sizes and thus, the required concrete material required.
- Incorporating the tensile strength of UHPC into the design can significantly impact the number of required prestressing strands.
- The required shear capacity can be achieved by considering the shear capacity of the crack-bridging fibers. In cases when the required tensile strength cannot be met by the UHPC contribution alone, traditional transverse mild steel reinforcement can be included in critical regions, or the size of the structural member can be modified (i.e., increasing the girder web width). Note that the amount of required traditional transverse mild steel reinforcement is significantly reduced compared to a high strength concrete girder.
- For continuous span bridges, the required deck steel in the negative moment regions over the pier does not change.
- It was shown that the tensile strength of UHPC is large enough to remove the confinement steel (i.e., the bursting stress is less than the allowable tensile limit).

The results of the parametric bridge study based on UHPC properties identified in literature. At this time, there are no standard design procedures that incorporate these properties and thus, assumptions had to be made. Typically, these assumptions were made to be as conservative as possible. As more research is conducted on this new material, design procedures and equations to model the behavior of UHPC will become available which could potentially further impact the efficiency of UHPC employment.

10.3 CONCLUSIONS OF ECONOMIC ANALYSIS

Based on the results of the economic analysis, the following conclusions were drawn:

- UHPC has the potential to reduce the life-cycle costs of bridge girders. UHPC is expected to provide at least twice the service life expected from HPC. Savings are made at 75 years when the HPC girder bridge has to be replaced and the UHPC girder bridge does not.
- The estimated material cost of UHPC using local materials is approximately 5.5 times the cost of HPC, whereas the patented Ductal® material is about 10 times the cost of HPC.

- If girder sizes or girder lines can be reduced due to the mechanical properties of UHPC, less material is required reducing the overall cost. Smaller and/or fewer members also can decrease construction time and costs.
- An additional way to save money would be to reduce the amount of steel fibers from 2% volume to 1% volume and use typical mild steel reinforcement. To determine if this is a good design, testing will need to be conducted.
- Industry must see a clear financial benefit to using UHPC before they invest in it. This study shows that the greatest benefit will be long term, but the state of New Mexico will have to commit to using UHPC before manufacturers will be confident enough to bid UHPC projects competitively.

UHPC has the potential to significantly impact structural projects. However, with Ductal®, the cost of implementing this material in design is still rather high at approximately 10 times the cost of high strength concrete. It is recommended that further investigations into UHPC mixture proportions using local materials be developed and tested for use in bridge design in New Mexico.

THIS PAGE LEFT BLANK INTENTIONALLY

PHASE II:

DEVELOPMENT OF MIXTURE PROPORTIONS FOR AN ULTRA HIGH PERFORMANCE CONCRETE USING LOCAL MATERIALS

THIS PAGE LEFT BLANK INTENTIONALLY

11 INTRODUCTION – PHASE II

Following the findings from Phase I of this research project, it was determined that more economical and readily available UHPC mixture proportions would be required for successful implementation of UHPC into bridge design in New Mexico. To achieve this, mixture proportions for UHPC materials needed to be developed and optimized. Two constituents in the original UHPC proportions were targeted for optimization. First, the silica fume content was reduced by replacing silica fume with an equivalent mass of Class F fly ash. This helps to reduce the cost of producing UHPC in New Mexico. The addition of fly ash also helps to control any potential alkali-silica reactions and delayed ettringite formation. The second constituent optimized was the fine sand. Scalping sand at the No. 30 sieve is a practice that requires labor and can waste material if the scalped material is not utilized. Therefore, larger aggregate top sizes were investigated. Each of these changes required adjustment of the mixture proportions to maintain compressive strength and a workable consistency. After the mixture proportions were optimized, the curing regimen was optimized for use in local precast plants. The curing regimen was optimized for economy by using readily achievable temperatures for both the wet and dry curing periods. Finally, the durability of the optimized mixture for resistance to alkali-silica reaction, freezing and thawing, and delayed ettringite formation was established.

THIS PAGE LEFT BLANK INTENTIONALLY

12 BACKGROUND

UHPC is composed of cement, fine sand, quartz powder, micro silica, steel fibers, and high range water reducing admixture (HRWRA). When used in optimum dosages, the HRWRA reduces the water-to-cementitious materials (w/cm) ratio while improving the workability of concrete. The addition of micro-silica enhances the mechanical properties of the paste by filling voids, enhancing rheology, and producing secondary hydrates. The quartz powder is useful for its reactivity during heat treatment (Dili and Santhanam 2004). The constituents of the mixture and proportions (by fraction of cement mass) proposed by various investigators (Richard and Cheyrezy 1995, Shaheen and Shrive 2006, and Matte and Moranville 1999) are presented in Table 12.1.

TABLE 12.1 Mixture proportions (by fraction of cement) of UHPC from literature.

Constituent	Richard and Cheyrezy (1995)				Shaheen and Shrive (2006)		Matte and Moranville (1999)
	Plain		Steel fibers [0.5 in. (13 mm) long]		Plain	Carbon Fibers [0.118 in. (3 mm) long]	Steel fibers
Portland cement	1	1	1	1	1	1	1
Silica fume	0.25	0.23	0.25	0.23	0.23	0.23	0.325
Quartz Sand	1.1	1.1	1.1	1.1	1.1	0.5	1.43
Quartz powder	-	0.39	-	0.39	-	-	0.3
Crushed quartz	-	-	-	-	0.39	0.39	-
Superplasticizer	0.016	0.019	0.016	0.019	0.019	0.019	0.018
Steel fibers	-	-	0.175	0.175	-	-	0.275
Carbon fibers	-	-	-	-	-	0.125	-
Water	0.15	0.17	0.17	0.19	0.13	0.13	0.2
w/c[1]	0.15	0.17	0.17	0.19	0.13	0.13	0.2
w/cm[2]	0.12	0.138	0.136	0.154	0.11	0.11	0.15
Pre-setting pressure, ksi (MPa)	-	-	-	-	3.8 (26)	3.8 (26)	-
Post-setting heat treatment temperature, ˚F (˚C)	68 (20)	194 (90)	68 (20)	194 (90)	212 (100)	212 (100)	194 (90)

[1]water-to-cement
[2]water-to-cementitious materials

Roux *et al*. (1996) demonstrated that the mechanical properties of UHPC are obtained by lowering the w/cm ratio, using HRWRAs, and including silica fume. The lower w/cm ratio reduces the porosity of the cement paste and improves durability. Richard and Cheyrezy (1995) recommended the following principles to develop UHPC:

- Removal of coarse aggregate to enhance homogeneity of the concrete.
- Use of silica fume for pozzolanic reaction.
- Optimization of the granular mixture for enhancement of compacted density.
- Application of pre-setting pressure for better compaction.

- Post-setting heat treatment to enhance the mechanical properties of the microstructure.
- Addition of steel fibers to achieve ductility.

Further background information can be found in the literature review presented in Chapter 2.

The development of two mixtures of UHPC (one with and one without fibers) from a previous study (Allena and Newtson 2010) is discussed in the following section to establish the baseline for Phase II of this project. The compressive and flexural strength obtained from the UHPC mixtures are similar to those presented in literature.

12.1 MATERIALS

Type I/II portland cement, silica fume, and fine local sand [0.00295-0.0236 in. (75-600 μm)] from Las Cruces, New Mexico were used. Table 12.2 shows the grain size distribution for the fine sand. Steel fibers that were 0.5 in. (13 mm) long were used to provide ductility. The fibers are continuously deformed (wavy) in shape with an effective aspect ratio of 24. To achieve the desired workability, a commercially available polycarboxylate-based HRWRA (Glenium 3030 NS from BASF Chemicals) was used.

TABLE 12.2 Grain size distribution of fine sand.

Sieve No.	Sieve size, in. (mm)	Percent passing
30	0.0236 (0.60)	100
50	0.0118 (0.30)	40.1
100	0.0059 (0.15)	0

Table 12.3 shows the mixture proportions of the two mixtures of UHPC developed in previous work (Allena and Newtson 2010). Mixture EL00 was produced by introducing steel fibers to the mixture proportions from DL00. The volume of sand was reduced by the volume occupied by steel fibers in mixture EL00. The aggregates were thoroughly washed and dried prior to use to remove any dust. A better coating of cement paste over the sand particles was achieved by removing the dust, resulting in increased compressive strengths.

TABLE 12.3 Mixture proportions of UHPC.

Category	Mixture	Cement, lb/yd^3 (kg/m^3)	Silica fume, lb/yd^3 (kg/m^3)	Fine sand, lb/yd^3 (kg/m^3)	Steel fibers, lb/yd^3 (kg/m^3)	Water, lb/yd^3 (kg/m^3)	HRWRA, gal/yd^3 (l/m^3)	w/c	w/ (c+sf)[1]
D	DL00	1500 (890)	375 (222)	1411 (837)	-	375 (222)	6.00 (29.64)	0.25	0.20
E	EL00	1500 (890)	375 (222)	1347 (799)	200 (119)	375 (222)	6.00 (29.64)	0.25	0.20

[1]water-to-cement plus silica fume

12.2 SPECIMEN PREPARATION

Sand used in this study was passed through a No. 30 sieve to obtain the desired particle sizes. The aggregates were then thoroughly washed over a No. 200 sieve. After washing, the sand was oven dried at 110°F (44°C) to achieve 0% moisture content.

The constituents of each mixture were mixed for 15 to 20 minutes using a laboratory pan mixture. The dry constituents were mixed for two minutes and then 75% of the water was added. After thorough mixing, the HRWRA was added and the remaining 25% of the water was added to the mixture. Steel fibers were added at the end. This process of mixing seemed to improve the action of the HRWRA.

Compressive strength specimens included 2 in. (50 mm) cubes and 4 in. (100 mm) cubes. All specimens were consolidated using a high frequency vibrating table. After the specified curing period, the cube specimens were tested according to British Standard (BS) 1881-116.

12.3 CURING REGIMEN

The concrete specimens were cured at room temperature, 65°F (20°C), for the first 24 hours. After demolding, the specimens were heat cured in a water bath at 122°F (50°C). Then, the specimens were removed from the water bath and dry cured at 392°F (200°C) for two days prior to testing. This curing regimen was designated as OV.

12.4 COMPRESSIVE STRENGTH RESULTS

Average compressive strengths of specimens produced from each mixture category are presented in Table 12.4. To investigate the repeatability of the compressive strengths of these mixtures, testing was conducted on three specimens cast from each batch. Compressive strengths were measured at 7 and 28 days.

TABLE 12.4 Compressive strength of UHPC mixtures.

Mixture details				Compressive Strength, psi (MPa)			
				7 days		28 days	
Category	Mixture	w/c ratio	w/(c+sf)	2 in. (50 mm) Cube	4 in. (100 mm) Cube	2 in. (50 mm) Cube	4 in. (100 mm) Cube
D	DL00 (OV)	0.25	0.20	21,240 (146.4)	18,900 (130.3)	23,480 (161.9)	20,480 (141.2)
E	EL00 (OV)	0.25	0.20	22,210 (153.1)	19,850 (136.9)	24,010 (165.5)	21,680 (149.5)

The greater compressive strength of the fiber reinforced UHPC mixture is consistent with results reported by Reda *et al*. (1999).

This research provided the foundation for the work conducted in Phase II of this project. These mixture proportions served as the baseline and were optimized for the UHPC mixture proportions developed using materials local to New Mexico.

13 OPTIMIZATION OF MIXTURE PROPORTIONS

Based on the results from the two UHPC mixtures described in Chapter 12, several additional batches of UHPC were mixed, cured, and tested for 7-day compressive strengths. To reduce the required curing temperature and increase the aggregate top size, the water-to-cementitious material (w/cm) ratio was decreased incrementally. The batches used w/cm ratios of 0.20, 0.18, 0.15, and 0.14. A w/cm ratio of 0.13 was also attempted, but due to poor workability, this w/cm ratio was not considered further in this project. To improve workability, a HRWRA, Glenium 3030 NS, was used. Silica fume, Rheomac SF 100, was used in the mixture proportions to improve the density of the microstructure and provide secondary calcium silicate hydrates in UHPC. Angular sand with a specific gravity of 2.58 from the Placitas Quarry near Albuquerque, New Mexico passing through a No. 30 sieve was used in all of the batches. Prior to sieving, the sand was oven-dried to remove moisture. It was then washed over a No. 200 sieve to remove dust particles and oven-dried again. Type I/II portland cement, water, and carbon steel fibers were the additional constituents used.

Using a laboratory pan mixer, the dry ingredients were first mixed for five minutes. Next, 75% of the water was added and again allowed to mix for five minutes. The HRWRA was then added slowly to ensure thorough mixing. The remaining water was added to the mixer and mixed until a slurry was formed. Figure 13.1 shows the slurry in the pan mixer. Finally, the steel fibers were added (see Figure 13.2). Decreasing the w/cm ratio required greater mixing times to develop the slurry. Therefore, total mixing time ranged from 20 to 30 minutes.

FIGURE 13.1 Photograph of formation of slurry.

FIGURE 13.2 Photograph of steel fibers being added to slurry.

Once mixing was completed the concrete was placed into steel molds and consolidated on a vibrating table. Specimens were cast in 2 in. (50 mm) and 4 in. (100 mm) cube molds. UHPC was placed in three lifts into the 4 in. (100 mm) molds and two lifts into the 2 in. (50 mm) molds. Each lift was rodded 25 times. The vibrating period varied depending on the fluidity of the mix. The vibrating table was turned on while each lift was rodded. However, it was found that for mixtures with better workability due to higher w/cm ratios (e.g., 0.20 and 0.18), too much vibration would cause the steel fibers to sink to the bottom of the mold. Therefore, the vibration table was turned off while placing the next lift. Mixtures with 0.15 and 0.14 w/cm ratios were vibrated for the entire casting process (during placing and rodding of the concrete). Once the specimens were cast they were covered with plastic sheeting to prevent bleeding. After 24 hours, the specimens were removed from the molds and placed in an oven to cure. Figure 13.3 shows casted specimens prior to being covered with the plastic sheeting.

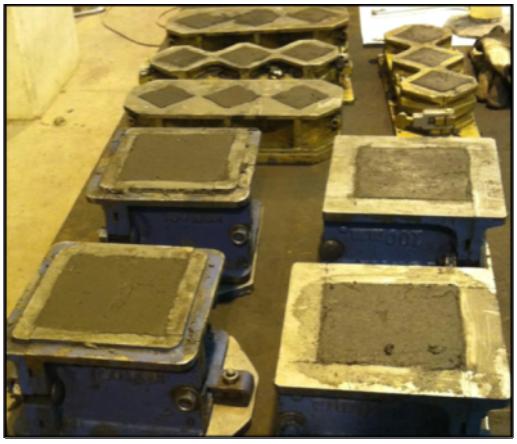

FIGURE 13.3 Photograph of test specimens.

To produce an economically feasible UHPC product with these mixture proportions, the curing regimen had to be modified from Allena and Newtson (2010). For more information on the curing regimen and optimization, please refer to Chapter 14. Following casting, the specimens were allowed to cure in an ambient environment for 24 hours until they were removed from their molds. After demolding, the specimens were wet cured at a temperature of 203°F (95°C) for four days. They were then transferred to dry heat at the same temperature [203°F (95°C)] for an additional two days (for a total of six days of heat curing). Finally, the specimens were removed from their curing environment and tested for seven day compressive strength following BS 1881: Part 116 standard methods. The loading rate was modified to achieve failure in a reasonable period of time. Graybeal (2006) concluded a load rate of 9000 psi/min (62 MPa/min) was acceptable for cylindrical UHPC specimens. Typically, it is expected that higher load rates will result in higher compressive strengths. However, the results indicated that there was no statistically significant difference in the compressive strength, the modulus of elasticity, or Poisson's ratio. Consequently, it was determined that an increased rate of loading would be beneficial to reduce the overall testing time while having negligible effect on the material characteristics.

The testing apparatus (see Figure 13.4) used in this research was a Tinius Olsen universal testing machine that has a maximum capacity of 400,000 lb (1780 kN). The average compressive strengths from the different batches are presented in Table 13.1.

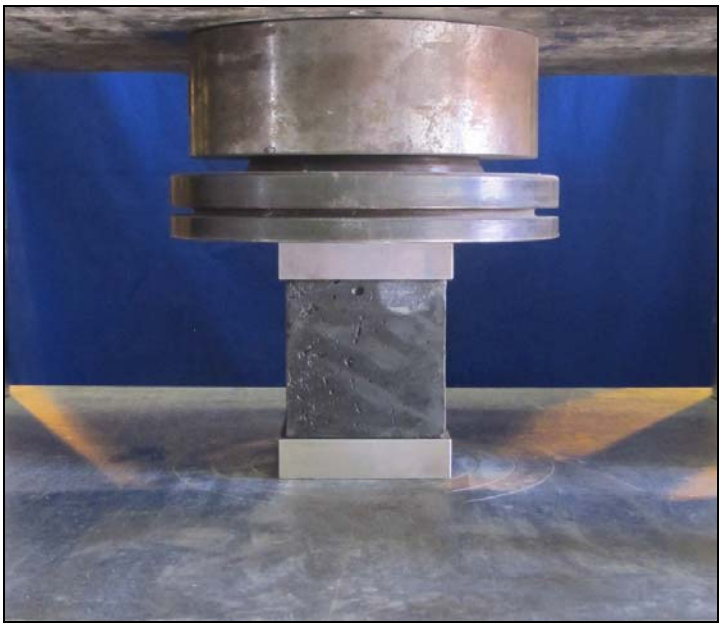

FIGURE 13.4 Photograph of Tinius Olsen universal testing machine and specimen prior to loading.

TABLE 13.1 Compressive strength of UHPC mixtures.

w/cm ratio	Average compressive strength, psi (MPa)	
	2 in. (50 mm) cubes	4 in. (100 mm) cubes
0.20	19,120 (131.8)	17,820 (122.9)
0.18	23,020 (158.7)	18,410 (126.9)
0.15	22,430 (154.7)	19,640 (135.4)
0.14	25,080 (172.9)	20,470 (141.1)

Based on the compressive strength results and workability, mixture proportions with a w/cm ratio of 0.14 were selected as the basis for further optimization. The mixture proportions and curing regimen were kept constant for all the following tests except for the parameter variation described in each section.

13.1 FLY ASH OPTIMIZATION

To minimize the use of silica fume, and subsequently cost, in the UHPC mixture, silica fume was replaced with an equivalent mass of Class F fly ash. Several batches were tested with increasing

percentages (12.5% to 100%) of silica fume being replaced by fly ash. The average 7-day compressive strengths of three test specimens from each batch are presented in Table 13.2.

TABLE 13.2 Compressive strength of UHPC mixtures with fly ash replacement (w/cm = 0.14).

Percentage (%) of silica fume replaced by fly ash	Average compressive strength, psi (MPa)	
	2 in. (50 mm) cubes	4 in. (100 mm) cubes
12.5	23,690 (163.3)	22,120 (152.5)
25	24,560 (169.3)	21,530 (148.4)
37.5	24,200 (170.0)	21,190 (146.1)
40	23,640 (166.9)	20,140 (138.8)
45	20,360 (140.4)	21,220 (146.3)
50	20,110 (138.7)	20,850 (144.0)
55	23,970 (165.2)	20,590 (142.0)
60	24,590 (169.5)	20,770 (143.2)
75	23,600 (162.7)	21,450 (147.9)
100	14,840 (102.3)	15,030 (103.6)

The compressive strength results for all of the batches, except at 100% replacement of silica fume replaced by fly ash, were above 20,000 psi (138 MPa). However, variation in the data for fly ash percentages greater than 50% was considered excessive. Consequently, mixture proportions with fly ash contents of 37.5% and 50% of the supplementary cementitious materials were chosen for further optimization in this study.

13.2 MAXIMUM SIZE OF AGGREGATE

To further reduce the cost of the UHPC mixture, a study was conducted to evaluate the effects of aggregate top size. For this study, the maximum size of the sand was increased from No. 30 to No. 16, No. 8, and finally No. 4. The objective of this portion of the study was to utilize more of the raw sand and reduce labor cost associated with sieving. Scalping sand at the No. 30 sieve is a practice that requires labor and can waste material if the scalped material is not utilized. Therefore, the use of larger aggregates was investigated. The average compressive strength results are shown below in Table 13.3. The results show that increasing the maximum size of the sand resulted in a reduction in compressive strength. However, the reduced cost of processing the sand was considered to offset the strength sacrificed.

TABLE 13.3 Effect of maximum size of aggregate on compressive strength.

Sieve No.	Sieve Size, in. (mm)	Compressive Strength, psi (MPa)	
		2 in. (50 mm) cubes	4 in. (100 mm) cubes
30	0.0234 (0.595)	24,200 (170.0)	21,190 (146.1)
16	0.0469 (1.19)	24,640 (169.9)	24,030 (165.7)
8	0.0937 (2.38)	24,430 (168.4)	22,410 (154.4)
4	0.187 (4.76)	23,870 (165.2)	21,790 (150.3)

13.3 SAND PROPORTION OPTIMIZATION

To further improve the cost of the UHPC mixture proportions, a study was conducted on the optimal amount of sand. Increasing the amount of sand, allows for a reduction in the cementitious materials. Using the mixture proportions with a w/cm ratio of 0.14, the sand was increased in increments up to 2100 lb/yd^3 (1246 kg/m^3). The w/cm ratio was preserved for all mixture proportions. Seven day compressive strengths were measured on 2 in. (50 mm) and 4 in. (100 mm) cube specimens. The results of the study are presented in Table 13.4.

TABLE 13.4 Effect of amount of sand on compressive strength.

Sand, lb/yd^3 (kg/m^3)	Compressive Strength, psi (MPa)	
	2 in. (50 mm) Cubes	4 in. (100 mm) Cubes
1,500 (890)	24,110 (166.2)	22,310 (153.8)
1,700 (1009)	23,990 (165.4)	21,940 (151.3)
1,900 (1127)	24,340 (167.8)	21,010 (144.9)
2,100 (1246)	22,940 (158.2)	21,590 (148.9)

The results show that an increase in sand does not greatly affect the compressive strength of the mixture. As the sand content increases, there is a small reduction in strength. The average results fluctuate between 22,156 and 24,335 psi (152.8 – 167.8 MPa) for the 2 in. (50 mm) cubes and

21,010 and 22,313 psi (144.9 – 153.8 MPa) for the 4 in. (100 mm) cubes. Increasing the amount of sand helps reduce the cost of UHPC and also helps to improve the workability of the mixture. The mixture proportions with a sand content of 1900 lb/yd^3 (1127 kg/m^3) and 2100 lb/yd^3 (1246 kg/m^3) were selected for further work. Sand contents above 2100 lb/yd^3 (1246 kg/m^3) were not workable.

13.4 ADMIXTURE OPTIMIZATION

The effect of different admixtures on the workability and compressive strength was investigated through a study that used two different admixtures. Rheomac, a viscosity modifying admixture, and Navitas 33, a rheology modifying admixture, were used at varying dosages in the mixture proportions. For each admixture three batches were mixed using the minimum recommended dosage, the maximum recommended dosage, and an intermediate dosage. By inspection and ease of placement, the workability of the mixtures were evaluated as poor, fair, good, or very good. Finally, 2 in. (50 mm) and 4 in. (100 mm) cube specimens were tested for 7-day compressive strengths. The results of this study are provided in Tables 13.5 and 13.6. As the dosage of the admixtures increased, the workability of the mixture increased and a small reduction (5% - 9%) of compressive strength was observed. Neither admixture appeared to offer significant advantages so neither was investigated further.

TABLE 13.5 Effect of Rheomac on mixture proportions.

	Compressive strength, psi (MPa)		Workability description
Dosage	2 in. (50 mm) Cubes	4 in. (100 mm) Cubes	
minimum	22,170 (152.9)	22,380 (154.3)	poor
intermediate	24,540 (169.2)	21,590 (148.9)	poor
maximum	23,700 (163.4)	22,660 (156.2)	good

TABLE 13.6 Effect of Navitas 33 on mixture proportions.

Dosage	Compressive strength, psi (MPa)		Workability description
	2 in. (50 mm) Cubes	4 in. (100 mm) Cubes	
minimum	23,360 (161.1)	21,380 (147.4)	poor
intermediate	23,320 (160.8)	20,530 (141.5)	fair
maximum	23,950 (165.1)	21,060 (145.2)	good

13.5 COMPRESSIVE STRENGTH GAIN

To assess strength gain of UHPC, a study was conducted using two of the optimized mixtures. Both mixtures had a w/cm ratio of 0.14, a sand content of 1900 lb/yd^3 (1127 kg/m^3), and No. 4 maximum aggregate size. The difference between the two UHPC mixtures was the amount of fly ash of the pozzolanic materials. The proportions of the pozzolanic materials for one mixture were 37.5% fly ash and 62.5% silica fume. Proportions of the pozzolanic materials for the second mixture were 50% fly ash and 50% silica fume.

Both mixtures were cured using two curing regimens. In both regimens, specimens remained in their molds for 24 hours at room temperature, 77^{o}F (25^{o}C). For the first curing regimen, the specimens were heat cured after demolding in a waterbath at 203^{o}F (95^{o}C) for the following 4 days. Then, they were dry cured in an oven at 203^{o}F (95^{o}C) for two days. Finally, they were cured the rest of the time at room temperature, 77^{o}F (25^{o}C). For the second curing regimen, specimens were moist cured right after demolding at 73^{o}F (23^{o}C), until testing was performed.

Compressive strength testing was performed using 4 in. (100 mm) cubes at ages of 1, 7, 14, 28 and 56 days. The strength gain of the concrete is plotted in Figure 13.5. It is important to note that there is rapid strength gain during the first 24 hours. After one day, the rate of strength gain decreases.

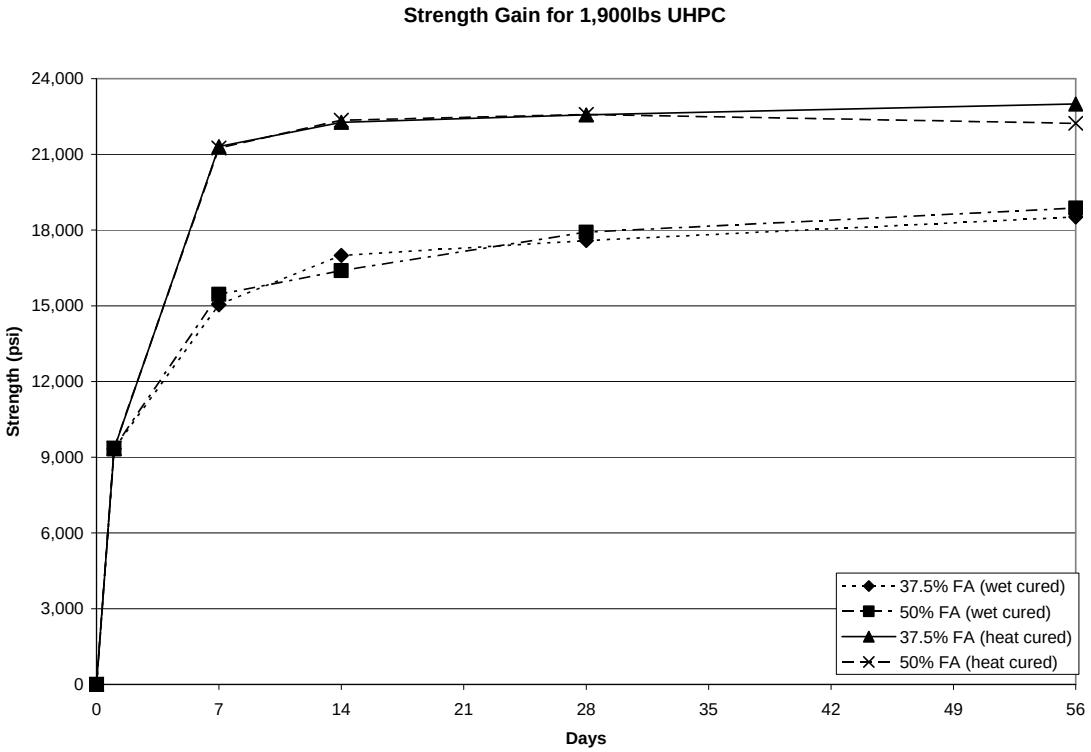

FIGURE 13.5 Compressive strength gain of UHPC.

Both mixtures exhibited similar behavior under ambient curing conditions during the first 24 hours. Additionally, providing heat and humidity during curing resulted in a greater strength gain at early age. However, strength gain plateaued after 14 days for mixtures provided with heat/humidity curing. Conversely, mixtures that were only wet cured continued to gain strength at a decelerating rate.

THIS PAGE LEFT BLANK INTENTIONALLY

14 OPTIMIZATION OF CURING REGIMEN

UHPC typically requires a heat curing regimen to achieve high compressive strength and improved durability properties. For implementation of UHPC in design, this curing regimen needs to be economical and readily achievable in a precast plant. Thus, the baseline curing regimen required modification. Discussions with local precasters indicate that temperatures of 203°F (95°C) are currently achievable. Therefore, those temperatures were used for the curing regimen optimized for the UHPC mixture.

Two heat treatment curing regimens were investigated in this research. Allena and Newtson's (2010) curing regimen was implemented to replicate seven day compressive strengths. This regimen required specimens to be cured at room temperature, 70°F (21°C), for the first 24 hours, then removed from the molds and placed in a heated water bath for four days at 122°F (50°C), and finally dry cured for two days at 392°F (200°C). This curing regimen will be referred to as the 50/200 regimen. The second curing regimen required the specimens to be cured at room temperature, 70°F (21°C), for the first 24 hours. After demolding, the specimens were heat cured in a water bath at 203°F (95°C) for four days. Then, they were removed from the water bath and dry cured at 203°F (95°C) for two days. This curing regimen will be referred to as the 95/95 regimen. Compressive strength testing of UHPC was conducted on 2 in. (50 mm) and 4 in. (100 mm) cubes and the results are presented in Table 14.1

TABLE 14.1 Compressive testing results for different curing regimens.

			Compressive Strength, psi (MPa)	
w/cm ratio	Curing regimen	No. of batches	2 in. (50 mm) cube	4 in. (100 mm) cube
0.20	50/200	3	25,200 (173.7)	23,430 (161.5)
0.20	95/95	2	19,120 (131.8)	17,820 (122.8)

After seven days, regardless of specimen size, samples cured at 203°F (95°C) experienced a decrease in compressive strength compared to samples cured according to Allena and Newtson's (2010) curing regimen. Specifically, the 2 in. (50 mm) cubes produced a 24.1% reduction in compressive strength, while the 4 in. (100 mm) cubes decreased in compressive strength by 23.9%. These results led to the conclusion that the w/cm ratio needed to be reduced to increase the compressive strength of UHPC cured in a 203°F (95°C) environment, since the curing regimen used by Allena and Newtson (2010) is not economically feasible.

To re-gain strength lost due to the reduced temperature in the heat curing regimen, the w/cm ratio was incrementally decreased from 0.2 to 0.14. The results of this portion of the study were presented in Chapter 13. Using the 95/95 curing regimen and a w/cm ratio of 0.14, compressive strengths of 25,080 (172.9MPa) and 20,470 psi (14.1 MPa) were measured for 2 in. (50 mm) and 4 in. (100 mm) cubes, respectively. By lowering the w/cm ratio, the use of the more economical 95/95 curing regimen to achieve the desire compressive strength was possible.

15 DURABILITY TESTING

The durability of the UHPC was established by studying resistance to freezing and thawing, alkali-slicia reaction, and delayed ettringite formation. Resistance to freezing and thawing of UHPC produced with optimized mixture proportions and curing methods was conducted according to ASTM C 666 (AASHTO T161). Fundamental frequency testing described in ASTM C 215 as the impact resonance method was used to monitor dynamic elastic modulus during the repeated cycles of freezing and thawing. Resistance to alkali-silica reaction was assessed using the mortar bar method (ASTM C 1260). Finally, resistance to delayed ettringite formation was established by evaluating the chemical composition of the cementitious materials.

15.1 RESISTANCE TO FREEZING AND THAWING

Resistance to freezing and thawing of UHPC produced with optimized mixture proportions and curing methods was conducted according to ASTM C 666 Procedure A (AASHTO T161). Fundamental frequency testing described in ASTM C 215 as the impact resonance method was used to monitor dynamic elastic modulus during the repeated cycles of freezing and thawing.

In this test, concrete specimens are subjected to rapid repeated freezing and thawing cycles under laboratory conditions. It is required that the specimens be submerged in distilled water throughout the experiment, surrounded by at least 1/32 in. (0.79 mm) of water at all times. The specimens are molded beams that are cured 14 days prior to testing. The dimensions of the beams are 3 x 4 x 16 in. (76 x 102 x 406 mm). On the last day of curing, the specimens are subjected to a 24 hour conditioning period in a 40^{o}F (4.4^{o}C) waterbath. After the conditioning period, the specimens are placed in the freezing and thawing chamber.

The freezing and thawing chamber consists of a chamber with the equipment necessary to refrigerate and heat the specimens in automatic, continuous, and reproducible cycles. For this application, the rapid freezing and thawing cabinet model H-3185SD from Humboldt Mfg. Co. was selected.

Following ASTM C 666, a four hour cycle was selected. The cycle starts by initially lowering the temperature of the conditioned specimens to 0^{o}F (-18^{o}C) in 2 hours and 42 minutes. Then, there is an 8 minute transition period between freezing and thawing. After the transition period, the temperature is raised to 40^{o}F (4.4^{o}C) in one hour. Finally, the temperature is kept constant in a second transition period for 10 minutes.

The specimens are removed from the apparatus in the thawed transition period for fundamental frequency testing. Fundamental transverse frequency, length, and weight are recorded at intervals not exceeding 36 cycles. The weight of each specimen is recorded and the effective length of the sample is measured using a length comparator with a resolution of 0.0001 in. (0.0025 mm).

The fundamental transverse frequency is obtained using the impact resonance method described in ASTM C 215. It requires the use of a computer, an instrumented hammer, an accelerometer, and an amplifier. To obtain the transverse frequency, the concrete specimen is supported on two

piano strings, allowing free vibration. The accelerometer is attached to an end of the specimen. Using an instrumented hammer, the specimen is excited over a wide range of frequencies, which are recorded by the computer. Dynamic modulus of elasticity, E_D, is computed using an ASTM equation that is a function of weight, natural frequency, and specimen dimensions as:

$$E_D = Cm\omega_r \qquad \text{Equation 15.1}$$

where C is a constant that accounts for Poisson's ratio and the geometry of the specimen, m is the mass of the specimen, and ω_r is the measured fundamental frequency.

Testing of the specimens continues until each of the beams has been subjected to at least 300 cycles of freezing and thawing, or until the relative dynamic modulus of elasticity falls below 60% of its initial value. Additionally, a 0.10% expansion may also be considered as a failure criteria.

When ASTM C 215 is used to monitor deteriorating concrete, it is common practice to present results in terms of the relative dynamic modulus, RDM, computed as:

$$\text{RDM} = \frac{E_n}{E_0}(100) \qquad \text{Equation 15.2}$$

where RDM is the relative dynamic modulus after n cycles of freezing and thawing, E_n is the dynamic elastic modulus after n cycles, and E_0 is the dynamic elastic modulus at zero cycles of freezing and thawing. After completion of freezing and thawing cycles, a durability factor, DF, can be computed as:

$$\text{DF} = \frac{\text{RDM} \cdot \text{N}}{\text{M}} \qquad \text{Equation 15.3}$$

where N is the number of cycles imposed, and M is the specified number of cycles (usually 300).

15.1.1 Results

Resistance to freezing and thawing for nine UHPC mixtures were evaluated in accordance to ASTM C 666 Procedure A. The mixtures had a w/cm ratio of 0.14 and variable aggregate top size and content. The cementitious materials consist of 80% portland cement and 20% other pozzolanic materials.

The specimens were cured for 14 days prior to testing. During the first seven days, the curing regimen was the same for all of the batches. The specimens remained in their molds for 24 hours at room temperature, 77°F (25°C). After demolding, the specimens were heat cured in a waterbath at 203°F (95°C) for the following 4 days. Then, they were dry cured in an oven at 203°F (95°C) for two days.

From an age of seven days to an age of 14 days, two different curing regimens were investigated to identify practices that might improve UHPC durability. In Regimen 1, specimens were air

cured for six days at room temperature, 77°F (25°C), followed by 24 hours of conditioning in a waterbath at 40°F (4.4°C). In regimen 2, specimens were moist cured for six days at 73°F (23°C), followed by 24 hours of conditioning in a waterbath at 40°F (4.4°C).

Series 1 consisted of three sets of UHPC mixtures that had a low sand content and a No. 30 aggregate top size. The difference between the three UHPC mixtures was the amount of fly ash of the pozzolanic materials. The proportions of the pozzolanic materials for Mixture 1 were 0% fly ash and 100% silica fume. Proportions of the pozzolanic materials for Mixture 2 were 37.5% fly ash and 62.5% silica fume. Finally, Mixture 3 pozzolanic material proportions were 50% fly ash and 50% silica fume. All three mixtures were evaluated using both curing Regimens 1 and 2.

NMDOT requires a durability factor (DF) greater than 95 to ensure that the concrete provides adequate resistance to freezing and thawing. Table 15.1 shows the durability factors for Series 1. The 0% fly ash mixture had one specimen subjected to dry curing that was adequate; however, the other specimens did not reach the required limit. The mixtures that used 37.5% and 50% fly ash appear to provide good resistance to freezing and thawing (DF > 95) regardless of the curing regimen. Also, it is important to note that Mixtures 2 and 3 under curing Regimen 1 provided greater durability factors. In fact, Mixtures 2 and 3 experienced an increase in dynamic elastic modulus.

TABLE 15.1 Durability factors for UHPC mixtures with low sand (Series 1).

Mixture		1	1	2	3	3
Percent Fly Ash, %		0	0	37.5	50	50
Curing Regimen		1 (dry)	2 (wet)	1 (dry)	1 (dry)	2 (wet)
Specimen	1	93.7	89.2	96.9	102.5	100.4
	2	95.4	92.2	104.8	101.2	100.9
	3	93.7	90.9	102.7	101.8	101.2
	AVG	94.3	90.8	101.5	101.9	100.8

Series 2 consisted of three sets of UHPC mixtures that had a higher sand content and a No. 30 aggregate top size. The difference between the three UHPC mixtures was the amount of fly ash of the pozzolanic materials and the sand content. The proportions of the pozzolanic materials for Mixture 4 are 37.5% fly ash and 62.5% silica fume with a sand content of 1,900 lb/yd^3 (1127 kg/m^3). Proportions of the pozzolanic materials for Mixture 5 were 37.5% fly ash and 62.5% silica fume with a sand content of 2,100 lb/yd^3 (1246 kg/m^3). Finally, mixture 6 pozzolanic material proportions were 50% fly ash and 50% silica fume and a sand content of 1,900 lb/yd^3 (1127 kg/m^3). All three mixtures were tested only under curing Regimen 2 (wet).

Figure 15.1 shows a plot of the average relative dynamic modulus (RDM) for the UHPC mixtures of Series 2. Table 15.2 presents the durability factors. All three UHPC mixtures provide good resistance to freezing and thawing (DF > 95) under curing Regimen 2.

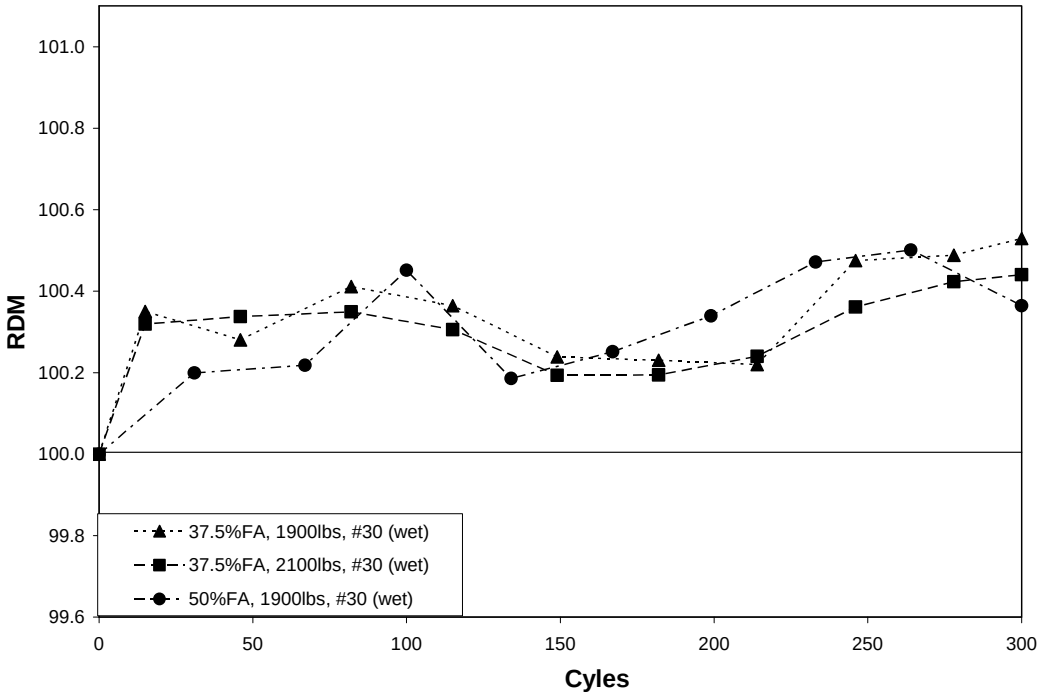

FIGURE 15.1 Average relative dynamic modulus for mixtures 4-5.

TABLE 15.2 Durability factors for UHPC mixtures with high sand (Series 1).

Mixture		4	5	6
Percent Fly Ash, %		37.5	37.5	50
Sand, lb/yd^3 (kg/m^3)		1900 (1127)	2100 (1246)	1900 (1127)
Curing Regimen		2 (wet)	2 (wet)	2 (wet)
Specimen	1	100.5	100.4	100.4
	2	100.5	100.5	100.3
	3	100.6	100.4	100.4
	AVG	100.5	100.4	100.4

The last series, Series 3, had three sets of UHPC mixtures that had a sand content of 1,900 lb/yd^3 (1227 kg/m^3) or higher, with an increment in aggregate top size from sieve size No. 30 to No. 4. The difference between the three UHPC mixtures was the amount of fly ash of the pozzolanic materials and the sand content. The proportions of the pozzolanic materials for Mixture 7 were 50% fly ash and 50% silica fume with a sand content of 1,900 lb/yd^3 (1127 kg/m^3). Proportions of the pozzolanic materials for Mixture 8 were 37.5% fly ash and 62.5% silica fume with a sand content of 1,900 lb/yd^3 (1127 kg/m^3). Finally, Mixture 9 pozzolanic material proportions were

37.5% fly ash and 62.5% silica fume and a sand content of 2,100 lb/yd^3 (1246 kg/m^3). All three mixtures were tested under curing regimens 1 (dry) and 2 (wet).

Figure 15.2 shows a plot of the average relative dynamic modulus (RDM) for the UHPC mixtures. Table 15.3 presents the durability factors. All three UHPC mixtures provided adequate resistance to freezing and thawing (DF > 95) under both curing regimens 1 and 2.

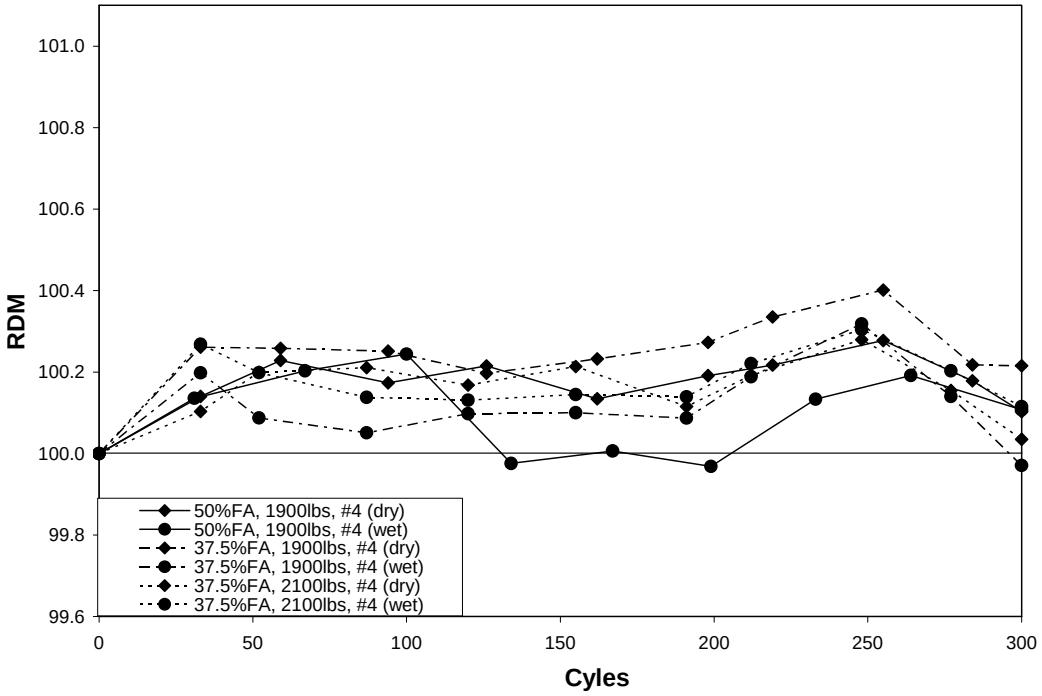

FIGURE 15.2 Average relative dynamic modulus for mixtures 7-9.

TABLE 15.3 Durability factors for UHPC mixtures with No. 4 maximum size aggregate (Series 3).

Mixture		7	7	8	8	9	9
Percent Fly Ash, %		50	50	37.5	37.5	37.5	37.5
Sand, lb/yd^3 (kg/m^3)		1900 (1127)	1900 (1127)	1900 (1127)	1900 (1127)	2100 (1246)	2100 (1246)
Curing Regimen		2 (wet)	1 (wet)	2 (wet)	1 (wet)	2 (wet)	1 (wet)
Specimen	1	100.2	100.1	99.9	99.9	100.0	100.1
	2	100.0	100.0	100.2	100.4	100.2	100.1
	3	100.1	100.2	99.8	100.3	100.1	99.9
	AVG	100.1	100.1	100.0	100.2	100.1	100.0

In general, most of the mixtures with pozzolanic material proportions of 37.5% fly ash and 62.5% silica fume exhibited greater durability factors for mixtures with the same top size, sand content and curing regimen. Similarly, lower sand contents resulted in greater durability factors for mixtures with the same pozzolanic material proportions, top size and curing regimen.

The increase from No. 30 to No. 4 in aggregate top size resulted in a decrease in durability factors. However, all UHPC mixtures with a No. 4 top size provided durability factors greater than 95. In most cases, curing regimen 1 provided greater durability factors. This indicates the possibility of reducing curing time.

15.2 RESISTANCE TO ALKALI-SILICA REACTION

Damage due to alkali-silica reaction (ASR) in concrete is a phenomenon that was first recognized in 1940 by Stanton in Southern California. The damage due to ASR is caused by expansion of alkali-silica gel that forms during the reaction. As the gel absorbs water, it swells and exerts pressure in the concrete that may be sufficient to cause cracking (Tuthill 1982). For ASR to occur, three factors must exist (CCANZ 2003):

(1) sufficient moisture in the pore structure of the concrete;
(2) sufficient alkalies supplied by the cement and other binder constituents, chemical admixtures and/or the aggregate in the pore solution; and
(3) reactive mineral(s) in the aggregate.

Typically, the reaction does not occur if the relative humidity in the concrete drops below 75%. However, if sufficient moisture is present, ASR will continue until the alkalinity of the pore solution falls below the required concentration for reaction, or until the one of the reactants is exhausted.

Cracking is usually considered to be the main damaging effect of ASR. The type and amount of ASR cracking is dependent upon the restraint provided by adjacent elements and/or reinforcement (mild steel or prestressing). Cracks will only develop where expansion restraint is not present. Cracking may be restricted to the outer (i.e., cover) concrete, with the interior concrete experiencing micro-cracking in the region of expanding particles. ASR can also cause damage that affects structural behavior. Concrete compressive strength, tensile/flexural capacity, shear strength, and elastic modulus may all be reduced. ASR expansion may affect the performance of the entire structure by imposing forces on adjacent members, inducing bending moments, closing expansion joints, increasing tensile strains in reinforcement, and/or reducing the bond between the concrete and reinforcement (CCANZ 2003).

Cracking of the cover concrete may also increase the risk of reinforcement corrosion by providing a route for water, air, and chlorides to reach steel reinforcement. It can also reduce resistance to freezing and thawing. Due to the detrimental effects that ASR can have on a structure, it is more important to minimize the risk of ASR damage at the time of construction, rather than to accommodate it in the design or to assess the significance of the effects if and when deterioration becomes evident.

The resistance to ASR of the UHPC mixtures developed using materials local to New Mexico was assessed using the mortar bar method (ASTM C 1260). ASTM defines the acceptable expansion limit as 0.10%. Several batches (see Table 15.4) were investigated, including batches with fibers and without fibers. For each batch, four 1.0 x 1.0 x 11.25 in. (25 x 25 x 285 mm) specimens were cast. Immediately after casting the concrete in the molds, the specimens were placed in a wet room for 24 hours, at room temperature. After 24 hours, the specimens were removed from the molds and a comparator was used to measure the initial length. The specimens were then placed in a water bath at 175°F (80°C) for 24 hours. Following the heated water bath, an initial calibration measurement for each specimen was recorded. Due to the temperature of the specimens being significantly higher than the ambient temperature (for the initial calibration measurement and subsequent measurements), the measurements were performed quickly (15 s ± 2 s) after removing the specimen from the container. After the initial calibration measurements were performed, the specimens were placed in a 1 N NaOH solution at 175°F (80°C). Four subsequent measurements (at 3, 7, 10, and 14 days) were performed after the zero measurement reading.

TABLE 15.4 UHPC batches tested.

Mixture	Percent Fly Ash, %	Sand weight, lb/yd^3 (kg/m^3)	Maximum Aggregate Size, (Sieve No.)	Percent volume of fibers, %
1	50	1900 (1127)	30	0
2	50	2100 (1246)	30	0
3	37.5	1900 (1127)	30	0
4	37.5	2100 (1246)	30	0
5	50	1900 (1127)	4	0
6	50	2100 (1246)	4	0
7	37.5	1900 (1127)	4	0
8	37.5	2100 (1246)	4	0
9	50	1900 (1127)	4	1.5
10	50	2100 (1246)	4	1.5
11	37.5	1900 (1127)	4	1.5
12	37.5	2100 (1246)	4	1.5

Results from the UHPC batches without fibers are shown in Figure 15.3. From these results, gradually increasing expansion can be seen throughout the testing period. Increasing the maximum aggregate size and the amount of sand caused a modest increase in expansion. However, at the end of the 16 day testing period, the greatest expansion was 0.025%, well below the acceptable limit of 0.10%. Figure 15.4 presents the results from the UHPC batches with steel fibers. The greatest expansion in any set of specimens was 0.016%, well below the ASTM allowable expansion limit of 0.10%.

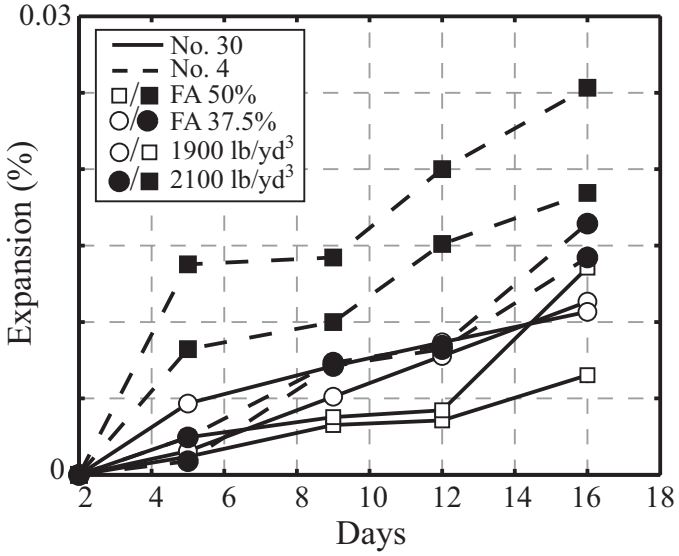

FIGURE 15.3 Expansion versus time for UHPC mixtures without fibers.

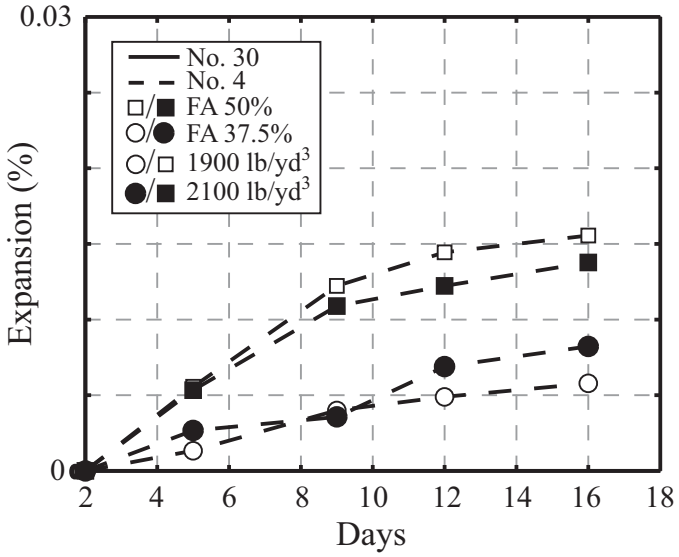

FIGURE 15.4 Expansion versus time for UHPC mixtures with fibers.

15.3 RESISTANCE TO DELAYED ETTRINGITE FORMATION

Delayed ettringite formation (DEF) is the formation of ettringite, a calcium aluminum sulfate mineral, in a cementitious material by a process that begins after hardening is substantially complete. DEF is different than the normal or secondary ettringite formation that takes place during normal hydration prior to the concrete hardening (Himes 1996). DEF occurs when

concrete is extensively exposed to water over a long duration or there are excessive amounts of sulfates present allowing for ettringite to "re-form." This creates significant expansion forces, and when left unrestrained, causes cracking of the concrete. DEF is observed in cases of elevated temperature curing [above 158°F (70°C)] where the concrete is exposed to moisture after curing and certain relationships exist between SO_3 content and some physical and chemical characteristics such as specific surface area, C_3A content, and Al_2O_3 content. Previous studies have discussed factors that affect DEF that may facilitate prediction of behavior for the new UHPC mixture.

15.3.1 Previous Research on DEF

Several investigations have been conducted to determine what factors affect DEF. Elevated curing temperatures greater than 158°F (70°C) are a common factor in all DEF studies. The data indicate that curing temperatures greater than 158°F (70°C) increase the expansion, while temperatures less than 158°F (70°C) produce no significant expansion.

Heinz and Ludwig (1987) concluded that the SO_3/Al_2O_3 ratio is the key to predicting DEF expansion. They stated that if the SO_3/Al_2O_3 ratio is less than 0.7 then DEF should not occur.

Odler and Chen (1995) showed that the SO_3/Al_2O_3 ratio is not as important as the individual SO_3 and Al_2O_3 contents. They concluded that only high C_3A (7-10%) and high SO_3 (3.5-5%) contents together produce significant expansion. However, the addition of fly ash with a high Al_2O_3 content reduced expansion substantially.

Ramlochan, Zacarias and Hooton (2003) concluded that approximately 8% silica fume replacement will not affect the long term expansion. Their study also concluded that lower replacement of fly ash (15-25%) effectively controlled expansion. They also suggested that a combination of silica fume and fly ash can control the expansion without loss of early strength.

Kelham (1996) studied different types of cement with different SO_3 contents. The maximum expansion occurred at an SO_3 content of 4%, less expansion was observed for lower SO_3 contents and no expansion occurred if the SO_3 content was 3% or less.

15.3.2 Analysis for UHPC in New Mexico

Due to the 203°F (95°C) curing used to achieve the high compressive strength of UHPC, DEF must be addressed. The SO_3/Al_2O_3 ratio for the cement in this work can be determined from the chemical composition provided in Table 15.5. The SO_3/Al_2O_3 ratio was 0.62, which is lower than the threshold identified by Heinz and Ludwig (1987) of 0.7. This ratio is not necessarily considered reliable, but it does indicate low DEF susceptibility.

To get significant expansion the SO_3 content should be 3.5-5% (Odler and Chen 1995). The cement in this study contains only 2.86% SO_3 (2.31% SO_3 for all cementitious materials). These values are lower than the effective limit of SO_3 (3.5%), indicating that DEF expansion should not be an issue for the UHPC mixtures. Odler and Chen (1995) also stated that at least 7% C_3A is necessary for DEF expansion. The cement used in the UHPC contains only 6% C_3A, indicating

again that DEF is unlikely to be problem. Mill certifications for the cement are required to ensure that this value remains bellows the limit.

TABLE 15.5 Chemical and physical characteristics of cement, Silica fume and fly ash.

	Cement	Silica fume	fly ash
Chemical Compound	Percentage of chemical composition (%)		
SiO_2	20.5	96.9	61.83
Al_2O_3	4.6	0.2	24.54
Fe_2O_3	3.6	0.2	4.22
CaO	64.5	0.3	1.45
K_2O	-	0.3	1.32
Na_2O	-	0.2	1.41
MgO	1.1	0.2	0.74
SO_3	2.8	0.1	0.18
Loss on ignition	2.3	2.17	0.36
Insoluble residue	0.21	-	-
pH	-	7.65	10-11
physical properties			
Relative Density	-	2.24	1.96
Specific Surface Area	335 m^2/kg	26,810 m^2/kg	2500 m^2/kg
Autoclave Expansion	0.0%	-	-0.03%
Moisture Content	-	0.04%	0.09%
C_3S, %	58	-	-
C_2S, %	17	-	-
C_3A, %	6	-	-
C_4AF, %	11	-	-

In this study, 7.5 and 10% fly ash additions have been used with 12.5 and 10% silica fume additions. Ramlochan *et al.* (2003) observed that fly ash with 18.23-21.89% Al_2O_3 effectively reduced expansion due to DEF. Similar benefits should be expected from the fly ash used in the UHPC since it contains 24.5% Al_2O_3.

In addition to the above factors there are other factors that may inhibit or reduce the expansion or expansion stresses. The dense microstructure produced by using 10% silica fume addition will decrease the permeability and the moisture content. Consequently the ettringite formation process will be prevented or slowed. Additionally, the steel fibers in the UHPC will restrain expansion if DEF occurs.

Evaluation of the possible factors that may influence the UHPC mixtures indicates that there should be no significant expansion in the UHPC mixtures. Most importantly, the low SO_3 content of the cement used in the UHPC [2.86% versus Kelham`s (1996) limit of 3%] and the low C_3A content [6% versus Odler and Chen's (1995) 7%] indicate that there should not be significant expansion.

THIS PAGE LEFT BLANK INTENTIONALLY

16 CONCLUSION AND RECOMMENDATIONS

Following the findings from Phase I of this research project, it was determined that more economical and readily available UHPC mixture proportions would be required for successful implementation of UHPC into bridge design in New Mexico. In Phase II, mixture proportions for UHPC with materials local to New Mexico were developed and optimized. After the mixture proportions were optimized, the curing regimen was optimized for use in local precast plants by using readily achievable temperatures for both the wet and dry curing periods. Finally, the durability of the optimized mixture for resistance to freezing and thawing, alkali-silica reaction, and delayed ettringite formation was established. The following conclusions and recommendations were drawn based on the work conducted as part of Phase II of this research project.

16.1 MIXTURE PROPORTIONS

Based on the findings of this research, the following characteristics are recommended for UHPC mixture proportions using materials local to New Mexico:

- Type I/II portland cement;
- water-to-cementitious material ratio of 0.14;
- 50% replacement of silica fume with Class F fly ash;
- No. 4 maximum size of aggregate;
- 1900 lb/yd^3 (1127 kg/m^3) of sand; and
- 1.5% steel fibers by volume.

TABLE 16.1 Recommended Mixture Proportions.

Constituents	Unit	Amount/yd^3 (Amount/m^3)
Cement	lb (kg)	1263.9 (749.8)
Silica fume	lb (kg)	158 (93.7)
Fly ash	lb (kg)	158 (93.7)
Sand	lb (kg)	1900 (1127)
Steel fibers	lb (kg)	200 (118.7)
HRWRA	gal (L)	8.6 (42.5)
Water	lb (kg)	221.2 (131.2)

16.2 CURING REGIMEN

Using temperatures that are readily achievable at local precast plants, the following 7-day heated curing regimen is recommended:

- 24 hours ambient environment;
- 4 day wet cure at of 203°F (95°C); and
- 2 day dry cure at of 203°F (95°C).

As research on UHPC continues to progress, this curing regimen recommendation may be revised. Many researchers are currently working toward developing UHPC that does not require a heated curing regimen. If that work is successful during the course of this continuing research, effort will be taken to implement similar curing methods in New Mexico.

16.3 DURABILITY

Based on the results of the durability study, it was established that the UHPC developed using material local to New Mexico provides excellent resistance to freezing and thawing, alkali-silica reaction, and delayed ettringite formation.

All durability factor values determined from freezing and thawing tests were greater than 100 versus the required limit of 95 to demonstrate resistance to freezing and thawing.

In the ASR tests, the greatest expansion was 0.025%, well below the ASTM limit of 0.1%.

Finally, the only factor indicating DEF formation susceptibility is a curing temperature greater than 158°F (70°C). All other factors indicate that the UHPC is not vulnerable to DEF.

16.4 FUTURE WORK

Following the development of UHPC mixture proportions using local materials, further testing to investigate the creep and shrinkage behavior of the UHPC is necessary. Due to the removal of coarse aggregate and the increased cementitious materials content of UHPC, shrinkage could be substantially greater than for normal and high strength concretes. Curing conditions can also affect shrinkage of concrete. To achieve the high compressive strengths and durability properties of UHPC, a heated wet and dry curing period is required. This curing regimen could lead to reduced post-curing shrinkage. As discussed in Chapter 2, research on UHPC has shown negligible shrinkage following the heated curing regimen; however, early age shrinkage prior to curing may still be substantial. The curing regimen and removal of coarse aggregate can also play a significant role on the creep behavior of the UHPC. Both creep and shrinkage can increase prestress losses; therefore, it is important to understand the behavior of both prior to implementing UHPC in prestressed concrete bridge design.

Large-scale testing of girder specimens is also necessary to develop design recommendations for the use of UHPC in bridge superstructures. Currently, there are no design procedures for UHPC which limits the potential for designers to use this material in design. Designing large-scale specimens and testing them in flexure will establish a basis to develop design procedures for incorporating UHPC into bridge design.

Finally, modifications to current standard specifications are required for the introduction of this material in precast plant production. Due to the regimented mixing and curing procedures required to achieve the high compressive strengths and durability properties of UHPC, specifications and guidelines are necessary to ensure quality production of this material.

THIS PAGE LEFT BLANK INTENTIONALLY

REFERENCES

Alborn, T.M., Peuse, E.J., Misson, D.L., *Ultra-High-Performance-Concrete for Michigan Bridges Material Performance-Phase I.* Research Report RC-1525. Michigan Department of Transportation, 2008.

Aïtcin, P. C., *Cements of Yesterday and Today: Concrete of Tomorrow*, Cement and Concrete Research, Vol. 30, 2000, pp. 1349-1359.

Allena, S., and Newtson, C., *Ultra-High Strength Mixtures Using Local Materials*, Concrete Sustainability Conference, National Ready Mix Concrete Association, Tempe, AZ, April 13-15, 2010.

Bache, H.H., *Densified cement/ultra fine particle based materials*, Second International Conference on Superplasticizers in Concrete. Ottawa, Ontario, Canada, June 10-12, 1981.

Bierwagen, D, Abu-Hawash, A., *Ultra High Performance Concrete Highway Bridge* Proceedings of the 2005 Mid-Continent Transportation Research Symposium, Ames, Iowa, August 2005. © 2005 by Iowa State University.

Bierwagen, D. and McDonald, N. *Ultra High Performance Concrete Highway Bridge*. Report by the Iowa Department of Transportation, 2005

CCANZ, *Technical Report 3 – Alkali Silica Reaction, Minimising the Risk of Damage to Concrete: Guidance Notes and Recommended Practice Second Edition*, Cement and Concrete Association of New Zealand, 2003.

Collepardi, S., Coppola, L., Troli, R., & Collepardi, M. *Mechanical Properties of Modified Reactive Powder Concrete*, www.encosrl.it/enco%20srl%20ITA/servizi/pdf/high/12.pdf, 2007.

Davila, R.S., *Recommendations for the Design of Ultra High Performance Concrete Structures*., Master's Thesis, Massachusetts Institute of Technology, 2007.

Degen, Brian *Evaluation of a Prestressed Concrete Bridge Constructed using Ultra High-Performance Concrete.* Master'sThesis, Iowa State University, Iowa. 2005.

de Lerrard, F., and Sedran, T., *Optimization of Ultra-High Performance Concrete by the Use of a Packing Model,* Cement and Concrete Research, Vol. 24, No. 6, 1994, pp. 997-1009.

Dili, A. S., Santhanam, M. *Investigations on Reactive Powder Concrete: A Developing Ultra High Strength Technology*, The Indian Concrete Journal, Vol. 78 No. 4, 2004, pp. 33-38.

Elkem. Particle size distribution software, LISA: http://www.materials.elkem.com/eway/default.aspx?pid=243&trg=Main_7170&Main_7170=7197:0:4,4710:1:0:0:::0:0. Site accessed 2009

Ferraris, C.F., & Larrard, F.de. *Testing and Modeling of Fresh Concrete Rheology*, Building and Fire Research Laboratory, No. NISTIR 6094, National Institute of Standards and Technology, Gaithersburg, MD, 1998 pp. 1-61.

Gao,R., Stroeven, P., Hendriks, C.F. *Mechanical Properties of Reactive Powder Concrete Beams*, Seventh International Symposium on the Utilization of High Strength/High Performance Concrete, SP-228-79, ACI, 2005.

Garcia, H. and Graybeal, B. *Analysis of an Ultra high Performance Two-Way Ribbed Bridge Deck Slab*, National Technical Information Service Report No. PB2007-112112, Springfield, VA, 2007.

Gowripalan, N. and Gilbert, R.I., *Design Guidelines for UHPC Prestressed Concrete Beam*, The University of New South Wales, January 2000.

Graybeal, B. A. and Hartmann, J.L. *Rapid Construction of an Ultra High Performance Concrete Bridge*. 2004.

Graybeal, B., Hartmann, J., Perry,V. *Ultra High Performance Concrete for Highway Bridge*, Symposium - Avignon, France, April 26-28, 2004.

Graybeal, B. *Structural Behavior of Ultra high Performance Concrete Prestressed I-Girders*, Federal Highway Administration Report No. FHWA-HRT-06-115, McLean, VA, 2006a.

Graybeal, B. *Material Property Characterization of Ultra High Performance Concrete*, Federal Highway Administration Report, No. FHWA-HRT-06-103, McLean, VA, 2006b.

Graybeal, B. and Tanesi, J. *Durability of an Ultra High Performance Concrete*. ASCE Journal of Materials in Civil Engineering, Vol. 19, No.10, 2007, pp. 848-854.

Graybeal, B., *Flexural Behavior of an Ultrahigh-Performance Concrete I-Girder*. ASCE Journal of Bridge Engineering,Vol.13, No. 6, pp. 602-610. November-December 2008.

Graybeal, B.A., *UHPC Making Strides*, U.S. Department of Transportation Federal Highway Administration Public Road, Vol. 72, No.4, 2009.

Heinz, D. & Ludwig,U., *Mechanism of secondary ettringite formation in mortars and concretes subjected to heat treatment*. Concrete Durability, Katherine and Bryant Mather International Conference, SP-100. Vol. 2, edited by J.M. Scanlon, American Concrete Institute, Detroit, MI, 1987, pp. 2059-2071.

IBRC Homepage. Federal Highway Administration http://www/fhwa.dot.gov/bridge/ibrc/ Accessed August 20, 2009.

Interim Recommendations produced by the Service d`études techniques des routes et autoroutes of the Association Française de Génie Civil (AFGC/SETRA), January 2002.

Keierleber, B., Phares, B., Bierwagen, D., Couture,I., Fanous, F. *Design of Buchanan County, Iowa, Bridge Using Ultra High Performance Concrete and PI Girders*, Proceedings of the 2007 Mid-Continent Transportation Research Symposium, Ames, Iowa, August 2007. © 2007 by Iowa State University.

Kelham, S., *The effect of cement composition and fineness on expansion associated with delayed ettringite formation*. Cement and Concrete Composites, Vol. 18, No. 3, 1996, pp. 171-179.

Kleymann, M.J., Girgis, A.M., Tadros., M.K. *Developing User Friendly and Cost Effective Ultra High Performance Concrete*. Concrete Bridge Conference. The Nugget, Reno, Nevada. May 7-10, 2006.

Lafarge Canada Inc. "Ductal® Frequently Asked Questions," http://87.230.81.56/imagineductal/faq.php, Accessed June 4, 2009a.

Lafarge Canada Inc. "Technical Characteristics," http://87.230.81.56/imagineductal/technical.php, Accessed June 4, 2009b.

Matte, V., & Moranville, M. *Durability of Reactive Powder Composites: Influence of Silica Fume on the Leaching Properties of Very Low Water/Binder Pastes*. Cement and Concrete Composites, Vol. 21, 1-9, 1999.

Odler, I. and Chen, Y., *Effect of cement composition on the expansion of heat-curing cement pastes*. Cement and Concrete Research, No. 25, 1995, pp. 853-862.

Ramlochan, T., Zacarias, P., Thomas, M.D.A., and Hooton, R.D., *The effect of pozzolans and slag on the expansion of mortars cured at elevated temperature: part I: expansive behavior*, Cement and Concrete Research, Vol. 33, No. 6, 2003, pp. 807-814.

Rebentrost, M. and Cavill, B. *Australian Experience with Ductal®: An Ultra High Performance Concrete*, FIB 2nd International Congress, Naples, Italy, 2006.

Recommendations for Design and Construction of Ultra High Strength Fiber Reinforced Concrete Structures, Published by Subcommittee on Research of Ultra High Strength Fiber Reinforced Concrete of the Japan Society of Civil Engineers (JSCE), 2006

Reda, M.M., Shrive, N.G., and Gillott, J.E., *Microstructural Investigation of Innovative UHPC*, Cement and Concrete Research, Vol. 29, No. 3, 1999, pp. 323-329.

Resplendino, J. and Petitjean, J. *Ultra High Performance Concrete: First Recommendations and Examples of Application*, ISHPC, France, 2003.

Richard, P., and Cheyrezy, M. H. *Reactive Powder Concretes With High Ductility and 200-800 MPa Compressive Strength*, Concrete technology: past, present and future, Proceedings of the V.

Mohan Malhotra symposium, Mehta, P.K. (Ed.), ACI SP 144-24, pp. 507-518. Detroit: Victoria Wieczorek, 1994.

Richard, P., & Cheyrezy, M. *Composition of Reactive Powder Concrete*, Cement and Concrete Research, Vol. 25, No. 7, pp. 1501-1511, 1995.

Roux, N., Andrade, C., & Sanjuan, M. A. *Experimental Study of Durability of Reactive Powder Concretes*, Journal of Materials in Civil Engineering, Vol. 8, No. 1, pp. 1-6, 1996.

Shaheen, E., & Shrive, N. J. *Optimization of Mechanical Properties and Durability of Reactive Powder Concrete*, ACI Materials Journal, Vol. 103, No. 6, 444-451, 2006.

Stanton T. E., *Expansion of Concrete Through Reaction Between Cement and Aggregate,* Proc. of the American Society of Civil Engineers*,* Vol. 66, No. 10, 1940, pp. 1781-1811.

Tuthill, L., *Alkali-Silica Reaction – 40 Years Later*, Concrete International, April 1982, pp. 32-36.

Ulm, F.-J. "Bending & Shear Design of Iowa DOT Sample Bridge – Update. Design Review of Mars Hill Bridge", Massachusetts Institute of Technology. May 24, 2004.

Wen-yu, J., Ming-zhe, A., Gui-ping, Y., & Jun-min, W. *Study on Reactive Powder Concrete Used in Sidewalk System of The Qinghai-Tibet Railway Bridge*," http://www.cptechcenter.org/publications/sustainable/jireactive.pdf, Accessed 2007.

New Mexico Department of Transportation
RESEARCH BUREAU
7500B Pan American Freeway NE
PO Box 94690
Albuquerque, NM 87199-4690
Tel: (505) 841-9145